ISAS - INTERNATIONAL SCHOOL FOR ADVANCED STUDIES

The Environments of BL Lacertae Objects

Thesis submitted to the
International School for Advanced Studies, Trieste, Italy
- Astrophysics Sector -
in partial fulfilment of the requirements for the degree of

Philosophiæ Doctor

CANDIDATE

Joseph E. Pesce

SUPERVISORS

Prof. Aldo Treves
Dr. Renato Falomo

October 1993

TRIESTE

SISSA - SCUOLA INTERNAZIONALE SUPERIORE STUDI AVANZATI
TRIESTE
Strada Costiera 11

To my Tata

The Environments of BL Lacertae Objects

Thesis submitted to the
International School for Advanced Studies, Trieste, Italy
- Astrophysics Sector -
in partial fulfilment of the requirements for the degree of

Philosophiæ Doctor

CANDIDATE

Joseph E. Pesce

SUPERVISORS

Prof. Aldo Treves
Dr. Renato Falomo

October 1993

ABSTRACT

This thesis reports the results of an environmental study of seventeen BL Lacertae objects (BL Lacs). We performed a detailed, multicolor analysis of the fields around the BL Lacs, and obtained spectra of selected galaxies near a subgroup of seven objects.

We find that BL Lac objects are often located in regions of higher-than-average galaxy density. The host galaxies of BL Lacs are probably the dominant members of small groups or clusters of galaxies, rarely richer than Abell richness class 0. The richest environment of the sample is around the X-ray selected object, H 0414+009, also the first BL Lac to be found in such a cluster.

Spectroscopy gives direct proof of the physical association between the BL Lac and at least one other galaxy in the field in six of seven cases observed. For five sources we note the BL Lac has a very close ($\lesssim$ 5 arcsec) companion galaxy, which is, perhaps, in the process of interacting. Spectra confirm the association of a galaxy, with a projected distance of 11 kpc from the bright BL Lac, PKS 2155–304, and of galaxies within 90 kpc of three objects.

The imaging results for BL Lacs are compared to those (taken from the literature) for F-R I and II radio galaxies, the proposed BL Lac parent population. While the scarcity of the data available hinders our interpretation, BL Lac environments are consistent with those of both F-R I and II galaxies.

Acknowledgements

I would like to thank my parents, Michael and Lucille Pesce, and the rest of my family, for their support and for encouraging me, from the age of five, along the path of astronomy. My supervisors, Aldo Treves and Renato Falomo put up with my naive questions and absented-mindedness; for this, and everything else (*e.g.* funding!), goes my gratitude. Renato taught me how to analyze and interpret data, and, in general, how to be an astronomer.

Special thanks go to my ex-collaborators and friends Bob Stencel and Chris Moss who advised me and accepted my continual requests for letters of recommendation! Prof. Alfonso Cavaliere provided the impetus for my coming to Italy, and Prof. Dennis Sciama first introduced me to S.I.S.S.A. and provided funding for my research throughout my stay here, for which I am grateful.

My friends all over the world have been a special asset and have given me much advice and encouragement. To list them risks leaving someone out, but I will do so anyway: Chris Blair, Paolo Catelan, Miguel Chavez, Francesca and Alberto Conti, Marilyn and Rob Clifton, Li-Cai Deng, Paul Haines, Eric Hooper, Pavel Kroupa, Hugo Tecotl Morales, Mark Oliver, Elena Pian, David Valls-Gabaud, Gerry Williger, and all the rest I have failed to include.

My gratitude to the many people who assisted me, financially and otherwise, at the conferences I attended and official visits I made, especially George V. Coyne, S.J., Sabino Maffeo, S.J., the staff of the Specola Vaticana, and the Scuole Nazionale di Astrofisica.

I wish to acknowledge Francesco Valdes for his assistance with the installation of FOCAS and for subsequent suggestions, the IRAF support staff during the installation of the software, and after, and Allyn Tennant for his

assistance during the installation of QDP and PGPLOT. However, all of this 'installing' would not have been possible without the tremendous amount of help from Antonio Lanza. Finally, thanks go to Roberto Innocente, Marina Picek, and Luisa Urgias, the efficient European Southern Observatory support staff in Chile and Germany, and the staff and members of S.I.S.S.A. and the Asiago/Padova Observatories.

This research has made use of the NASA/IPAC Extragalactic Database (NED), operated by the Jet Propulsion Laboratory, Caltech, under contract with NASA, and the High Energy Astrophysical Science Archive Research Center Online Service (HEASARC), provided by the NASA – Goddard Space Flight Center.

This thesis is the result of my own work except where acknowledged otherwise. It is not substantially the same as any work that I have submitted or will submit for a degree, diploma or other qualifications at any other university.

Joseph E. Pesce

October 1993

Haec sic pernosces parva perductus opella;
namque alid ex alio clarescet, nec tibi caeca
nox iter eripiet quin ultima naturai
pervideas: ita res accendent lumina rebus.

"If you take a little trouble you will attain
a thorough understanding of these truths. For one thing
will be illumined by another, and eyeless night will
not rob you of your road till you have looked into
the heart of nature's darkest mysteries. So surely will
facts throw light upon facts."

Lucretius, *De rerum natura*, I.1114 – 1117

CONTENTS

I Introduction 1

II BL Lacertae Objects 5

2.1 The Beaming Model of BL Lacs 5

2.1.1 The BL Lac Parent Population 7

2.2 Gravitational (micro)Lensing 10

III Environmental Studies of BL Lacertae Objects 15

3.1 Early History 15

3.2 Host Galaxies 20

3.3 Zwicky and Abell Clusters Associated with BL Lac Objects 21

IV Observations and Data Analysis 23

4.1 The Sample 23

4.2 The Instruments 27

4.3 Data Reduction 30

4.4 Analysis Method 31

4.5 Post FOCAS Analysis 35

4.5.1 Background Counts 39

V Results 43

5.1 Analysis Methods 43

5.1.1 Simple Statistics 43

5.1.2 Cluster Richness 44

5.1.3 The Angular Correlation Amplitude 46
5.1.4 Evaluating the Amplitudes 48
5.2 Individual Objects 48
5.2.1 PKS 0118–272 48
5.2.2 PKS 0301–243 53
5.2.3 H 0414+009 56
5.2.4 PKS 0537–441 61
5.2.5 PKS 0823+033 64
5.2.6 PKS 0829+046 67
5.2.7 H 1101–232 71
5.2.8 PKS 1400+162 76
5.2.9 MS 1402+042 80
5.2.10 PKS 1514–241 (AP Lib) 83
5.2.11 PKS 1538+149 87
5.2.12 PG 1553+113 90
5.2.13 H 1722+119 93
5.2.14 1749+096 96
5.2.15 PKS 2005–489 99
5.2.16 PKS 2155–304 103
5.2.17 PKS 2335+031 110

VI Discussion 113
6.1 Comparisons with Other Studies 116
6.1.1 Quasar Environments 116
6.1.2 Radio Galaxy Environment 119
6.2 Conclusions 127

References 129

A Images of Program Objects 141

B Density Distributions 159

C Miscellaneous FOCAS Output 175

TABLES

4.1 Program Objects 28

4.2 Source Properties 29

4.3 Various Parameters 30

4.4 Imaging Data 40

4.5 Matched Galaxies 42

5.1 Excess Galaxies 45

5.2 Richness - $N_{0.5}$ Calibration 46

5.3 Imaging Results 49

6.1 Spectra Results 114

6.2 Richness Classifiers 120

6.3 Comparisons 125

FIGURES

2.1 Beaming Model Geometry 6

4.1 The Redshift Distribution 24

4.2 The Apparent Magnitude Distribution 25

4.3 Host Galaxy Absolute Magnitude 26

4.4 Scale-Magnitude Diagram 34

4.5 Differential Galaxy Counts 37

5.1 Contour: PKS 0118–272 51

5.2 Radial Distribution: PKS 0118–272 52

5.3 Contour: PKS 0301–243 54

5.4 Radial Distribution: PKS 0301–243 55

5.5 Contour: PKS 0414+009 57

5.6 Radial Distribution: H 0414+009 58

5.7 H 0414+009: Spectra 60

5.8 Contour: PKS 0537–441 62

5.9 Radial Distribution: PKS 0537–441 63

5.10 Contour: PKS 0823+033 65

5.11 Radial Distribution: PKS 0823+033 66

5.12 Contour: PKS 0829+046 68

5.13 Radial Distribution: PKS 0829+046 69

5.14 Spectra: PKS 0829+046 70

5.15 Contour: H 1101–232 72

5.16 Radial Distribution: H 1101–232 73
5.17 The Host Galaxy of H 1101–232 74
5.18 Spectra: H 1101–232 75
5.19 Contour: PKS 1400+162 77
5.20 Radial Distribution: PKS 1400+162 78
5.21 Spectra: PKS 1400+162 79
5.22 Contour: MS 1402+042 81
5.23 Radial Distribution: MS 1402+042 82
5.24 Contour: PKS 1514–241 84
5.25 Radial Distribution: PKS 1514–241 85
5.26 Spectra: PKS 1514–241 86
5.27 Contour: PKS 1538+149 88
5.28 Radial Distribution: PKS 1538+149 89
5.29 Contour: PG 1553+113 91
5.30 Radial Distribution: PG 1553+113 92
5.31 Contour: H 1722+119 94
5.32 Radial Distribution: H 1722+119 95
5.33 Contour: 1749+0962 97
5.34 Radial Distribution: 1749+096 98
5.35 Contour: PKS 2005–489 100
5.36 Radial Distribution: PKS 2005–489 101
5.37 Spectra: PKS 2005–489 102
5.38 Contour: PKS 2155–304 104
5.39 Radial Distribution: PKS 2155–304 105
5.40 PKS 2155–304: Spectra 108
5.41 PKS 2155–304 - G4 109

5.42 Contour: PKS 2335+096 111

5.43 Radial Distribution: PKS 2335+031 112

6.1 Average Density 118

6.2 $N_{0.5}$ Distribution, Combined Sample 121

6.3 $N_{0.5}$ Distribution, By Redshift 123

6.4 Richness Indicators and Redshift 124

6.5 Correlation Amplitude Distributions 126

A.1 Image: PKS 0118–272 142

A.2 Image: PKS 0301–243 143

A.3 Image: H 0414+009 144

A.4 Image: PKS 0537–441 145

A.5 Image: PKS 0823+033 146

A.6 Image: PKS 0829+046 147

A.7 Image: H 1101–232 148

A.8 Image: PKS 1400+162 149

A.9 Image: MS 1402+042 150

A.10 Image: PKS 1514–241 151

A.11 Image: PKS 1538+149 152

A.12 Image: PG 1553+113 153

A.13 Image: H 1722+119 154

A.14 Image: 1749+096 155

A.15 Image: PKS 2005–489 156

A.16 Image: PKS 2155–304 157

A.17 Image: PKS 2335+031 158

B.1 Density V: PKS 0118–272 160

B.2 Density I: PKS 0118–272 160
B.3 Density V: H 0414+009 161
B.4 Density I: H 0414+009 161
B.5 Density V: PKS 0537–441 162
B.6 Density I: PKS 0537–441 162
B.7 Density I: PKS 0823+033 163
B.8 Density V: PKS 0829+046 164
B.9 Density I: PKS 0829+046 164
B.10 Density V: H 1101–232 165
B.11 Density I: H 1101–232 165
B.12 Density V: PKS 1400+162 166
B.13 Density I: PKS 1400+162 166
B.14 Density I: MS 1402+042 167
B.15 Density V: PKS 1514–241 168
B.16 Density V: PKS 1538+149 169
B.17 Density I: PKS 1538+149 169
B.18 Density V: PG 1553+113 170
B.19 Density I: PG 1553+113 170
B.20 Density V: H 1722+119 171
B.21 Density V: PKS 2005–489 172
B.22 Density I: PKS 2005–489 172
B.23 Density V: PKS 2155–304 173
B.24 Density I: PKS 2155–304 173

The Environments of BL Lacertae Objects

CHAPTER I

Introduction

BL Lacertae objects (in the following, BL Lacs or BL Lac objects) are a class of highly luminous, core-dominated Active Galactic Nuclei (AGNs). One of the major characteristics defining the BL Lac phenomena is strong polarization ($\geq$ 3 %). This varies on timescales of a few hours and up, and is wavelength dependent in the optical-IR (with changes in both position angle and strength). BL Lacs also exhibit rapid flux variability at all wavelengths, and featureless (weak or undetectable emission lines), non-thermal continua with most of the luminosity radiated in the Infrared. All BL Lacs are both X-ray and radio emitters (*e.g.* Madejski & Schwartz 1989; Stocke *et al.* 1991) and some are superluminal sources (Urry, Padovani, & Stickel 1991). When observed, the hosts of BL Lacs are generally giant elliptical galaxies (see below, Chapter III, Section 3.2).

Because of the inherent variability of these sources, defining objects as BL Lacs is not straightforward. A good working definition, however, is that of Stocke *et al.* (1991). In order to be included as a BL Lac, the optical counterpart of an X-ray source (in the case of Stocke *et al.*) must have a featureless optical spectrum, here considered when the equivalent widths of any lines in emission are less than 5 Å. In addition, the Ca II break 'strength', that is the relative depression of the continuum below 4000 Å in the rest frame, must be less than 25% (a typical giant elliptical or F-R I radio galaxy has a break strength of 50%).

BL Lac objects can be divided into radio-selected and X-ray-selected subclasses, depending on whether they are found in radio (Stickel *et al.* 1991) or X-ray surveys (Maccacaro *et al.* 1982; Gioia *et al.* 1984; Stocke *et al.* 1991; Giommi *et al.* 1991). However, this classification is not unambiguous; some radio selected sources are strong X-ray sources as well (*e.g.* Mushotzky *et al.* 1978; Schwartz *et al.* 1978). A more quantitative criterion refers to the ratio of the radio and X-ray flux (Ledden & O'Dell 1985).

X-ray selected BL Lacs (XBLs) are generally similar to radio selected ones (RBLs) in that they both have the same X-ray luminosity, but the continua are flatter in XBLs (Ghisellini & Maraschi 1989), and they probably share the same parents (Kollgaard *et al.* 1992). However, XBLs are much more numerous than RBLs (about ten times more, Morris *et al.* 1991; Urry, Padovani, & Stickel 1991). In addition, they have, in general, a higher fraction of starlight in their optical spectra when compared to RBLs (Morris *et al.* 1991), and lesser amounts of optical variability and polarized light (Stocke *et al.* 1989).

Several models have been proposed to explain the BL Lac phenomena and its characteristics. By far the most accepted is that of Blandford & Rees (1978) who hypothesize that the BL Lac spectra are dominated by emission from a relativistic jet closely aligned to the line of sight (for more details, see below, Chapter II, Section 2.1). Among other things, the beaming model naturally predicts a large number of unaligned objects, the parent population.

The alternative, more exotic, theory proposed by Ostriker & Vietri (1985), is the gravitational microlensing model. In this view, a significant fraction of BL Lacs are gravitationally microlensed Optically Violently Variable quasars (OVVs) whose continuum emission is greatly amplified relative to the line emission, the lenses being stars and compact objects in foreground galaxies. The enhancement of the continuum is possible because the line-emitting regions are too large to be lensed by stars (see below, Chapter II, Section 2.2).

Some of the outstanding problems in BL Lac research include a better understanding of the emission processes. The recent detection of BL Lacs as γ-ray emitters is assisting in this, as are observations with the new generations of X-ray satellites (ROSAT, ASTRO-D). For example, X-ray spectra have been modelled in terms of synchrotron self-Compton emission from a jet, thermal emission from a nuclear disk, and inverse Compton emission from the interaction of an ultra-relativistic jet with the disk radiation field. Measurements of γ-rays would search for the predicted high energy signature of jet deceleration model (Königl 1989). The modelling of X-ray spectra (such as by, for example, Sambruna *et al.* 1993) will help to answer questions about emission processes.

Questions concerning the XBL/RBL division include: Are X-rays produced in a weakly beamed part of the jet (Ghisellini & Maraschi 1989) or, as suggested by Melia & Königl (1989), do they come from an isotropic flow that is still strongly beamed? Is there a thermal emission component present in BL

Lacs (perhaps in the form of the 6.4 keV feature due to Iron), or X-ray absorption features due to intrinsic gas? Are high and low redshift BL Lacs the same class of object, or do they differ substantially (Antonucci 1993)?

One way of understanding the BL Lac phenomena is by studying their *environments*. In particular, the beaming model requires the identification of a parent population. Thus, we would expect BL Lac environments to be identical to those of their parents.

For the case of quasars, evidence is growing that the environments play an important role in triggering and fueling the nuclear activity (*e.g.* Hutchings et al. 1984; Hutchings & Neff 1990, 1992). The way in which the environment causes this activity is through galaxy-quasar interactions and mergers. Perhaps similar processes instigate the BL Lac phenomena.

The study of the environment of BL Lacs can also be used to test the lensing model. Most lensing galaxies are expected to be at relatively low redshifts ($z < 0.5$), and if these galaxies are located in clusters, the clusters should be found around BL Lacs regardless of the object's intrinsic emission-line redshift. In particular, high redshift BL Lacs should also be associated with clusters (which are foreground).

The observed differences between high and low redshift BL Lacs, between BL Lacs and optically violently variable quasars, and between XBL and RBL can all be addressed and, perhaps, understood by an environmental analysis.

The work presented below is an analysis of the environments of seventeen BL Lac objects. We perform multicolor imaging of a large (> 7 arcmin) field around the targets. All objects in the fields are classified as stars or galaxies, and we determine whether there is a significant enhancement of galaxies (indicating the presence of a, possibly, associated group or cluster) around the BL Lacs. Furthermore, we have obtained spectra of selected galaxies in the fields of seven BL Lac objects. The imaging data are then compared to similar data (from the literature) for radio loud quasars and the proposed BL Lac parent population. We stress that our sample of BL Lac objects is **not** to be considered statistically complete.

This thesis is organized as follows. In Chapter II we describe the main aspects of the beaming and lensing models. Chapter III is a summary of historical studies of the BL Lac environments. A description of the sample and of

the data reduction is given in Chapter IV. In Chapter V we present the final analysis methods and the results. Finally, in Chapter VI we discuss the results and compare the environmental properties of BL Lacs with those of the proposed parent population.

Part of the results of this thesis were published in Falomo, Pesce, & Treves 1993a [*Astron. J.*, **105**, 2031], Falomo, Pesce, & Treves 1993b [*Astrophys. J. Lett.*, **411**, L63], and Pesce, Falomo, & Treves 1993 [*Astron. J.*, submitted].

CHAPTER II

BL Lacertae Objects

2.1 The Beaming Model of BL Lacs

The hypothesis proposed by Blandford & Rees (1978; see also Blandford & Königl 1979) to explain the BL Lac phenomena, namely that these objects are characterized by bulk relativistic motion in a jet aligned nearly to the line of sight, is still dominant today. Below, we will briefly introduce this theory.

Blandford & Rees were motivated by two problems in the observations of BL Lacs, the rapid variability and the formulation of dynamical models to explain the outburst of the source PKS 0235+164 in 1975. At the outburst, the radio brightness temperature of PKS 0235+164 was calculated to be $> 10^{15}$ K, far too high to be compatible with the Compton limit for a non-relativistic outburst.[1] The high polarization observed in BL Lacs provided an argument in favor of the Compton-synchrotron models for these objects, *i.e.*, their continua are non-thermal in origin. Further observations placed constraints on any models for the compact non-thermal sources.

Based on the fact that compact radio sources have large scale, extended double or linear structures, the authors assumed that small scale structures ($<$ pc) are linked to the large scale structures by two straight jets along which matter flows at supersonic and possibly relativistic speeds. The opening angles of the jets are typically about 10°, and for some fraction of the sources we should look directly along either jet. In this case, one would expect to see unscattered (rapidly variable and polarized) non-thermal emission directly.

Thus, Blandford & Rees made the following proposal, "...*[BL Lacs] are*

[1]This is part of the 'Compton catastrophe', discussed in light of discrepancies between radio X-ray flux by, for example, Madejski & Schwartz 1983.

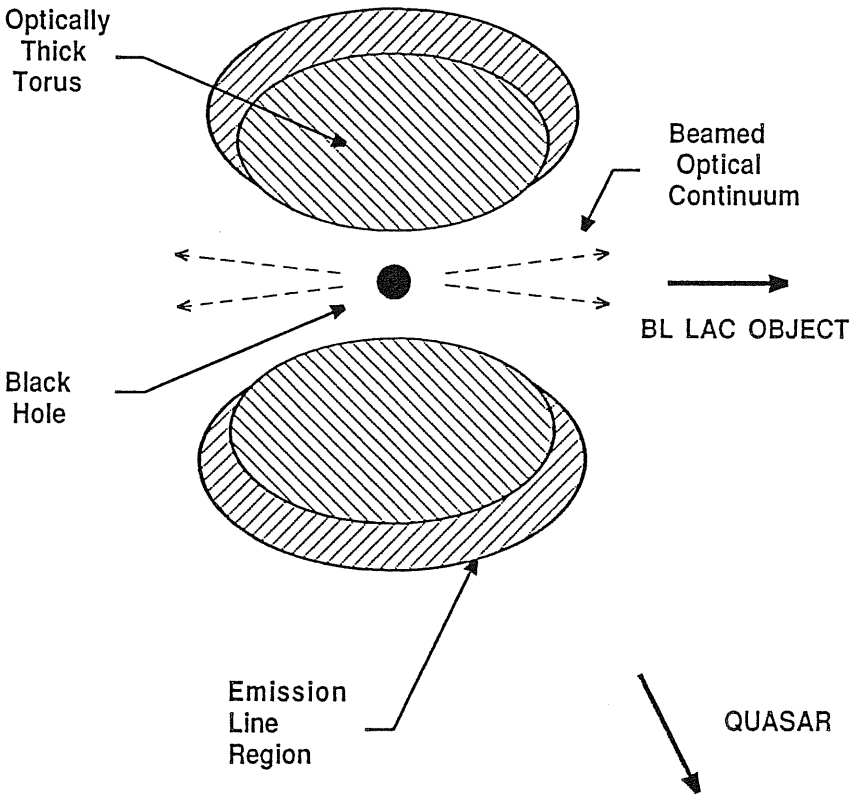

Figure 2.1: Geometry for the beaming model. Adapted from Blandford & Rees 1978.

active galactic nuclei where the continuum emission is enhanced by being beamed toward us. This may occur because the emitting region moves relativistically outwards in the form of a jet...." See Figure 2.1.

Königl (1989) reviewed the findings and developments in light of the beaming model, over the ten years from the original Blandford & Rees paper. Support for beaming comes from several observations. At least four objects had been confirmed as superluminal sources (Zensus 1989). VLBI maps of BL Lacs exhibit a core-jet morphology which is interpreted in terms of the relativistic beaming model: the counter-jet is Doppler-boosted away. Many BL Lacs exhibit rapid flux variation whose timescales decrease toward shorter wavelengths, interpreted by invoking relativistic motions at the source. Strong variability in the polarized flux is also attributed to relativistic effects.

Evidence in support of small observing angles with respect to the jet axes is provided by measurement of the extended radio emission. A prediction

by Blandford & Rees that some BL Lacs should show halo emission corresponding to a double source viewed along its symmetry axis has been demonstrated observationally by Antonucci & Ulvestad (1985).

Königl (1989) states that a test of the Blandford & Rees proposal is the ability of synchrotron emission models of relativistic jets to account for the observed BL Lac spectra, and, indeed, models reproduce well the shape of the spectra (*cf.* references in Königl). In addition, the discovery of BL Lacs as γ-ray sources (*e.g.* Hunter *et al.* 1993; Thompson *et al.* 1993) is further confirmation of the jet model, since a high energy component was predicted (*cf.* Maraschi, Ghisellini, & Celotti 1992).

Further predictions, still awaiting confirmation, deal not with the central source but with the parent population (see below). If BL Lacs represent those objects for which we observe the jet end on, there must be a population of objects for which the jet is unaligned to the line of sight; the parents.

2.1.1 The BL Lac Parent Population

It is widely argued that the compact radio emission, and the highly variable and polarized optical emission of BL Lac objects is the result of a relativistic jet seen end-on. In this case, there must be a large number of unaligned objects, the parent population.

Many studies have addressed the question of the BL Lac parent population. Based upon an analysis of X-rays, Schwartz & Ku (1983) estimated the local volume density of BL Lacs. This was then compared to the density of Seyfert I galaxies and X-ray emitting quasars. They find that the volume density for all three types of objects is similar. Thus if the X-ray emission is isotropic, the hypothesis that BL Lac objects are a subclass of quasars is excluded.

Browne (1983) took these results to be consistent with a subset of giant elliptical galaxies being the parent population. This author argues that the existence of extended radio emission (see, *e.g.,* Wardle, Moore, & Angel 1984) places strong constraints on any unaligned parent population. If Seyferts have been excluded (*cf.* Schwartz & Ku 1983), the only other possibility is elliptical radio galaxies. Ulrich (1989) agrees with this, finding the parents to be bright radio galaxies such as those in the Bologna sample.

Based on VLA observations of BL Lacs, Wardle, Moore, & Angel (1984) found that the luminosity distribution of their extended radio structure (if radi-

ated isotropically) is similar to that of Fanaroff-Riley (F-R) type I radio galaxies, but is weaker than F-R II radio galaxies.[2]

Padovani & Urry (1990) began a detailed analysis of BL Lacs and F-R I radio galaxies, by studying the X-ray properties of these two classes. Starting with the luminosity function of F-R I radio galaxies, these authors then estimated the shapes of the luminosity function of sources beamed toward us (BL Lacs), normalizing it to the observed X-ray counts and constraining the fit by the partial redshift distribution (this approach simultaneously tests the beaming hypothesis and determines the effectiveness of F-R I galaxies as the parent population).

The authors compare number density of BL Lacs and parents, combining a large, complete sample of BL Lacs, corrected for the effects of beaming on the luminosity function, and explicitly identify the F-R I galaxies as the parent population. The ratio between the total number density of BL Lacs and F-R I galaxies is 1:7. In addition, the predicted luminosity function of BL Lacs is found to be in good agreement with previous, direct estimates which were based on a limited number of BL Lacs with known redshift. They stress that the results are not strongly dependent on the details of their models, and that the hypothesis that BL Lacs are beamed F-R I galaxies can easily explain their observed X-ray properties

In the continuing series, Padovani & Urry (1991) undertook a study of the optical properties of F-R I galaxies and BL Lacs. In a way analogous to the X-ray study, they first constructed the F-R I optical luminosity function, then calculated the predicted BL Lac luminosity function (considering effects of beaming and contamination by light from the host galaxy). Finally, BL Lac counts are derived and compared (along with the redshift distribution) to those predicted by their model. Although of low luminosity in the radio, F-R I galaxies are bright optically ($L \geq L^*$).[3] Again in this case the results are consistent with F-R I radio galaxies as the parent population.

Finally, Urry, Padovani, & Stickel (1991) studied the radio properties of F-R I galaxies and BL Lacs in a similar fashion. They noted that a more

[2]Fanaroff & Riley (1974) classified radio galaxies as one of two groups, type I or type II, defined as follows. Type I are characterized by low radio power ($P_{178MHz} < 10^{25.5}$ W Hz^{-1}), are generally compact, lack terminal hotspots, and are highly distorted with diffuse, edge-darkened, narrow, two-sided jets. Type II are the classical double sources, with $P_{178MHz} > 10^{25.5}$ W Hz^{-1}, and have edge-brightened jets with terminal hotspots.

[3]The BL Lac hosts are also found in brighter elliptical galaxies (Ulrich 1989).

complex model is required because more detailed data are available in the radio than in any other waveband. Their results are that the predicted luminosity function of a subset of F-R I galaxies beamed toward us is in good agreement with the observed luminosity function of BL Lacs.

Detailed radio observations of 17 BL Lacs by Kollgaard *et al.* (1992) provided some interesting results. In general, sources with the most luminous extended emission exhibit F-R II characteristics in both *morphology* and *polarization* (and, hence, are not just the high luminosity tail of F-R I sources), while less luminous sources exhibit F-R I characteristics. The main conclusion is that *the parent population of BL Lac objects contains both F-R I and F-R II radio sources* (their italics). In addition, BL Lacs show distinctive polarization properties at milli-arcsecond resolution, and no object exhibits quasar-like polarization. This finding argues against the view that the most luminous BL Lacs are merely an extension of the quasar/OVV population or that most BL Lacs are gravitationally microlensed images of distant quasars (see below).

The authors conclude that not all radio galaxies can contain a nucleus that would appear as a radio selected BL Lac if properly oriented, and thus only some do (most probably those with stronger cores). For X-ray selected BL Lacs (which are less beamed and more numerous), a larger fraction of radio galaxies may be the parent population.

Thus, to summarize this section: F-R I radio galaxies have been proposed as the parent population of BL Lac objects based on their space density, X-ray luminosity and unbeamed (extended) optical and radio properties. Their X-ray, optical, and radio luminosity functions are consistent with those of BL Lacs (in the beaming hypothesis) and they are the only AGNs with sufficient space density to be the parent population. A small number of radio selected BL Lacs have radio properties incompatible with the beamed F-R hypothesis and thus may be F-R II sources. X-ray selected BL Lacs may be the transition objects between the unbeamed parents and the highly beamed radio selected BL Lacs, as expected in the beaming model. Not all radio galaxies have a BL Lac nucleus.

2.2 Gravitational (micro)Lensing

In order to explain apparent anomalous features of BL Lac observations which are inconsistent with the beaming model, Ostriker & Vietri (1985; hereafter OV85) developed the microlensing model. Physical problems with the beaming model included the fact that ionizing radiation from the nucleus would be expected to be absorbed by ambient gas in an elliptical galaxy (assuming such gas has not been ejected). Some of this radiation will degrade to the Hα line, which should be detected in nearby BL Lac objects. One of the major problems is of a statistical nature. Put simply, there are far too many BL Lacs at redshift less than 0.2 and too few at high redshift ($z \gtrsim 1$).

OV85 proposed that BL Lacs are the results of the microlensing of distant Optically Violently Variable quasars (OVVs) by compact objects in foreground galaxies. Thus the nebulosity of BL Lacs should not be physically associated with the active nuclei but will only be on the same line of sight. OVVs were chosen because of the similarities between their properties and those of BL Lacs (*e.g.*, high polarization and rapid variability), and because they are intrinsically small (derived from variability arguments). These objects differ from BL Lacs in exhibiting strong lines. The magnification of the continuum over the line emission is possible because of the difference in size between the small continuum-emitting region ($\sim 10^{15}$ cm) and the line-emitting region (0.1 – 1 pc). The latter is too large to be lensed by stars in a microlensing situation. Because of the strong emission lines in OVVs, magnification of the continuum by a factor of at least 10 is required for a BL Lac classification.

The best lensing candidates were found to be elliptical galaxies with $z \sim 0.05 - 0.1$, consistent with the observed distribution of BL Lacs. Thus, OV85 conjectured, BL Lacs are at cosmological distances and the apparent enhancement at low redshift is just due to the fact that the best lens candidates are found there.

In the intervening years, a number of studies have been produced which seem to reject the microlensing hypothesis. This model predicts that the extended radio properties of OVVs and BL Lacs should be similar. Ulvestad & Antonucci (1986) find that the properties of the extended radio emission in several nearby BL Lacs are inconsistent with the expectation. The emission observed for Mrk 180, PKS 2155–304, and 1727+502 would imply extensions of

600 kiloparsec to 1.1 megaparsec at z = 1. On the contrary, emission around OVVs extends to only tens of kiloparsecs (Antonucci & Ulvestad 1985).

Other differences between BL Lacs and OVVs that are hard to reconcile if they are truly related are that BL Lacs have steeper X-ray spectra than OVVs, and while the latter can be fit with a single spectral index, this may not to be the case for the former (*e.g.* Worrall & Wilkes 1990). The parsec scale polarization of BL Lacs is distinct and non-quasar like (Kollgaard *et al.* 1992), while the extended radio emission and line luminosities ([O III]) of the classes are significantly different (Padovani 1992). BL Lacs appear not to be quasars with emission lines swamped by an enhanced optical continuum, but have intrinsically weak lines. Another strong argument against BL Lacs and OVVs being the same type of object is the difference of their redshift distributions; the large number of low redshift BL Lacs is inconsistent with these objects coming from the same parent population (Browne 1989). BL Lacs are almost exclusively found in luminous elliptical galaxies (Ulrich 1989) which may be F-R I radio galaxies, while OVVs may have F-R II hosts. Thus there is no one, unified model for OVVs and BL Lacs (Browne 1989).

Some testable consequences of the model are given by OV85. Absorption systems should be observed in a significant fraction of BL Lacs. One can expect to find $z_{\rm abs} > z_{\rm gal}$ in some cases. In fact, while absorption systems with redshifts lower those of the BL Lac are found in some cases (*e.g.* PKS 0235+164) no cases have been observed of an absorption system with redshift higher than the redshift of the BL Lac determined from the host galaxy spectrum.

The position of the optical continuum source should not be centered on the image of the associated galaxy, when observed. Re-examining the issue, Merrifield (1992) finds that the *majority* of BL Lacs should be projected away from the center of the lensing galaxy. In the 12 objects clearly resolved by Abraham, M$^{\rm c}$Hardy, & Crawford (1991), the mean offset from the central source and the isophote where the galaxy dominates is only 0.04 arcsec. Incidentally, OV85 use the example of OX 290 (Craine & Warner 1976), a radio source 6 arcsec from a Zwicky galaxy. Ulvestad & Johnston (1984) showed that the radio emission is centered on the Zwicky galaxy. Thus the proposed BL Lac object, OX 290A, is not a confirmed radio emitter and probably not a BL Lac (Ulvestad & Antonucci 1986).

In addition, lensing can be expected to produce multiple images (Narayan

& Schneider 1990). No such multiple images have been observed associated with BL Lacs, though Ostriker & Vietri (1990) suggest that this is because one of the images is brighter than the others, thus outshining them.

In the lensing model, the radio source does not necessarily have to be coincident with the optical galaxy. The reference quoted by OV85 as proof of this statement, Danziger *et al.* (1979), reported that the BL Lac object 0521–26 [4] has an unresolved radio component centered on the galaxy and an extended component to the Northeast. However, there is no expectation that extended radio emission should be coincident with the galactic center (Ulvestad & Antonucci 1986). We note that Danziger *et al.* (1979), based on an analysis of weak emission lines, and, in particular, Hα, find the presence of a quantity of gas typical for other active galaxies. This is contrary to one of the main points against the beaming mode.

Ostriker & Vietri (1990) list a number of specific cases which seem to favor their model. The object 0846+51 W1, when in the bright state, has all of the attributes of a BL Lac. In the low state, however, it looks like a quasar, exhibiting emission lines that yield a redshift of $z = 1.86$ (Arp *et al.* 1979; Nottale 1986). This is normal behavior for BL Lacs (and is one reason why they are so difficult to classify; see Antonucci 1993 for a discussion of this point).

Another lensing candidate is the BL Lac object PKS 0537–441. Despite a redshift of 0.894, Stickel, Fried, & Kühr (1988c) find that the object is extended, spatially resolved, and that image decomposition reveals a foreground disk galaxy (centered on the BL Lac). A second, similar galaxy 11 arcsec away from the BL Lac has $z = 0.186$. The authors contend that this is a prime example of a gravitationally lensed quasar. However, Falomo, Melnick, & Tanzi (1992) point out that a detailed modelling of the Point-Source Function (PSF) is crucial. The analysis of an image of PKS 0537–441, obtained under subarcsecond conditions, revealed that there is **no** evidence the source is extended, and thus, does not support the suggestion that there is a galaxy superposed on the image of the BL Lac object.

One of the best studied BL Lac objects is PKS 0235+164, with $z = 0.94$. A nearby (2 arcsec) compact object has $z = 0.524$ and other galaxies in the field share this redshift (Stickel, Fried, & Kühr 1988b). Absorption line systems

[4]There is some question as to whether this object is indeed a BL Lac because it exhibits broad emission lines when the continuum is in a low state.

at $z = 0.524$ and $z = 0.851$ are found in the spectrum of PKS 0235+164. In addition, emission features are also detected at $z = 0.524$. From two-dimensional image decomposition, Stickel, Fried, & Kühr (1988b) propose there is a bright galaxy, displaced 0.5 arcsec from the BL Lac and superposed on it. However, the analysis is very complex as there are a number of objects very near the BL Lac source, and we recall that the extended image may be an artefact due to improper modelling of the PSF (as in the case of 0537–441). It is also possible that PKS 0235+164 is truly unique.

In conclusion, while individual cases of microlensing may exist, it is probably not a general explanation of the phenomena. The most significant argument against the hypothesis being the fact that OVVs and BL Lacs are intrinsically different, contrary to the predictions.

CHAPTER III

Environmental Studies of BL Lacertae Objects

3.1 Early History

From the earliest period, even before they were recognized as a distinct class of objects, BL Lacs were noticed in connection with groups of galaxies. The first study of this 'early phase' was that of Disney, Peterson, & Rodgers (1974) who found several galaxies within three arcmin of AP Lib (PKS 1514–241, $z = 0.0486$). The nearest galaxy (one arcmin) to the North has approximately the same diameter as AP Lib and may be at the same distance. These authors suggested that the BL Lac source may be a member of a small group or cluster of galaxies. Later analysis of this same field by Visvanathan & Griersmith (1977) showed that after subtraction of the contribution from a foreground group about 20 arcmin to the Northeast (velocity = 2260 km s^{-1} and dominant members NGC 5898 and NGC 5903; Sandage 1975) and the background galaxy density, the high number of galaxies within nine arcmin (eight) suggests the presence of a group of galaxies in the direction of AP Lib.

For Disney (1974) the fact that PKS 0548–322 appeared to be located at the center of a group of galaxies added evidence for the extragalactic nature of BL Lac objects, a fact which was not yet completely clear at the time. The cluster appears to be of Abell richness class 0 and spectroscopy of three galaxies in the field yielded a cluster redshift of $z = 0.042$, while the spectra of PKS 0548–322 was found to be featureless. Disney argued that the similarity of the angular sizes of the BL Lac halo and the cluster galaxies supported the hypothesis of cluster membership for the BL Lac. However, spectra of the halo of the luminous giant elliptical obtained by Fosbury & Disney (1976) showed absorption lines from a population of late-type stars with $z = 0.069$. This finding effectively ruled out

the BL Lac-cluster connection in the case of PKS 0548–322.

A successive study (Craine, Tapia, & Tarenghi 1975) of the nebulosity underlying the BL Lac objects PKS 1538+149, PKS 2254+074, and PKS 2335+031 found evidence for many faint galaxies in the fields of these three sources, suggesting their possible membership in distant galaxy clusters. The authors state, "since the majority of the BL Lac objects seem to be somehow related to galaxies, it seems of interest to ask whether isolated BL Lac objects really exist or will they eventually be found to be associated with galaxies?" Because of the technology of the period, a definitive response to this question would have to wait awhile yet.

Contemporarily, Butcher *et al.* (1976) found that the BL Lac 3C 66A is located near the apparent center of a distant rich cluster of galaxies. These authors were motivated to study the object because it lies in the same direction as the Abell cluster A347 (with $z \sim 0.02$); if the BL Lac were an elliptical galaxy at this distance, detection of its outer envelope would be possible. While the authors detected no evidence of surrounding 'fuzz' they did notice a "swarm of faint objects, nearly centered on 3C 66A, almost all of which are fainter than 20^{th} magnitude." Comparison of plates of distant clusters with known redshift indicated that the group could well be a cluster with $z \geq 0.4$. The apparent radius at which the density of objects falls to about half its central value is 20–30 arcsec, again consistent with $z \geq 0.4$.

Multicolor photometry of all objects within one arcmin of 3C 66A and fainter than $V \sim 19$ indicated that the sample is complete down to $V = 22$ and contains 15 probable cluster members brighter than this limit. The swarm of faint objects surrounding 3C 66A have a color distribution and luminosity function of a distant, rich cluster of galaxies at $z \sim 0.37^{+0.07}_{-0.03}$. Spectra of 3C 66A were later obtained by Miller, French, & Hawley (1978). A feature detected in a noisy area was identified with Mg II λ 2800 Å giving a redshift $z = 0.444$. These authors stress, however, that this is not a definitive measurement, and the redshift can not be considered reliable. No further spectroscopy of 3C 66A, nor of any galaxies in the field, has since been performed, to our knowledge.

In the meantime, Baldwin *et al.* (1977) identified the weak emission feature of [O II] λ 3727 Å in the spectra of PKS 1400+162 giving $z = 0.244$. These authors noted that PKS 1400+162 is superposed on the western edge of a small group of galaxies, the nearest member of which is only about six

arcsec to the Southwest of the BL Lac. Baldwin *et al.* also obtained a (noisy) spectrum of this galaxy and identified the Ca II H and K features and the 4000 Å discontinuity at a redshift of $z = 0.245$. PKS 1400+162 was thus the first BL Lac object for which the probable physical association with nearby galaxies had been established spectroscopically.[1]

In a later study of the field of PKS 1400+162, Weistrop *et al.* (1983) obtained photometry of some galaxies in the group. The estimated redshifts are consistent with the $z = 0.245$ determined by Baldwin *et al.* (1977) for the nearest galaxy to PKS 1400+162.

In a largely ignored paper, Ulrich (1978) obtained spectra of B2 1101+38, and of five galaxies within 15 arcmin of the BL Lac. For B2 1101+38 (Mrk 421), the redshift derived from the host galaxy is $z = 0.03$. Three of the galaxies (plus one additional galaxy, the velocity of which was measured by R. Lynds, as reported in Colla *et al.* 1975) have nearly the same velocity, corresponding to $z \sim 0.03$. Ulrich found the galaxies form part of the Zwicky cluster CGCG 1057.2+3804 and that the surface density of galaxies is fairly uniform, with two low-contrast condensations, one near the BL Lac and the other near the opposite edge of the cluster at $10^h\ 50^m + 38°\ 00'$.

A few years later, Weistrop *et al.* (1981) performed surface photometry of 1218+304, 1827+50 (I Zw 187), and 1219+28 (W Com). The former two objects were found to be typical elliptical galaxies, while no nebulosity was found associated with 1219+28. More importantly, these authors conclude by noting an apparent absence of galaxies around the BL Lacs studied. They detect no galaxies in the images, nor find nearby Abell clusters, and state, "...the BL Lac phenomena may preferentially avoid a cluster environment."

Other than Weistrop *et al.* (1983), no further work on the environment of BL Lacs was attempted for almost ten years. It was almost as if the words of Weistrop *et al.* (1981) frightened everyone out of the field!

With the advent of CCDs, allowing fainter objects to be imaged and spectra of faint galaxies more easily obtained, the study of the BL Lac environment experiences a renaissance and takes off. We enter the 'modern' phase. The use of larger scale CCDs has also assisted in this development.

[1]The object is also found to be the first BL Lac for which the low frequency radio emission arises almost entirely in an extended double-lobed structure typical of radio galaxies. Another is 2007+777 (Antonucci *et al.* 1986).

Based on a preliminary analysis of BL Lacs observed in the 1 Jy catalog of radio sources (Kühr *et al.* 1981), Stickel, Fried, & Kühr (1989) observed that 1418+546 appeared to be located in a previously unknown group of galaxies. They obtained spectra of six galaxies in the field and found that two have the same redshift as the BL Lac ($z \sim 0.15$), though this value is uncertain.

The same authors later performed a more detailed analysis of the BL Lacs in the 1 Jy catalog (Stickel, Fried, & Kühr 1993) and found five objects with at least one to three galaxies in the field at the same redshift as the BL Lac source (1418+546, 1652+398, 1807+698, 2005–489, and 2254+074). In addition, they note that there is a grouping of seven faint, compact galaxies near 1749+096, but were unable to determine a redshift from the spectrum of the brightest galaxy in the group.

A statistical analysis of this sample was performed by Fried, Stickel, & Kühr (1993), who determined the average excess of galaxies versus distance from the BL Lac source. BL Lacs in the low ($\langle z \rangle = 0.28$) and medium ($\langle z \rangle = 0.65$) redshift ranges are found, *on average*, in clusters as rich as Abell richness class 0 – 1. The high ($\langle z \rangle = 0.97$) redshift range is particularly interesting. No significant *average* excess of surrounding galaxies was found, although in individual cases (PKS 0537–441 and 0820+225) an excess may be present. This result is not surprising, and in fact is expected, since at the magnitude limit of the study ($m \leq 22$) a typical cluster galaxy ($M^* = -21$; $m = 23.7$) would not be detected. Moreover, such a finding is evidence against the microlensing theory, since if the lensing galaxy is in a cluster, these objects will have $z < 0.5$ and should be observed, regardless of the high redshift of the BL Lac (see Chapter II, Section 2.2, above).

For two newly discovered BL Lacs found in the HEAO 1 survey (H 1101–232 and H 1426+428) Remillard *et al.* (1989) obtained R– band CCD images and remarked that the host galaxy of both sources may be the central members of a cluster of galaxies. An aggregation of 15 – 20 marginally resolved objects are within two arcmin of H 1426+428 and there are about 15 surrounding H 1101–232. The galaxies are all similar in color and have a brightness range of $22 < V < 20$. Nothing further is known about these objects.

The present analysis was stimulated by several works. The first of these (Falomo, Melnick, & Tanzi 1990) noted the presence of close companion objects near PKS 0048–097, H 0323+022, H 0414+009, H 1722+119, PKS 2155–304,

and H 2351–31. Falomo (1991) detected about 15 faint galaxies in the field of PKS 0118–272, which are symmetrically distributed within 30 arcsec of the BL Lac object; the nearest is eight arcsec away.

Falomo, Pesce, & Treves (1991) reported the presence of at least two galaxies within ten arcsec of PKS 0829+046 and two galaxies near PKS 2005–489. Spectra of one of these galaxies in each field show them to be associated with the BL Lac sources. Falomo, Tanzi, & Treves (1991) observed a number of galaxies in a peculiar disposition surrounding the X-ray object H 0414+009. This field was more thoroughly analyzed by M^{c}Hardy *et al.* (1992) and Falomo, Pesce, & Treves (1993a) (see also below). The object was found to be the dominant member of a moderately rich cluster of galaxies (Abell richness class 0). H 0414+009 is the first case of the unequivocal identification of a BL Lac in such a rich environment.

Furthermore, Falomo *et al.* (1991) performed high resolution imaging of PKS 2155–304, and showed that the previously attributed redshift of the source was instead mistakenly derived from a nearby (4.5 arcsec) companion galaxy ($z = 0.117$), until then hidden by the glare of the BL Lac source. These authors obtained spectra of one other nearby galaxy, finding a redshift of $z = 0.116$ and noting numerous other galaxies in the field. PKS 2155–304 was further studied by Falomo, Pesce, & Treves (1993b) (see below), who determined the BL Lac's true redshift ($z = 0.116$) and found it to be the dominant member of a poor cluster with an interesting binary structure.[2]

Recently, Wurtz and collaborators performed an imaging analysis of four BL Lacs. These workers find two X-ray selected objects (MS 1207+39 and MS 1407+59) in rich clusters, evidence for a poor cluster around 3C 66A, and confirm the rich cluster around H 0414+009 (Wurtz *et al.* 1993a, 1993b). Similarly, Smith, O'Dea, & Baum (1993) analyzed the images of 17 BL Lacs and find these objects in regions of enhanced galaxy density.

As seen above, most studies only commented on the presence of companion galaxies or groups/clusters surrounding BL Lacs. Certainly no work specifically devoted to the environmental properties of BL Lacs appears in either of the two big BL Lac conferences (Pittsburgh, 1978 and Como, 1988). Our

[2]In addition, galaxies with various redshifts have been observed around both PKS 0235+164 and PKS 0537–441. These are two candidates for lensing, and we will not reference them here. They have been discussed above in Chapter II, Section 2.2.

present analysis is, as far as known, the first systematic imaging *and* spectroscopic study of the environment of a large sample of BL Lac objects.

3.2 Host Galaxies

The present work is not the forum in which to discuss the topic of BL Lac host galaxies, although it is extremely important for the understanding of the phenomena. However, a few words are in order.

It was recognized early on (*e.g.* Disney, Peterson, & Rodgers 1974; Thuan, Oke, & Gunn 1975; Ulrich *et al.* 1975; Ulrich 1978) that BL Lacs reside in elliptical galaxies with $\langle M_V \rangle = -23.05 \pm 0.71$ (Ulrich 1989). To our knowledge, all BL Lacs to date have been found in elliptical galaxies, with the following exceptions (and counter arguments).

M^{c}Hardy *et al.* (1991) obtained multicolor images of PKS 1413+135. They find the R and I surface brightness distributions are best fit by the combination of a large exponential disk and a small central bulge. Based on the disk-to-bulge ratio and the red colors, these authors classify the object as an S0b–c galaxy.

Carilli, Perlman, & Stocke (1992) detected strong neutral hydrogen 21cm absorption and confirmed the 'host' galaxy as a spiral of type later than S0. Stocke *et al.* (1992) concluded that while there is strong evidence for a spiral host to the BL Lac nucleus, this is an improbable situation since the highly extincted optical/UV/X-ray continuum would produce thermal Infrared emission and strong, narrow emission lines which are **not** observed. The continuum would need to be narrowly beamed ($\theta <$ few degrees) in order not to heat the gas and dust. The evidence argues for the AGN to be background to the spiral and not hosted by it.

PKS 1413+135 might be gravitationally lensed by the foreground spiral. However, while expected, multiple images are not observed. Thus, PKS 1413+135 remains an enigmatic object.

The only other BL Lac thought to be hosted by a spiral is 1E 1415.6+2557. Halpern *et al.* (1986) fit the resolved component with an exponential disk of scale length 18 kpc. However, the study of surface brightness profiles can be very delicate, and after a careful examination of the image, Romanishin (1992) showed

that, in fact, the BL Lac host is most likely a luminous elliptical galaxy.[3]

Abraham, M^{c}Hardy, & Crawford (1991) studied a number of BL Lacs and classified two as being located in disk systems. One is PKS 1413+135, discussed above. The other is OQ 530. However, there may be problems with the classifications.

3.3 Zwicky and Abell Clusters Associated with BL Lac Objects

BL Lacs might be found in or near Zwicky and Abell clusters. To date, observations indicate that in only one case, Mrk 421, is a BL Lac object definitely associated with a Zwicky cluster (Ulrich 1978). The cluster, CGCG 1057.2+3804, is indicated by Zwicky *et al.* (1961–68) to be 'open' and 'rich' and contains about 535 members within a radius of 1.°23.

Fried, Stickel, & Kühr (1993) claim that H 0414+009 is a member of CGCG 0414.3+0103, though this is unsubstantiated. The cluster is 'medium compact' and lies 20 arcmin away from the BL Lac, with a distance class indicating it to be foreground to H 0414+009.

Similarly for Abell clusters, only one BL Lac is thought to be a member. The redshift of the Abell cluster A2295 is based upon that of the BL Lac 3C 371 (1807+698) (Sandage 1966; Sandage 1978; Struble & Rood 1982). (3C 371 was originally, and erroneously, thought to be part of A2301). However, such an association is highly unlikely since 3C 371 is about 1.°8 (or 8 Mpc for $z = 0.05$) from the cluster center.

In the course of the present work, it was found that the Abell cluster A1969 and the BL Lac MS 1443+638 share the same redshift ($z \sim 0.299$), both determined independently, although the BL Lac is about 5 Mpc from the cluster center. It could be that the BL Lac is an outlying member or part of a subcluster in the outskirts of the cluster proper. As of yet, we have no information on the environment of this object.

BL Lacs do not appear to reside, on average, in Zwicky or Abell clusters. However, this does not mean they are not found in clusters or groups of galaxies.

---

[3]This author further detects the presence of what appears to be an optical jet. Only one other BL Lac has been reported to have an optical jet (PKS 0521–36: Keel 1986; Macchetto *et al.* 1991).

CHAPTER IV

Observations and Data Analysis

4.1 The Sample

The program objects are listed in Table 4.1, which gives the object and other names in columns 1 and 2, respectively, the right ascension and declination (1950) in columns 3 and 4, and apparent visual magnitude in column 5. The redshift and reference for this value are in columns 6 and 7, respectively, while column 8 gives the selection method (X-ray selected or radio selected). The selection method has been determined following Ledden & O'Dell (1985) who find that a majority of objects have X-ray luminosity to radio luminosity ratios in the range $35 \leq L_x/L_r \leq 7000$. These objects we call 'X-ray selected'. Those with $1 \leq L_x/L_r \leq 35$ are called 'radio selected'.

The sample consists of seventeen objects, with a mixture of radio and X-ray selected targets, and does not satisfy any selection criteria. The redshifts range from $z = 0.0486$ to 0.896 and there are three objects with undetermined redshifts. The redshift distribution is given in Figure 4.1 and that of the apparent magnitudes is in Figure 4.2.

Further source information appears in Table 4.2, which lists the polarization values (column 2) and whether there is evidence for a host galaxy (column 3). For eight objects, the host galaxy absolute visual magnitude is given (column 4). These values have been taken from the literature (references given in column 5), and, where necessary, have been recalculated using $H_0 = 50$ and $q_0 = 0.5$, and K-corrected. Figure 4.3 shows the distribution of the absolute magnitudes, with an average $\langle M_V \rangle = -22.99 \pm 0.71$, in good agreement with that for a larger sample of BL Lacs (-23.05 ± 0.71; Ulrich 1989).

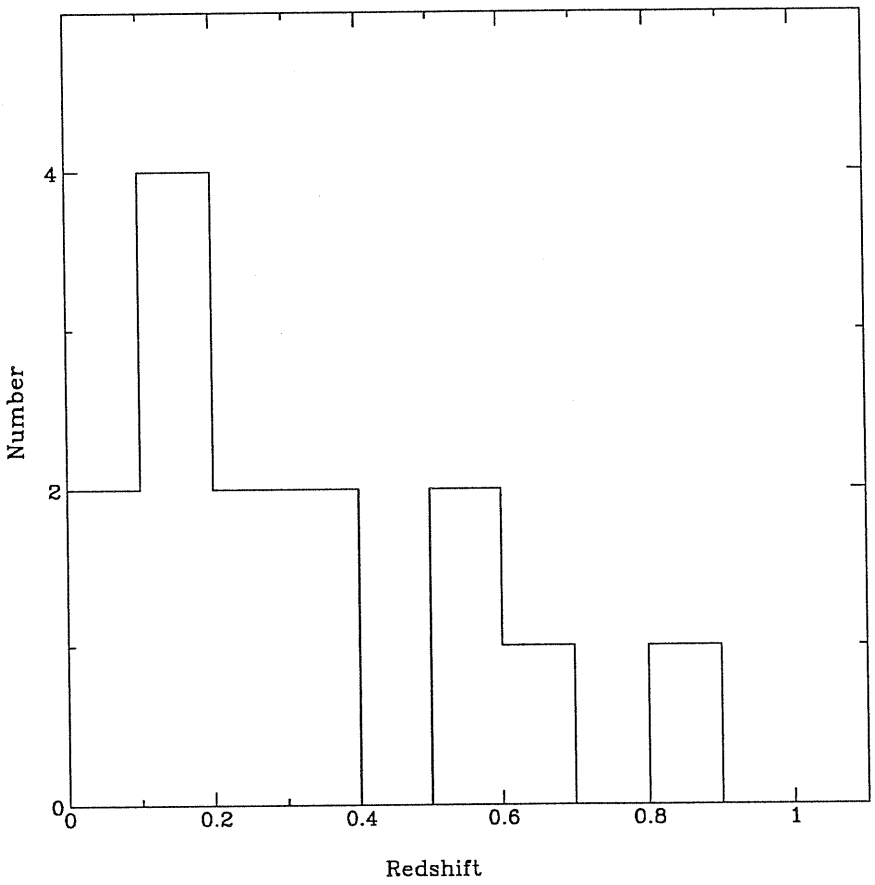

Figure 4.1: The sample redshift distribution.

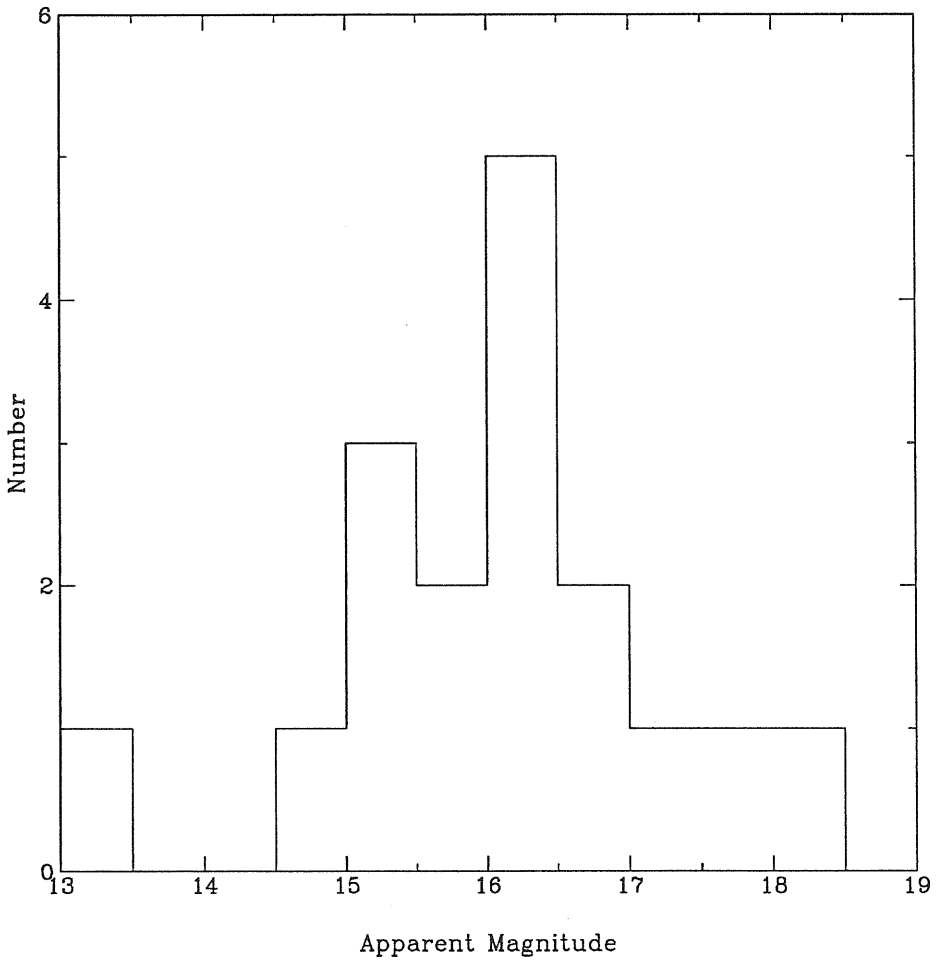

Figure 4.2: The sample apparent magnitude distribution.

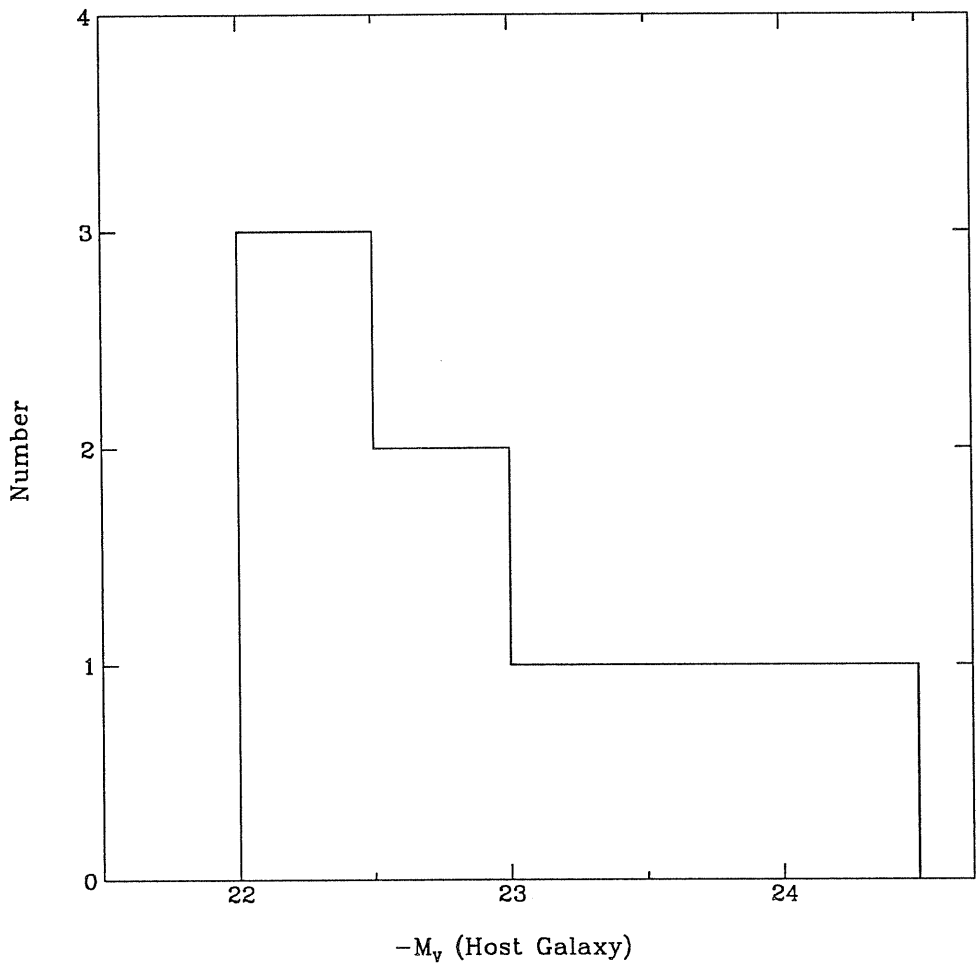

Figure 4.3: The host galaxy absolute visual magnitude distribution. The average is $\langle M_V \rangle = -22.99 \pm 0.71$.

4.2 The Instruments

Data for this thesis were obtained during observing runs on 15 – 18 February 1991 and 28 July – 1 August 1992. Observations were acquired with the 3.5m New Technology Telescope (NTT), at the European Southern Observatory (ESO) La Silla (Chile) site, equipped with the ESO Multi-Mode Instrument (EMMI; Melnick, Dekker, & D'Odorico 1992). Renato Falomo of the Osservatorio Astronomico di Padova performed the observations. General details about the telescope and instrumentation can be found in the *ESO User's Manual* (Schwartz & Melnick 1989).

We used EMMI in the Red Imaging and Low Dispersion mode (RILD) in which the instrument works as a normal focal reducer with the possibility of performing imaging and low dispersion (grism) spectroscopy. The detector employed in this mode was the THX 1024 CCD and the F/2.5 red camera, giving a pixel size of 19 μm and a useful field size of 7.5×7.5 arcmin, or 0.4397 arcsec pixel^{-1}. Observations were obtained in the Cousins B, V, R, and I filters (although not for every object). It was later found that there were problems with the few B images obtained, and, thus, these have not been used.

In addition to direct images, we obtained spectra of some galaxies in the fields of selected BL Lac objects. A long slit (2″ wide) was oriented in such a way as to secure at least two galaxies in the field at a time. Exposure times were between 30 and 40 minutes. In some cases, we also obtained the spectrum of the nebulosity surrounding the BL Lac object. For all spectra, we employed a grism of 300 gr mm^{-1} giving a dispersion of 246 Å mm^{-1} in the range 4000 to 8000 Å. Spectra were wavelength calibrated using an Helium-Argon lamp, and relative flux calibration was derived from observations of the standard star Feige 110 (Stone 1977).

In the following thesis, all images have been reduced and analyzed by the author. The spectral material has been kindly provided by Renato Falomo.

Table 4.1: Program Objects.

Coordinate Name	Other Names	R.A. (1950)	Dec (1950)	m	z [a]		Selection [b]
		h m s	° ′ ″				
(1)	(2)	(3)	(4)	(5)	(6)	(7)	(8)
0118–272	PKS, OC–230	01 18 09	–27 17 07	16.5	>0.559 a	1	R
0301–243	PKS, OE–202	03 01 16	–24 22 00	16.5	···	···	R
0414+009	1H	04 14 17	+00 58 03	16.4	0.287 g	2	X
0537–441	PKS	05 37 21	–44 06 45	15.5	0.896 e	3	R
0823+033	PKS, MG, OJ 038	08 23 14	+03 19 15	18.5	0.506 e	4	R
0829+046	PKS, OJ 049, IRASF	08 29 11	+04 39 51	16.5	0.18 g	1	R
1101–232	H, 2A 1058–226	11 01 11	–23 13 20	16.6	0.186 g	5	X
1400+162	PKS, MC3, MRC, 4C 16.39	14 00 21	+16 14 21	16.5	0.244 e	6	R
1402+042	MS 1402.3+0416, 1E	14 02 20	+04 16 22	17.1	0.200 g	7	X
1514–241	AP Lib, PKS, MRC	15 14 45	–24 11 22	15.1	0.0486 a,e	8	R
1538+149	PKS, OR 165, 4C 14.60	15 38 30	+14 57 22	16.0	0.605 e	4	R
1553+113	PG	15 53 21	+11 20 03	15.	···	···	X
1722+119	H, 4U, 1H1720+117	17 22 45	+11 54 52	15.8	···	···	X
1749+096	4C 09.57, OT 81, MRC	17 49 10	+09 39 42	16.8	0.322 e	9,13	R
2005–489	PKS, IRASF	20 05 47	–48 58 43	15.3	0.071 g	10	X
2155–304	PKS, H, 1H	21 55 58	–30 27 53	13.1	0.116 g	11	X
2335+031	PKS, OZ 061, 4C 03.59	23 35 34	+03 10 12	17.7	0.31 g	12	R

References: (1) Falomo 1991; (2) Halpern *et al.* 1991; (3) Stickel, Fried, & Kühr 1988c; (4) Stickel, Fried, & Kühr 1993; (5) Remillard *et al.* 1989; (6) Baldwin *et al.* 1977; (7) Morris *et al.* 1991; (8) Disney *et al.* 1974; (9) Stickel *et al.* 1988a; (10) Falomo *et al.* 1987; (11) Falomo, Pesce, & Treves 1993b; (12) Romanishin 1987; (13) White *et al.* 1988.

Notes:

[a] Columns 6 and 7: Redshift (a = intervening absorption system, g = galaxy = absorption from underlying galaxy, e = emission lines), and references.

[b] Selection method: R = Radio, X = X-ray, see text.

Table 4.2: Source Properties.

Object	P (%)	HG	M_V	
(1)	(2)	(3)	(4)	(5)
0118–272	17.2 (IT)	N	...	...
0301–243	10.6 (IT)	Y [a]	...	...
0414+009	2.8 (IT)	Y	–23.6	1
0537–441	14.6 (IT)	N	...	...
0823+033	18.5 (IT)	N	...	...
0829+046	...	Y	$\sim$ –22.4	2
1101–232	2.0 (JSE)	Y	–22.4	3
1400+162	...	Y	–23.3	4
1402+042	4.8 (JSE)	N	...	...
1514–241	6.9 (SFK)	Y	–22.8	5
1538+149	32.8 (SFK)	N	...	...
1553+113	...	N	...	...
1722+119	7.8 (JSE)	N	...	...
1749+096	32.0 (SFK)	Y	...	...
2005–489	2.0 (SFK)	Y	–24.3	6
2155–304	6.3 (JSE)	Y	–22.9	7
2335+031	...	Y	–22.2	8

Columns: (1) Object; (2) Polarization, from IT = Impey & Tapia (1988), JSE = Jannuzi, Smith, & Elston (1993), SFK = Stickel, Fried, & Kühr (1993). When more than one value was available, the average has been computed. All sources are variable; (3) Evidence for host galaxy. Where seen, all are ellipticals; (4) Absolute visual magnitude recalculated with $H_0 = 50$, $q_0 = 0.5$, where necessary. Values for Galactic extinction and the K correction are given after each reference, below. (5) Magnitude references.

References: (1) Falomo & Tanzi 1991, $A_V = 0.35$, K = 0.3; (2) Falomo 1991; (3) Remillard *et al.* 1989, $A_V = 0.2$; (4) Hutchings, Crampton, & Campbell, 1984, K $\sim$ 0.1; (5) Baxter, Disney, & Phillipps 1987, $A_V = 0.21$, K = 0.09; (6) Wall *et al.* (1986), $A_V \sim 0.1$, K $\sim$ 0.35; (7) Falomo *et al.* 1991; (8) Romanishin 1987, $A_V \sim 0.2$.

Notes: [a] See Falomo *et al.* (1993).

Table 4.3: Zero points and sky magnitudes.

Filter	K	Sky
(1)	(2)	(3)
V	24.47	21.6
R	24.65	20.7
I	23.73	19.5

Column 1: Filter in the Cousins system.

Column 2: Photometric zero points as determined from the field of T Phoenicis.

Column 3: Average sky magnitudes for the images.

4.3 Data Reduction

The images have been reduced using the Image Reduction and Analysis Facility (IRAF). This is a general purpose software system for the reduction and analysis of scientific data, designed at Kitt Peak National Observatory.

Data reduction followed standard procedures and was performed automatically, using the IRAF applications program CCDPROC. The reduction process consisted of calculating the image bias from the overscan region of the CCD, subtracting this bias, and trimming the image to remove the overscan regions. Bad columns were then cleaned. Sky flat fields were obtained during the runs and used to correct science frames (images) for sensitivity non-uniformity.

Each image was inspected at the end of the reduction process, and was 'cleaned' using the IRAF application program IMEDIT. During this stage, cosmetic defects such as saturated rows and columns were removed. In certain cases, some saturated stars were removed as these were found to cause problems in a later phase of the analysis.

For each object, single images were cleaned of defects due to cosmic rays using the IRAF application program COSMICRAYS. Two images in the same filter were averaged using the IRAF application program IMCOMBINE.

In the case of three or more images in the same filter, IMCOMBINE was used with the 'AVSIGCLIP' option, which automatically removes cosmic rays as well as averaging the images. Some images were not used because of defects such as satellite trails, or because of bad (> 1.8 arcsec FWHM) seeing. In general, the February 1991 observing run had relatively good seeing (1.0 – 1.2 arcsec) while it varied from 1.0 to 1.9 arcsec for the July – August 1992 run. For some objects, observations were taken both in February and in July – August. When the image quality varied in these cases, only the higher quality data were used.

Photometric calibration was obtained from observations of standard stars (Landolt 1983). In Table 4.3 we report typical NTT zero-point constants, K[1], and the average sky magnitudes determined from our images. Appendix A provides representative images for each field. We give information about the observations in Table 4.4, at the end of this chapter. Column 1 is the object name, and column 2 is the date of observation. The filters used appear in column 3 along with the number of frames per filter, the exposure times (in seconds) and seeing (arcsec FWHM) in columns 4, 5, and 6, respectively. The magnitude limit is listed in column 7 while the background galaxy counts, and the number of galaxies and stars detected to the magnitude limit are in columns 8 – 10. When there is more than one frame per filter, the data in columns 5 – 10 refer to the averaged frame.

Because of the removal of saturated stars and certain cleaning operations, area was lost in some images. In most cases the lost area amounted to a small fraction of a square arcmin ($\sim$ 0.1 – 0.7 arcmin^2), and has not been considered further. However, due to a number of bright stars in the field of PKS 2155–304, a total of 2.9 arcmin^2 has been removed from the image. Further analysis of this object takes the lost area into account.

4.4 Analysis Method

Because we want to determine the existence of excess galaxy counts around our program objects, the most important part of the analysis involves the classification of objects in each image as stars, galaxies, or noise. To detect and classify objects, we adopted the Faint Object Classification and Analysis Software (FOCAS), developed by Jarvis & Tyson (1981), revised and expanded

[1]Defined as $K = m_{true} - m_{inst} - 2.5 \times \log\Delta t$, where Δt is the exposure time in seconds.

by Francisco Valdes of the National Optical Astronomy Observatories. The software was used in the UNIX operating environment and as a package within IRAF

FOCAS is a set of programs for creating and manipulating catalogs of objects from digital astronomical images. The creation of a catalog is accomplished by an automatic threshold 'detector' where the threshold is measured relative to a simultaneously determined background. Manipulation of catalogs includes the separation of merged objects, the measurement of position, shape, and photometric parameters, the astronomical classification, and the display and analysis of the catalogs. While a detailed description of FOCAS is beyond the scope of this work, because of its importance in the present project, we will briefly outline some critical aspects.

In order for FOCAS to generate a catalog of objects, the catalog header must be first initialized. This involves providing the name of the image to be analyzed, its exposure time, *et cetera.* A number of parameters used in subsequent analysis must be provided as well; these are the detection threshold sigma, the minimum detection size, and the detection filter. The threshold sigma used for this project was 3.5σ above the background and 5.0σ below the background. These values should give only the detection of real objects. A minimum detection size of six pixels was employed. Objects with dimensions (including diagonals) less than this value will be excluded. Finally, the default detection filter was used. The filter could be optimized for different projects, but the default was found to give satisfactory results.

After the header is set, FOCAS first determines the background value and sigma, then all objects are detected. Evaluation of these objects follows, in which their positions, shapes, and luminosities are determined. Objects which are merged at the detection isophote are separated. Stellar objects are found, based on an analysis of their intensity-weighted moments. These are then used to define the average Point Spread Function (PSF), if this function is not given by the user.

The last step is object classification, a detailed description of which can be found in Valdes (1982). Briefly, the resolution classifier fits to each object a series of templates, derived from the image PSF by broadening to various **scales.** The scale of the best fitting template is then a measure of the degree of resolution of the object, and the classification is made from this scale value; scales near

the PSF are stars while larger resolved scales are galaxies and very large scales are diffuse sky enhancements. Other templates have a stellar component plus a broader component. The **fraction** of broad component is also used as part of the classification scheme. The resolution classifier uses the additional criterion that even if a template is not a true model of a galaxy's shape, if it is resolved (*i.e.,* does not agree with the PSF better than a broader PSF) then it cannot be a star and must be a galaxy.

After classification, an object has a *scale* and a *fraction* value. These parameters are compared to classification rules defined by the user. The classification rules used in the present analysis were optimized by experimentation and by comparison to a similar analysis by Hintzen, Romanishin, & Valdes (1991). They are:

Scale Range	Fraction Range	Object Classification
0.10 – 0.79	0.00 – 1.00	NOISE
0.80 – 1.15	0.00 – 1.00	STARS
1.16 – 6.00	0.00 – 1.00	GALAXIES
6.01 – 100.0	0.00 – 1.00	DIFFUSE NOISE

Figure 4.4 shows a typical scale versus magnitude diagram. Note the differentiation between stars and galaxies. The quantized values for scale greater than two are due to the individual templates used by FOCAS.

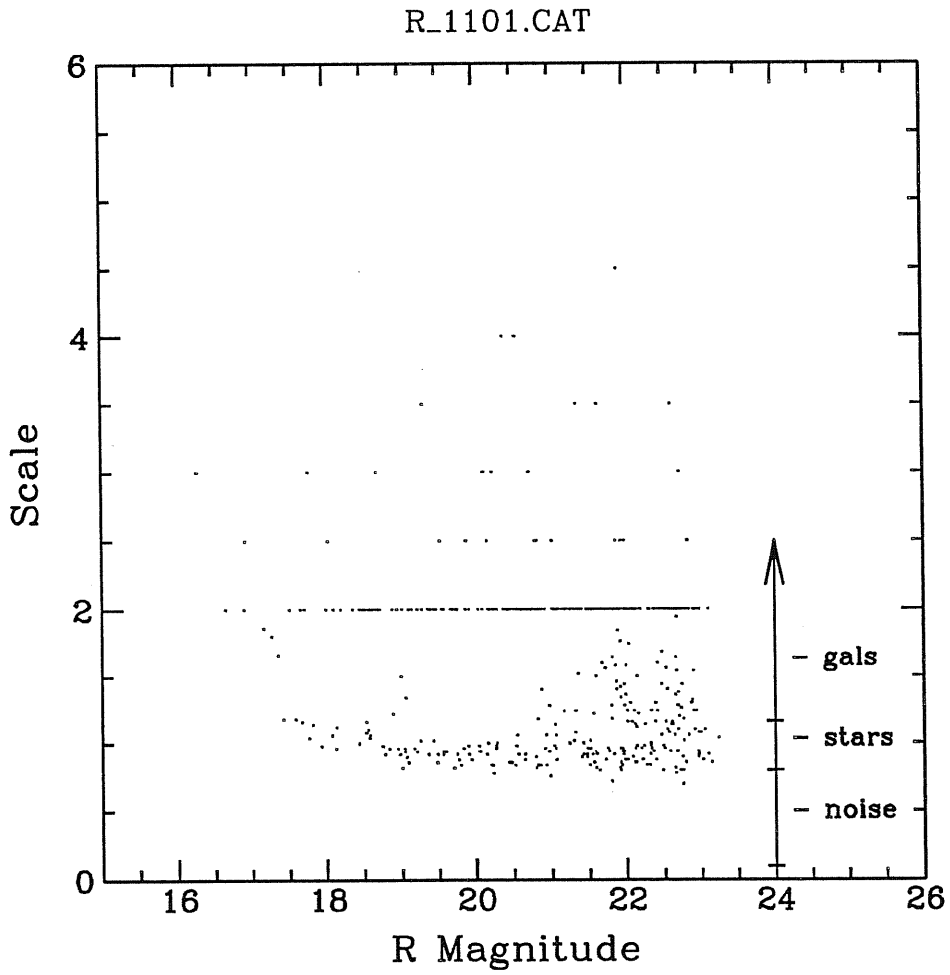

Figure 4.4: A typical Scale-Magnitude diagram, with the classification rules as given in the text. The *R*-band image of H 1101–232 is used in this example.

After running FOCAS, the user can define the output catalog, which gives information such as position, magnitude, scale and fraction values, *et cetera.* This then forms the basis for subsequent analysis.

In the initial stages, all FOCAS-classified objects were examined manually to determine the accuracy of the program. Later, only objects classified as noise and merged objects were examined, as were all objects nearby the target source. While differentiation between stars and galaxies becomes difficult at faint magnitudes, this was determined not to be a problem and almost always occurred for magnitudes fainter than the magnitude limit (see below and Table 4.4). Certain types of saturated stars also gave spurious galaxy identifications, but these were always very bright objects and hence easy to remove. However, such objects were subsequently removed from the images *before* the FOCAS analysis. Although individual cases of misclassification of stars and galaxies probably do exist, the fraction of such identifications is small (on the order of 1 – 3%), and does not affect the results of the analysis, since 95% of these objects have magnitudes fainter than the magnitude limit.

4.5 Post FOCAS Analysis

Using the output FOCAS catalogs, a SuperMongo routine was implemented to plot various diagrams used for an initial interpretation of the results. An example is presented in Appendix C. This appendix also includes a catalog and header example. Further information regarding the analysis output can be obtained by contacting the author.

We have determined the magnitude limits given in Table 4.4 in the following way. All objects classified as galaxies over the entire frame are sorted into bins of width 0.5 magnitudes. These are then used to calculate the differential magnitude counts (the total number of galaxies within each 0.5 mag bin). In turn, the counts from the individual fields are compared to the average counts (determined from 14 independent fields) of Metcalfe *et al.* (1991). Figure 4.5 shows an example of such a differential count diagram, with our data plotted as circles with error bars and those of Metcalfe *et al.* as the line. The point where our counts 'turn over' and deviate significantly from the curve of the average counts defines the faintest complete magnitude, the magnitude limit. In the case of Figure 4.5, this magnitude limit occurs at $m_R = 22.0$. The under-

counting and loss of galaxies is evident for magnitudes fainter than the limit. A comparison of this sort with average counts is possible only for the R-band images. For the other images, we determine the magnitude limit as the point where the distribution turns over.

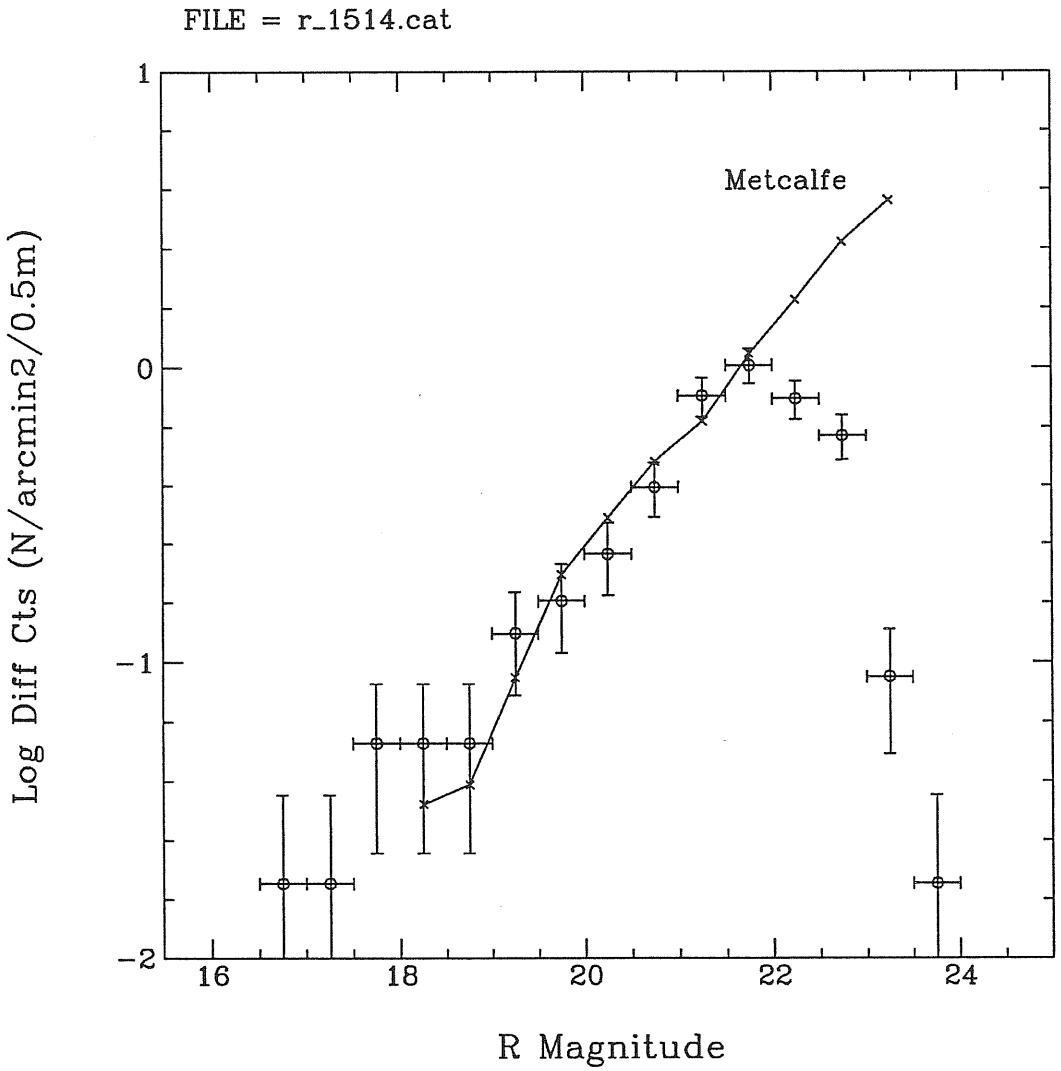

Figure 4.5: The differential galaxy count diagram, used to demonstrate how the magnitude limits are determined. The circles with error bars represent our data for the field of AP Lib (R-band), while the curve is from the average counts of Metcalfe *et al.* (1991). The point where our distribution turns over represents the magnitude limit for the frame, here $m_R = 22.0$.

An example of the differential count and the integral count diagrams is given in Appendix C. For the R and I-band images, the latter is compared to average values of Hintzen, Romanishin, & Valdes (1991).

Finally, objects are matched using a FORTRAN matching program developed for this project. An example of a matched table is provided in Appendix C. Results of matching for galaxies, and with no magnitude limits, are shown in Table 4.5, where the total number of galaxies in the V-, R-, and I-band images are given in columns 2, 3, and 4 respectively. The number of objects matched on the R- and I-band images are given in column 5, for the R- and V-band images in column 6 and for the I- and V-band in column 7. The total number of galaxies on two or more images is given in column 8.

The number of galaxies on two or more images is a conservative estimate of the real number of galaxies observed. The requirement that a galaxy be observed and classified as such on two or more images reduces the number of mis-identifications due to noise or spurious CCD defects. However, the final number is controlled by the exposure of each image and by the seeing. In the latter case, when bad, the number of misidentifications can be high (as appears to be the case for the R-band image of PKS 2005-489) or the number of detected galaxies low. Compare the case of the V-band image of PKS 1538+149 (seeing = 1.6 arcsec) with that of the R-band image (seeing = 1.1 arcsec). The number of galaxies detected on the latter is a factor of 2.5 times higher even though the exposure time is five times lower. When the seeing is the same, but the exposure times are disparate, as in the case of PKS 0823+033, the lowest exposure time will limit the number of matched galaxies. In the example highlighted, the long exposure image has over 100 more galaxies than both the short exposure image and the total number of matched galaxies. In this case, the total number of matched galaxies is an extremely conservative indicator of the true number of galaxies observed on the long exposure image.

It is interesting to note that the number of galaxies detected to the respective magnitude limits (Table 4.4, column 9) on individual frames is consistent with the number of galaxies detected on two or more frames for each object (Table 4.5, column 8).

4.5.1 Background Counts

The galaxy counts used for comparison with the values of Metcalfe *et al.* (1991) and Hintzen, Romanishin, & Valdes (1991) are determined from the entire frame. In general, our *background* counts are typically determined using galaxies beyond about 150 arcsec from the target (0.4 – 1.0 Mpc).

Our counts compare favorably with the average values from the larger studies of Metcalfe *et al.* and Jones *et al.* (1991) (see Table 5.3, the average values are given in parentheses). However, we found some cases where the background counts are lower or higher than the average values. In the analysis of individual objects we have used local background counts (and not average values, unless otherwise noted) for the following reasons.

If galaxies do not cluster it might be expected that counts from image to image and field to field will follow Poissonian statistics. This has repeatedly been shown not to be the case (Kron 1980; Jones *et al.* 1991; Metcalfe *et al.* 1991), with root-mean-square errors deviating substantially from the expected $\sqrt{N}$ errors. Large-scale galaxy clustering accounts for a significant part of these differences. A consequence of this is that variations of number counts from field to field will be relatively large. Jones *et al.* (1991) and Metcalfe *et al.* (1991) find these variations to be on the order of a factor of two.

The above indicates that an average value for the background galaxy counts may hide excess counts around *individual* objects situated in regions of lower-than-average galaxy density (and, vice versa, the average counts may enhance the excess counts in a region of abnormally high local galaxy density). In addition, the proper determination of richness depends on an accurate estimate of the true background. Thus, the conclusion drawn is that **local** background galaxy counts should be used when studying individual objects, instead of average counts.

Ideally, what is required is a large CCD covering a field around the object which is much greater (two – three times) than the typical dimension of the association (*e.g.* 1 Mpc). For the present study, the **local** background counts are defined as those determined from the same image as the target object.

Table 4.4: Imaging Data.

Object	Date	Filter	Frames	Exp (sec)	Seeing (″ FWHM)	Mag lim	Bkgd (gals arcmin^{-2})	# Objects Detected	
								Galaxies	Stars
(1)	(2)	(3)	(4)	(5)	(6)	(7)	(8)	(9)	(10)
PKS 0118–272	31JUL92	V	1	600	1.8	23.5	2.4 ± 0.3	130	43
	31JUL92	R	3	260	1.7	22.0	1.4 ± 0.2	88	33
	31JUL92	I	1	600	1.7	21.5	2.2 ± 0.3	137	36
PKS 0301–243	31JUL92	R	1	600	1.9	21.5	1.4 ± 0.2	77	32
H 0414+009	16FEB91	V	2	120	1.6	21.0	0.4 ± 0.1	32	38
	16FEB91	R	4	90	1.1	21.5	1.9 ± 0.2	119	63
	16FEB91	I	3	138	1.5	21.0	1.9 ± 0.2	123	78
PKS 0537–441	16FEB91	V	2	180	1.6	22.5	1.4 ± 0.2	85	112
	16FEB91	R	3	180	1.3	22.0	1.9 ± 0.2	112	114
	16FEB91	I	2	180	1.3	21.0	1.7 ± 0.2	103	127
PKS 0823+033	16FEB91	R	1	300	1.7	22.0	2.9 ± 0.3	200	135
	16FEB91	I	1	60	1.7	20.0	1.5 ± 0.2	103	88
PKS 0829+046	15FEB91	V	2	120	1.2	22.5	1.9 ± 0.2	107	115
	15FEB91	R	4	60	1.0	21.5	1.8 ± 0.2	108	121
	15FEB91	I	3	60	1.0	21.0	2.3 ± 0.3	137	134
H 1101–232	15FEB91	V	2	180	1.6	22.0	2.0 ± 0.2	131	89
	15FEB91	R	2	330	1.2	22.0	3.4 ± 0.3	203	103
	15FEB91	I	2	300	1.2	22.0	4.3 ± 0.4	254	159
PKS 1400+162	16FEB91	V	1	120	1.5	22.5	1.4 ± 0.2	96	65
	15FEB91	R	2	330	1.0	21.5	1.2 ± 0.2	75	45
	15FEB91	I	1	300	1.0	20.5	0.8 ± 0.2	52	40

Table 4.4 - *continued.*

Object	Date	Filter	Frames	Exp (sec)	Seeing (″ FWHM)	Mag lim	Bkgd (gals arcmin^{-2})	# Objects Detected	
								Galaxies	Stars
(1)	(2)	(3)	(4)	(5)	(6)	(7)	(8)	(9)	(10)
MS 1402+042	16FEB91	R	1	120	1.1	21.5	1.2 ± 0.2	71	66
	16FEB91	I	1	180	1.2	21.0	1.7 ± 0.2	93	77
PKS 1514–241	31JUL92	V	1	600	1.6	22.5	···	136	215
	31JUL92	R	1	600	1.5	22.0	···	165	240
PKS 1538+149	01AUG92	V	1	600	1.6	22.0	1.0 ± 0.2	70	62
	17FEB91	$R1$	1	120	1.1	22.0	3.3 ± 0.3	243	73
	17FEB91	I	1	120	1.1	20.5	2.0 ± 0.2	154	63
PG 1553+113	01AUG92	V	1	600	1.7	23.0	2.4 ± 0.3	130	104
	16FEB91	R	3	50	1.2	21.5	1.5 ± 0.2	86	110
	16FEB91	I	3	60	1.1	21.0	1.5 ± 0.2	98	113
H 1722+119	31JUL92	V	1	180	1.9	20.5	···	29	88
	31JUL92	R	1	60	2.3	100	···	33	93
1749+096	01AUG92	R	1	300	1.5	21.0	1.7 ± 0.2	88	390
PKS 2005–489	31JUL92	V	1	300	1.6	23.0	···	161	201
	31JUL92	R	1	180	1.7	22.0	···	230	150
	31JUL92	I	1	180	1.6	21.0	···	196	167
PKS 2155–304	31JUL92	V	1	180	2.0	21.5	0.4 ± 0.1	36	54
	31JUL92	R	2	150	1.8	21.5	1.0 ± 0.2	80	73
	31JUL92	I	1	180	2.0	20.5	0.7 ± 0.2	57	65
PKS 2335+031	02AUG92	$R4$	1	120	1.2	22.5	3.8 ± 0.3	200	55

Columns: (1) Object; (2) Date of observation; (3) Filter (Cousins); (4) Number of frames; (5) Exposure time in seconds. Refers to the average frame if more than one; (6) Seeing, in arcsec FWHM, from stars in the field. Refers the average frame if more than one; (7) Magnitude limit, determined as explained in the text. Refers to the average frame if more than one; (8) Local galaxy background to the magnitude limit, in galaxies arcmin^{-2}. The errors are $\sqrt{N}$; (9) The number of galaxies detected to the magnitude limit; (10) The number of stars detected to the magnitude limit.

Table 4.5: Matched galaxies.

Object	V	R	I	RI	RV	IV	Total
(1)	(2)	(3)	(4)	(5)	(6)	(7)	(8)
0118–272	147	142	229	125	91	107	153
0414+009	63	193	147	125	55	54	130
0537–441	119	166	162	121	103	93	139
0823+033	...	284	149	104	...	...	104
0829+046	107	121	140	110	98	90	120
1101–232	179	314	257	225	156	147	235
1400+162	132	108	62	60	69	45	88
1402+042	...	129	128	101	...	...	101
1514–241	205	248	...	...	131	...	131
1538+149	98	257	235	181	70	71	188
1553+113	177	104	102	76	80	69	97
1722+119	34	33	...	...	18	...	18
2005–489	221	369	289	203	163	145	272
2155–304	44	93	67	57	43	41	61

Column descriptions: (1) Object; (2) number of galaxies on the V-band image (no magnitude limit); (3) number of galaxies on the R-band image (no magnitude limit); (4) number of galaxies on the R-band image (no magnitude limit); (5) Total number of galaxies matched on the R-band and I-band images; (6) Total number of galaxies matched on the R-band and V-band images; (7) Total number of galaxies matched on the I-band and V-band images; (8) Number of galaxies matched on at least two images.

CHAPTER V

Results

In this chapter we discuss the results of the analysis for individual objects. We start by using simple statistics to determine excesses of galaxies above the background. We study the radial distribution of the galaxies around the BL Lacs, and then employ more robust statistical tests to assess the significance of clustering. Only the R-band images are used because the results for the other filters are similar. For seven objects (*i.e.* H 0414+009, PKS 0829+046, H 1101–232, PKS 1400+162, PKS 1514–241, PKS 2005-489, and PKS 2155–304) we will also discuss results of spectroscopy of selected galaxies in the field.

The R-band images for all of the fields are presented in Appendix A.

5.1 Analysis Methods

5.1.1 Simple Statistics

One can determine the excess of galaxies in a region of space with various means. The simplest of these is by assuming galaxies are Poisson distributed randomly. Counting galaxies and then comparing these counts with the expected values will give a very rough idea of whether or not an excess of galaxies above the background (the normal distribution) exists. This process can be performed in two ways. The first involves counting the total number of galaxies in the images and determining the total image area. A subset of the area will then have some fraction of the total area, and, in the Poissonian assumption, will contain the same fraction of galaxies. The probability of an excess can be easily calculated.

The results of this analysis for the R-band images are presented in Table 5.1, which gives the number of galaxies to the magnitude limit used,

within 0.5 Mpc of the target object. For the objects with unknown redshift we have calculated the excess galaxies over the whole frame. The area of the 0.5 Mpc radius is listed as is the expected number of galaxies, and the significance of the excess (given as the probability that the excess is due to background fluctuations). Expected galaxies counts are computed with the local background values, given in Chapter IV, Table 4.4 and below in Table 5.3. In all cases, whether saturated or not, the target has been included as a galaxy. We use H_0 = 50 km s^{-1} Mpc^{-1} and $q_0 = 0.5$ throughout this work.

As can be seen, in many cases there is a significant excess of galaxies within 0.5 Mpc of the BL Lac. Note that this is only proof of the existence of clustering, not of physical association with the BL Lac. For those objects with no significant excess, we are unable to determine if this is an intrinsic property. In these cases, the results are most likely affected by poor seeing (*e.g.* PKS 0301–243, for which the redshift is unknown as well), or because the images are not deep enough (*e.g.* PKS 0829+046, MS 1402+042, PKS 1514–241, 1749+096).

Counts of galaxies in annular areas of increasing radius, r, with constant width, Δr, have been determined for all fields. These are shown for each object (in the R-band), below. The distributions in the other bands are given in Appendix B. For these figures, the dotted lines represent background counts determined from galaxies beyond 150 arcsec from the BL Lac object. The arrow marks the location of the 0.5 Mpc radius.

5.1.2 Cluster Richness

We have employed the method of Abell (1958) in order to calculate the Abell Richness. This parameter is defined as the number, N_R, of galaxies within 3 Mpc of the cluster center and with magnitudes within the range $m \leq m_3 + 2$, where m_3 is the third-ranked cluster galaxy.

Instead of the 3 Mpc radius, which is outside our images, we have determined the number of *excess* galaxies within 0.5 Mpc, $N_{0.5}$. Bahcall (1981) has determined an empirical relation between $N_{0.5}$ and N_R. This takes the form $N_R = 3.3 \times N_{0.5}$. Table 5.2 gives the mean values of $N_{0.5}$ for 23 Abell clusters of Richness class 0, 1, and 2 corrected for richness effects (Bahcall 1981). We also provide the values of N_R for the three classes.

The 0.5 Mpc radius for each object is given in Table 5.3. This table also reports the R magnitude limit, the background to that limit, the value of m_3,

Table 5.1: Excess galaxies in the R- band Images.

Object	Galaxies Observed	$A_{0.5Mpc}$ (arcmin^2)	Galaxies Expected	P (%)
(1)	(2)	(3)	(4)	(5)
0118–272	11	3.95	5.5 ± 2.4	2
0301–243	77	56.25 [a]	78.8 ± 8.9	... [b]
...	11	3.14	4.4 ± 2.1	0.3 [c]
0414+009	28	7.60	14.4 ± 3.8	1.2
0537–441	12	3.09	5.9 ± 2.4	1.2
0823+033	22	4.26	12.4 ± 3.5	0.7
0829+046	32	14.23	25.6 ± 5.1	... [d]
1101–232	63	13.57	46.1 ± 6.8	1.2
1400+162	18	9.32	11.2 ± 3.3	3.6
1402+042	16	12.23	14.7 ± 3.8	... [d]
1514–241	41	56.25 [a]	39.9 ± 6.3 [f]	... [b]
1538+149	19	3.74	12.3 ± 3.5	5.7
...	243	56.25	185.6 ± 13.6	$\ll 0.1$ [e]
1553+113	86	56.25 [a]	101.3 ± 10.1	... [d]
1749+096	14	6.63	11.3 ± 3.4	... [d]
2005–489	120	56.25 [a]	68.6 ± 8.3 [g]	$\ll 0.1$
2155–304	58	28.13	28.1 ± 5.3	$\ll 0.1$
2335+031	28	6.93	26.3 ± 5.1	...

Column descriptions: (1) Object; (2) Observed number of galaxies (on the R-band image, within 0.5 Mpc of the target, and to the magnitude limit of the frame); (3) Area of the 0.5 Mpc radius, in arcmin^2; (4) Expected number of galaxies within 0.5 Mpc, calculated using the local background. Errors are $\sqrt{N}$; (5) Probability that the excess of galaxies above the background is due only to background fluctuations. Poissonian statistics are assumed. The ellipses imply no statistical significance.

Notes: (a) The entire frame has been used, either because the redshift is unknown or because the redshift is too low; (b) Counts are probably affected by poor seeing; (c) For PKS 0301–243: counts within 1 arcmin; (d) The image probably is not deep enough; (e) For PKS 1538+149: counts on the full frame; (f) for a magnitude limit of 20.5; (g) for a magnitude limit of 21.0.

Table 5.2: Richness - $N_{0.5}$ Calibration.

Richness	$\langle N_{0.5} \rangle$	σ	N_R
0	12	3	30 - 49
1	20	5	50 - 79
2	32	8	80 - 129

and the value of $N_{0.5}$ for each object. We note that the value of $N_{0.5}$ determined as above may be underestimated for several reasons: 1.) contamination by foreground galaxies, and 2.) $m_3 + 2$ can be lower than the magnitude limit of the frame, in which case the richness was calculated for galaxies with magnitudes up to the magnitude limit only.

5.1.3 The Angular Correlation Amplitude

An alternative, more robust method of determining the existence and significance of galaxy clustering is by way of the angular correlation function. The correlation function (Peebles 1980) is one of the best statistical tools to measure quantitatively the clustering of objects in a sample, providing both clustering strength and extent. Let us assume galaxy counts have been made over a portion of the sky (to some limiting apparent magnitude, $m_{\rm lim}$). Their apparent distribution in the sky, around any particular point, i, can be described by the *angular correlation function*, $\omega(\theta)$, defined by (Seldner & Peebles 1978)

$$n(\theta)\,\mathrm{d}\Omega = N_{\rm b}\,[1 + \omega(\theta)]\mathrm{d}\Omega\,, \tag{5.1}$$

where $n(\theta)d\Omega$ is the number of galaxies lying in the solid angle $d\Omega$ at angular distance θ from the reference point i, and $N_{\rm b}$ is the mean surface density of galaxies. The function $\omega(\theta)$ may be interpreted as the excess probability of finding a galaxy at distance θ from the reference object i with respect to a uniform Poisson distribution. In this last case, $\omega(\theta) \equiv 0$. If $\omega(\theta) > 0$ then the positions of galaxies are correlated and anti-correlated if $-1 \leq \omega(\theta) < 0$. In other words, the function $\omega(\theta)$ describes the 'strength' of clustering in the sky.

The two-point galaxy angular correlation function is described by a power law

$$\omega(\theta) = A\,\theta^{1-\gamma}\,, \tag{5.2}$$

where $\gamma \simeq 1.77$, consistent with estimates made from a number of catalogs (*cf.* Groth & Peebles 1977 and references therein. See also Tyson 1986 and Yee & Green 1987). Prestage & Peacock (1988) find that errors introduced if the correct value of γ is not 1.77 are negligible, provided $\gamma \simeq 2$. The value A is referred to as the *angular correlation amplitude* and is a measure of the amplitude of the average enhancement of the number of galaxies about a particular point in the sky.

The expected number of neighbors within distance θ of the object i may be obtained by integrating equation (5.1). Thus,

$$\int_0^\theta n(\theta')\,\mathrm{d}\Omega = N_\mathrm{b} \int_0^\theta [1+\omega(\theta')]\,\mathrm{d}\Omega\,, \tag{5.3}$$

or, by defining N as the mean number density of neighbors,

$$N\,\frac{\theta^2}{2} = N_\mathrm{b} \int_0^\theta \theta'\,\mathrm{d}\theta' + N_\mathrm{b} \int_0^\theta \omega(\theta')\,\theta'\,\mathrm{d}\theta'\,, \tag{5.4}$$

where we have used the small angle approximation. The first term on the R.H.S. of equation (5.4) is simply the total number of background galaxies, while the second term describes the excess galaxies above the background, within radius θ and assuming a Poissonian distribution.

Replacing $\omega(\theta)$ with the form in equation (5.2) we can obtain the amplitude, A

$$N\,\frac{\theta^2}{2} = N_\mathrm{b} \int_0^\theta \theta'\,\mathrm{d}\theta' + N_\mathrm{b} \int_0^\theta A\,\theta'^{2-\gamma}\,\mathrm{d}\theta'$$

and

$$\frac{\theta^2}{2}\,N = N_\mathrm{b} \left\{ \frac{\theta^2}{2} + \frac{A}{3-\gamma}\theta^{3-\gamma} \right\}\,,$$

thus

$$A_\mathrm{gBL} = \frac{N - N_\mathrm{b}}{\frac{2}{3-\gamma} N_\mathrm{b}\,\theta^{1-\gamma}}\,.$$

Or, explicitly with $\gamma = 1.77$, we have

$$A_\mathrm{gBL} = 0.62\,\frac{N_\mathrm{obs} - N_\mathrm{bc}}{N_\mathrm{b}}\,\theta^{0.77}\,, \tag{5.5}$$

where N_obs and N_bc are the total counts observed on the source frame and the observed background counts (within a circle of radius θ, in degrees). We have introduced the notation, A_gBL to signify the angular correlation amplitude

between BL Lacertae objects and galaxies. This value is essentially the excess of galaxies associated with each source, with an extra factor to account for the fact that galaxies are correlated with each other on the sky. As can be seen, $A_{\rm gBL}$ is model independent and is based directly on the observed data.

The errors on $A_{\rm gBL}$ can be calculated assuming Poisson statistics. Following Yates, Miller, & Peacock (1989), the error on the number of objects assumed to be associated with the BL Lac ($N_{\rm obs} - N_{\rm bc}$) is $\sqrt{2}\sqrt{N_{\rm bc}}$. Of course the real errors are not Poissonian. In particular we might worry about intercepting a foreground or background cluster along the line of sight. Yates, Miller, & Peacock argue that this should be a minor effect, and in any case, our background counts have an equal chance of being contaminated as well. Such contamination would lead to large, negative values of $A_{\rm gBL}$, which we do not observe.

5.1.4 Evaluating the Amplitudes

We now proceed with the method suggested by Hartwick & Schade (1990) to enable us to better compare $A_{\rm gBL}$ to other studies. Normalizing $A_{\rm gBL}$ to $A_{\rm gg}$, the galaxy-galaxy auto-correlation amplitude, allows for differing background galaxy counts. Based on the correlation analysis results for deep galaxy samples of Stevenson *et al.* (1985), Hartwick & Schade (1990) find

$$\log A_{\rm gg} = -0.7 \log n - 2.39\,, \tag{5.6}$$

where n is the background galaxy counts ($N_{\rm b}$ in our notation) in galaxies per square arcmin. These values are discussed at length in Chapter VI. They are calculated for a radius of 0.5 Mpc, except for the cases of PKS 1514–241 and PKS 2005–489.

5.2 Individual Objects

5.2.1 PKS 0118–272

Falomo (1991) determined the redshift of $z = 0.559$ for PKS 0118–272 based on an absorption feature identified as the Mg II λ 2800 Å doublet. This object was previously noted (Falomo, Melnick, & Tanzi 1990) to be surrounded

Table 5.3: R-band Imaging results.

Object (1)	z (2)	$R_{\rm lim}$ (3)	Bkgd (4)	$r_{0.5Mpc}$ (5)	m_3 (6)	$N_{0.5}$ (7)
0118–272	>0.559	22.0	1.4±0.2 (2.9)	67.3	21.07	5.5 [a]
0414+009	0.287	21.5	1.9±0.2 (1.9)	93.3	19.23	13.0
0537–441	0.896	22.0	1.9±0.2 (2.9)	59.5	19.39	2.3 [g]
0823+033	0.506	22.0	2.9±0.3 (2.9)	69.9	17.35	9.2 [b]
0829+046	0.18	21.5	1.8±0.2 (1.8)	127.7	18.49	8.5
1101–232	0.186	22.0	3.4±0.3 (2.9)	124.7	18.78	4.3 [f]
1400+162	0.244	21.5	1.2±0.2 (1.8)	103.3	19.61	6.8 [a]
1402+042	0.200	21.5	1.2±0.2 (1.8)	118.4	20.08	1.3 [a]
1514–241	0.0486	22.0	... (2.9)	384.3	...	... [c]
1538+149 [d]	0.605	22.0	3.3±0.3 (2.9)	65.5	19.76	8.3 [f]
1749+096	0.322	21.0	1.7±0.2 (1.2)	87.2	18.63	3.7 [f]
2005–489	0.071	22.0	... (2.9)	273.0	...	... [c]
2155–304	0.116	21.5	1.0±0.2 (1.8)	179.6	17.43	7.2 [e]
2335+031	0.31	22.5	3.8±0.3 (4.6)	89.2	20.00	0.0

Column descriptions: (1) Object name; (2) Redshift; (3) Magnitude limit for R; (4) Local background (beyond 150 arcsec from object), with the average value in parenthesis. The local value is always used in the analysis. Units are galaxies arcmin^{-1}; (5) Radius of 0.5 Mpc in arcsec; (6) R-band magnitude of the 3^{rd}-ranked cluster galaxy; (7) Background corrected counts within 0.5 Mpc (richness).

Notes:

[a] For richness calculations, $m_3 + 2$ is fainter than the magnitude limit, thus the richness is calculated for $m < R_{\rm lim}$ and is underestimated.

[b] Since m_3 appears to be foreground, m_4 (= 19.16) was used. With m_3, $N_{0.5} = 2.9$.

[c] Entire field is within 0.5 Mpc.

[d] There appears to be a rich cluster 121 arcsec (0.9 Mpc) to the Southeast (assuming the same redshift as for 1538+149, the cluster richness parameter $N_{0.5} = 31$, equivalent to Abell richness class 2).

[e] Since m_3 appears to be foreground, m_4 (= 17.88) was used. With m_3, $N_{0.5} = 2.1$.

[f] $N_{0.5}$ and A_{gBL}/A_{gg} may be low due to an (anomalously) high local background.

[g] The image is probably not deep enough, and/or the redshift is too high.

by a roughly symmetrical grouping of about 15 galaxies. These authors were unable to resolve the host galaxy of the BL Lac.

Our R-band image (Figure 5.1) clearly show the galaxies surrounding the BL Lac, the nearest of which has a projected distance of only 8 arcsec (or 60 kpc at $z = 0.559$). Their average magnitude is $m_{\rm R} \sim 22$, approximately the magnitude of M^* at $z = 0.5$. There is a statistically significant excess of galaxies within 0.5 Mpc, which is clearly seen in the radial distribution (see Figure 5.2). A lower limit of $N_{0.5}$ of 5.5 in R indicates a cluster slightly poorer than Abell class 0.

The redshift of the BL Lac is derived from an absorption system, possibly associated with material in the presumed cluster (perhaps from the halo of the nearby galaxy). Further spectroscopy is needed in order to determine the association of PKS 0118–272 with the surrounding cluster.

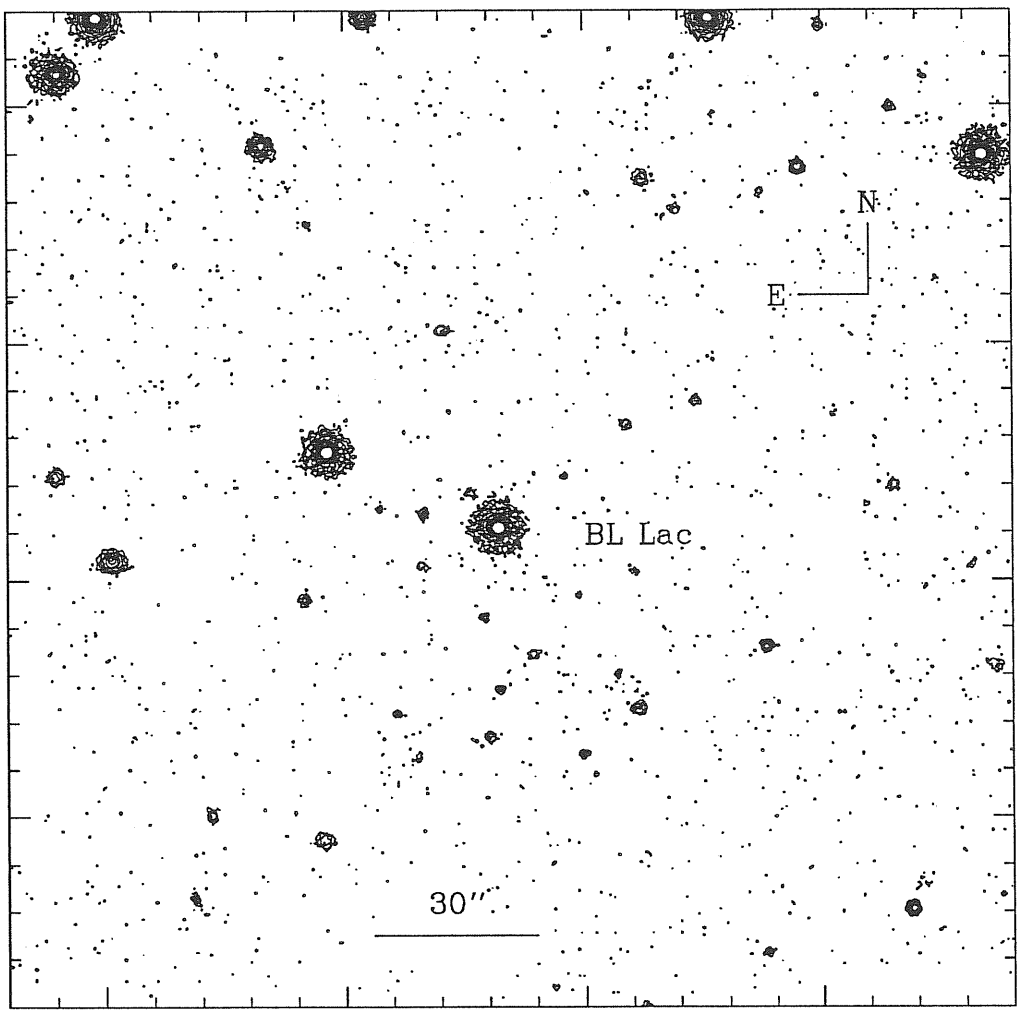

Figure 5.1: The contour plot of the R-band image of PKS 0118–272. Only the central portion is shown. Notice the numerous faint galaxies symmetrically distributed around the BL Lac object.

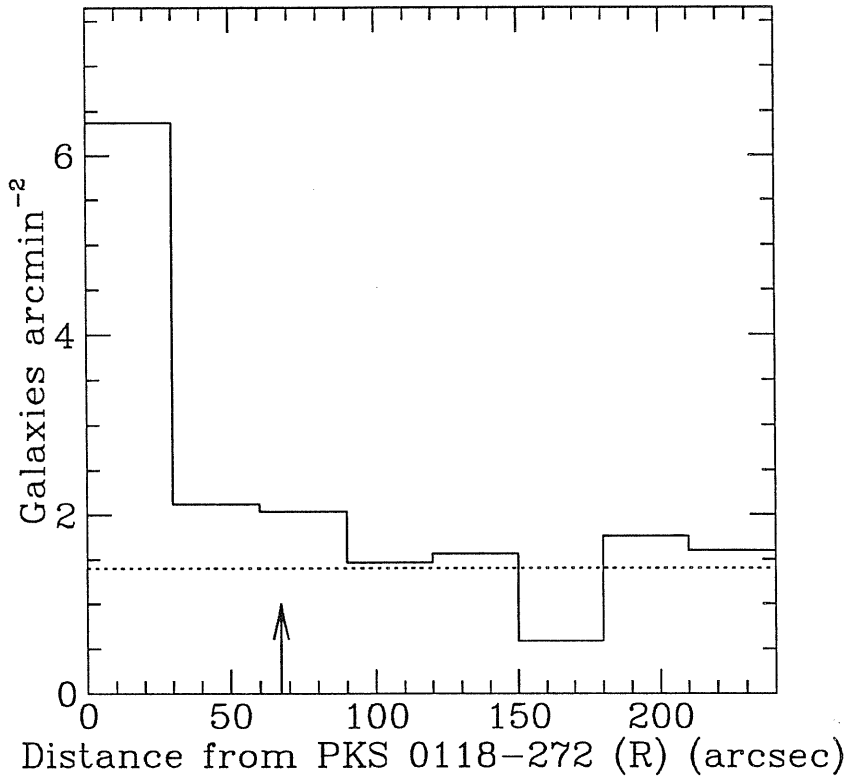

Figure 5.2: The radial distribution of galaxies around PKS 0118–272 (R band). The dashed line indicates the local background and the arrow is the 0.5 Mpc radius. The magnitude limit is 22.0.

5.2.2 PKS 0301–243

There is no measured redshift for this object. Falomo *et al.* (1993) noted that the near Infrared-to-optical region of the spectrum for PKS 0301–243 exhibits a small curvature, possibly arising from the host galaxy contribution.

Our image is affected by poor seeing (1.9 arcsec) but shows a faint object six arcsec to the Southwest of the BL Lac (see Figure 5.3). In the radial galaxy distribution (Figure 5.4), there appears to be an excess of galaxies within 60 arcsec of PKS 0301–243. This excess is statistically significant (see Table 5.1).

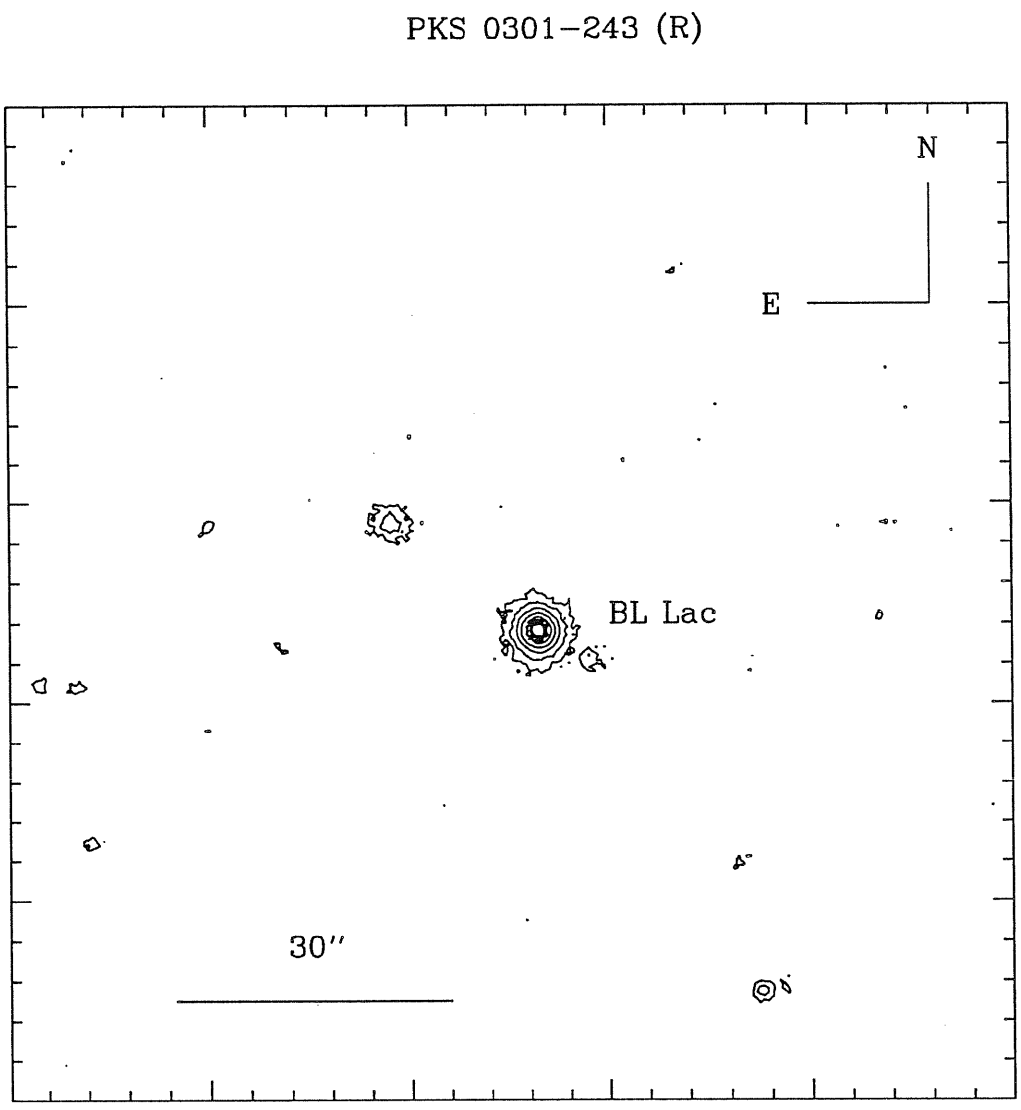

Figure 5.3: The contour plot of the R-band image of PKS 0301–243. Only the central portion is shown.

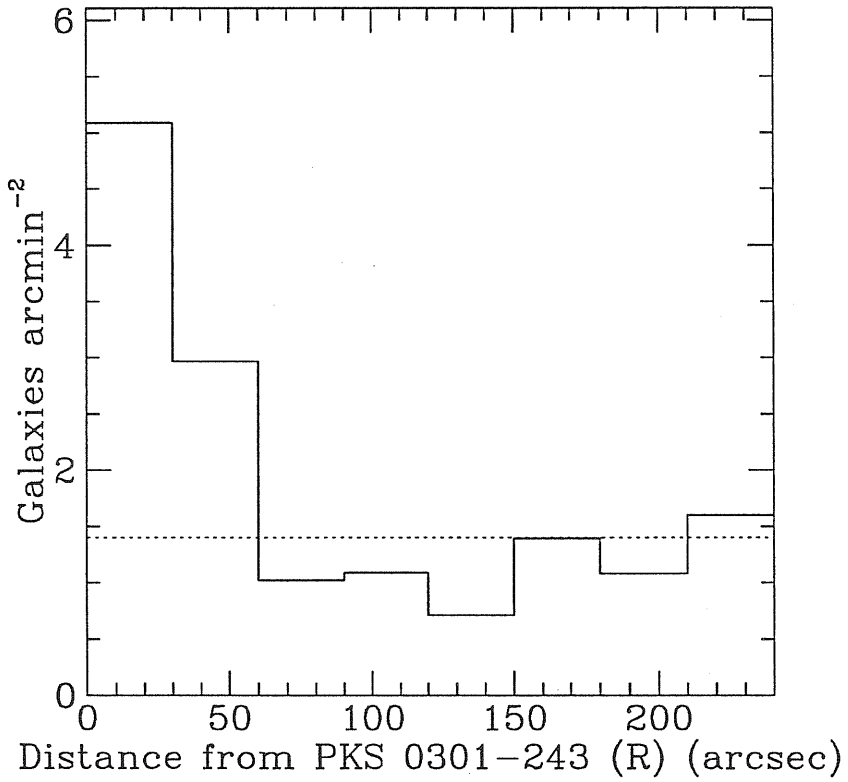

Figure 5.4: The radial distribution of galaxies around PKS 0301–243. The dashed line indicates the local background and the magnitude limit is 21.5.

5.2.3 H 0414+009

This is a moderately high redshift BL Lac ($z = 0.287$; Halpern *et al.* 1991) hosted by a luminous ($M_V \sim -23.5$) elliptical galaxy (Falomo & Tanzi 1991).[1] H 0414+009 is surrounded by many faint galaxies exhibiting a peculiar disposition (Falomo, Tanzi, & Treves 1991). The clustering of the galaxies around the object suggests that they form a loose group (see Figure 5.5).

M^{c}Hardy *et al.* (1992) recently studied the field in the radio, optical, and X-ray bands. Multicolor photometry was given for a large number of objects around the BL Lac and spectroscopy for some of the brightest sources. In addition, it was found that the radio morphology and emission of the host are typical of an F-R I radio galaxy.

Our imaging results show a significant excess of galaxies within 0.5 Mpc, clearly seen in the radial distribution profile (Figure 5.6). We calculate a richness measure of $N_{0.5} = 13.0$, or indicative of an Abell richness class 0 cluster. This is consistent with the finding of M^{c}Hardy *et al.* (1992) who used a different, more uncertain method.

Spectra have been obtained for five objects (A1, A2, B1, B2, C1), and are shown in Figure 5.7. We detected clear absorption features (mainly Ca II, Mg I) in the spectra of galaxies A1, A2, and B2 which give redshifts of 0.288, 0.289, and 0.284, respectively, with typical errors of 0.001. The spectrum of object B1 reveals that it is a red M dwarf star. For galaxy C1 the spectrum is noisy and exhibits only one certain absorption feature at $\sim$ 6255 Å which, if identified with Mg I 5175 Å, yields a redshift of 0.21.

The redshifts of A1, A2, and B2 are very similar to the redshift of the giant elliptical hosting the BL Lac ($z = 0.287$) thus confirming that they form a physical group. Moreover, the redshifts of galaxies A1 and A2 are identical within the errors, confirming that they form a physical pair, separated by only 24 kpc (and 300 km s^{-1}).

[1]This section is a summary of the full report which appears in Falomo, Pesce, & Treves (1993a).

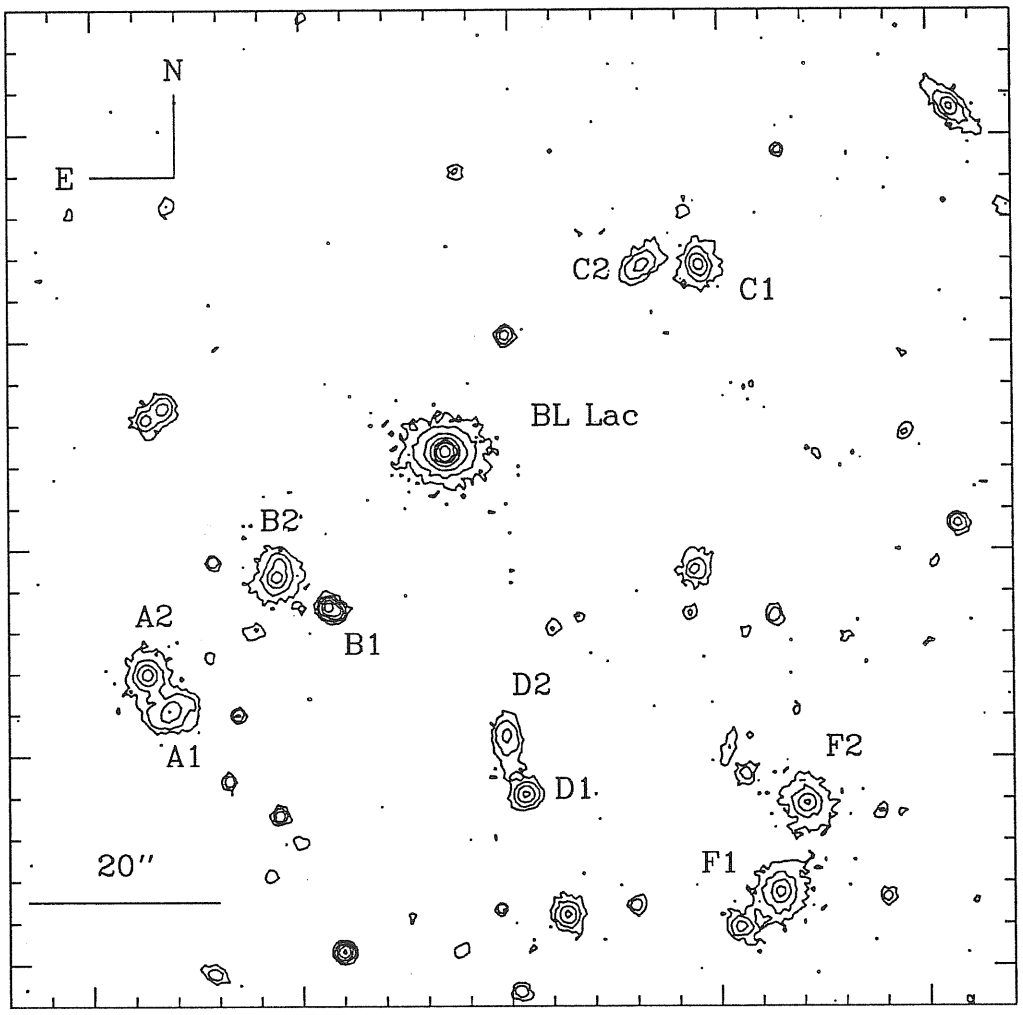

Figure 5.5: Contour plot of the central part of the field around H 0414+009 (in R). Surrounding galaxies are labelled as in Falomo, Tanzi, & Treves (1991), see text.

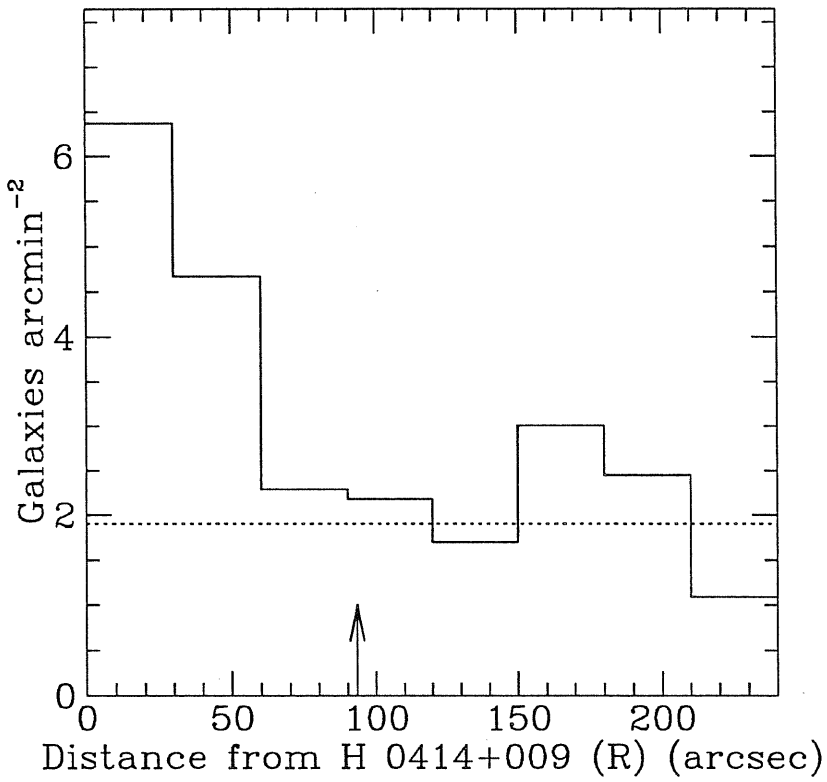

Figure 5.6: The radial distribution of galaxies around H 0414+009. The dashed line indicates the local background and the arrow is the 0.5 Mpc radius. The magnitude limit is 21.5.

M^{c}Hardy *et al.* (1992) also obtained spectra for some of the galaxies in the field. However, we found some differences for the galaxies in common with their study (A2, B2, and C1). For galaxy B2 we obtain $z = 0.284$ while they report $z = 0.287$ and, for galaxy C1, we find z = 0.21 while from their noisy spectrum they derive $z = 0.289$. Our spectrum of object A2 clearly shows galaxian absorption features at $z = 0.289$ while the spectrum of M^{c}Hardy *et al.* does not exhibit believable features.

Our spectral results confirm the imaging findings and demonstrate that at least one of the galaxy pairs is physically associated (A1/A2). While they are certainly close enough to be interacting, there is no evidence for such activity.[2] The B1/B2 pair has been shown to be due to projection effects (B1 is, in fact, a foreground star). More spectroscopic work is required to prove the reality of the other pairs in the field. The present results substantially weaken the exotic possibility of gravitational focusing by a cosmic string considered by Falomo, Tanzi, & Treves (1991).

[2]Galaxy A1 appears to be barred. If this is indeed the case the bar could be interaction induced, see *e.g.* Elmegreen, Elmegreen, & Bellin (1990).

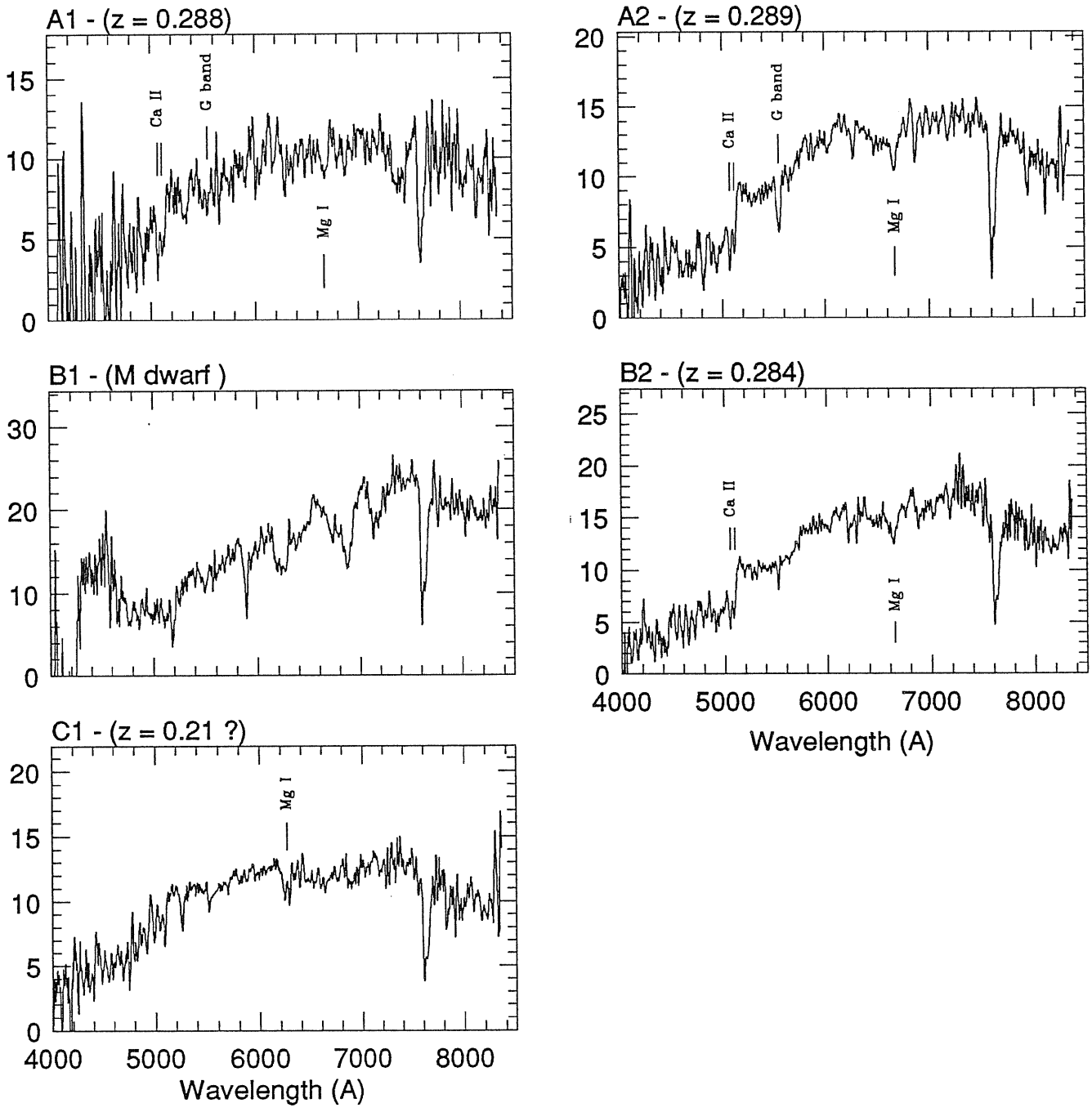

Figure 5.7: Spectra of some objects in the field of H 0414+009. Flux is in units of 10^{-17} erg cm^{-2} s^{-1} Å^{-1}.

5.2.4 PKS 0537–441

This object was classified as a BL Lac and then shown to have broad emission lines at $z = 0.894$ (Peterson *et al.* 1976), confirmed by Surdej & Swings (1981) for Mg II λ 2787 Å. PKS 0537–441 exhibits rapid and large optical variations and is one of the most luminous blazars (Impey & Neugebauer 1988).

Stickel, Fried, & Kühr (1988c) found the object to be spatially resolved despite it high redshift. This claim however was dismissed by Falomo, Melnick, & Tanzi (1992) as due to improper analysis. A thorough discussion of this point has been given above in Chapter II.

In our images, PKS 0537–441 is offset from the center to avoid a bright star (see Figure A.4). The contour plot of the region centered on the source is given in Figure 5.8. The close companion galaxies, about four to five arcsec to the Northeast and Southwest, noted by Falomo, Melnick, & Tanzi (1992) can just be seen in Figure 5.8.

Inspection of Figure 5.9 suggests an enhancement of galaxies within 0.5 Mpc and this is found to be statistically significant (Table 5.1). Our value of $N_{0.5} = 2.3$ implies a very poor cluster, or group. However, it is noted that the image is probably not deep enough to observe galaxies at $z \sim 0.9$, for which $m^* \sim 23.5$, well below our limit of 22.

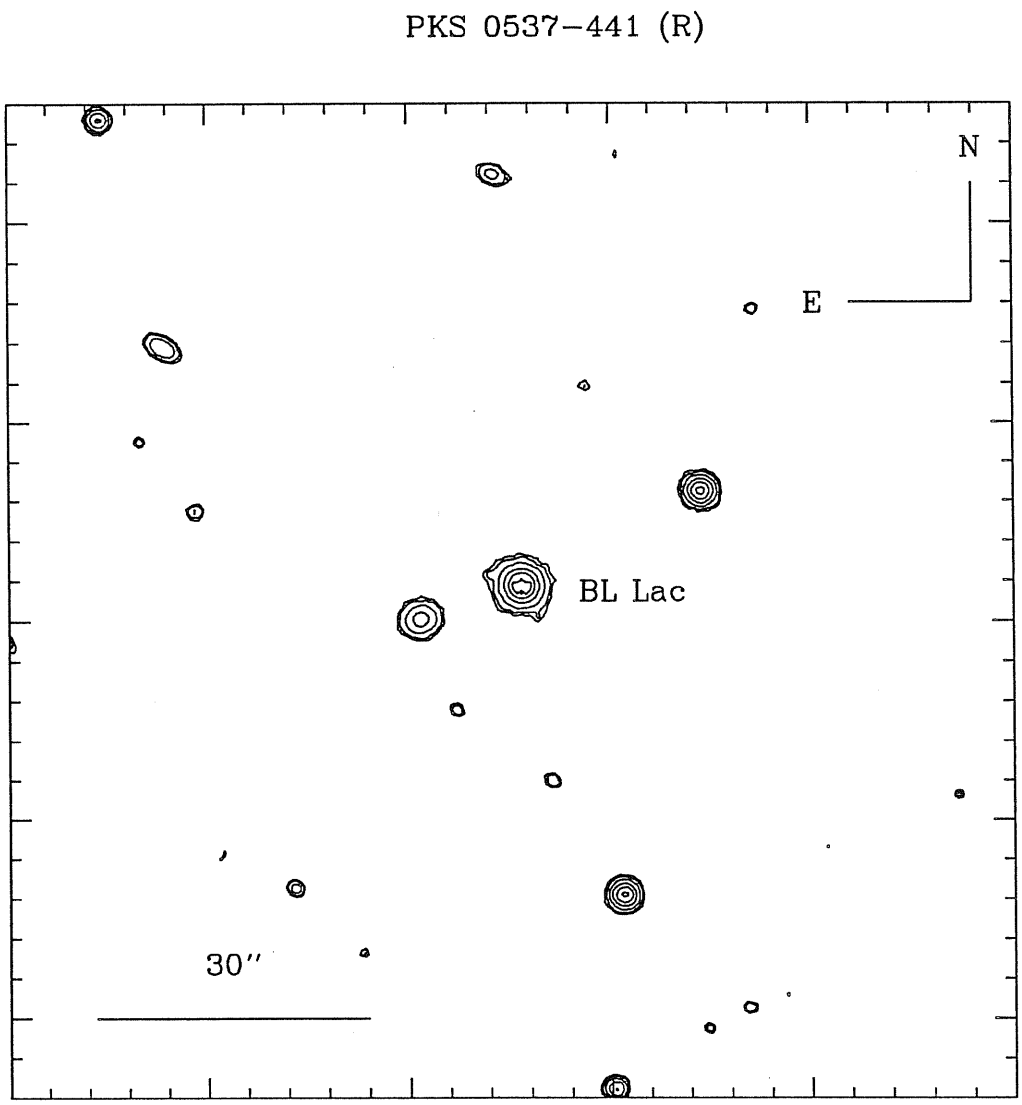

Figure 5.8: Contour plot of the central part of the field around PKS 0537–441 (in R).

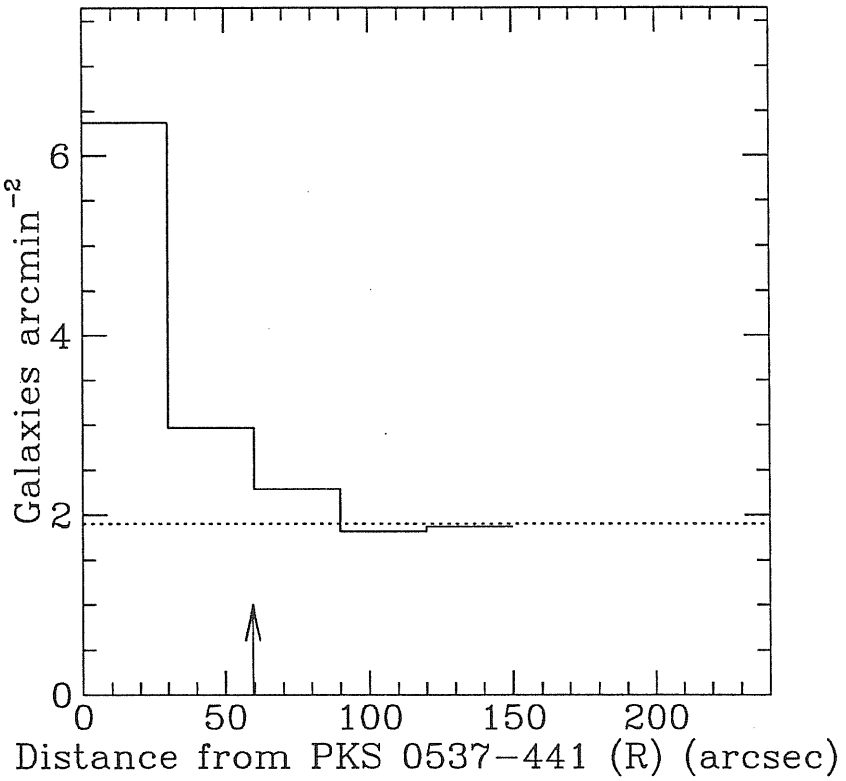

Figure 5.9: The radial distribution of galaxies around PKS 0537–441. The dashed line indicates the local background and the arrow is the 0.5 Mpc radius. The magnitude limit is 22.0.

5.2.5 PKS 0823+033

The redshift ($z = 0.506$) of this object is derived from two weak features identified with Mg II λ 2798 Å and [O II] λ 3727 Å (Stickel, Fried, & Kühr 1993), though it has not yet been confirmed. These authors obtained spectra of three galaxies in the field, none of which are associated with the BL Lac.

Our images (*cf.* Figure 5.10), while taken during relatively poor seeing, exhibit a significant enhancement of galaxies within 0.5 Mpc. This is seen in the radial distribution (Figure 5.11). The richness measure indicates a cluster of Abell richness class 0, though this may be underestimated, due to a bright magnitude limit.

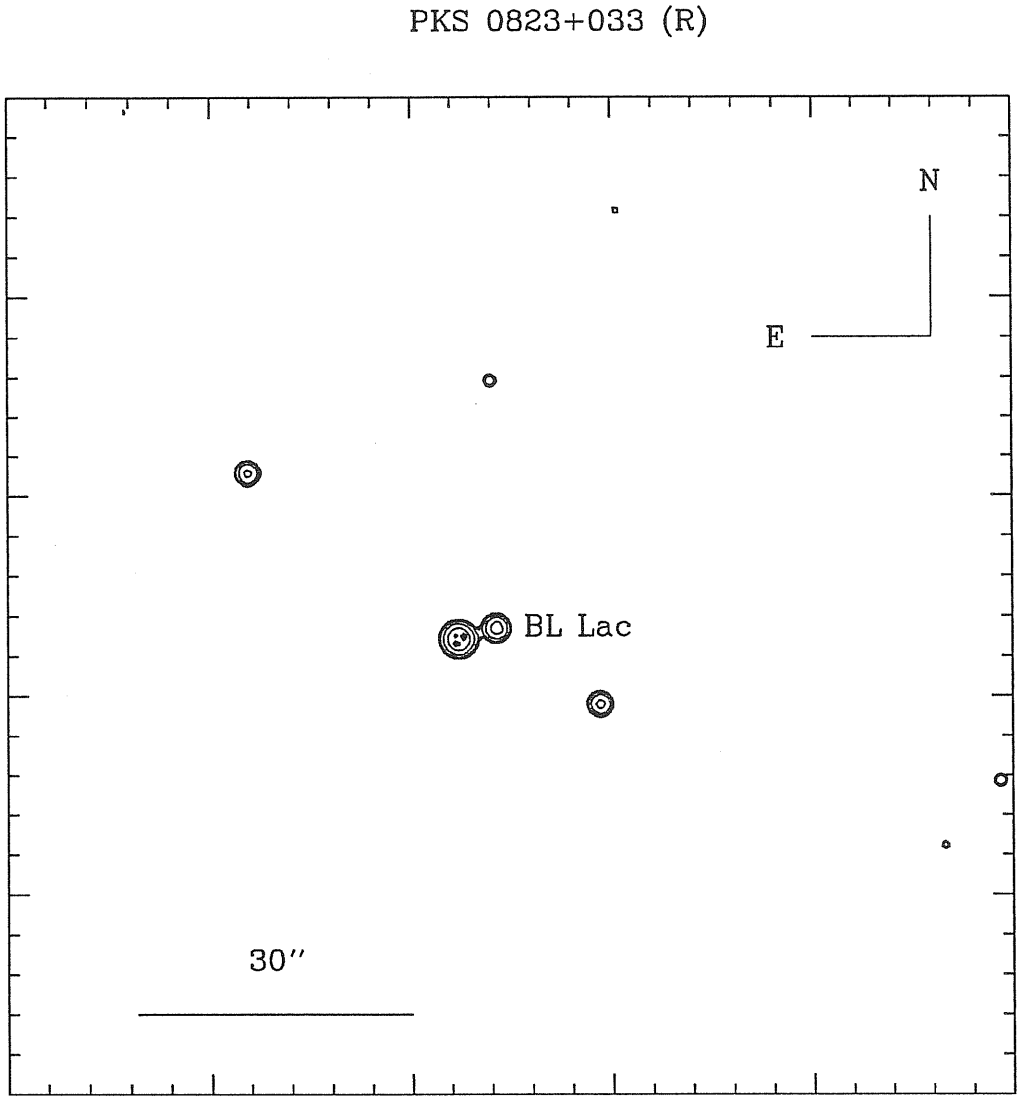

Figure 5.10: Contour plot of the central part of the field around PKS 0823+033 (in R).

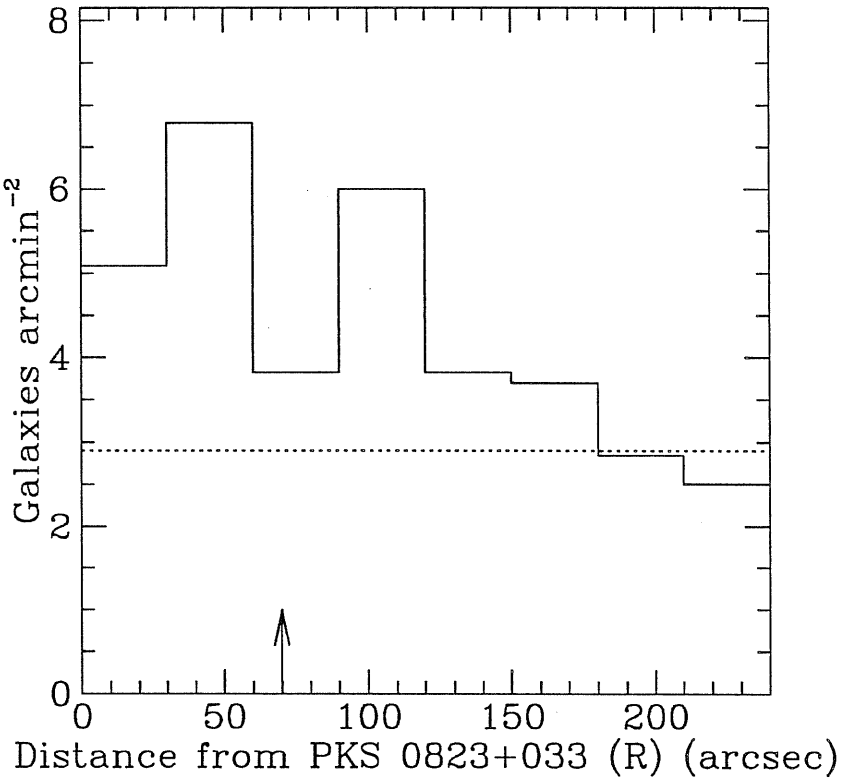

Figure 5.11: The radial distribution of galaxies around PKS 0823+033. The dashed line indicates the local background and the arrow is the 0.5 Mpc radius. The magnitude limit is 22.0.

5.2.6 PKS 0829+046

PKS 0829+046 [3] is optically very active and on the basis of broad spectral features attributed to the host galaxy, a redshift of $z = 0.18$ was proposed (Falomo 1991). The object is spatially extended and its radial brightness profile is well fitted by both a disk and an elliptical galaxy model at $z \sim 0.24$ (Abraham, M^{c}Hardy, & Crawford 1991).

Our images show PKS 0829+046 is surrounded by a number of galaxies (see Figure 5.12). A marked excess of galaxies within 60 arcsec of PKS 0829+046 is evident (see Figure 5.13), dropping to the local background beyond this radius. From this excess we derive a richness indicator $N_{0.5} = 8.5$, which may be low due to the short exposure (60 sec) and the bright magnitude limit ($R = 21.5$).

Spectra were obtained for the two nearest galaxies, G1 and G2 (5 arcsec, PA $\sim 190°$ and 27 arcsec, PA $\sim 85°$ respectively; see Figure 5.12). Galaxy G1 exhibits both absorption (Ca II, G band) and emission lines ([O III] and H_α + [N II]) at $z = 0.24$, superposed on a non-thermal continuum (see Figure 5.14, left panel). The spectrum and line ratios suggest this object is a LINER (a type of active galaxy). Absorption lines (Ca II, the G band, Mg I, and Na I) of a typical elliptical galaxy at $z = 0.204 \pm 0.001$ are seen in the spectrum of galaxy G2 (Figure 5.14, right panel).

Thus, the redshift of galaxy G2 is marginally consistent with that of PKS 0829+046 as determined by Falomo (1991), and galaxy G1 appears to be a background source. While the galaxy density suggests a clustering of galaxies around PKS 0829+046, this is not well supported by spectroscopy. Spectra of other galaxies in the field are needed to clarify this point.

[3] This object is discussed in Pesce, Falomo, & Treves (1993).

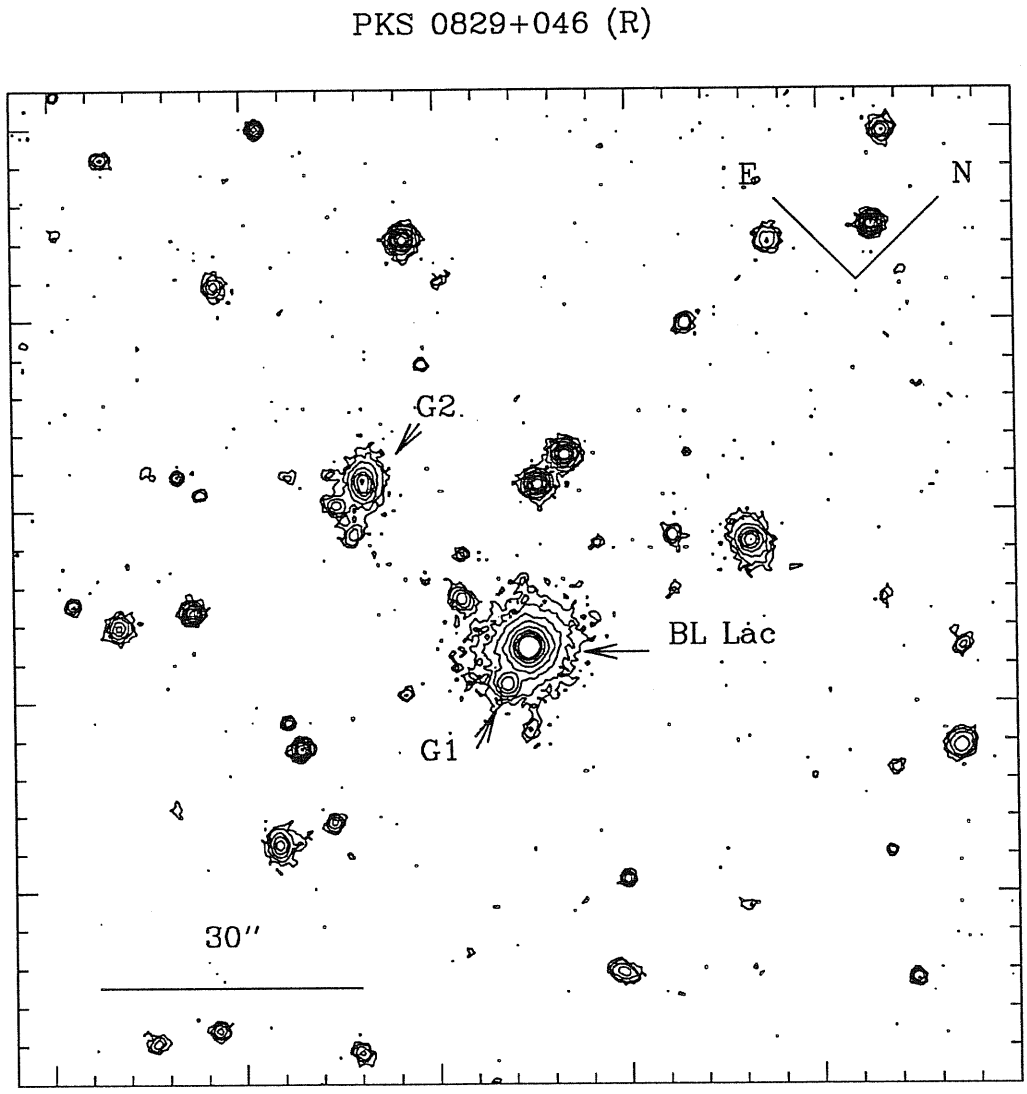

Figure 5.12: Contour plot of the central part of the field around PKS 0829+046 (in R).

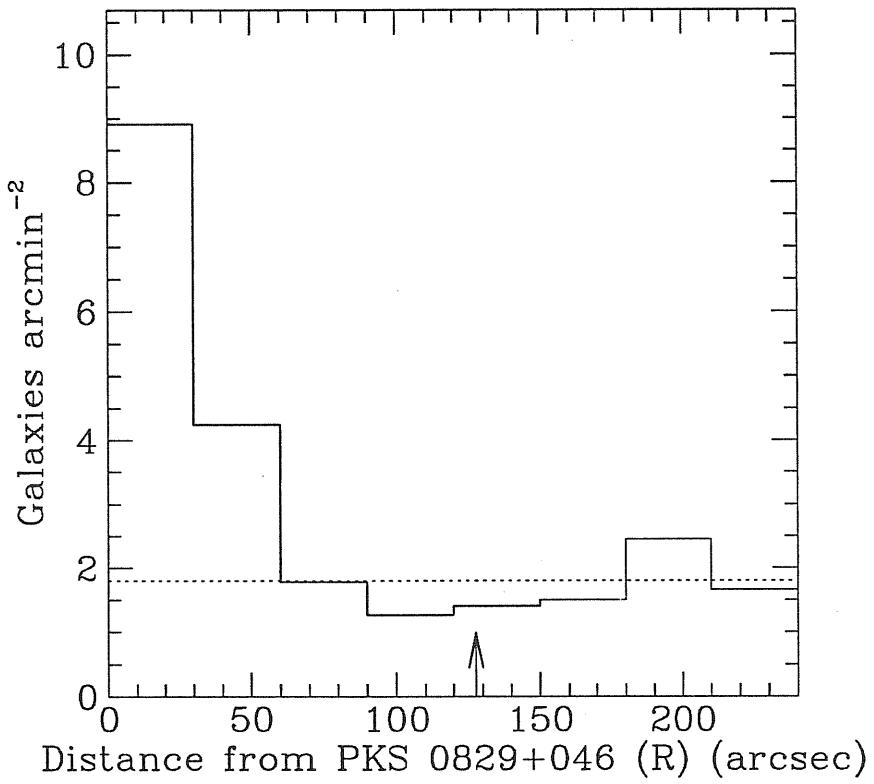

Figure 5.13: The radial distribution of galaxies around PKS 0829+046. The dashed line indicates the local background and the arrow is the 0.5 Mpc radius. The magnitude limit is 21.5.

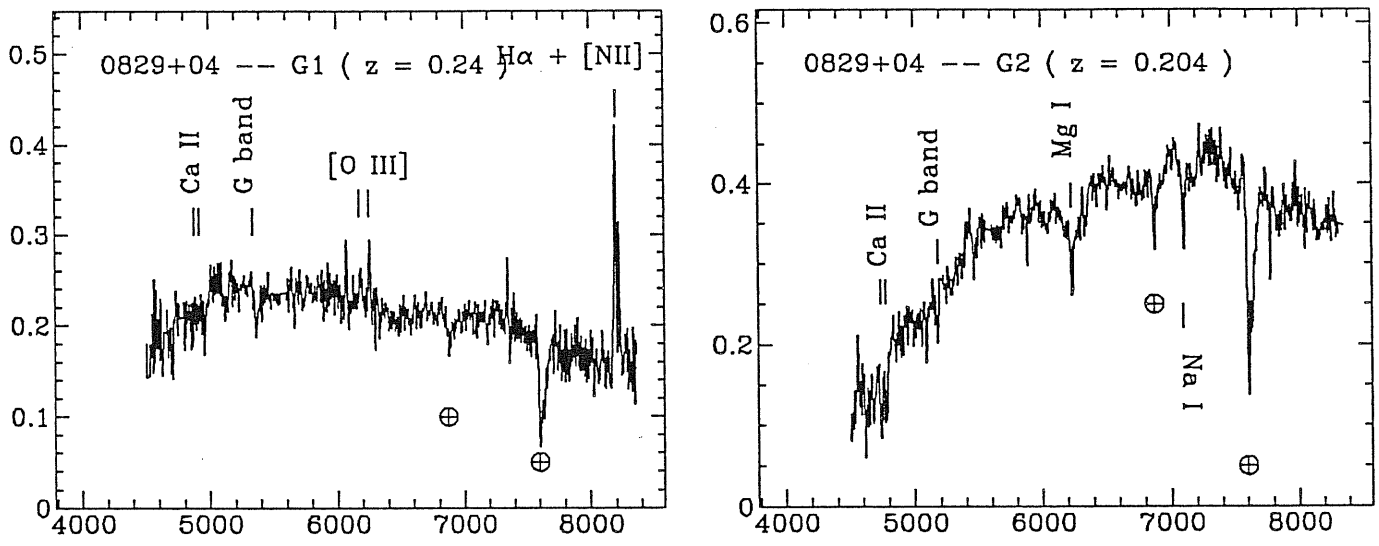

Figure 5.14: Spectra of galaxies in the field of PKS 0829+046. Flux is in relative units of ergs cm^{-2} s^{-1} $Å^{-1}$ and the abscissa is wavelength in units of Å.

5.2.7 H 1101–232

H 1101–232 [4] is surrounded by a substantial nebulosity for which Remillard *et al.* (1989) proposed $z = 0.186$, confirmed by Falomo, Scarpa, & Bersanelli (1993). The field (see Figure 5.15) is extremely rich in galaxies, especially lenticular ones, though they are not distributed symmetrically around the BL Lac (*cf.* Figure A.7). We note the local background is higher than the average (see Table 5.3), perhaps signalling a large, rich cluster associated with, or near to, the BL Lac, the existence of which our images are too small to determine properly.

The galaxy density (Figure 5.16) exhibits a peak near the object and rapidly drops to the background at 25 arcsec. A second peak between 50 and 75 arcsec is probably due to substructure. We calculate the excess of galaxies within 0.5 Mpc (125 arcsec) and determine $N_{0.5} = 4.3$. Because the local background is high and inhomogeneous, the value of the richness may be a lower limit.

We performed a surface brightness analysis of the host galaxy (see Figure 5.17) using the Numerical Mapping Package (Barbon, Benacchio, & Capaccioli 1976). From the average image in the R filter we derived isophotes down to $\mu_R = 25.7$ mag and fitted each isophote by an ellipse with free parameters. External isophotes are found to be substantially *boxy*, possibly due to activity (*e.g.* Bender *et al.* 1989). The radial brightness profile extends to 15 arcsec along the major axis (PA = 15°; ellipticity = 0.45) and can be well fitted either by a central point (modelled by the PSF) plus a $r^{1/4}$ de Vaucouleurs law, or by a central point plus an exponential disk. In both cases the total magnitude of the galaxy is $m_R = 16.4$ corresponding to $M_R = -24$, and assuming $V - R = 0.8$ yields $M_V = -23.2$. In the case of the $r^{1/4}$ decomposition we found the galaxy has $r_e = 8.5$ arcsec (34 Kpc at $z = 0.186$).

Spectra were obtained for two galaxies in the field, G1 at 104 arcsec (PA $\sim$ 225°) and G2 at 134 arcsec (PA $\sim$ 229°). The spectrum of G1 (see Figure 5.18, left) exhibits absorption due to Ca II, the G band, Mg I, and Na I at $z = 0.187 \pm 0.001$, identical to that of the BL Lac host. The projected distance is 0.4 Mpc. G2's spectrum shows emission lines ([O II], H_β, and H_α + [N II]) at $z = 0.14$ superposed onto a non-thermal continuum (see Figure 5.18, right). As for the case of PKS 0829+046 G1, this too appears to be a LINER.

[4] This object is discussed in Pesce, Falomo, & Treves (1993).

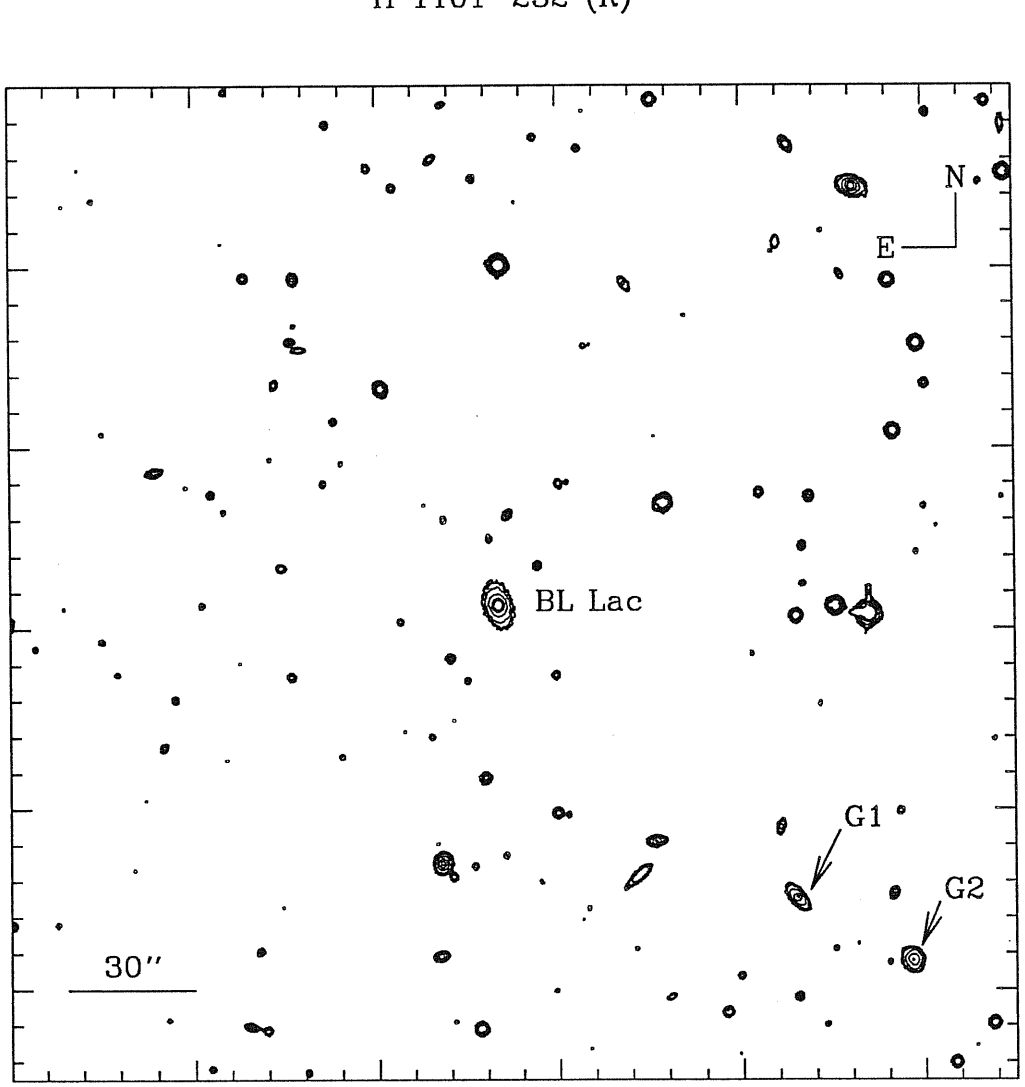

Figure 5.15: Contour plot of the central part of the field around H 1101–232 (in R).

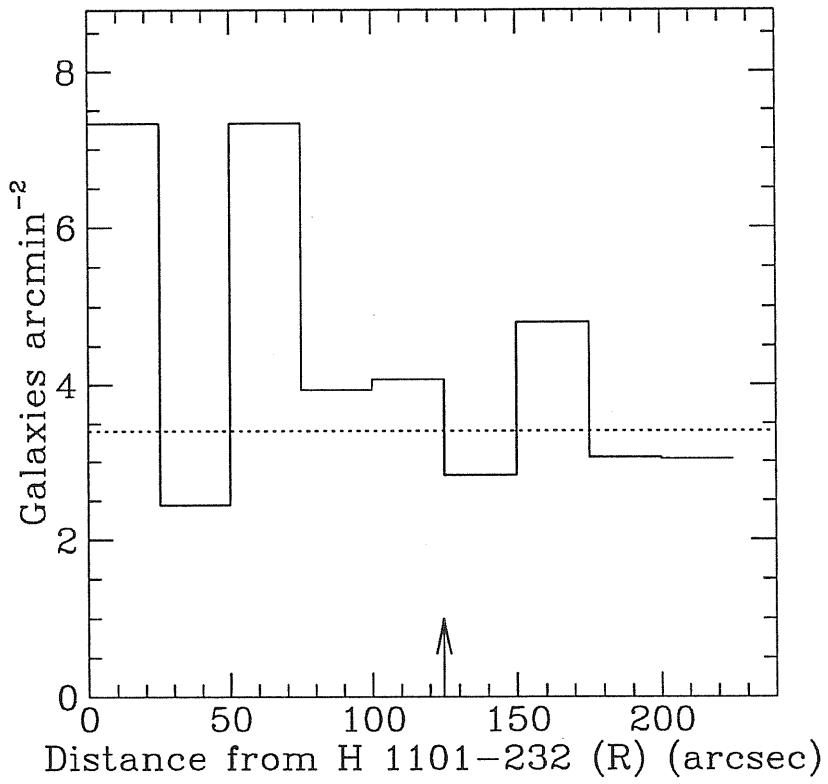

Figure 5.16: The radial distribution of galaxies around H 1101–232. The dashed line indicates the local background and the arrow is the 0.5 Mpc radius. The magnitude limit is 22.0.

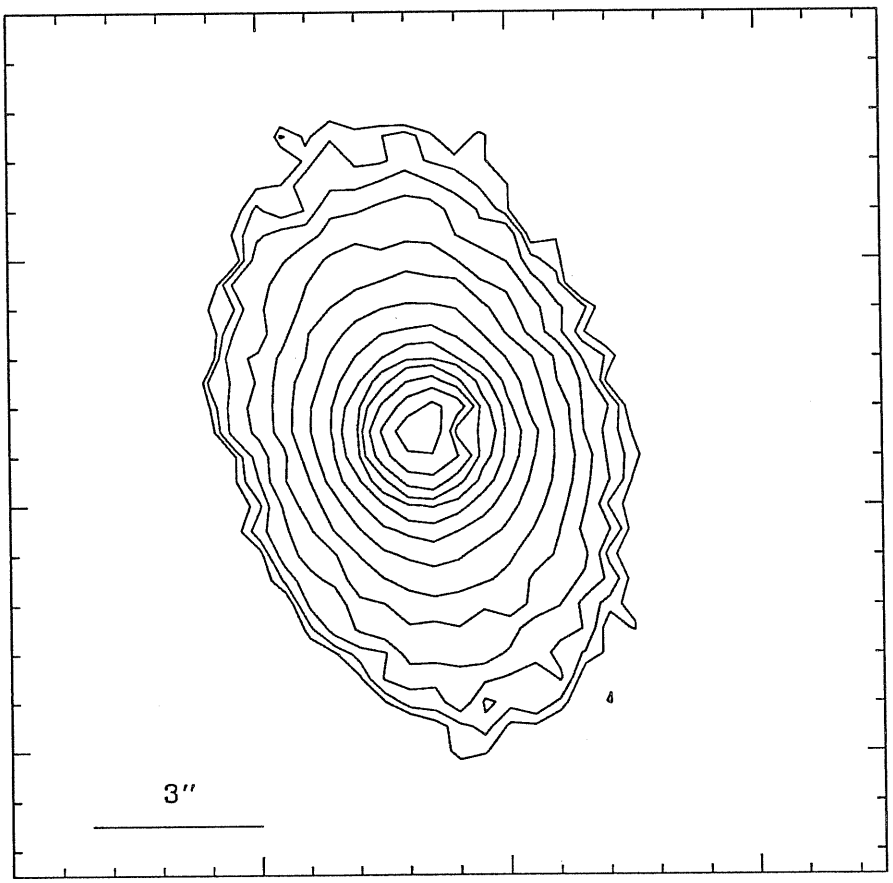

Figure 5.17: The host galaxy of H 1101–232.

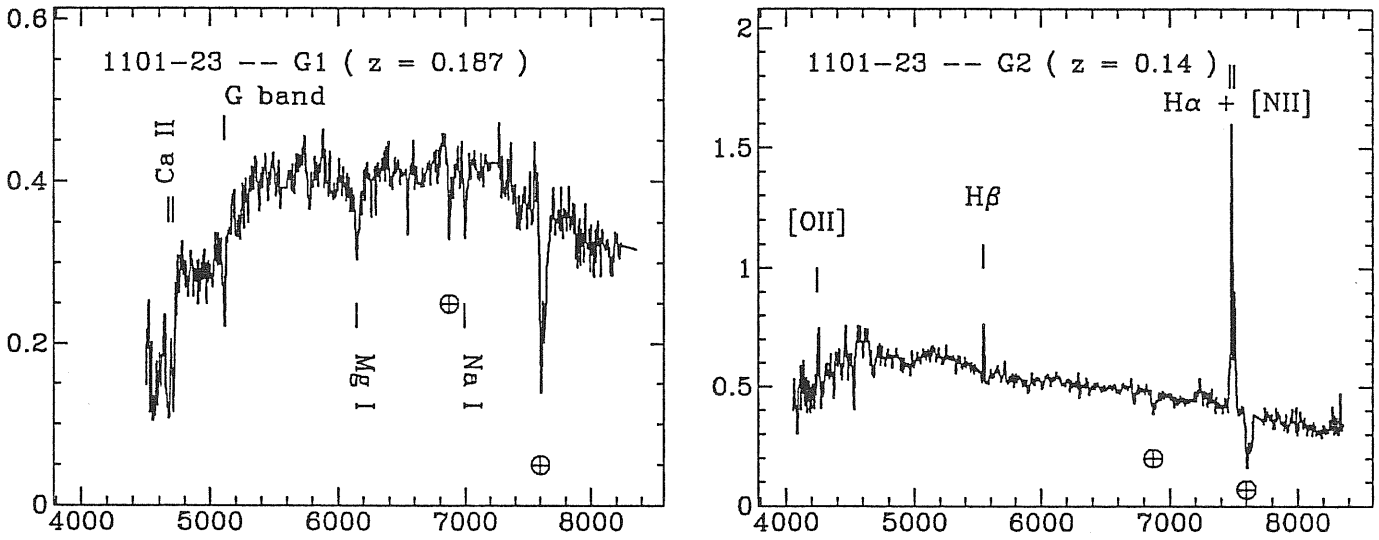

Figure 5.18: Spectra of galaxies in the field of H 1101–232. Flux is in relative units of ergs cm^{-2} s^{-1} $Å^{-1}$ and the abscissa is wavelength in units of Å.

5.2.8 PKS 1400+162

The field of this source was studied by Baldwin *et al.* (1977) who determined the redshift of the BL Lac and that of the nearest galaxy (labelled 'I' below), 6 arcsec Southwest, both as $z = 0.244$.[5] Based on statistical methods, Weistrop *et al.* (1983) found a small group, with consistent redshift, around PKS 1400+162. Later imaging studies of the BL Lac host (Hutchings *et al.* 1984; Hutchings & Neff 1992) found no evidence for interactions, even though galaxy I has a projected distance from the BL Lac of only 29 kpc.

Figure 5.19 is a contour plot of the field around the BL Lac with galaxies labelled as in Weistrop *et al.* (1983). We note that three of the nine galaxies assumed by Weistrop *et al.* (objects A, B, and G) are, in fact, stars.

The density distribution (Figure 5.20) shows a marked, significant excess of galaxies within the central 30 arcsec, dropping rapidly to the local background. We calculate a richness measure $N_{0.5} = 6.8$, but note that this is a lower limit due to the low magnitude limit.

For this field we obtained spectra of the host galaxy of PKS 1400+162 and of galaxies I = G1 (at 6 arcsec, PA $\sim 215°$) and D = G2 (at 20 arcsec, PA $\sim 35°$). The spectrum of the nebulosity of PKS 1400+162 (see Figure 5.21) clearly shows emission ([O II] λ 3727 Å and [O III] λ 5007 Å) and absorption lines (Ca II H and K) at a redshift $z = 0.244$, thus confirming the earlier value of Baldwin *et al.* (1977).

The spectrum of galaxy G1 (Figure 5.21) is very noisy, but Ca II H and K, the G band, and Mg I λ 5175 Å are present at $z = 0.224$. For galaxy G2, our spectrum (see Figure 5.21) shows a very strong [O II] λ 3727 Å line as well as [O III] λ 5007 Å in emission and Ca II H and K in absorption yielding $z = 0.230$.

Our results are clearly at odds with previous findings. We are unable to confirm the redshift of $z = 0.244$ for galaxy G1 (I). While it appears that two of the closest galaxies to PKS 1400+162 are not at the same redshift, it may be that they are members of small foreground group. Spectra of the other galaxies in the field are necessary in order to resolve this puzzle.

[5]These data are discussed in Pesce, Falomo, & Treves (1993).

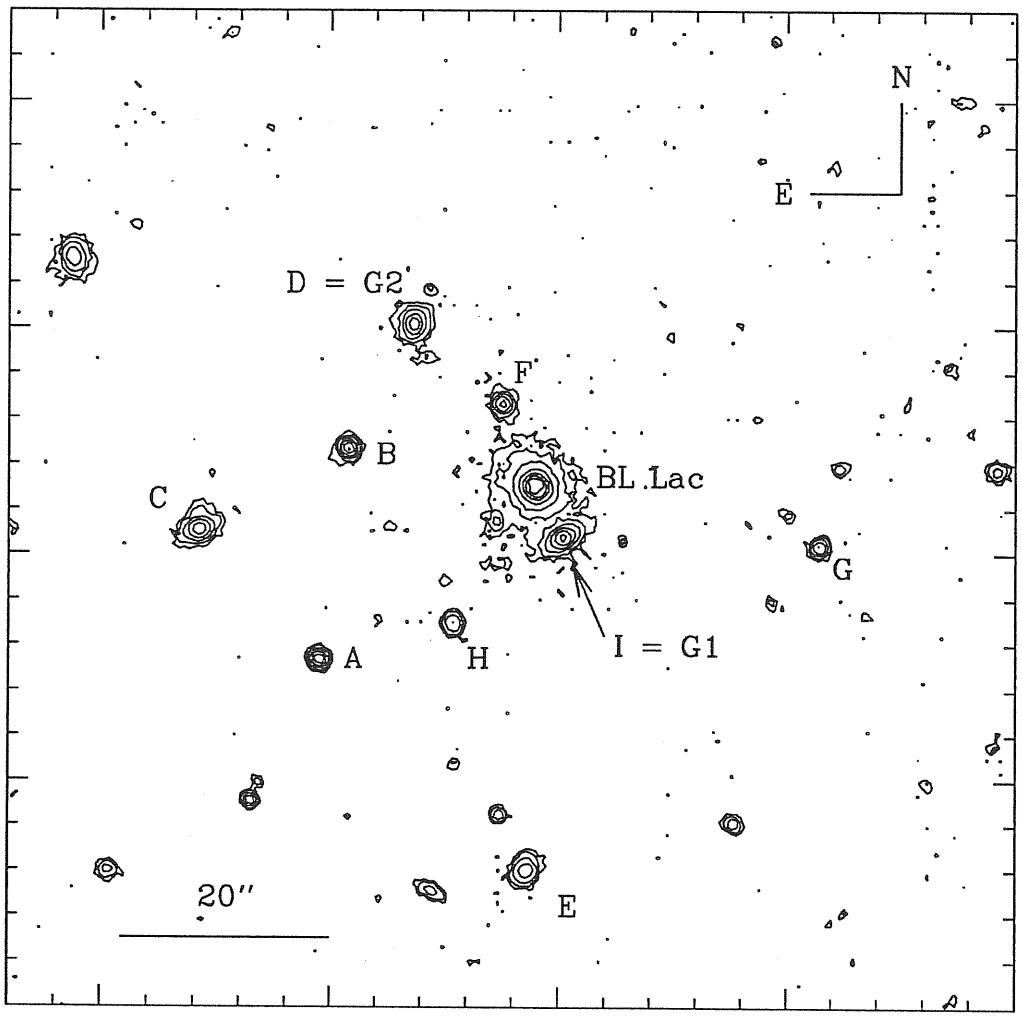

Figure 5.19: Contour plot of the central part of the field around PKS 1400+162 (in R).

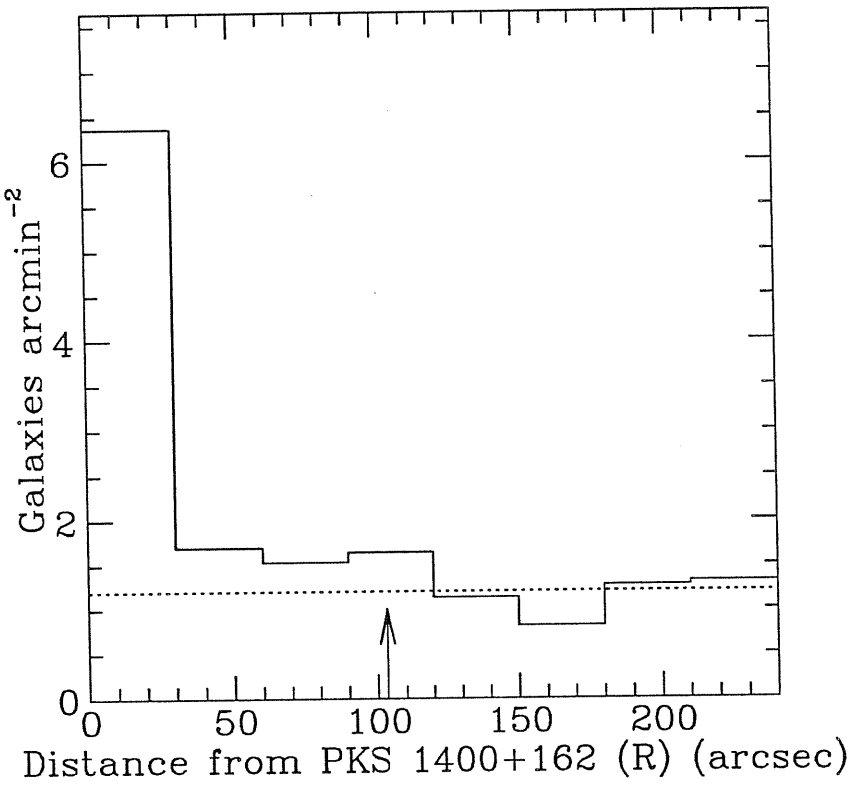

Figure 5.20: The radial distribution of galaxies around PKS 1400+162. The dashed line indicates the local background and the arrow is the 0.5 Mpc radius. The magnitude limit is 21.5.

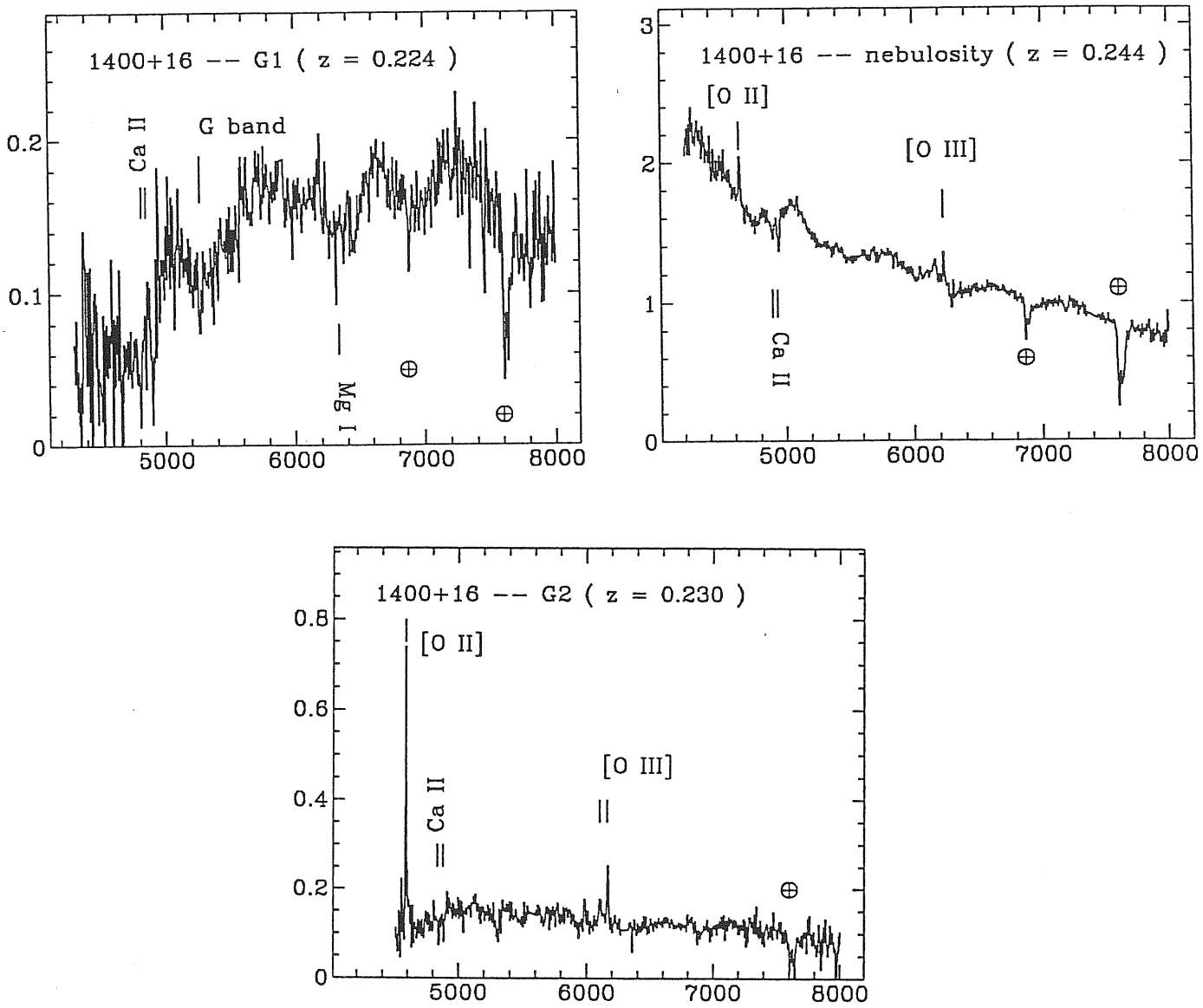

Figure 5.21: Spectra of galaxies in the field of PKS 1400+162 and the nebulosity of the BL Lac object. Flux is in relative units of ergs cm^{-2} s^{-1} $Å^{-1}$ and the abscissa is wavelength in units of Å.

5.2.9 MS 1402+042

This is the first BL Lac to be discovered as the optical counterpart of a faint X-ray source detected with the *Einstein* satellite. It is optically bluer than most known BL Lacs and very weak in the radio (Stocke *et al.* 1982). Giommi *et al.* (1986) noted rapid optical and X-ray variability.

A tentative redshift of $z = 0.2$ is given by Morris *et al.* (1991) who noted that the bump around 5000 Å, from which they derived the redshift, is suggestive of the Ca II break. However, this feature could be an artefact since it occurs in the region where they splice the red and blue parts of their spectra together. The lack of the Mg b or Na D features casts doubt on the redshift. Abraham, M^{c}Hardy, & Crawford (1991) report the object as unresolved.

Our images were taken in relatively good seeing (see Figure 5.22 for the R-band contour plot). We find no evidence for excess galaxies in the field around this source (see Figure 5.23 and Tables 5.1 and 5.3). We note, however, that the image may not be deep enough, and/or the object may have a much higher redshift than the one quoted by Morris *et al.* (1991).

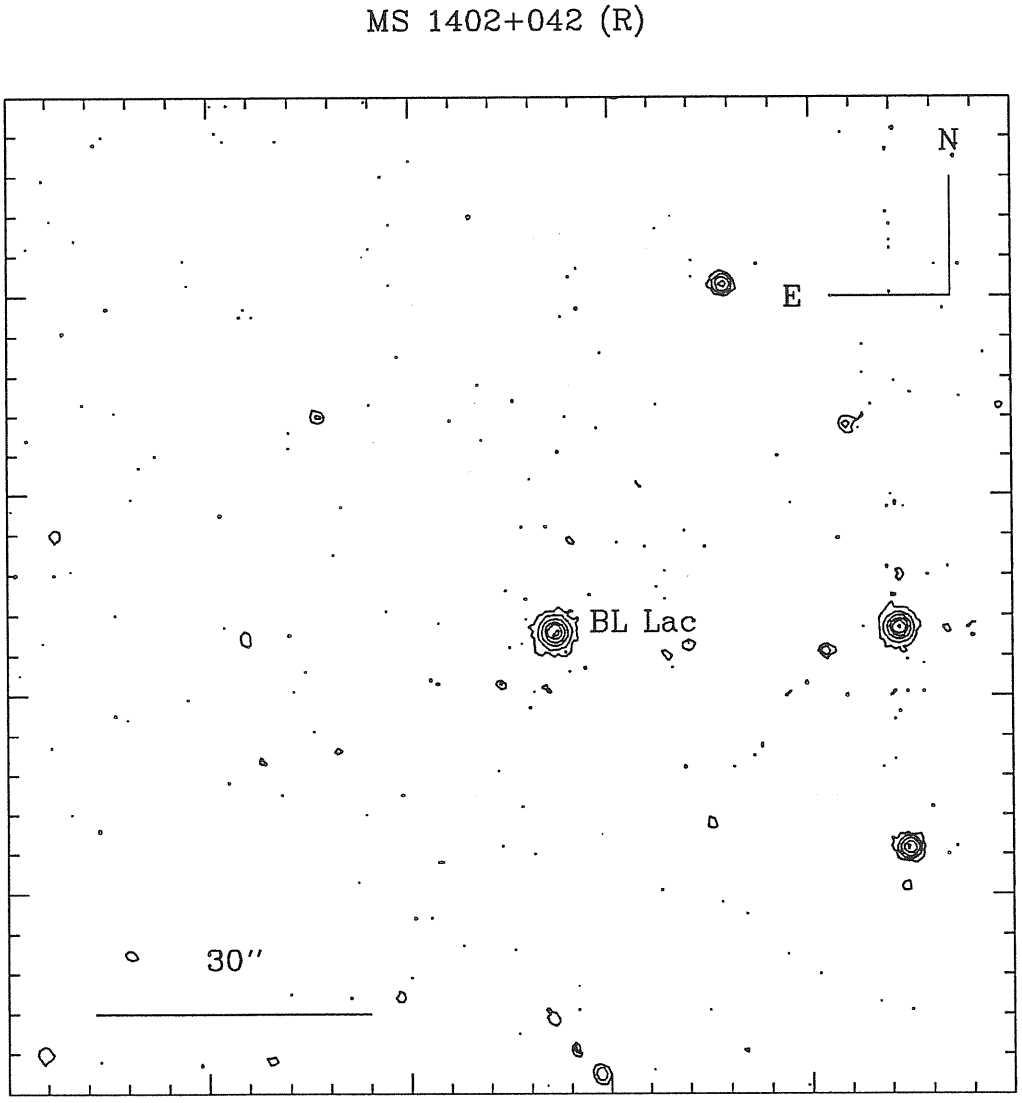

Figure 5.22: The *R*-band Contour plot of the central part of the field around MS 1402+042.

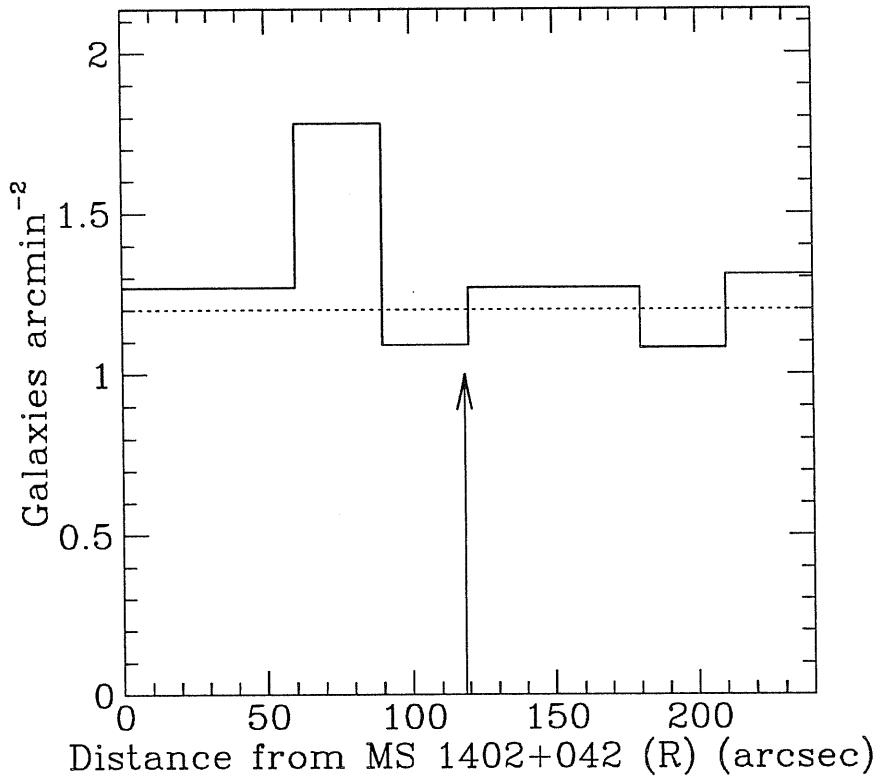

Figure 5.23: The radial distribution of galaxies around MS 1402+042. The dashed line indicates the local background and the arrow is the 0.5 Mpc radius. The magnitude limit is 21.5.

5.2.10 PKS 1514–241 (AP LIB)

PKS 1514–241 (AP Lib)[6] is a classical, nearby BL Lac object (z = 0.0486; Disney, Peterson, & Rodgers 1974). These authors noted several galaxies surrounding the BL Lac, in particular a lenticular galaxy one arcmin to the North which has the same radius as the extended halo of the BL Lac host galaxy (R = 11 kpc). This latter was found to have an absolute magnitude M_V $\sim$ –21.4, consistent with that typical for BL Lac hosts (Ulrich 1989). Stickel, Fried, & Kühr (1993) noted that the isophotes of the host galaxy of AP Lib are asymmetric and elongated towards the large, nearby lenticular (m_R = 16.62, 64 arcsec Northeast at PA = 26°; G1 in the following), suggesting tidal interaction between the two.

The field of PKS 1514–241 (see Figure 5.24) was difficult to analyze since the image covered only the central 0.2 – 0.5 Mpc of the presumed cluster (the object was offset from the center to avoid a bright star in the field). Thus, we were unable to determine the values of the local background and the richness parameter, $N_{0.5}$. Instead, we have calculated the number of galaxies to m_R = 20.5 using the average background and expect 40 while 41 are observed. We do not detect a significant excess over the average background, but we can not exclude the possibility that the intrinsic, local background is lower than average. Larger scale images are required in this case. Figure 5.25 shows the radial galaxy distribution.

We obtained a spectrum of G1, which shows Ca II H and K, the G band, Mg I λ 5175 Å, and Na I λ 5892 Å in absorption giving z = 0.048 (see Figure 5.26). Thus, the BL Lac host and this galaxy are associated, with a projected separation of 83 kpc.

[6]This object is discussed in Pesce, Falomo, & Treves (1993).

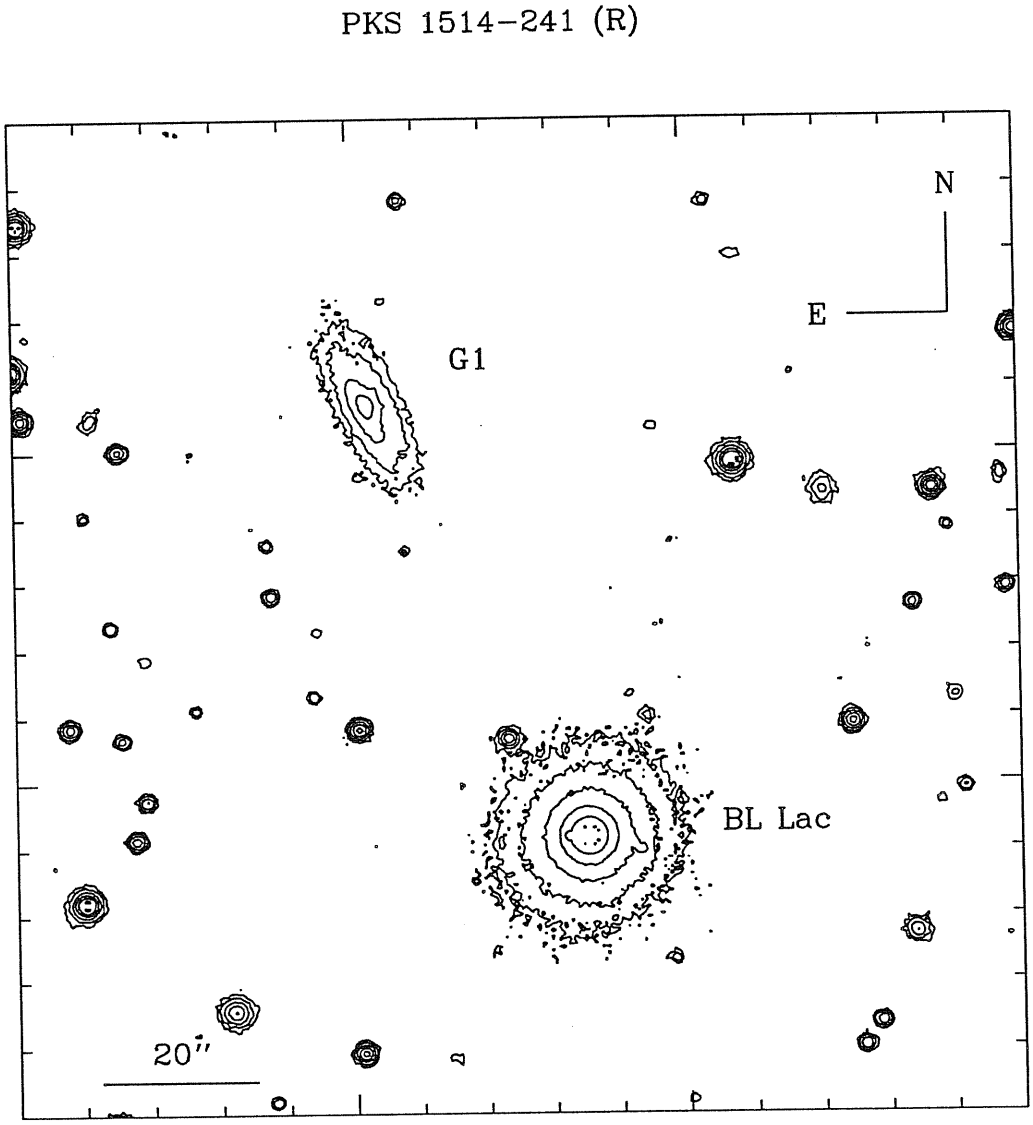

Figure 5.24: Contour plot of the central part of the field around PKS 1514–241 (in R).

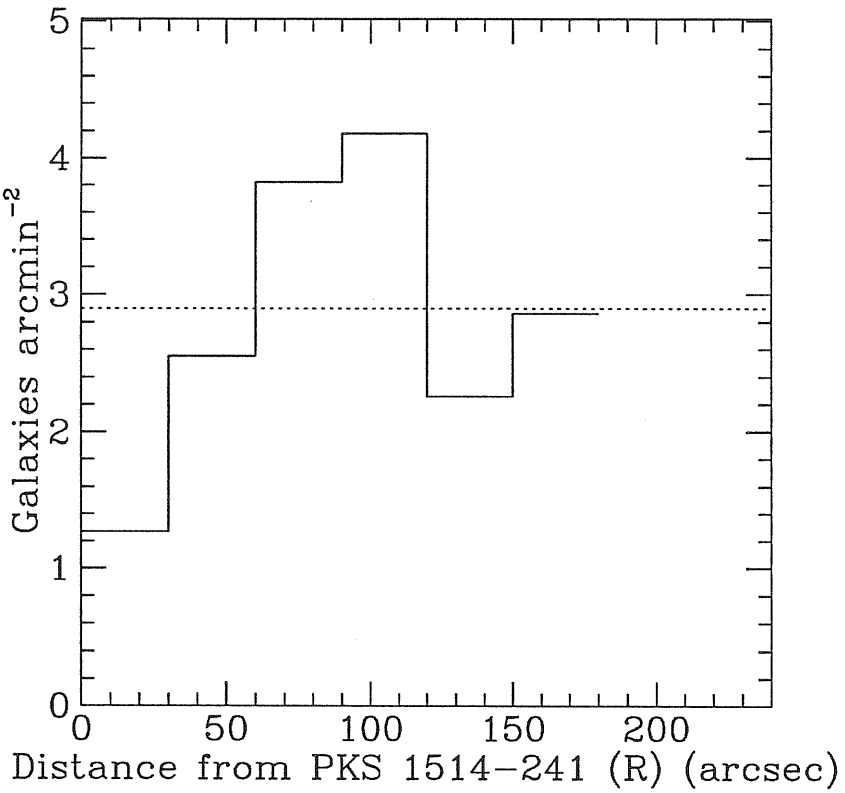

Figure 5.25: The radial distribution of galaxies around PKS 1514–241. The dashed line indicates the average background from Metcalfe *et al.* (1991). The radius of 0.5 Mpc is at 384 arcsec and the magnitude limit is 22.0.

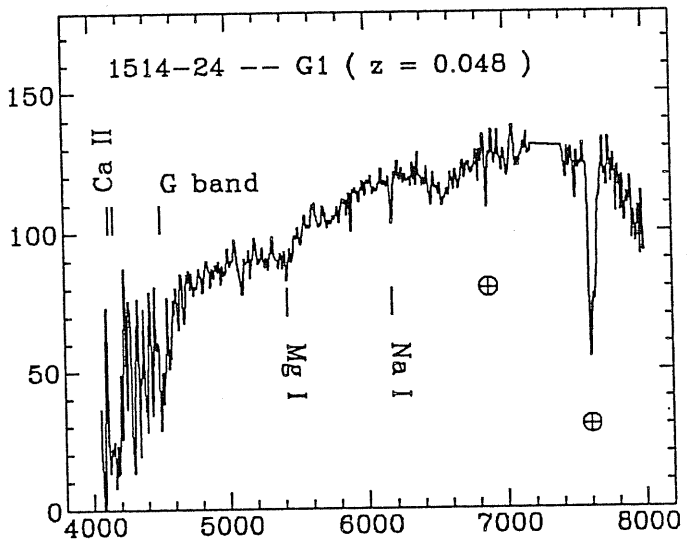

Figure 5.26: The spectrum of galaxy G1 in the field of PKS 1514–241. Flux is in relative units of ergs cm^{-2} s^{-1} $Å^{-1}$ and the abscissa is wavelength in units of Å.

5.2.11 PKS 1538+149

Wills & Wills (1976) noted this object as blue and with a featureless continuum. Craine, Tapia, & Tarenghi (1975) commented on the numerous faint galaxies surrounding the BL Lac. Hutchings, Johnson, & Pyke (1988) reported that the outer isophotes appear to be off center and note two galaxies about 16 arcsec away. The asymmetry may be caused by three faint, overlapping galaxies (Stickel, Fried, & Kühr 1993). A spectrum obtained by these authors shows weak broad and narrow emission lines identified with Mg II λ 2798 Å and [O II] λ 3727 Å at $z = 0.605$.

Our high quality images show what appears to be a rich cluster about 120 arcsec to the Southeast (see Figure 5.27). The galaxy excess within 0.5 Mpc of the BL Lac is barely significant, but over the whole field it is highly significant (see Table 5.1). This is seen graphically in Figure 5.28, where the high galaxy density within 0.5 Mpc of PKS 1538+149 is evident. The large excess at 80 to 170 arcsec is the cluster.

For $z = 0.605$, PKS 1538+149 is located approximately 0.9 Mpc from the cluster center. Calculations of the richness parameter for the BL Lac object give $N_{0.5} = 8$, just consistent with an Abell richness class 0 cluster (we note that at such a redshift, we may loose some galaxies due to the low magnitude limit of the image). On the other hand, the richness measure for the cluster (assuming a redshift of 0.6) is $N_{0.5} = 31$, representative of an Abell richness class 2 cluster.

The average $V - R$ color of 1.55 for the cluster galaxies is similar to the average color of ellipticals at a redshift of 0.37 or 0.61 (Butcher *et al.* 1976). This agrees well with the redshift range of 0.3 – 0.9, based on the colors and R magnitudes, determined from Coleman, Wu, & Weedman (1980).

Clearly spectroscopy is needed to confirm the physical association of PKS 1538+149 with this rich cluster. However, irrespective of whether the BL Lac is associated with the cluster or not, it is found in a region of higher-than-average galaxy density. One possible explanation is that the BL Lac is the center of a small subcluster at the outskirts of a larger system, similar, perhaps, to the case of PKS 2155–304 (see below).

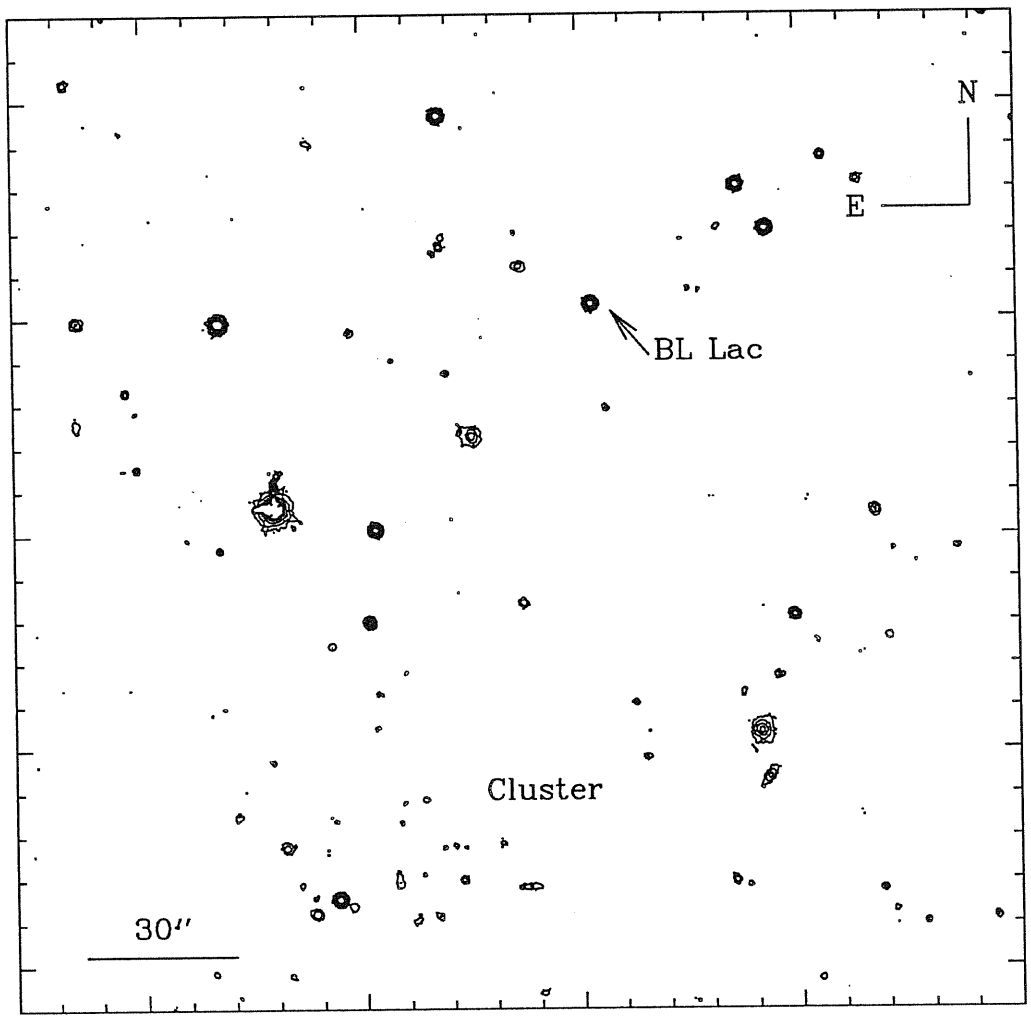

Figure 5.27: The *R*-band contour plot of the field around PKS 1538+149. The cluster 120 arcsec to the Southeast can be clearly seen.

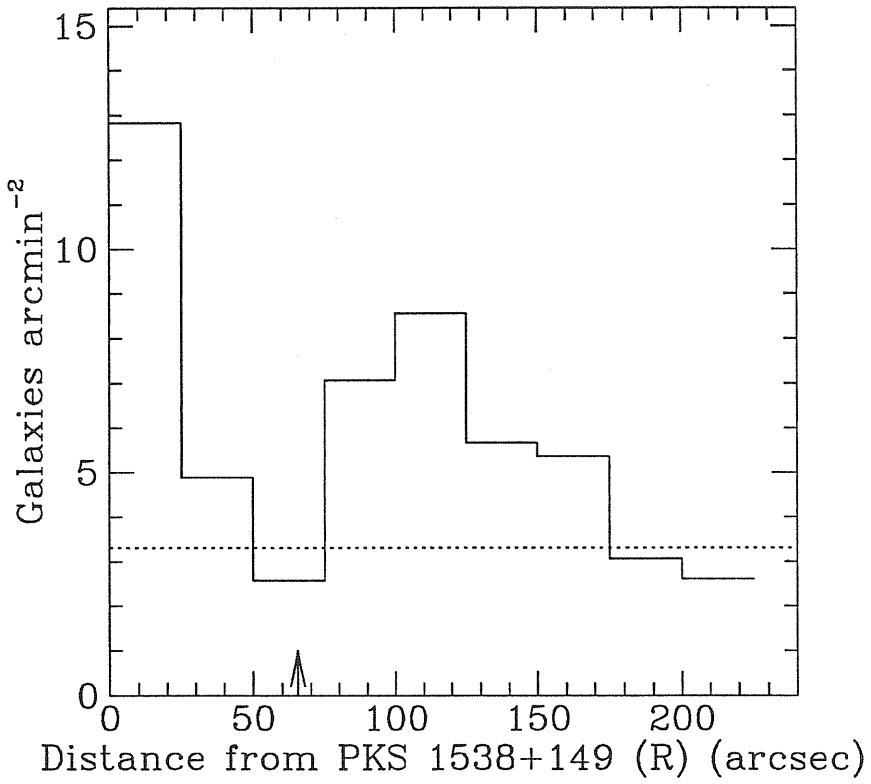

Figure 5.28: The radial distribution of galaxies around PKS 1538+149. The dashed line indicates the local background and the arrow is the 0.5 Mpc radius. There is an excess of galaxies within 0.5 Mpc of the BL Lac and the excess around the cluster at $\sim$ 120 arcsec is evident. The magnitude limit is 22.0.

5.2.12 PG 1553+113

This is the only BL Lac discovered in the Palomar-Green sample of UV excess objects. Featureless spectra (Miller & Green 1983) and optical variability (Miller *et al.* 1988) led to its classification as a BL Lac object.

Miller & Green (1983) identified Lyman-α at $z = 0.36$ in a spectrum obtained with the *International Ultraviolet Explorer* satellite. This feature was later shown to be spurious by Falomo & Treves (1990), who also find its overall spectral distribution to be similar to those of X-ray selected objects.

Falomo & Treves (1990) further noted that due to the object's brightness and stellar appearance (and lack of host galaxy signature), the host galaxy is either very under luminous or the object is very distant ($z > 0.5$), luminous ($L \sim 10^{46} - 10^{47}$ ergs s^{-1}), and possibly strongly beamed. Ellingson, Yee, & Green (1991) find many galaxies in the field, and Hutchings & Neff (1992) did not detect signs of either the host galaxy or nearby companions.

Our images (see Figure 5.29) show no evidence for a significant excess of objects around PG 1553+113 (*cf.* Figure 5.30 and Tables 5.1 and 5.3). However, we note that our exposures are short and that the images are not very deep (except for the V-band image which was, however, taken under relatively poor conditions). We would not expect to observe the majority of galaxies in a cluster with $z > 0.5$ in our images.

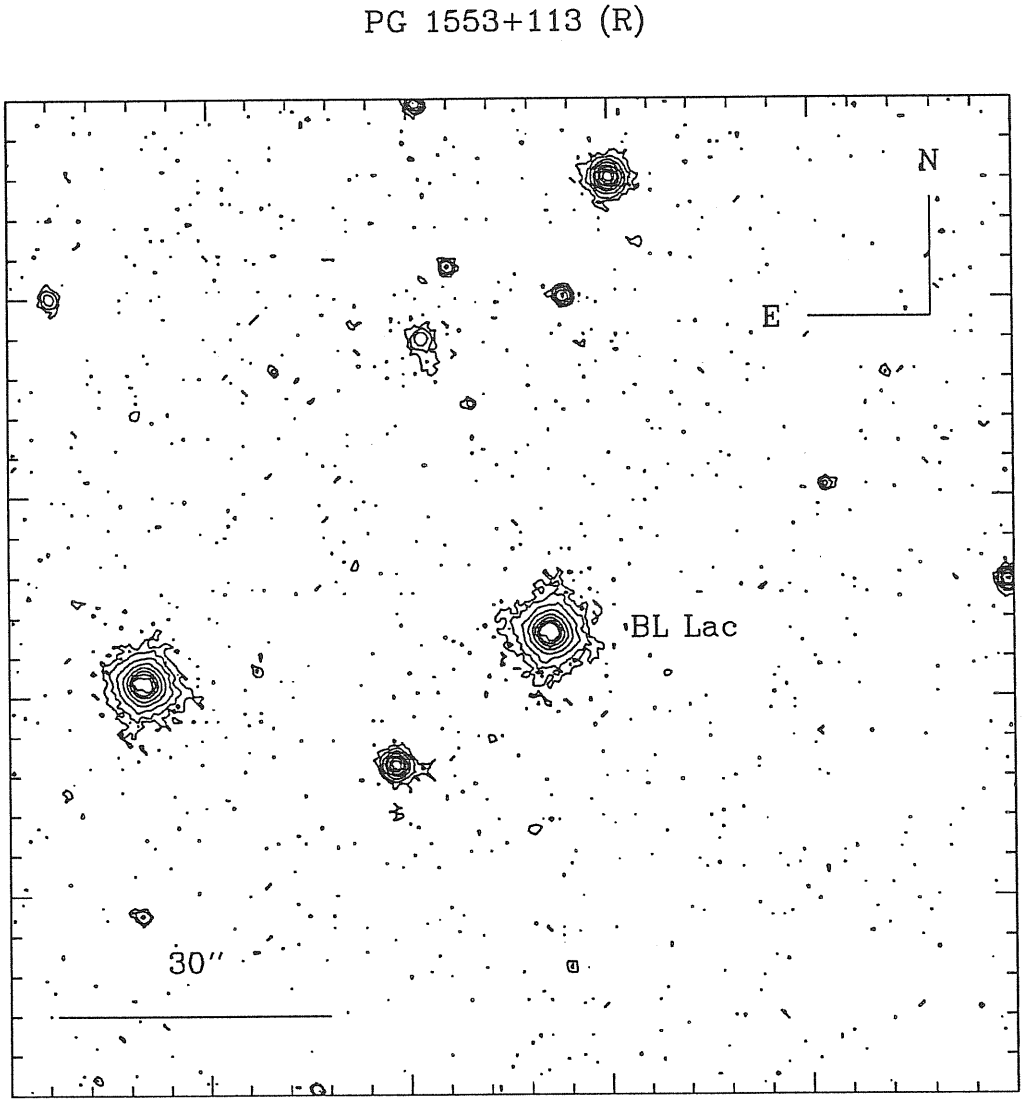

Figure 5.29: The *R*-band contour plot of the central part of the field around PG 1553+113.

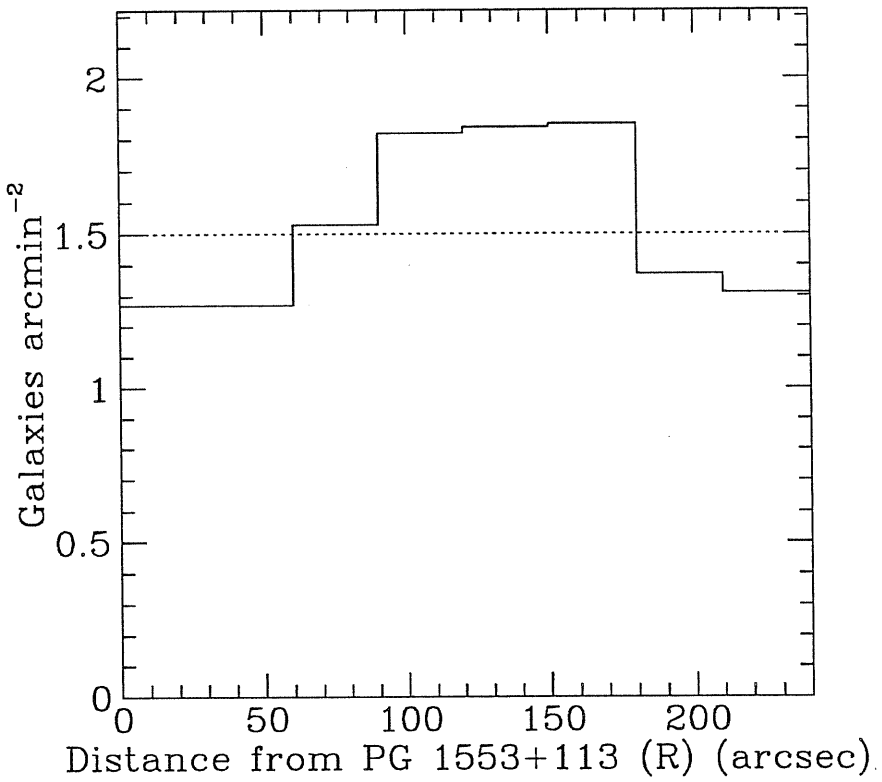

Figure 5.30: The radial distribution of galaxies around PG 1553+113. The dashed line indicates the local background and the magnitude limit is 21.5.

5.2.13 H 1722+119

This is among the brightest BL Lac objects ($m_V = 13 - 15$), but has no measured redshift nor is there any indication of the host galaxy.

The object was discovered in the HEAO-I all sky survey (Brissenden *et al.* 1990). It is a strong X-ray source, originally detected by the Uhuru satellite and the *Einstein* High Resolution Imager. In the optical, the spectra are featureless and, as for PG 1553+113, the bright magnitude and lack of host galaxy signature argue for a high redshift or an extremely luminous source.

Unfortunately, our images were taken under very poor conditions (Figure 5.31) and show no evidence for clustering (Figure 5.32). This negative result, however, is probably due to a number of factors, the most important being the poor image quality. A high redshift would effectively rule out the detection of excess galaxies in this case.

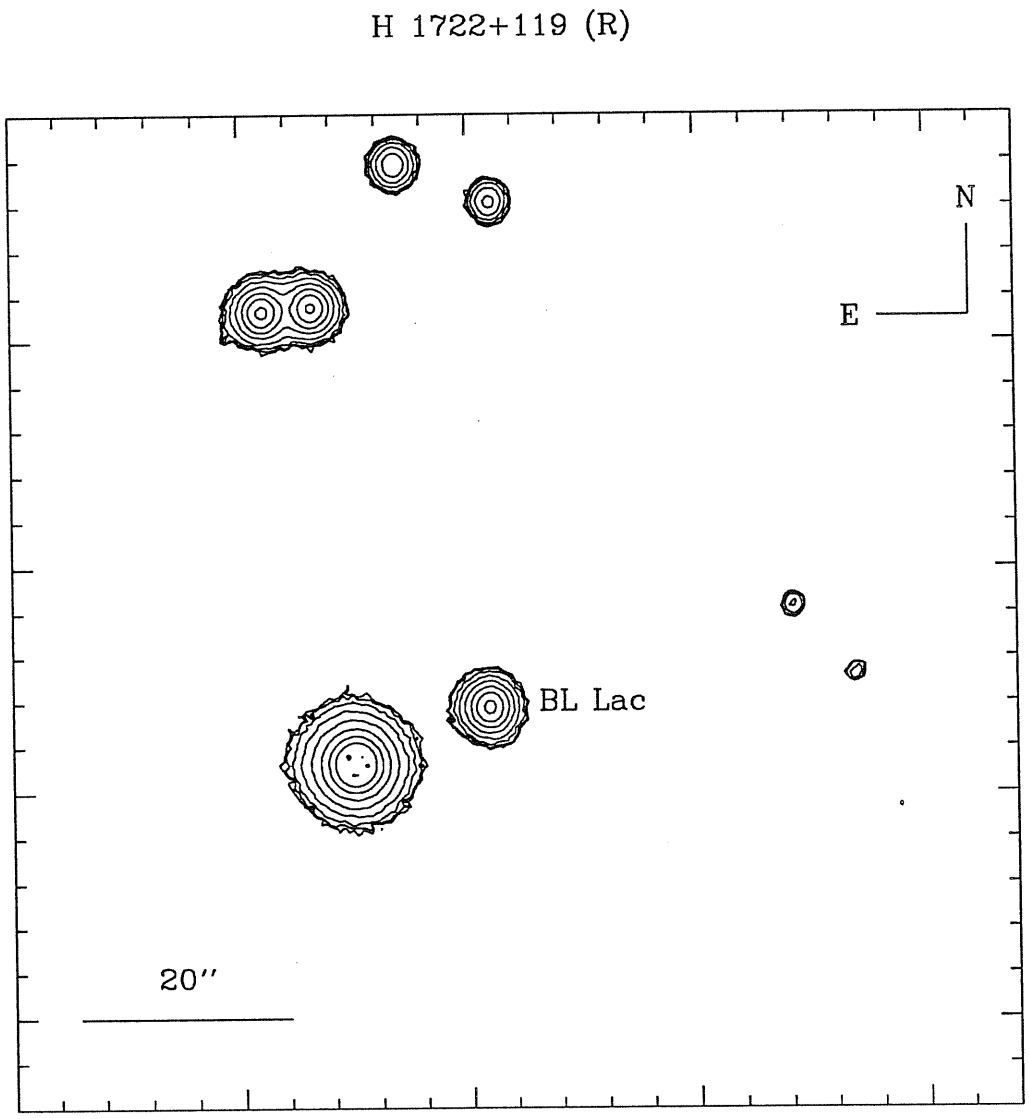

Figure 5.31: Contour plot of the central part of the field around H 1722+119 (in R).

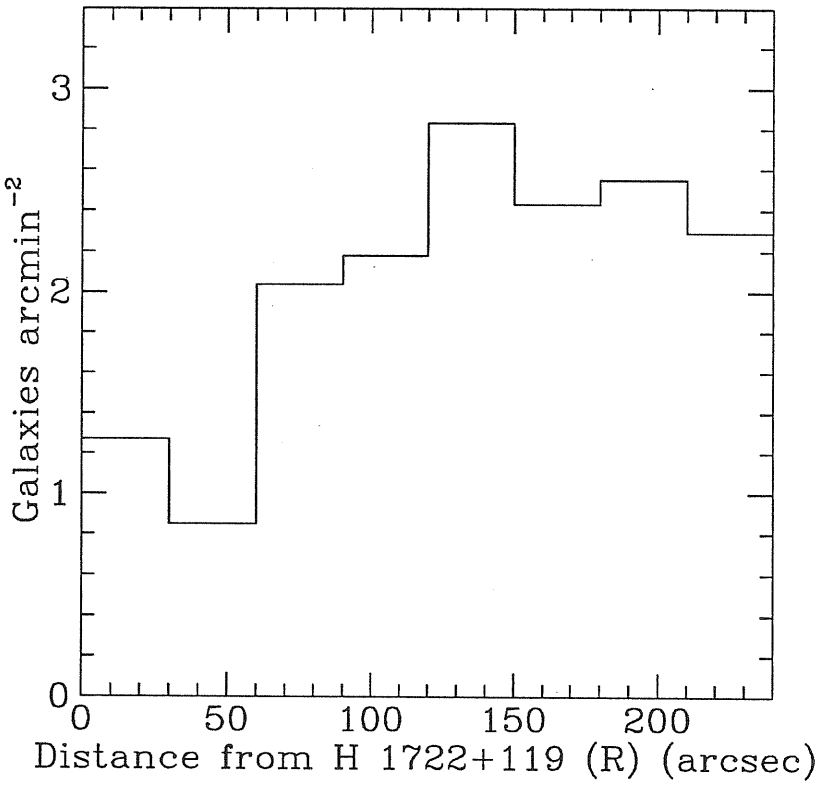

Figure 5.32: The radial distribution of galaxies around H 1722+119. Due to the poor image quality, no local background was computed.

5.2.14 1749+096

Browne, Crowther, & Adgie (1973) identified the radio source PKS 1749+096 with a neutral colored, stellar object and suggested it may be found to have a featureless continuum typical of BL Lacs. Craine, Tapia, & Tarenghi (1975) were unable to detect a signature of the host galaxy.

Stickel, Fried, & Kühr (1988a) observed the object and found emission lines of H_β and [O III] $\lambda\lambda$ 4959,5007 Å at $z = 0.32$. No absorption due to the underlying galaxy was found, but the continuum is well-fitted by a standard elliptical galaxy spectrum plus power law. The redshift was confirmed by White *et al.* (1988).

Stickel, Fried, & Kühr (1993) noted a close group of seven galaxies in the field around 1749+096. They observed five of these but were unable to determine the redshift for any of them.

Our image was taken in average conditions, but is not very deep (see Figure 5.33). The density distribution (Figure 5.34) shows what might be an excess of galaxies within 30 arcsec of the BL Lac, but this is not found to be significant. However, the local background is higher than average and may be the reason for this, though the largest controlling factor is almost certainly the low magnitude limit. We note a large number of stars in the field.

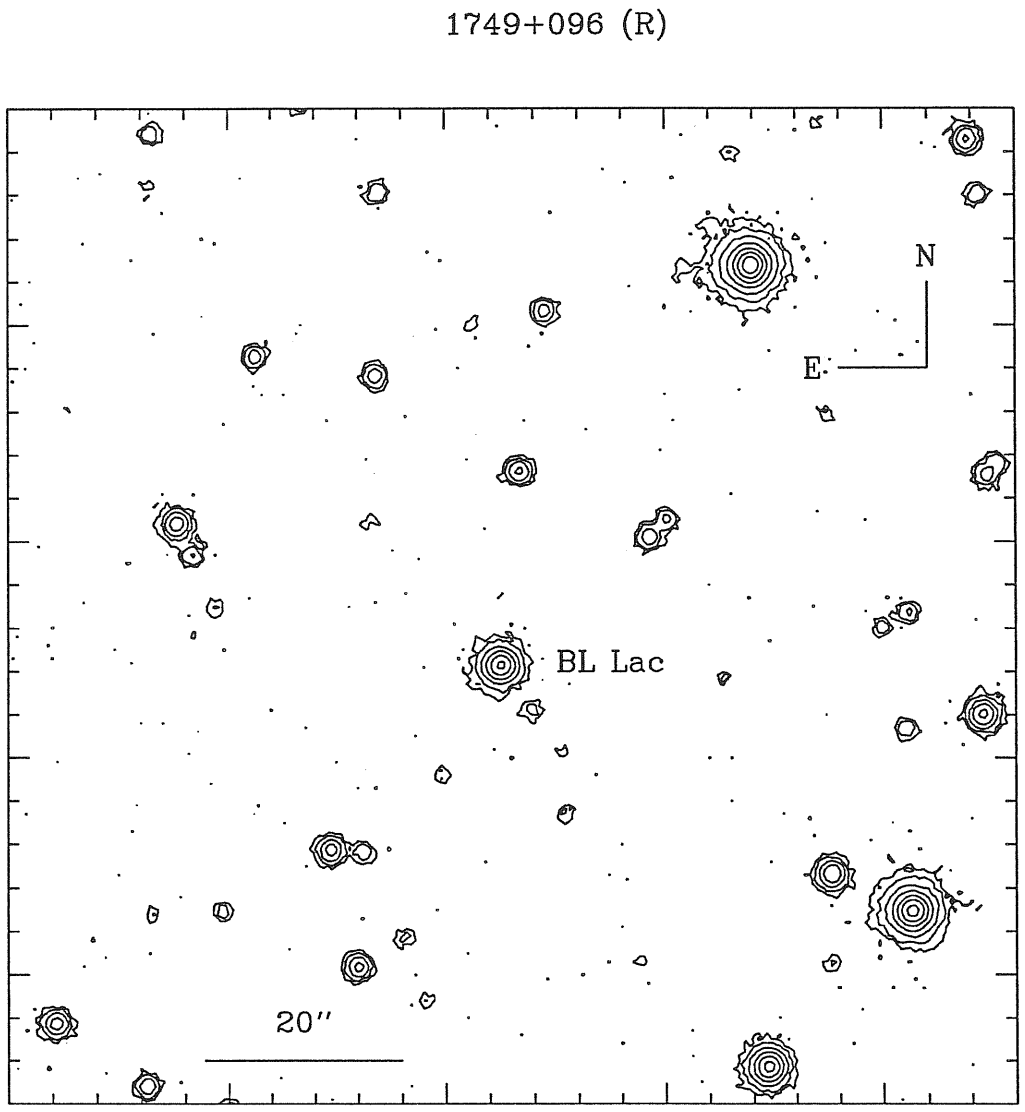

Figure 5.33: The *R*-band contour plot of the central part of the field around 1749+096.

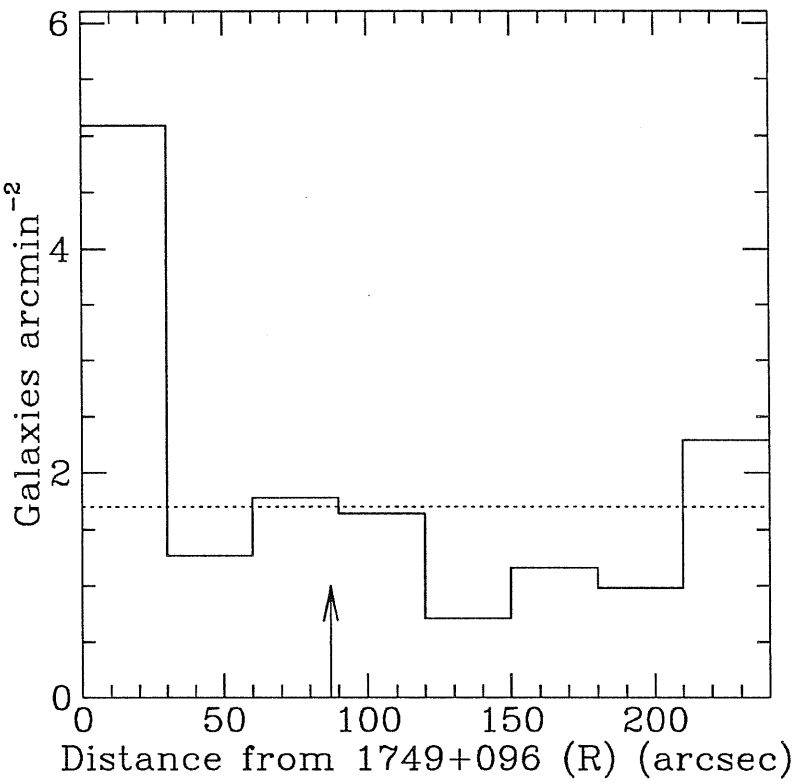

Figure 5.34: The radial distribution of galaxies around 1749+096. The dashed line indicates the local background and the arrow is the 0.5 Mpc radius. The magnitude limit is 21.0.

5.2.15 PKS 2005–489

PKS 2005–489 [7] is one of the brightest known BL Lac sources (Wall *et al.* 1986). Falomo *et al.* (1987) obtained spectra exhibiting weak emission (H_α + [N II]) lines at $z = 0.071$, which is confirmed by the spectrum reported below.

The object is surrounded by a number of galaxies (see Figure 5.35), but as for AP Lib, the field covers only about 0.5 Mpc from the BL Lac. Thus, the local background and richness classifier were not determined. For a magnitude limit of $m_R = 21.0$ we detect 120 galaxies (though in a long exposure with poor (1.7 arcsec) seeing) when 69 are expected. There is clearly a significant excess of galaxies in the total field. The presence of a foreground ($z = 0.01$) Abell cluster (A851s) 28 arcmin to the Northeast should not affect this result significantly since the cluster is noted as sparsely populated with about 20 members (Sersic 1974). The radial distribution of galaxies is given in Figure 5.36.

The two low redshift BL Lacs (AP Lib and PKS 2005–489) highlight the need for large-scale detectors in the study of environments around nearby objects, where even our relatively large CCD field was of insufficient size.

We obtained spectra of the BL Lac host and galaxies G1 (at 48 arcsec North, PA $\sim 15°$) and G2 (at 74 arcsec Northeast, PA $\sim 70°$). Our spectrum of the BL Lac nebulosity confirms the redshift of $z = 0.071$ based on absorption features of Ca II H and K, Mg I λ 5175 Å, and Na I λ 5892 Å (see Figure 5.37). Galaxy G1 also shows absorption lines of Ca II, the G band, Mg I, and Na I at a redshift of $z = 0.071$ (Figure 5.37). Similarly, galaxy G2 has a redshift $z = 0.070$ (see Figure 5.37).

For galaxy G1, we confirm the redshift found by Stickel, Fried, & Kühr (1993) who, in addition, determine $z = 0.069$ for the galaxy at 56 arcsec (PA $\sim$ 244) (G, see Figure 5.35). Thus, PKS 2005–489 is definitely associated with at least three surrounding galaxies.

[7] This object is discussed in Pesce, Falomo, & Treves (1993).

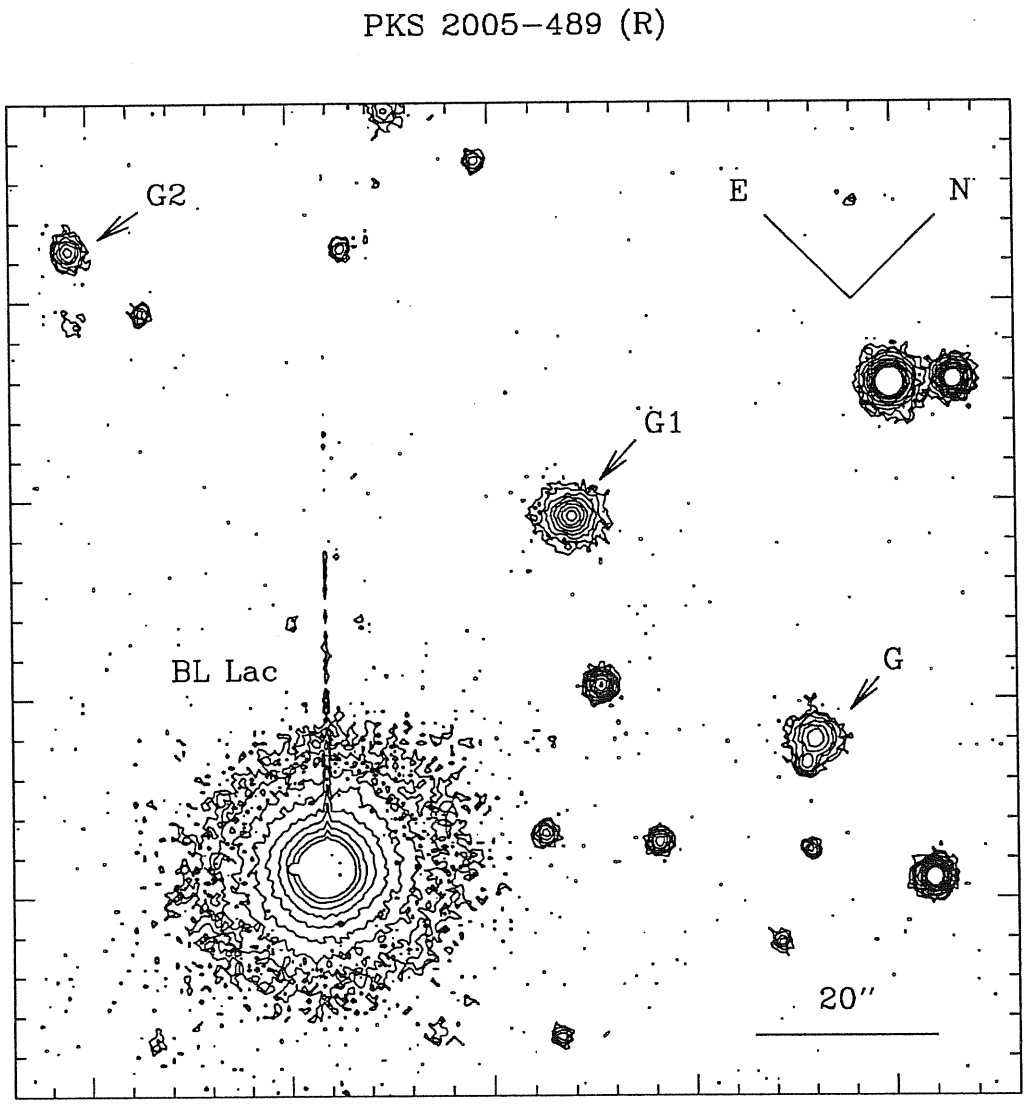

Figure 5.35: The *R*-band contour plot of the central part of the field around PKS 2005–489.

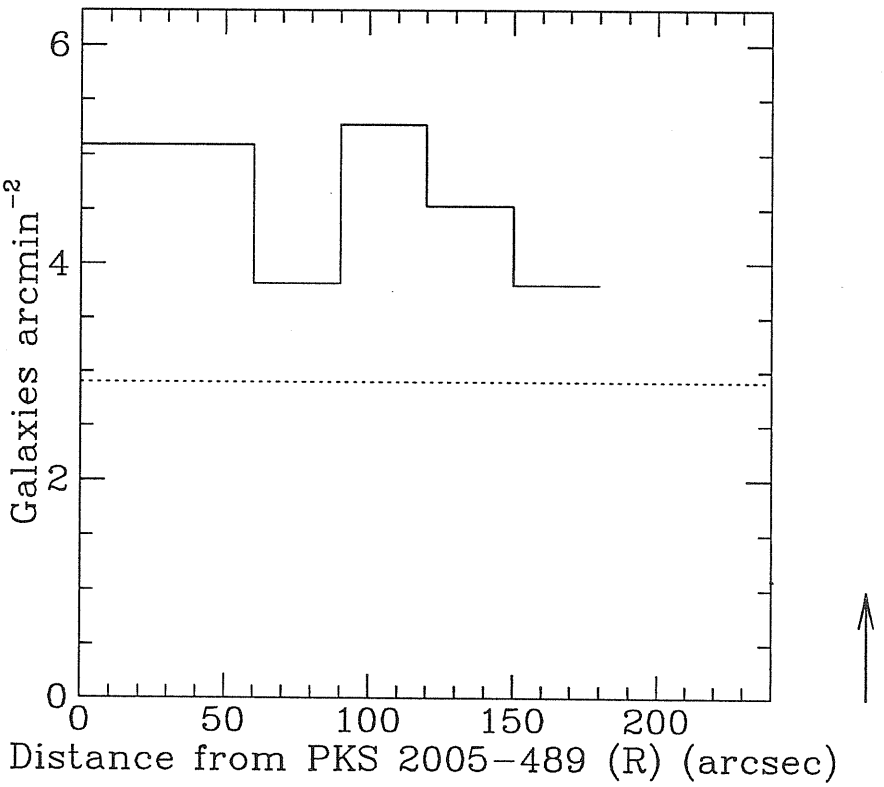

Figure 5.36: The radial distribution of galaxies around PKS 2005–489. The dashed line indicates the average background from Metcalfe *et al.* (1991) and the arrow the 0.5 Mpc radius. The magnitude limit is 22.0.

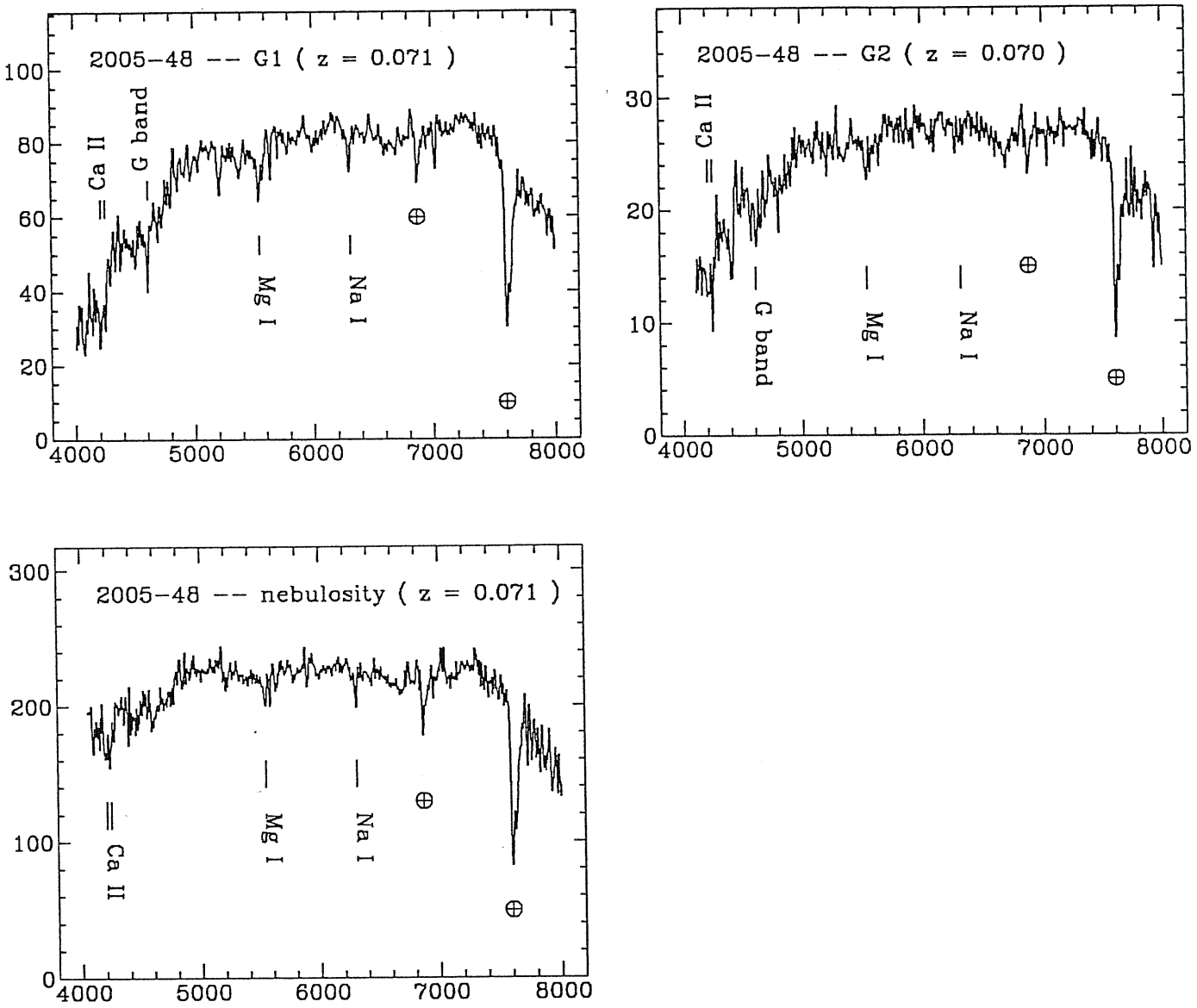

Figure 5.37: Spectra of galaxies in the field of PKS 2005–489 and the nebulosity of the BL Lac. Flux is in relative units of ergs cm^{-2} s^{-1} $Å^{-1}$ and the abscissa is wavelength in units of Å.

5.2.16 PKS 2155–304

The X-ray selected BL Lac object PKS 2155–304 [8] is one of the brightest ($m_V = 13$) of its class. A first image of the field surrounding the object was published by Griffiths *et al.* (1979) who noted an asymmetric nebulosity, with a wider extension to the East, around the source. A spectrum centered on this extension was obtained by Bowyer *et al.* (1984) who found stellar absorption features yielding a redshift $z = 0.117$. High resolution imaging by Falomo, Melnick, & Tanzi (1990) showed that the eastern extension is due to a faint ($m_R = 20$) galaxy $\sim 4''$ from the center of the object. In the following, this object will be referred to as G1.

Falomo *et al.* (1991) demonstrated that the redshift reported by Bowyer *et al.* pertains to this companion galaxy, and found that the galaxy (G2) $\sim 25''$ to the Southeast is at $z = 0.116$. Moreover, detailed surface photometry of the nebulosity showed the host galaxy has $M_V \sim -22.5$ and an effective radius $r_e = 4.5''$, and is likely a giant elliptical at a redshift $z \sim 0.1$. The R-band contour plot is given in Figure 5.38.

Figure 5.39 shows the galaxy density in filter R as a function of distance from the BL Lac object. A correction of 2.9 arcmin^2 for area lost due to interference by bright stars in the field is included in the subsequent analysis. The distribution exhibits an enhancement of galaxy density near the source. We also note that the small enhancement of galaxy density at $\sim 130''$ corresponds to the galaxies surrounding G4 (the second brightest galaxy in the field; see below). While the local background is lower than average, the excess is highly significant ($P \ll 0.1\%$), even using the average background. We calculate a richness indicator of $N_{0.5} = 7.2$ (see Table 5.3).

[8] This is a summary of the full report which appears in Falomo, Pesce & Treves (1993b).

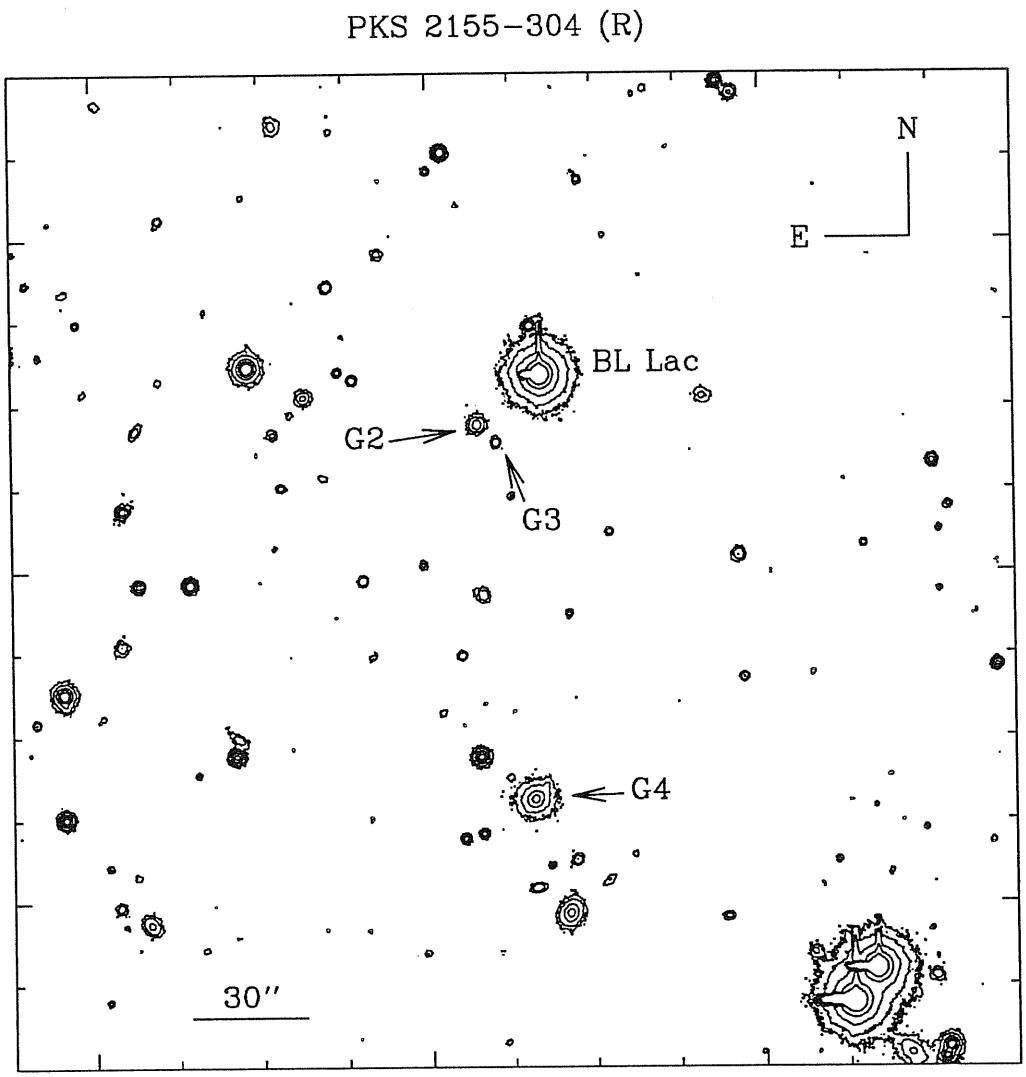

Figure 5.38: The *R*-band contour plot of the central part of the field around PKS 2155–304. The galaxy referred to as G1 in the text does not appear in this figure due to the resolution of the image.

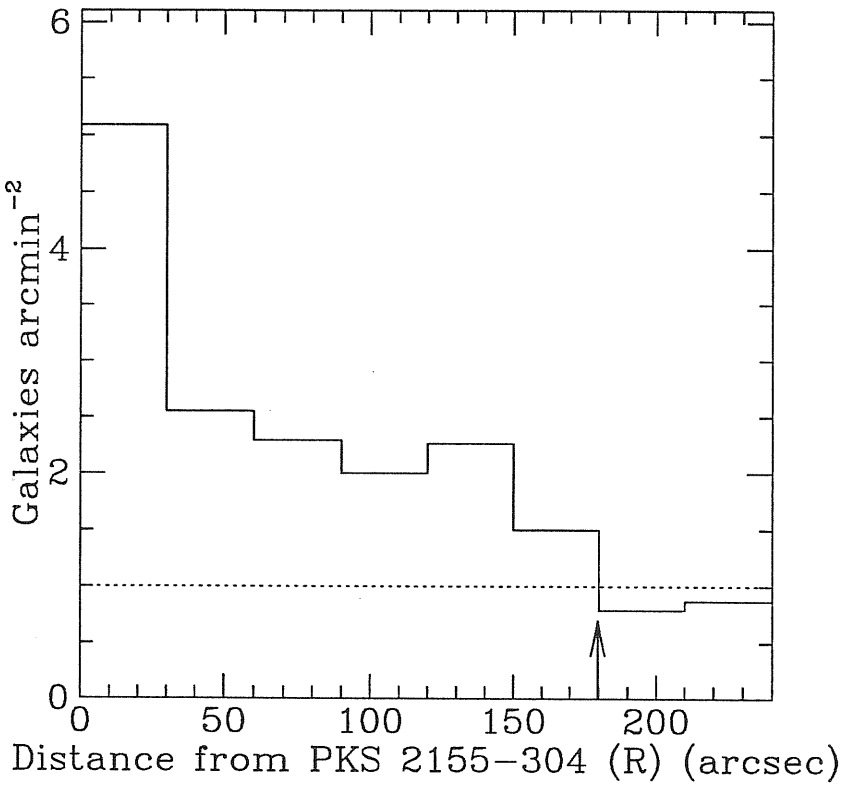

Figure 5.39: The density distribution of galaxies surrounding PKS 2155–304, showing the excess of objects around the BL Lac source. The arrow indicates the radius of 0.5 Mpc at $z = 0.116$ and the dotted line is the average background determined for objects beyond 150″ from PKS 2155–304. The slight excess at $\sim$ 130″ is due to the group around galaxy G4 (see text). The magnitude limit is 21.5.

We acquired three spectra of the nebulosity ($\sim 3''$ West of the nucleus). Although the slit was centered far from the nucleus, the contribution from the wing of the PSF of the central source is still the dominant component. The individual spectra exhibit the characteristic continuum of power law shape. To increase the S/N we combined the three spectra using the average, weighted by the exposure time. The combined spectrum (Figure 5.40a) shows some weak absorption features and we checked that these were not spurious artefacts due to poor sky subtraction. The regions of the spectrum heavily contaminated by the presence of intense night-sky emission lines were removed in the analysis. Apart from the telluric oxygen absorption bands, the strongest absorption features are at $\lambda\lambda$ 4795, 5773, 6575 Å and we identify them with, respectively, the G band, Mg I λ 5175 Å and Na I λ 5892 Å at a redshift $z = 0.116 \pm 0.002$. We verified, *a posteriori*, the consistency of these absorption features in the individual spectra and found reasonable agreement. Therefore we conclude that the host galaxy of PKS 2155–304 is at $z = 0.116$.

Our determination of the redshift does not change the interpretation of the 600 eV absorption feature discovered by Canizares & Kruper (1984) and further discussed by Bowyer *et al.* (1984) and Krolik *et al.* (1985).

The second brightest galaxy (G4) in our field is the $m_V \sim 18$ elliptical galaxy at $\sim 113''$ South of the BL Lac object (see Figure 5.38). The average of the two spectra obtained (Figure 5.40b) very clearly shows absorption features of Ca II H & K, the G band, Mg I λ 5175 Å, and Na I λ 5892 Å at redshift $z = 0.116 \pm 0.002$. The object is highly extended and surrounded by numerous faint galaxies (see Figure 5.41). Moreover, we detected an emission feature $\sim 4.5''$ (PA $\sim 320°$) from the center of G4. This could be either a jet-like structure associated with, or a faint galaxy superimposed onto the image of, G4.

We performed surface photometry in the R band on the galaxy using the Numerical Mapping Package (Barbon, Benacchio, & Capaccioli 1976). Isophotes down to $\mu_R = 25$ mag arcsec^{-2} were computed and then fitted by ellipses to study the radial profile. We found the profile is well described by a $r^{1/4}$ de Vaucouleurs law with $r_e = 3''$ and ellipticity $e = 0.15$ (PA = 310°). The total magnitude (*a la* de Vaucouleurs) is $m_R(tot) = 16.5$, while the magnitude computed integrating the flux within limits of detectability is $m_R = 17.0$, and the absolute magnitude of G4 is $M_V = -21.4$.

Therefore, G4 belongs to the cluster and lies at ~ 300 kpc from PKS

2155–304. Although fainter and smaller than the BL Lac host galaxy it is probably a giant elliptical at the center of a small subcluster. While such binary clusters are not unusual, this seems the first example involving a BL Lac object.

Our observations of PKS 2155–304 allow us to comment on the UV absorption features discovered with the *International Ultraviolet Explorer* satellite (Maraschi *et al.* 1988), and studied in greater detail with the *Hubble Space Telescope* (Allen *et al.* 1993). The most prominent features are at $\lambda\lambda$ 1281, 1284 Å and λ 1344 Å, and if interpreted as Lyα absorption yield $z_{\rm abs} = 0.056$ and $z_{\rm abs} = 0.104$. These values represent lower limits on the redshift of the BL Lac object and are fully consistent with $z = 0.116$ of the host galaxy. The images do not show any reasonable galaxies near PKS 2155–304 to which these absorption features could be attributed. Therefore we believe it is unlikely that these absorption lines are produced by material in the halo of a normal foreground galaxy. Instead, the most reasonable interpretation is that they are due to intervening low z Lyα absorption systems.

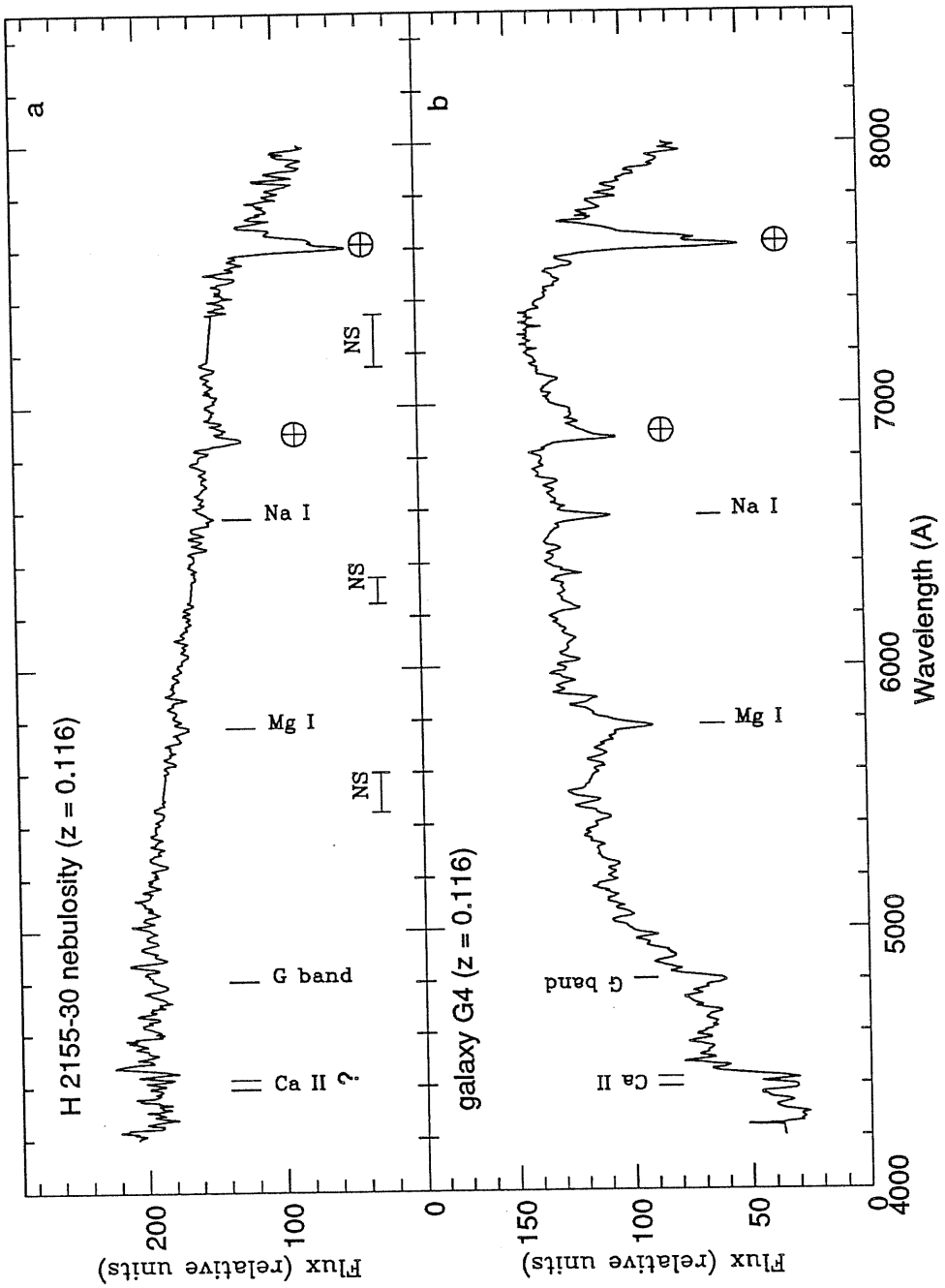

Figure 5.40: (a) The averaged spectrum of the host galaxy of PKS 2155–304. The absorption features labelled correspond to a redshift $z = 0.116 \pm 0.002$. Strong night-sky emission lines have been removed and their locations are marked with 'NS'. (b) The spectrum of the galaxy G4. This is an elliptical galaxy at $z = 0.116 \pm 0.002$. For both spectra, flux is in relative units of ergs cm^{-2} s^{-1}.

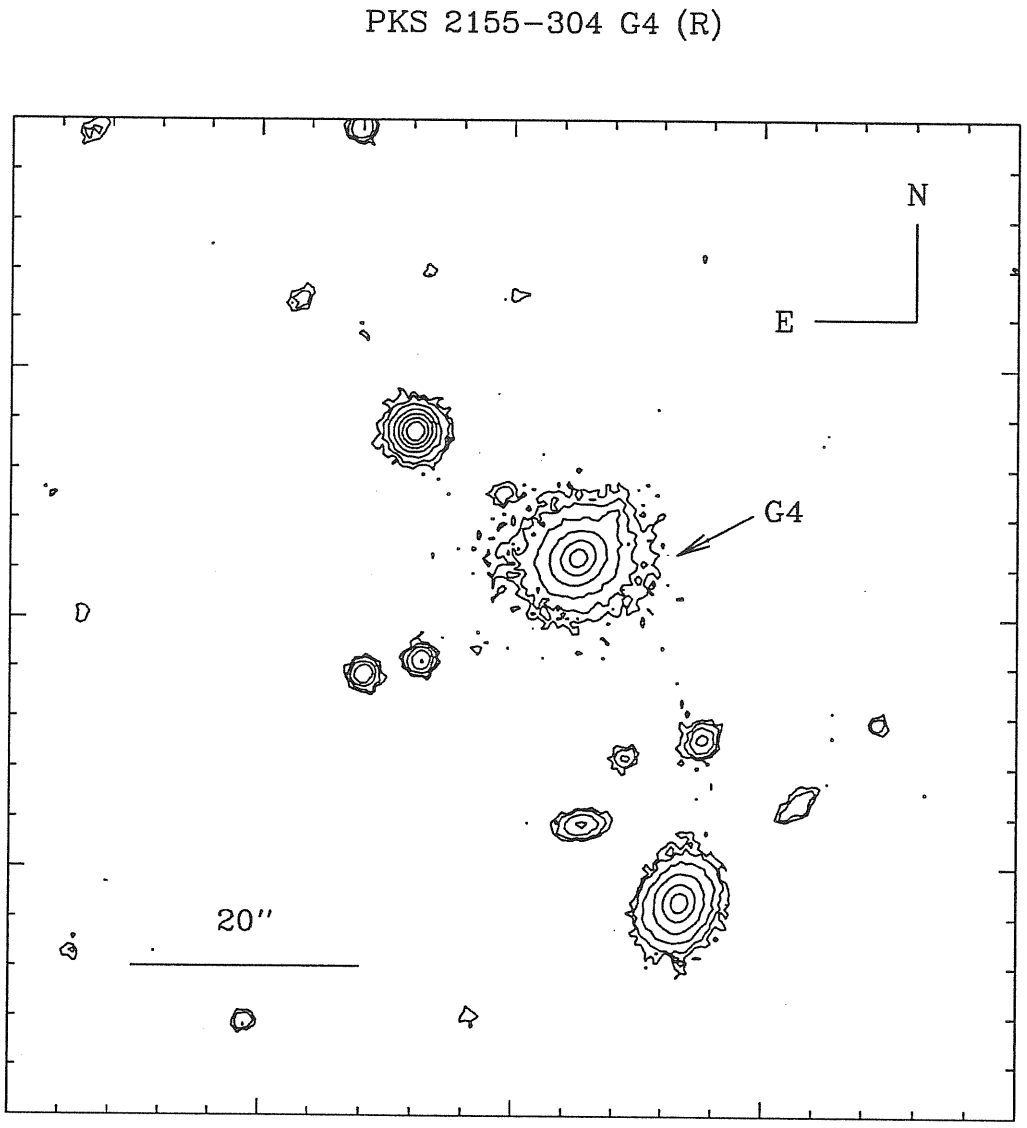

Figure 5.41: A contour plot of the region around the galaxy G4. Note the numerous faint galaxies surrounding this elliptical. The large galaxy to the Southwest is the third brightest galaxy in the field.

5.2.17 PKS 2335+031

Craine, Tapia, & Tarenghi (1975) noted this object to be non-stellar, with an extension to the East (resembling a jet or an extremely close companion). They further remarked that the field contains many faint galaxies.

Using the photometric properties of the host galaxy, assumed to be elliptical, Romanishin (1987) determined a redshift $z = 0.31$. Abraham, M^{c}Hardy, & Crawford (1991) observed this object, but it is impossible to glean information from their article, except to note that they were unable to constrain a model (either disk or elliptical) to the surface brightness profile.

A detailed inspection of our images (see Figure 5.42) shows that the eastward extension is separated by 2.6 arcsec. High resolution images taken under excellent conditions show that the object is clearly a galaxy (R. Falomo, 1993, private communication). This galaxy was not detected by FOCAS because it is too close to the BL Lac, but we have added it *a posteriori*. If at the same redshift, the projected distance is only 15 kpc, analogous to the companion galaxy of PKS 2155–304.

While the radial galaxy distribution shows a reasonably strong excess of galaxies within 30 arcsec of PKS 2335+031 (see Figure 5.43), this is not found to be significant.

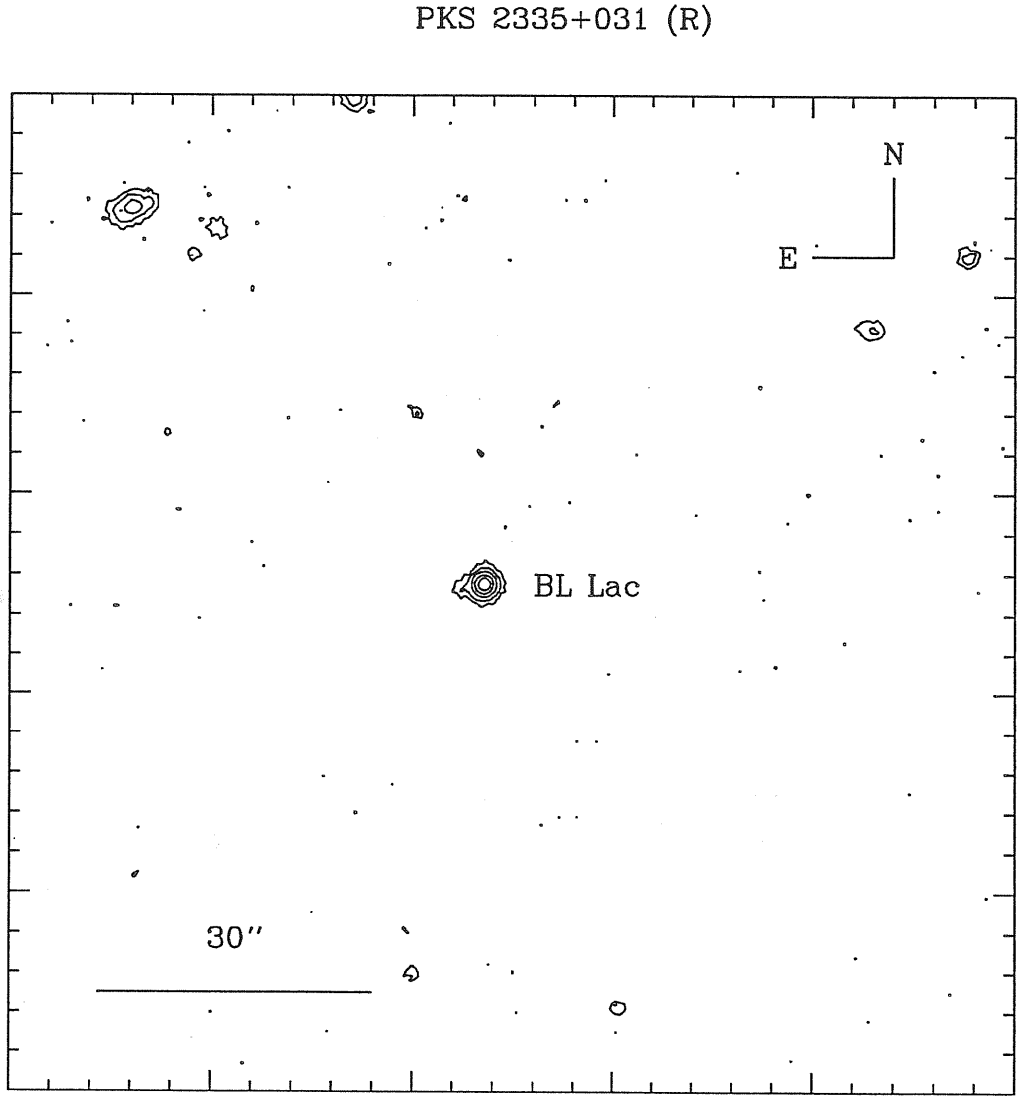

Figure 5.42: The *R*-band contour plot of the central part of the field around PKS 2335+096.

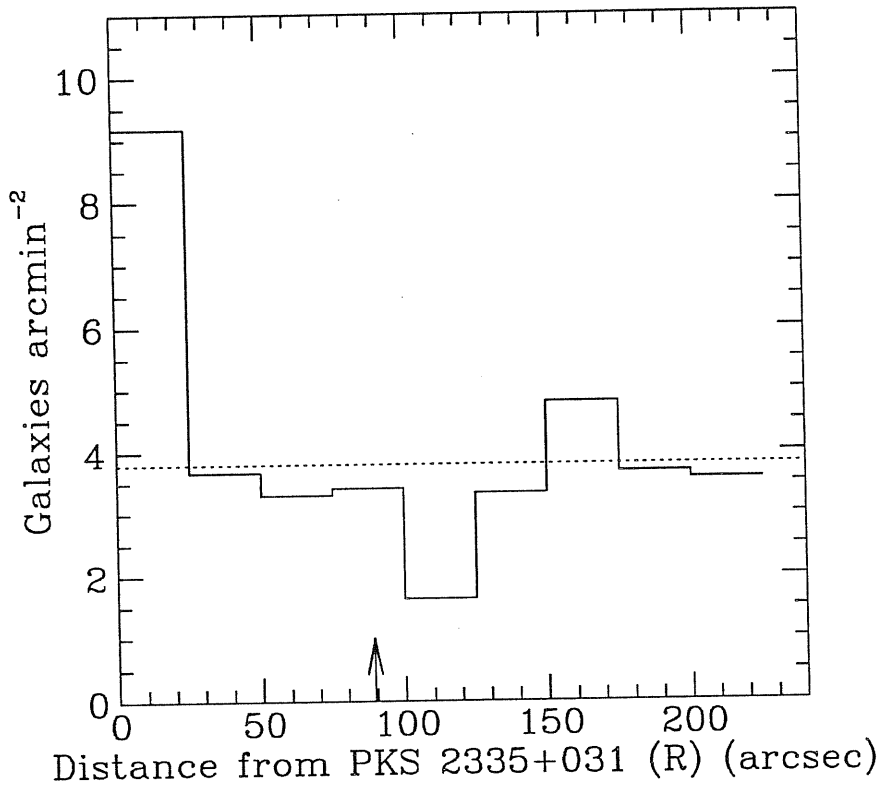

Figure 5.43: The radial distribution of galaxies around PKS 2335+031. The dashed line indicates the local background and the arrow is the 0.5 Mpc radius. The magnitude limit is 22.5.

CHAPTER VI

Discussion

In this chapter we present the discussion of our results. We start by highlighting the most important individual findings. A comparison with the studies of the quasar environments is made, and then with those of the proposed BL Lac parent population, the Faranoff-Riley radio galaxies. Finally the conclusions are given.

Table 6.1 gives a listing of the spectroscopy results for seven BL Lacs. We have also included PKS 0301–243 and PKS 2335+031, for which extremely close companions were detected. Spectra of these companions have not been obtained, and hence it remains to be seen if they are associated with the BL Lac object. Furthermore, spectroscopy confirms the redshift of two BL Lacs, PKS 1400+162 and PKS 2005–489.

Our analysis shows the X-ray BL Lac, H 0414+009, to be located in a cluster environment of Abell richness class 0. This object is the first BL Lac to be found in such an environment, the richest in our sample. Three galaxies surrounding H 0414+009 are found at the same redshift as the BL Lac. Of these, two are most likely interacting spiral galaxies.

Another very interesting object is PKS 2155–304, also found in an unusual environment. This source is surrounded by several galaxies sharing its redshift, the closest of which has a projected distance of only 11 kpc. If this is indeed the true distance, the two objects are almost certainly interacting, though we find no evidence for such interactions.

Located 300 kpc away from PKS 2155–304 is a large elliptical galaxy (G4, the second brightest galaxy in the field) at the same redshift as the BL Lac. This elliptical is itself surrounded by numerous faint galaxies. We hypothesize the existence of a 'double' cluster, such as Coma, with PKS 2155–304 and G4 forming the centers of subgroupings of galaxies.

Table 6.1: Observed galaxies in the fields of BL Lac objects.

Object	z_{BL}	Galaxy	z_{gal}	Distance		PA
				arcsec	kpc	
PKS 0301–243	...	G1	...	6.5	...	315
H 0414+009	0.287	A1	0.288	40	215	134
		A2	0.289	39	210	126
		B2	0.284	22	117	126
		C1	0.21:	33	...	307
PKS 0829+046	0.18	G1	0.24	5	...	190
		G2	0.204	27	116	85
H 1101–232	0.186	G1	0.187	104	419	225
		G2	0.14	134	...	229
PKS 1400+162	0.244	G1 (I)	0.224	6	...	215
		G2 (D)	0.230	20	...	35
PKS 1514–241	0.0486	G1	0.0486	64	83	26
PKS 2005–489	0.071	G1	0.071	48	88	15
		G2	0.071	74	136	70
		G [a]	0.069	56	100	330
PKS 2155–304	0.116	G1	0.117	4	11	70
		G2	0.116	25	70	135
		G3	0.116	113	315	357
PKS 2335+031	0.31	G1	...	2.6	...	90

[a] Results from Stickel, Fried, & Kühr (1993).

A similar case is that of H 1101–232, for which we find a galaxy 400 kpc distant to have the same redshift as the BL Lac host. The field around the source is rich in galaxies, one of which is shown to be a foreground LINER (a type of active galaxy). The fact that the field is rich in galaxies and that a galaxy 0.4 Mpc from the BL Lac shares its redshift may indicate the presence of a large, rich cluster. A further interesting observation is that the immediate area surrounding the BL Lac seems to be devoid of galaxies (this is evident in the galaxy density distribution shown in Chapter V, Figure 5.16). The lack of nearby galaxies may indicate a 'cleaning' of the neighborhood by the BL Lac.

We find one galaxy near PKS 1514–241 at the same redshift as the BL Lac. These two objects may be interacting. Our discovery of two galaxies surrounding PKS 2005–489 with the same redshift, brings to three the number of galaxies associated with this BL Lac. For PKS 0829+046 we find a background LINER and a galaxy which may be associated with the BL Lac.

Our only 'negative' spectroscopic result has been for the case of PKS 1400+162, historically the first BL Lac found to be associated with a cluster. We are unable to confirm the redshift for the galaxy nearest to the source, but, instead, find evidence for a foreground grouping.

The case of PKS 1538+149 is particularly interesting. The BL Lac is surrounded by a higher-than-average density of galaxies. It is also located about 1 Mpc from a rich, distant cluster. Average colors and magnitudes of the cluster members indicates a redshift of between 0.3 and 0.6 (the BL Lac has $z = 0.605$). We note the angular correlation amplitude, calculated for a radius of 1 Mpc from PKS 1538+149, is extremely large and highly significant (see Table 6.2). These results may imply that PKS 1538+149 is the dominant galaxy of a small group or cluster on the outskirts of a larger system. Redshifts of some of the cluster galaxies will quickly provide answers to these speculations.

Our imaging of MS 1402+042 may indicate that the tentative redshift ($z = 0.2$) of this X-ray selected object is incorrect. The source may be found to have a higher redshift.

6.1 Comparisons with Other Studies

6.1.1 The Environment of Quasars

Yee & Green (1984) performed the first systematic, quantitative survey of the galaxies associated with quasars by determining the galaxy-quasar angular correlation amplitudes (A_{gq}). Their sample consisted of 108 quasars, both radio loud and radio quiet, and with redshifts in the range 0.05 – 2.05. The survey shows that there is a clear excess of galaxies around the quasars. Clustering is observed only for objects with $z < 0.5$, and there is no significant excess of galaxies around quasars with $z > 0.5$. This result is, however, an observational effect due to the magnitude limit of the survey (equivalent to first-ranked cluster galaxies at $z \sim 0.5$). In fact, in this study, the data are of sufficient depth only for objects to $z \sim 0.3$.

On average, the quasars are in significantly richer associations than the average galaxy, but not in clusters richer than Abell richness class 0. There are a few exceptional cases (*e.g.* 3C 206, at $z = 0.198$ and in an Abell richness class 1 cluster; Ellingson *et al.* 1989).

A follow-up survey was obtained by Yee & Green (1987) which permitted the analysis of clustering properties to $z = 0.65$. For the objects with $0.3 < z < 0.5$, the results were similar to those of Yee & Green (1984): A higher-than-average density (consistent with an Abell richness class of 0), but not rich clusters. For the nine radio loud quasars in the range $0.55 < z < 0.65$, on the other hand, these researchers found significantly richer environments, with more than one-half of the sample in clusters of Abell richness class 1 or richer. The environment of the high redshift objects is a factor of four times richer than for the low redshift sample.

Yee & Green took this fact as evidence for strong luminosity evolution of radio loud quasars in rich environments, with a dimming of several magnitudes from $z = 0.6$ to $z = 0.3$. Quasars in environments richer than Abell class 0 evolve more rapidly than those in poorer environments (Ellingson, Yee, & Green 1991).

Moreover, Yee & Green (1984, 1987) and Ellingson, Yee, & Green (1991)

find that low redshift radio loud quasars are found in slightly richer environments than radio quiet quasars. Thus, the existence of radio emission may be a function of the environment. For radio quiet quasars the correlation amplitudes are low near the source, but can be a factor of three times higher farther away (1 – 2 Mpc), perhaps suggesting that these objects are found near the edges of rich clusters (Yee 1992).

Qualitatively our results are consistent with the findings for quasars. On average we observe an excess of galaxies around the BL Lacs (see Figure 6.1). In this figure we plot the average density of galaxies around the targets in bins of 30 arcsec. While this diagram does not include corrections for magnitude limits (which should be small) or redshift differences, it shows the major result of our analysis; there is a slight but significant excess of galaxies around BL Lac objects.

In order to quantitatively compare the samples, the normalized angular correlation amplitudes (defined above, in Chapter V) are useful. From the values in Table 6.2 we determine an average $\langle A_{gBL}/A_{gg} \rangle$ for our sample (with $\langle z \rangle = 0.37$) of 6.9 ± 4.9, excluding the three objects without redshifts and the two low redshift BL Lacs, PKS 1514–241 and PKS 2005–489 (all errors quoted are the standard deviations). We stress, however, that the full dataset is not a real sample in the statistical sense.

Excluding objects with $z > 0.5$ from the sample of Yee & Green (1984), the average redshift is 0.22. Their average normalized amplitude, $\langle A_{gq}/A_{gg} \rangle$, is 6.5 ± 2.7. Similarly, from Yee & Green (1987), for $\langle z \rangle = 0.41$ the average value is 5.9 ± 2.8 while for $\langle z \rangle = 0.64$ the average is 7.3 ± 2.8.

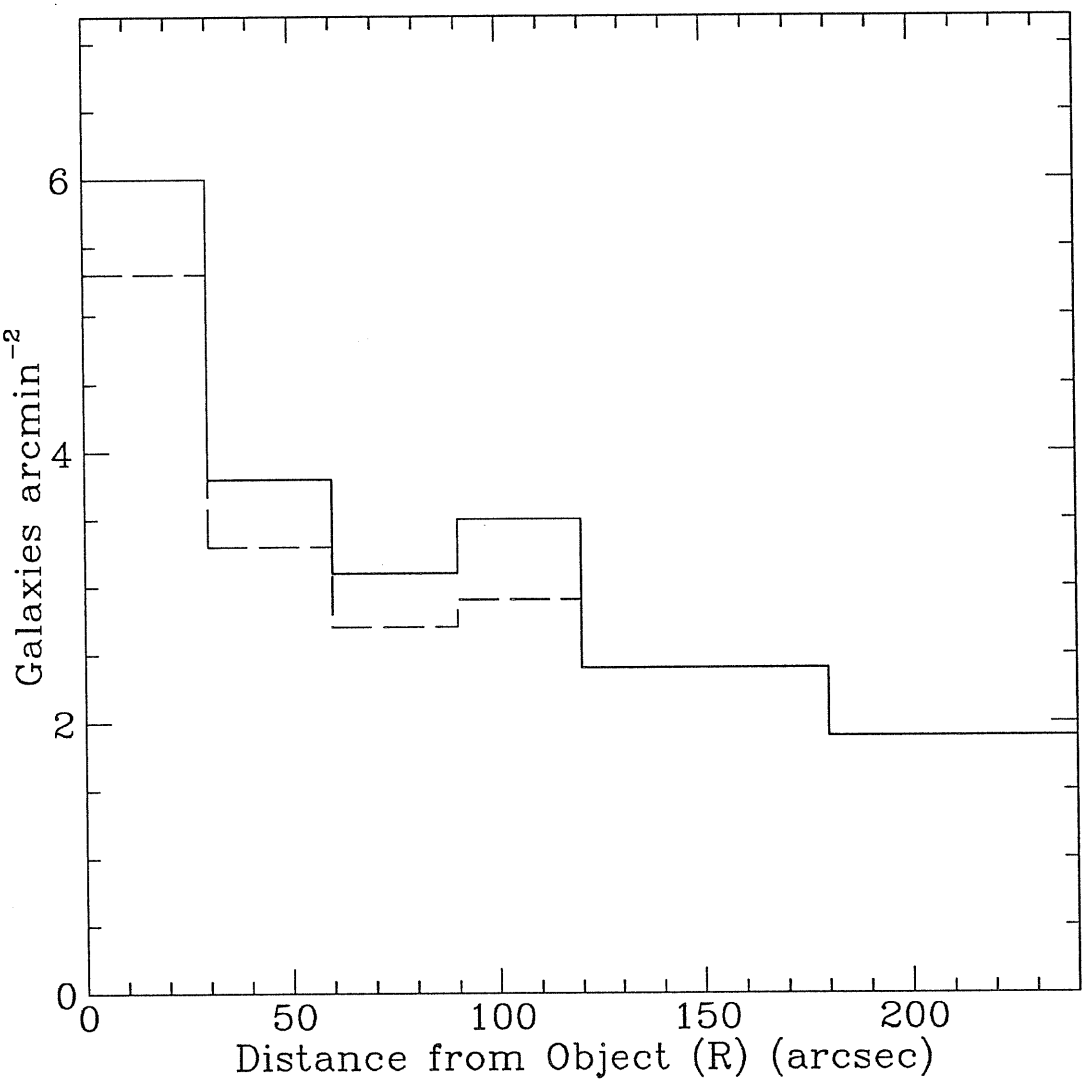

Figure 6.1: The average radial galaxy density distribution for the entire sample (minus H 1722+119), dashed line, and for a cleaned subsample (minus PKS 0301–243, PKS 0537–441, PKS 0829+046, PKS 1514–241, PG 1553+113, H1722+119), solid line. The average background is approximately 2 – 2.5 galaxies arcmin^{-2}.

6.1.2 The Environment of Radio Galaxies

Based on a statistical analysis of low redshift F-R I ($\langle z \rangle = 0.032$) and F-R II ($\langle z \rangle = 0.064$) radio galaxies, Prestage & Peacock (1988, see *erratum*, 1989) concluded that F-R I galaxies inhabit richer clusters than do F-R II galaxies. The average F-R I environment is approximately equivalent to an Abell richness class 0 cluster.

Higher redshift samples were analyzed by Yates, Miller, & Peacock (1989; mostly F-R II galaxies with $0.15 < z < 0.82$) and by Hill & Lilly (1991; $\langle z \rangle = 0.48$ for F-R II sources and $\langle z \rangle = 0.42$ for F-R I sources). These studies found that high redshift F-R II galaxies are found in richer environments than F-R I galaxies, while for the latter group there is no change in environment from high to low redshift. Few objects in either group are found in clusters richer than Abell class 1 (see Figure 8 of Hill & Lilly).

We note, however, that the analysis of the environments of radio galaxies is far from complete. The set of data for F-R galaxies is scarce and we can not perform a solid evaluation of the differences or similarities between their environments and those of BL Lacs.

With this caveat in mind, we compare our values of $N_{0.5}$ for BL Lacs to those of the $z \sim 0.5$ sample of Hill & Lilly. For the $z \sim 0.05$ sample of Prestage & Peacock, and the sample of Yates, Miller, & Peacock, we calculate $N_{0.5}$ using the reported values of the spatial correlation amplitude (B_{gg}) and the empirical relation, $B_{gg} = 34 \times N_{0.5}$ (Hill & Lilly 1991).[1] Finally, we directly compare our normalized angular correlation amplitudes (A_{gBL}/A_{gg}) to those of Yates, Miller, & Peacock (1989).

The distribution of $N_{0.5}$ for our entire sample is shown in Figure 6.2, compared with the entire samples of Yates, Miller, & Peacock, Hill & Lilly, and Prestage & Peacock, without distinguishing between F-R I and II galaxies.

[1]The reader is reminded that the values of $N_{0.5}$ corresponding to Abell richness classes of 0, 1, and 2, are 12 ± 3, 20 ± 5, and 32 ± 8, respectively.

Table 6.2: Richness classifiers.

Object	z	$N_{0.5}$	A_{gBL} ($\times 10^{-2}$)	A_{gg} ($\times 10^{-3}$)	A_{gBL}/A_{gg}
(1)	(2)	(3)	(4)	(5)	(6)
0118–272	>0.559	5.5 [a]	1.38 ± 0.84	1.9	7.3 ± 4.4
0414+009	0.287	13.0	3.70 ± 1.50	2.7	13.7 ± 5.6
0537–441	0.896	2.3 [i]	1.78 ± 1.00	1.9	9.2 ± 5.3
0823+033	0.506	9.2 [b]	2.55 ± 1.20	1.9	13.4 ± 6.3
0829+046	0.18	8.5	1.19 ± 1.33	2.7	4.4 ± 4.9
1101–232	0.186	4.3 [h]	0.46 ± 1.13	1.9	2.4 ± 5.9
1400+162	0.244	6.8 [a]	1.63 ± 1.13	2.7	6.0 ± 4.2
1402+042	0.200	1.3 [a]	0.26 ± 1.10	2.7	0.96 ± 4.07
1514–241	0.0486	... [c]	–0.07 ± 0.99	1.9	–0.4 ± 5.2 [d]
1538+149	0.605	8.3 [h]	1.72 ± 1.29	1.9	9.1 ± 6.8
...	...	...	5.52 ± 1.12	1.9	29.1 ± 5.9 [e]
1749+096	0.322	3.7 [h]	1.20 ± 2.13	3.6	3.3 ± 5.9
2005–489	0.071	... [c]	2.81 ± 1.03	1.9	14.5 ± 5.4 [f]
2155–304	0.116	7.2 [g]	3.50 ± 0.91	2.7	12.96 ± 3.37
2335+031	0.31	0.0	–0.05 ± 0.83	1.4	–0.4 ± 5.9

Column descriptions: (1) Object name; (2) Redshift; (3) Background corrected counts within 0.5 Mpc (richness); (4) Galaxy - BL Lac angular correlation amplitude, calculated for R < 0.5 Mpc; (5) Galaxy - Galaxy angular correlation amplitude, using average background values; (6) Ratio of columns (4) and (5).

Notes:

[a] For richness calculations, $m_3 + 2$ is fainter than the magnitude limit, thus the richness is calculated for $m < R_{\rm lim}$ and is underestimated.

[b] Since m_3 appears to be foreground, m_4 (= 19.16) was used. With m_3, $N_{0.5} = 2.9$.

[c] Entire field is within 0.5 Mpc.

[d] A_{gBL} is calculated for r = 0.2 Mpc, the largest, complete radius.

[e] For r = 1 Mpc.

[f] A_{gBL} is calculated for r = 0.26 Mpc, the largest, complete radius.

[g] Since m_3 appears to be foreground, m_4 (= 17.88) was used. With m_3, $N_{0.5} = 2.1$.

[h] $N_{0.5}$ and A_{gBL}/A_{gg} may be low due to an (anomalously) high local background.

[i] The image is probably not deep enough, and/or the redshift is too high.

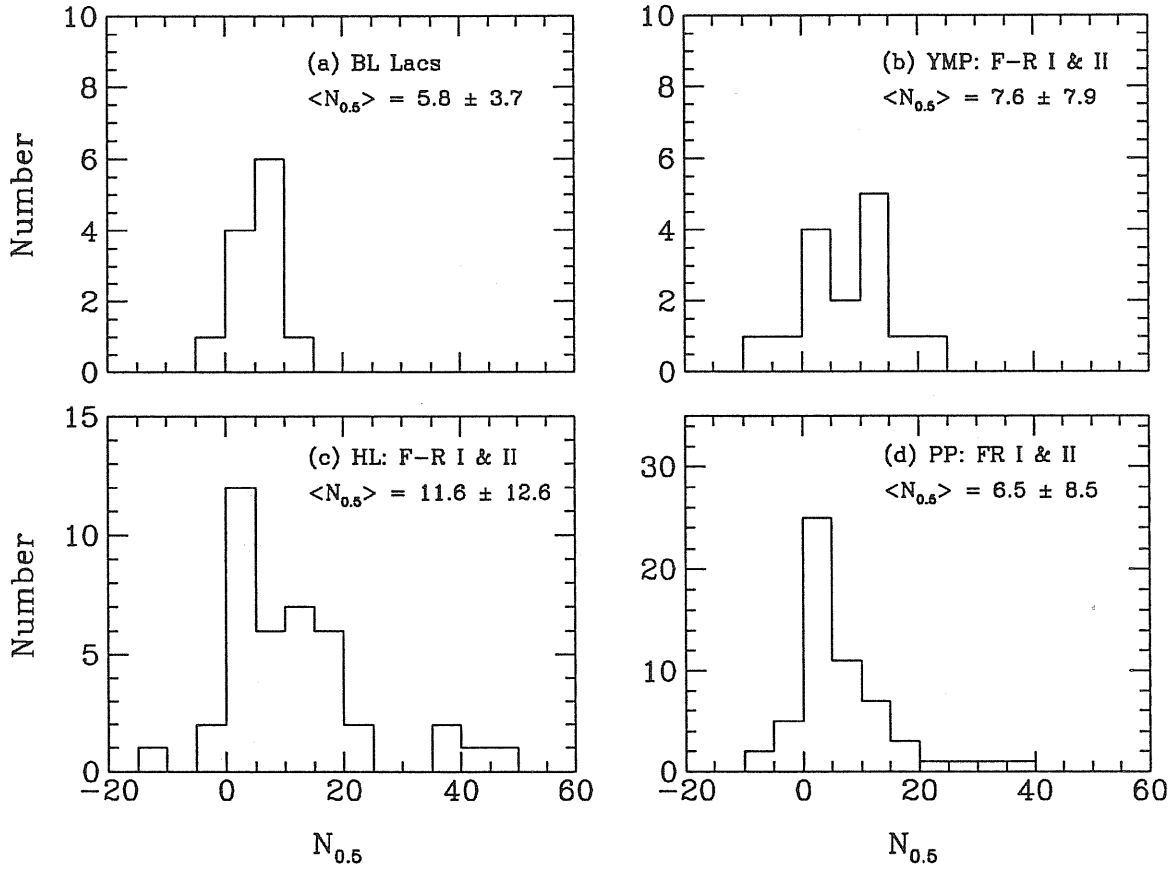

Figure 6.2: The distributions of $N_{0.5}$ for the combined samples of F-R I and II galaxies from Yates, Miller, & Peacock (1989), Hill & Lilly (1991), and Prestage & Peacock (1988) compared to the distribution of our BL Lacs.

Figure 6.3 shows the distribution of $N_{0.5}$ for the high redshift sample of Hill & Lilly (top and center left panels) and for the low redshift sample of Prestage & Peacock (top and center right panels). Our data for two redshift bins are shown in the bottom panels. We see that the distributions of $N_{0.5}$ in both redshift bins are consistent with those for F-R I and II galaxies. With the present data it is not possible, however, to determine whether or not the environments of BL Lacs are more similar to those of F-R I or II galaxies.

The $N_{0.5}$ values versus redshift are compared to the values for radio galaxies from Prestage & Peacock, Yates, Miller, & Peacock, and Hill & Lilly in Figure 6.4a. We note no redshift correlation with our data, which is very similar to the sample of Yates, Miller, & Peacock. The redshift correlation for F-R II galaxies, as noted by Hill & Lilly, is evident. We see that both F-R radio galaxies and BL Lacs are, in general, slightly less rich than Abell richness class 0 clusters, though some objects are found in richer clusters (*e.g.* H 0414+009).

Combining the three samples we calculate, for F-R I galaxies, $\langle N_{0.5} \rangle = 7.1 \pm 8.3$ and for F-R II galaxies, $\langle N_{0.5} \rangle = 9.5 \pm 11.5$. Our average value for BL Lacs, $\langle N_{0.5} \rangle = 5.8 \pm 3.7$, is consistent with the values for radio galaxies.

A Kolmogorov-Smirnov test was employed to determine differences between the samples based on the $N_{0.5}$ values. With the caveat of small numbers, we find no significant ($P \geq 95\%$) difference between BL Lacs and F-R I and II galaxies, either at high or low redshift. There is a slightly significant difference between the $N_{0.5}$ values of BL Lacs and F-R II galaxies, specifically those at high redshift ($P > 95\%$). This, however, is due to the six radio galaxies in rich environments ($N_{0.5} > 20$).

Figure 6.4b shows the distributions of the normalized angular correlation amplitude with redshift. As for $N_{0.5}$ there is no redshift correlation. The values for BL Lacs are in close agreement with those for radio galaxies (though these have a rather large spread). The average for radio galaxies is 13 ± 14 while we find an average of 7 ± 5. Another way of comparing the angular correlation amplitudes is shown in Figure 6.5.

There is a difference (though slight; $P = 96\%$) between the BL Lac sample and the sample of Yates, Miller, & Peacock, based on the A/A_{gg} values. However, when the large, highly uncertain value at $z = 0.3$ (in the sample of Yates, Miller, & Peacock) is removed, the two samples are not significantly different.

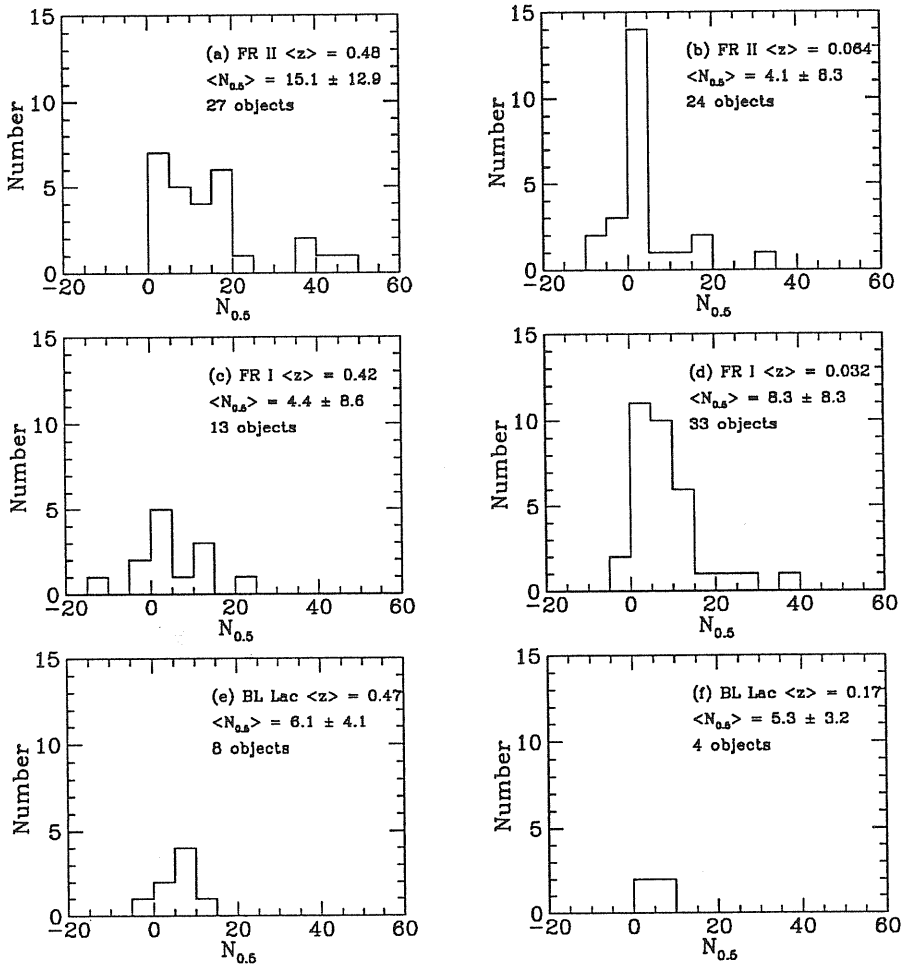

Figure 6.3: The distributions of $N_{0.5}$ for low and high redshift objects and for F-R I and II galaxies compared to the distributions for our BL Lacs in two redshift bins.

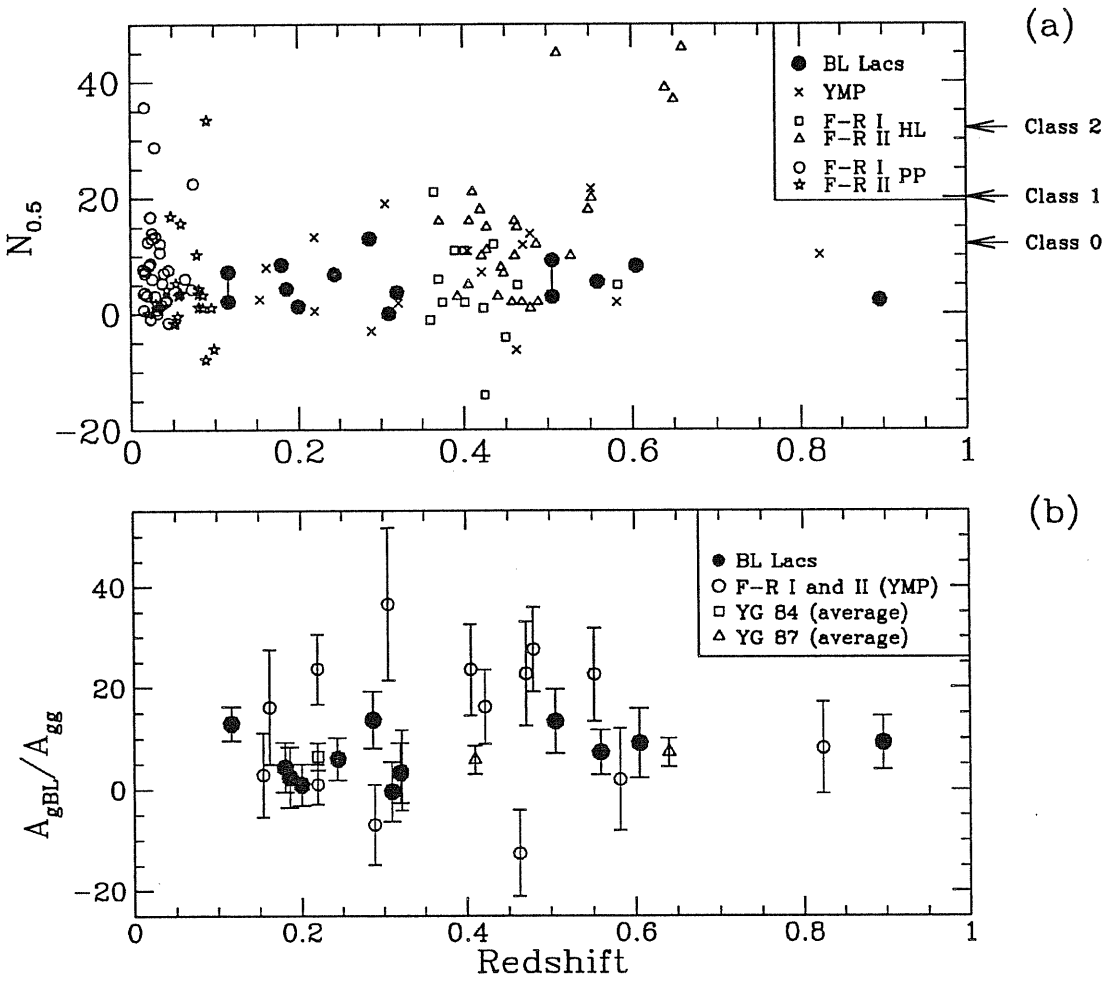

Figure 6.4: (a) $N_{0.5}$ for BL Lacs and for three samples of radio galaxies versus redshift. The values of $N_{0.5}$ for Abell richness class 0, 1, and 2 clusters are depicted to the right. (b) The values of the normalized angular correlation amplitude for radio galaxies from Yates, Miller, & Peacock (1989) compared to those for our BL Lacs. Also shown are the average values for quasars from Yee & Green (1984, 1987).

Table 6.3: Interstudy Comparisons.

	$\langle N_{0.5} \rangle$	$\langle A/A_{gg} \rangle$	$\langle z \rangle$	
		BL Lacs		
	5.8 ± 3.7	6.9 ± 4.9	0.37	
		Radio Galaxies		
YMP	7.6 ± 7.9	13 ± 14	0.39	
PP	6.5 ± 8.5	...	0.048	
HL	11.6 ± 12.6	...	0.45	
F-R I	7.1 ± 8.3	...	0.14	combined samples
F-R II	9.5 ± 11.5	...	0.31	combined samples
		Radio loud Quasars		
YG84	...	6.5 ± 2.7	0.22	
YG87	...	5.9 ± 2.8	0.41	
	...	7.3 ± 2.8	0.64	

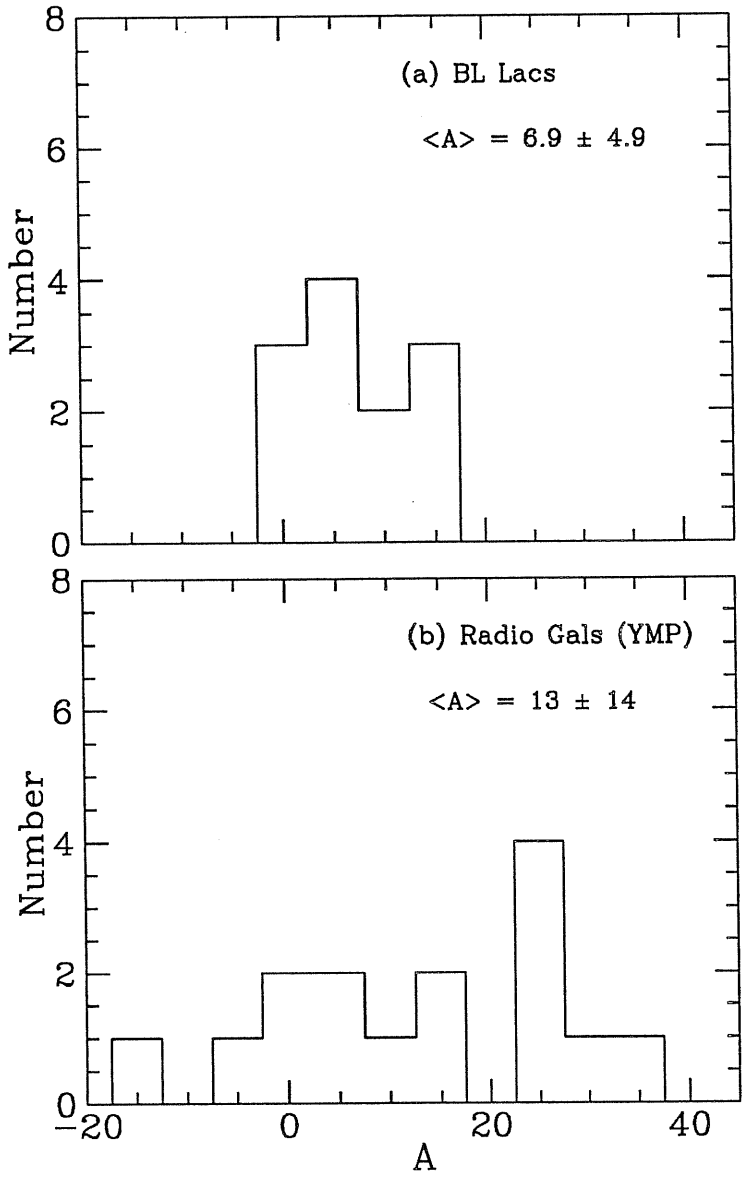

Figure 6.5: The distribution of our angular correlation amplitudes compared to those for radio galaxies from Yates, Miller, & Peacock (1989).

A summary of the results for BL Lacs, radio galaxies, and radio loud quasars is given in Table 6.3.

6.2 Conclusions

We have presented imaging results for seventeen BL Lacertae objects and spectroscopy for galaxies around a subsample of seven targets. This analysis is one of the first such surveys to date.

Our major conclusion is that BL Lacs are often located in regions of higher-than-average galaxy density. In all but one of the seven cases, we demonstrate spectroscopically the physical association of the BL Lac with at least one other galaxy in the field.

A further point which deserves some attention refers to the projected distance of the galaxies which have the same redshift of the BL Lacs. These are reported in Table 6.1. In five cases the BL Lacs have very close ($\lesssim$ 5 arcsec) companion galaxies and there are various examples of galaxies with distances $<$ 90 Kpc from the target, which suggests a search for tidal distortion or for line absorption in extended halos.

The nuclear activity of BL Lacs may be caused by interactions, as seems to be the case for quasars, where studies (*e.g.* Hutchings, Campbell, & Crampton 1982, 1984; Hutchings & Campbell 1983; Hutchings *et al.* 1984; Hutchings & Neff 1990, 1992) indicate that these objects are commonly found with companion galaxies and show signs of interactions. There is growing evidence that these interactions fuel the nuclear engine leading to activity (*e.g.* Hutchings *et al.* 1984; De Robertis 1985; Hutchings & Neff 1990, 1992).

Much more work needs to be done in obtaining high resolution images of BL Lacs to look for companions and/or signs of interactions. Similarly for F-R I galaxies, high resolution imaging will support the preliminary evidence indicating that these objects frequently have companion galaxies.

The clusters around BL Lacs are rarely very rich, the average being just consistent with an Abell richness class of 0, a result confirmed by two independent richness indicators ($N_{0.5}$ and A_{gBL}/A_{gg}). Thus, BL Lacs are the dominant members of small groups or poor clusters. The conclusions of our large imaging and spectroscopic analysis are consistent with other recent studies (*e.g.* Fried, Stickel, & Kühr 1993; Smith, O'Dea, & Baum 1993; Wurtz *et al.* 1993a, 1993b).

These were, however, all imaging studies of, in most cases, a small number of objects.

We demonstrate that the environments of BL Lacs are consistent with those of the proposed parent population, the F-R class of radio galaxies. This finding is similar to that reached by Smith, O'Dea, & Baum (1993) in an analysis of BL Lac environments. Because the data for radio galaxies, from the literature, are limited, we are unable to differentiate between the environments of F-R I and F-R II galaxies, and our comparisons are as of yet inconclusive.

Our sample is not statistically complete. Thus, future work would require observations of both XBL and RBL over a large redshift range to search for differences between these two subgroups, and evolutionary changes in BL Lacs and their environments. In addition, observations of both radio galaxy and OVV environments will allow comparisons with those of BL Lacs.

For nearby objects ($z \lesssim 0.1$), large scale CCDs are required, but the clustering properties can also be determined from an analysis of the Palomar or ESO Schmidt sky survey plates. Intermediate redshift ($0.1 \lesssim z \lesssim 1$) BL Lacs can be observed with large telescopes providing fields of view of 10 arcmin or more, while for higher redshift objects, observations with the *Hubble Space Telescope* are necessary.

* * *

References

Abell, G. O., 1958. *Astrophys. J. Suppl.*, **3**, 211.

Abraham, R. G., M^{c}Hardy, I. M., & Crawford, C. S., 1991. *Mon. Not. R. astr. Soc.*, **252**, 482.

Allen, R. G., Smith, P. S., Angel, J. R. P., Miller, B. W., Anderson, S. F., & Margon, B., 1993. *Astrophys. J.*, **403**, 610.

Antonucci, R. R. J., 1993. *Ann. Rev. Astron. Astrophys.*, in press.

Antonucci, R. R. J., Hickson, P., Olszewski, E. W., Miller, J. S., 1986. *Astron. J.*, **92**, 1.

Antonucci, R. R. J., & Ulvestad, J. S., 1985. *Astrophys. J.*, **294**, 158.

Arp, H., Sargent, W. L. W., Willis, A. G., & Oosterbaan, C. E., 1979. *Astrophys. J.*, **230**, 68.

Bahcall, N. A., 1981. *Astrophys. J.*, **247**, 787.

Baldwin, J. A., Wampler, E. J., Burbidge, E. M., O'Dell, S. L., Smith, H. E., Hazard, C., Nordsieck, K. H., Pooley, G., & Stein, W. A., 1977. *Astrophys. J.*, **215**, 408.

Barbon, R., Benacchio, L., & Capaccioli, M., 1976, *Astron. & Astrophys.*, **51**, 25.

Baxter, D. A., Disney, M. J., & Phillipps, S., 1987. *Mon. Not. R. astr. Soc.* **228**, 313.

Bender, R., Surma, P., Döbereiner, S., Möllenhoff, C., & Madejsky, R., 1989, *Astron. & Astrophys.*, **217**, 35.

Blandford, R. D., & Königl, A., 1979. *Astrophys. J.*, **232**, 34.

Blandford, R. D., & Rees, M. J., 1978. In: *The Pittsburgh Conference on BL Lacs*, ed. A. M. Wolfe, (Pittsburgh: The University of Pittsburgh Press), p. 328.

Bowyer, S., Brodie, J., Clarke, J. T., & Henry, J. P., 1984. *Astrophys. J. Lett.*, **278**, L103.

Brissenden, R. J. V., Remillard, R. A., Tuohy, I. R., Schwartz, D. A., & Hertz, P. L., 1990. *Astrophys. J.*, **350**, 578.

Browne, I. W. A., 1983. *Mon. Not. R. astr. Soc.*, **204**, 23P.

Browne, I. W. A., 1989. In: *BL Lac Objects*, eds. L. Maraschi, T. Maccacaro, & M.-H. Ulrich, (Berlin: Springer-Verlag), p. 401.

Browne, I. W. A., Crowther, J. H., & Adgie, R. L., 1973. *Nature*, **244**, 146.

Butcher, H. R., Oemler, A., Tapia, S., & Tarenghi, M., 1976. *Astrophys. J. Lett.*, **209**, L11.

Canizares, C. R., & Kruper, J., 1984. *Astrophys. J. Lett.*, **278**, L99.

Carilli, C. L., Perlman, E. S., & Stocke, J. T., 1992. *Astrophys. J. Lett.*, **400**, L13.

Coleman, G. D., Wu, C.-C., & Weedman, D. W., 1980. *Astrophys. J. Suppl.*, **43**, 393.

Colla, G, Fanti, C., Fanti, R., Gioia, I., Lari, C., Lequeux, J., Lucas, R., & Ulrich, M.-H., 1975. *Astron. & Astrophys. Suppl.*, **20**, 1.

Craine, E. R., Tapia, S., & Tarenghi, M., 1975. *Nature*, **258**, 56.

Craine, E. R., & Warner, J. W., 1976. *Astrophys. J.*, **206**, 359.

Danziger, I. J., Fosbury, R. A. E., Goss, W. M., & Ekers, R. D., 1979. *Mon. Not. R. astr. Soc.*, **188**, 415.

De Robertis, M., 1985. *Astron. J.*, **90**, 998.

Disney, M. J., 1974. *Astrophys. J. Lett.*, **193**, L103.

Disney, M. J., Peterson, B. A., & Rodgers, A. W., 1974, *Astrophys. J. Lett.*, **194**, L79.

Ellingson, E., Yee, H. K. C., & Green, R. F., 1991. *Astrophys. J.*, **371**, 49.

Ellingson, E., Yee, H. K. C., Green, R. F., & Kinman, T. D., 1989. *Astron. J.*, **97**, 1539.

Elmegreen, D. M., Elmegreen, B. G. & Bellin, A. D., 1990. *Astrophys. J.*, **364**, 415.

Falomo, R., 1991. *Astron. J.*, **102**, 1991.

Falomo, R., Giraud, E., Maraschi, L., Melnick, J., Tanzi, E. G., & Treves, A., 1991. *Astrophys. J. Lett.*, **380**, L67.

Falomo, R., Maraschi, L., Tanzi, E. G., & Treves, A., 1987. *Astrophys. J. Lett.*, **318**, L39.

Falomo, R., Melnick, J., & Tanzi, E. G., 1990. *Nature*, **345**, 692.

Falomo, R., Melnick, J., & Tanzi, E. G., 1992. *Astron. & Astrophys.*, **255**, L17.

Falomo, R., Pesce, J., & Treves, A., 1991. In: *Galaxy Environments and the Large Scale Structure of the Universe*, eds. G. Giuricin, F. Mardirossian, & M. Mezzetti, (Trieste: SISSA).

Falomo, R., Pesce, J. E., & Treves, A., 1993a. *Astron. J.*, **105**, 2031.

Falomo, R., Pesce, J. E., & Treves, A., 1993b. *Astrophys. J. Lett.*, **411**, L63.

Falomo, R., Scarpa, R., & Bersanelli, M., 1993, *Astrophys. J. Suppl.*, submitted.

Falomo, R., & Tanzi, E. G., 1991. *Astron. J.*, **102**, 1294.

Falomo, R., Tanzi, E. G., & Treves, A., 1991. *Astron. & Astrophys.*, **249**, 341.

Falomo R., & Treves, A., 1990. *Publ. Ast. Soc. Pac.*, **102**, 1120.

Falomo, R., Treves, A., Chiappetti, L., Maraschi, L., Pian, E., & Tanzi, E. G., 1993. *Astrophys. J.*, **402**, 532.

Faranoff, B. L., & Riley, J. M., 1974. *Mon. Not. R. astr. Soc.*, **167**, 31P.

Fosbury, R. A. E., & Disney, M. J., 1976. *Astrophys. J. Lett.*, **207**, L75.

Fried, J. W., Stickel, M., & Kühr, H., 1993. *Astron. & Astrophys.*, **268**, 53.

Ghisellini, G., & Maraschi, L., 1989. *Astrophys. J.*, **340**, 181.

Gioia, I. M., Maccacaro, T., Schild, R., Stocke, J. T., Liebert, J., Danziger, J., Knuth, D., & Lub, J., 1984. *Astrophys. J.*, **283**, 495.

Giommi, P., Barr, P., Gioia, I. M., Maccacaro, T., Schild, R., Garilli, B., Maccagni, D., 1986. *Astrophys. J.*, **303**, 596.

Giommi, P., Tagliaferri, G., Beuermann, K., Branduardi-Raymont, G., Brissenden, R., Graser, U., Mason, K. O., Mittaz, J. D. P., Murdin, P., Pooley, G., Thomas, H.-C., & Tuohy, I., 1991. *Astrophys. J.*, **378**, 77.

Griffiths, R. E., Tapia, S., Briel, U., & Chaisson, L., 1979. *Astrophys. J.*, **234**, 810.

Groth, E. J., & Peebles, P. J. E., 1977. *Astrophys. J.*, **217**, 385.

Halpern, J. P., Chen, V. S., Madejski, G. M., & Chanan, G. A., 1991. *Astron. J.*, **101**, 818.

Halpern, J. P., Impey, C. D., Bothun, G. D., Tapia, S., Skillman, E. D., Wilson, A. S., & Meurs, E. J. A., 1986. *Astrophys. J.*, **302**, 711.

Hartwick, F. D. A., & Schade, D., 1990. *Ann. Rev. Astron. Astrophys.*, **28**, 437.

Hill, G. J., & Lilly, S. J., 1991. *Astrophys. J.*, **367**, 1.

Hintzen, P., Romanishin, W., & Valdes, F., 1991. *Astrophys. J.*, **366**, 7.

Hunter, S. D., Bertsch, D. L., Dingus, B. L., Fichtel, C. E., Hartman, R. C., Kanbach, G., Kniffen, G., Kwok, P. W., Lin, Y. C., Mattox, J. R., Mayer-Hasselwander, H. A., Michelson, P. F., von Montigny, C., Nolan, P. L., Schneid, E., Sreekumar, P., & Thompson, D. J., 1993. *Astron. & Astrophys.*, **272**, 59.

Hutchings, J. B., & Campbell, B., 1983. *Nature*, **303**, 584.

Hutchings, J. B., Campbell, B., & Crampton, D., 1982. *Astrophys. J. Lett.*, **261**, L23.

Hutchings, J. B., Crampton, D., & Campbell, B., 1984. *Astrophys. J.*, **280**, 41.

Hutchings, J. B., Crampton, D., Campbell, B., Duncan, D., & Glendenning, B., 1984. *Astrophys. J. Suppl.*, **55**, 319.

Hutchings, J. B., & Neff, S. G., 1990. *Astron. J.*, **99**, 1715.

Hutchings, J. B., & Neff, S. G., 1992. *Astron. J.*, **104**, 1.

Hutchings, J. B., Johnson, I., & Pyke, R., 1988. *Astrophys. J. Suppl.*, **66**, 361.

Impey, C. D., & Neugebauer, G., 1988, *Astron. J.*, **95**, 307.

Impey, C. D., & Tapia, S., 1988. *Astrophys. J.*, **333**, 666.

Jannuzi, B. T., Smith, P. S., & Elston, R. E., 1993. *Astrophys. J. Suppl.*, **85**, 265.

Jarvis, J. F., & Tyson, J. A., 1981. *Astron. J.*, **86**, 476.

Jones, L. R., Fong, R., Shanks, T., Ellis, R. S., & Peterson, B. A., 1991. *Mon. Not. R. astr. Soc.*, **249**, 481.

Keel, W. L., 1986. *Astrophys. J.*, **302**, 296.

Kollgaard, R. I., Wardle, J. F. C., Roberts, D. H., & Gabuzda, D. C., 1992. *Astron. J.*, **104**, 1687.

Königl, A., 1989. In: *BL Lac Objects*, eds. L. Maraschi, T. Maccacaro, & M.-H. Ulrich, (Berlin: Springer-Verlag), p. 321.

Krolik, J. H., Kallman, T. R., Fabian, A. C., & Rees, M. J., 1985. *Astrophys. J.*, **295**, 104.

Kron, R. G., 1980. *Physica Scripta*, **21**, 652.

Kühr, H., Witzel, A., Pauliny-Toth, I. I. K., & Nauber, U., 1981. *Astron. & Astrophys. Suppl.*, **45**, 367.

Landolt, A. U., 1983. *Astron. J.*, **88**, 853.

Ledden, J. E., & O'Dell, S. L., 1985. *Astrophys. J.*, **298**, 630.

Maccacaro, T., Feigelson, E. D., Fener, M., Giacconi, R., Gioia, I. M., Griffiths, R. E., Murray, S. S., Zamorani, G., Stocke, J., & Liebert, J., 1982. *Astrophys. J.*, **253**, 504.

Macchetto, F., Albrecht, R., Barbieri, C., Blades, J. C., Boksenberg, A., Crane, P., Deharveng, J. M., Disney, M. J., Jakobsen, P., Kamperman, T. M., King, I. R., Makay, C. D., Paresce, F., Weigelt, G., Baxter, D., Greenfield, P., Jedrzejewski, R., Nota, A., & Sparks, W. B., 1991. *Astrophys. J. Lett.*, **369**, L55.

Madejski, G. M., & Schwartz, D. A., 1983. *Astrophys. J.*, **275**, 467.

Madejski, G. M., & Schwartz, D. A., 1989. In: *BL Lac Objects*, eds. L. Maraschi, T. Maccacaro, & M.-H. Ulrich, (Berlin: Springer-Verlag), p. 267.

Maraschi, L., Blades, J. C., Calanchi, C., Tanzi, E. G., & Treves, A., 1988, *Astrophys. J.*, **333**, 660.

Maraschi, L., Ghisellini, G., & Celotti, A., 1992. *Astrophys. J. Lett.*, **397**, L5.

M^{c}Hardy, I. M., Abraham, R. G., Crawford, C. S., Ulrich, M.-H., Mock, P. C., & Vanderspeck, R. K., 1991. *Mon. Not. R. astr. Soc.*, **249**, 742.

M^{c}Hardy, I. M., Luppino, G. A., George, I. M., Abraham, R. G., & Cooke, B. A., 1992. *Mon. Not. R. astr. Soc.*, **256**, 655.

Melia, F., & Königl, A., 1989. In: *BL Lac Objects*, eds. L. Maraschi, T. Maccacaro, & M.-H. Ulrich, (Berlin: Springer-Verlag), p. 372.

Melnick, J., Dekker, H., & D'Odorico, S., 1992, *The EMMI and SUSI ESO Operating Manual.*

Merrifield, M. R., 1992. *Astron. J.*, **104**, 1306.

Metcalfe, N., Shanks, T., Fong, R., & Jones, L. R., 1991. *Mon. Not. R. astr. Soc.*, **249**, 498.

Miller, H. R., Carini, M. T., Gaston, B. J., & Hutter, D. J., 1988. In: *A Decade of UV Astronomy with the IUE Satellite*, ESA SP-281, 303.

Miller, H. R., & Green, R. F., 1983. *Bull. A. A. S.*, **15**, 957.

Miller, J. S., French, H. B., & Hawley, S. A., 1978. In: *The Pittsburgh Conference on BL Lacs*, ed. A. M. Wolfe, (Pittsburgh: The University of Pittsburgh Press), p. 176.

Morris, S. L., Stocke, J. T., Gioia, I. M., Schild, R. E., Wolter, A., Maccacaro, T., & Della Ceca, R., 1991. *Astrophys. J.*, **380**, 49.

Mushotzky, R. F., Boldt, E. A., Holt, S. S., Pravdo, S. H., Serlemitsos, P. J., Swank, J. H., & Rothschild, R. H., 1978. *Astrophys. J. Lett.*, **226**, L65.

Narayan, R., & Schneider, D. P., 1990. *Mon. Not. R. astr. Soc.*, **243**, 192.

Nottale, L., 1986. *Astron. & Astrophys.*, **157**, 383.

Ostriker, J. P., & Vietri, M., 1985. *Nature*, **318**, 446.

Ostriker, J. P., & Vietri, M., 1990. *Nature*, **344**, 45.

Padovani, P., 1992. *Mon. Not. R. astr. Soc.*, **257**, 404.

Padovani, P., & Urry, C. M., 1990. *Astrophys. J.*, **356**, 75.

Padovani P., & Urry, C. M., 1991. *Astrophys. J.*, **368**, 373.

Peebles, P. J. E., 1980. *The Large Scale Structure of the Universe.* (Princeton, NJ: Princeton Univ. Press).

Pesce, J. E., Falomo, R., & Treves, A., 1993. *Astron. J.*, submitted.

Peterson, B. A., Jauncy, D. L., Wright, A. E., Condon, J. E., 1976. *Astrophys. J. Lett.*, **207**, L5.

Prestage, R. M., & Peacock, J. A., 1988. *Mon. Not. R. astr. Soc.*, **230**, 131.

Prestage, R. M., & Peacock, J. A., 1989. *Mon. Not. R. astr. Soc.*, **236**, 959.

Remillard, R. A., Tuohy, I. R., Brissenden, R. J. V., Buckley, D. A. H., Schwartz, D. A., Feigelson, E. D., & Tapia, S., 1989. *Astrophys. J.*, **345**, 140.

Romanishin, W., 1987. *Astrophys. J.*, **320**, 586.

Romanishin, W., 1992. *Astrophys. J. Lett.*, **401**, L65.

Sambruna, R. M., Barr, P., Giommi, P., Maraschi, L., Tagliaferri, G., & Treves, A., 1993. *Astrophys. J.*, submitted.

Sandage, A., 1966. *Astrophys. J.*, **145**, 1.

Sandage, A., 1975. *Astrophys. J.*, **202**, 563.

Sandage, A., 1978. *Astron. J.*, **83**, 904.

Schwartz, D. A., Bradt, H. V., Doxsey, R. E., Griffiths, R. E., Gursky, H., Johnston, M. D., & Schwarz, J., 1978. *Astrophys. J. Lett.*, **224**, L103.

Schwartz, D. A., & Ku, W. H.-M., 1983. *Astrophys. J.*, **266**, 459.

Schwartz, H. E., & Melnick, J., 1989. *The ESO User's Manual.*

Seldner, M., & Peebles, P. J. E., 1978. *Astrophys. J.*, **225**, 7.

Sersic, J. L., 1974, *Astrophys. & Space Sci.*, **28**, 365.

Smith, E. P., O'Dea, C. P., & Baum, S. A., 1993. *Bull. A. A. S.*, **25**, #2, 791.

Stevenson, P. R. F., Shanks, T., Fong, R., & MacGillivray, H. T., 1985. *Mon. Not. R. astr. Soc.*, **213**, 953.

Stickel, M., Fried, J. W., & Kühr, H., 1988a. *Astron. & Astrophys.*, **191**, L16.

Stickel, M., Fried, J. W., & Kühr, H., 1988b. *Astron. & Astrophys.*, **198**, L13.

Stickel, M., Fried, J. W., & Kühr, H., 1988c. *Astron. & Astrophys.*, **206**, L30.

Stickel, M., Fried, J. W., & Kühr, H., 1989. In: *BL Lac Objects*, eds. L. Maraschi, T. Maccacaro, & M.-H. Ulrich, (Berlin: Springer-Verlag), p. 64.

Stickel, M., Fried, J. W., & Kühr, H., 1993. *Astron. & Astrophys. Suppl.*, **98**, 393.

Stickel, M., Padovani, P., Urry, C. M., Fried, J. W., & Kühr, H., 1991. *Astrophys. J.*, **374**, 431.

Stocke, J. T., Liebert, J., Stockman, H., Danziger, J., Lub, J., Maccacaro, T., Griffiths, R., & Giommi, P., 1982. *Mon. Not. R. astr. Soc.*, **200**, 27P.

Stocke, J. T., Morris, S. L., Gioia, I. M., Maccacaro, T., Schild, R. E., & Wolter, A., 1989. In: *BL Lac Objects*, eds. L. Maraschi, T. Maccacaro, & M.-H. Ulrich, (Berlin: Springer-Verlag), p. 242.

Stocke, J. T., Morris, S. L., Gioia, I. M., Maccacaro, T., Schild, R., Wolter, A., Fleming, T. A., & Henry, J. P., 1991. *Astrophys. J. Suppl.*, **76**, 813.

Stocke, J. T., Wurtz, R., Wang, Q., Elston, R., & Jannuzi, B. T., 1992. *Astrophys. J. Lett.*, **400**, L17.

Stone, R. P. S., 1977. *Astrophys. J.*, **218**, 767.

Struble, M. F., & Rood, H. J., 1982. *Astron. J.*, **87**, 7.

Surdey, J., & Swings, J. P., 1981. *Astron. & Astrophys. Suppl.*, **46**, 305.

Thompson, D. J., Bertsch, D. L., Fichtel, C. E., Hartman, R. C., Hunter, S. D., Kanbach, G., Kniffen, D. A., Kwok, P. W., Lin, Y. C., Mattox, J. R., Mayer-Hasselwander, H. A., Michelson, P. F., von Montigny, C., Nolan, P. L., Pinkau, K., Schneid, E. J., & Sreekumar, P., 1993. *Astrophys. J.*, **410**, 87.

Thuan, T. X., Oke, J. B., & Gunn, J. B., 1975. *Astrophys. J.*, **201**, 45.

Tyson, J., A., 1986. *Astron. J.*, **92**, 691.

Ulrich, M.-H., 1978. *Astrophys. J. Lett.*, **222**, L3.

Ulrich, M.-H., 1989. In: *BL Lac Objects*, eds. L. Maraschi, T. Maccacaro, & M.-H. Ulrich, (Berlin: Springer-Verlag), p. 45.

Ulrich, M.-H., Kinman, T. D., Lynds, C. R., Rieke, G. H., & Ekers, R. D., 1975. *Astrophys. J.*, **198**, 261.

Ulvestad, J. S., & Antonucci, R. R. J., 1986. *Astron. J.*, **92**, 6.

Ulvestad, J. S., & Johnston, K. J., 1984. *Astron. J.*, **89**, 189.

Urry, C. M., Padovani, P., & Stickel, M., 1991. *Astrophys. J.*, **382**, 501.

Valdes, F., 1982. In: *Instrumentation in Astronomy IV*, S.P.I.E. Proceedings vol. 331, "The Resolution Classifier".

Visvanathan, N., & Griersmith, 1977. *Astrophys. J.*, **215**, 759.

Wall, J. V., Danziger, I. J., Pettini, M., Warwick, R. S., & Wamsteker, W., 1986. *Mon. Not. R. astr. Soc.*, **219**, 23p.

Wardle, J. F. C., Moore, R. L., & Angel, J. R. P., 1984. *Astrophys. J.*, **279**, 93.

Weistrop, D., Shaffer, D. B, Mushotzky, R. F., Reitsema, H. J., & Smith, B. A., 1981. *Astrophys. J.*, **249**, 3.

Weistrop, D., Shaffer, D. B., Reitsema, H. J., & Smith B. A., 1983. *Astrophys. J.*, **271**, 471.

White, G. L., Jauncey, D. L., Savage, A., Wright, A. E., Batty, M. J., Peterson, B. A., & Gulkis, S., 1988. *Astrophys. J.*, **327**, 561.

Wills, D., & Wills, B. J., 1976. *Astrophys. J. Suppl.*, **31**, 143.

Worrall, D. M., & Wilkes, B. J., 1990. *Astrophys. J.*, **360**, 396.

Wurtz, R., Ellingson, E., Stocke, J. T., & Yee, H. K. C., 1993a. *Astron. J.*, in press.

Wurtz, R., Stocke, J. T., Ellingson, E., & Yee, H. K. C., 1993b. In: *The Evolution of Galaxies and their Environments*, eds. D. Hollenbach, H. Thronson, & J. M. Shull, (Moffet Field, Calif.: NASA), p. 299.

Yates, M. G., Miller, L., & Peacock, J. A., 1989. *Mon. Not. R. astr. Soc.*, **240**, 129.

Yee, H. K. C., 1992. In: *Clusters and Superclusters of Galaxies*, ed. A. C. Fabian, (Dordrecht: Kluwer), p. 293.

Yee, H. K. C., & Green, R. F., 1984. *Astrophys. J.*, **280**, 79.

Yee, H. K. C., & Green, R. F., 1987. *Astrophys. J.*, **319**, 28.

Zensus, J. A., 1989. In: *BL Lac Objects*, eds. L. Maraschi, T. Maccacaro, & M.-H. Ulrich, (Berlin: Springer-Verlag), p. 3.

Zwicky, F., Herzog, E., Wild, P., Karpowicz, M., & Kowal, C. T., 1961-68. *Catalogue of Galaxies and Clusters of Galaxies*, (Pasadena: California Institute of Technology), in 6 volumes.

Appendixes

APPENDIX A

Images of the Program Objects

This Appendix contains the full images of the program objects, in the R-band. North is at the top and East is to the right. The dimensions are 7.5×7.5 arcmin^2.

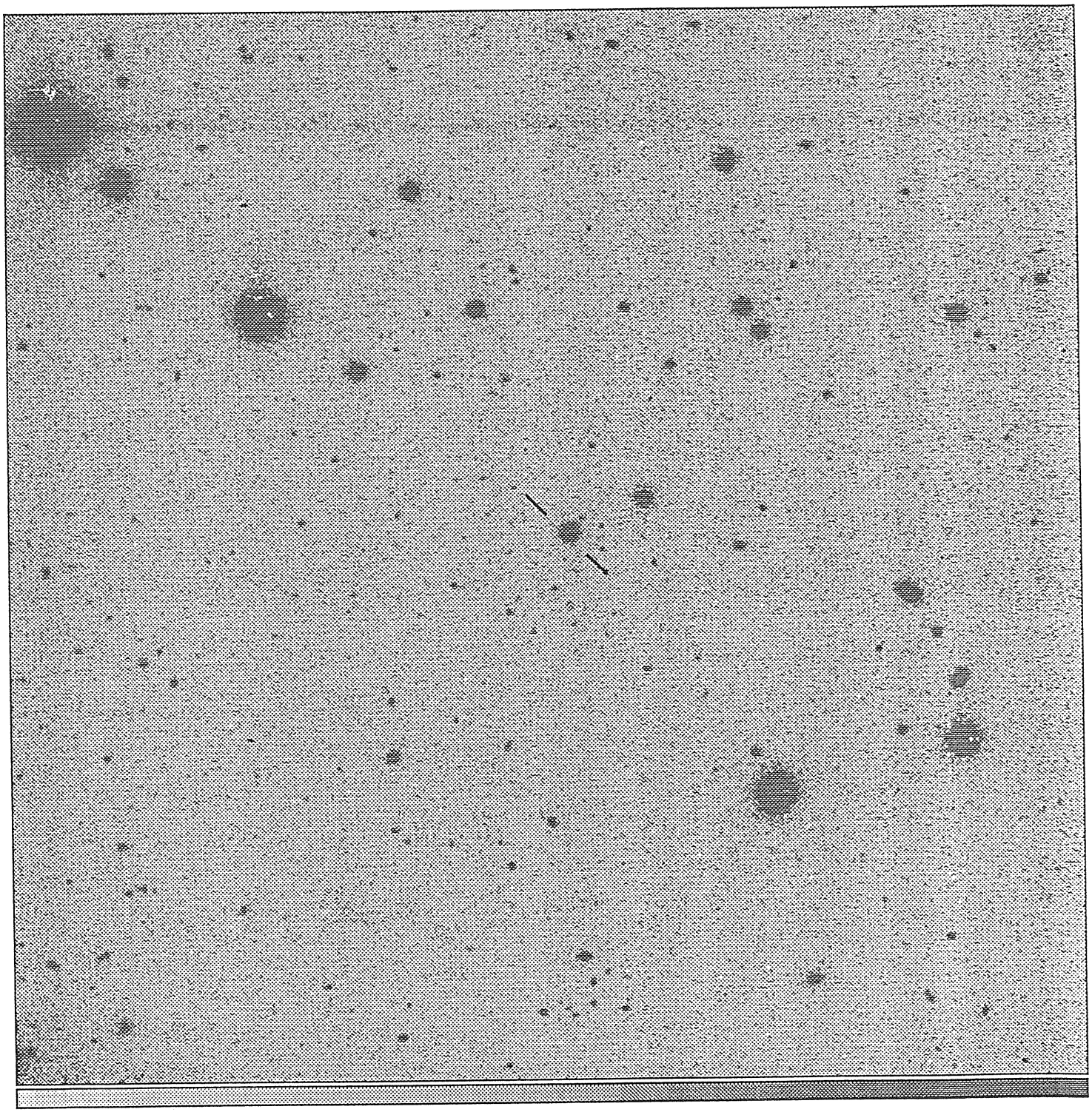

Figure A.1: PKS 0118–272 (average R frame), $z = 0.559$, exp = 260s.

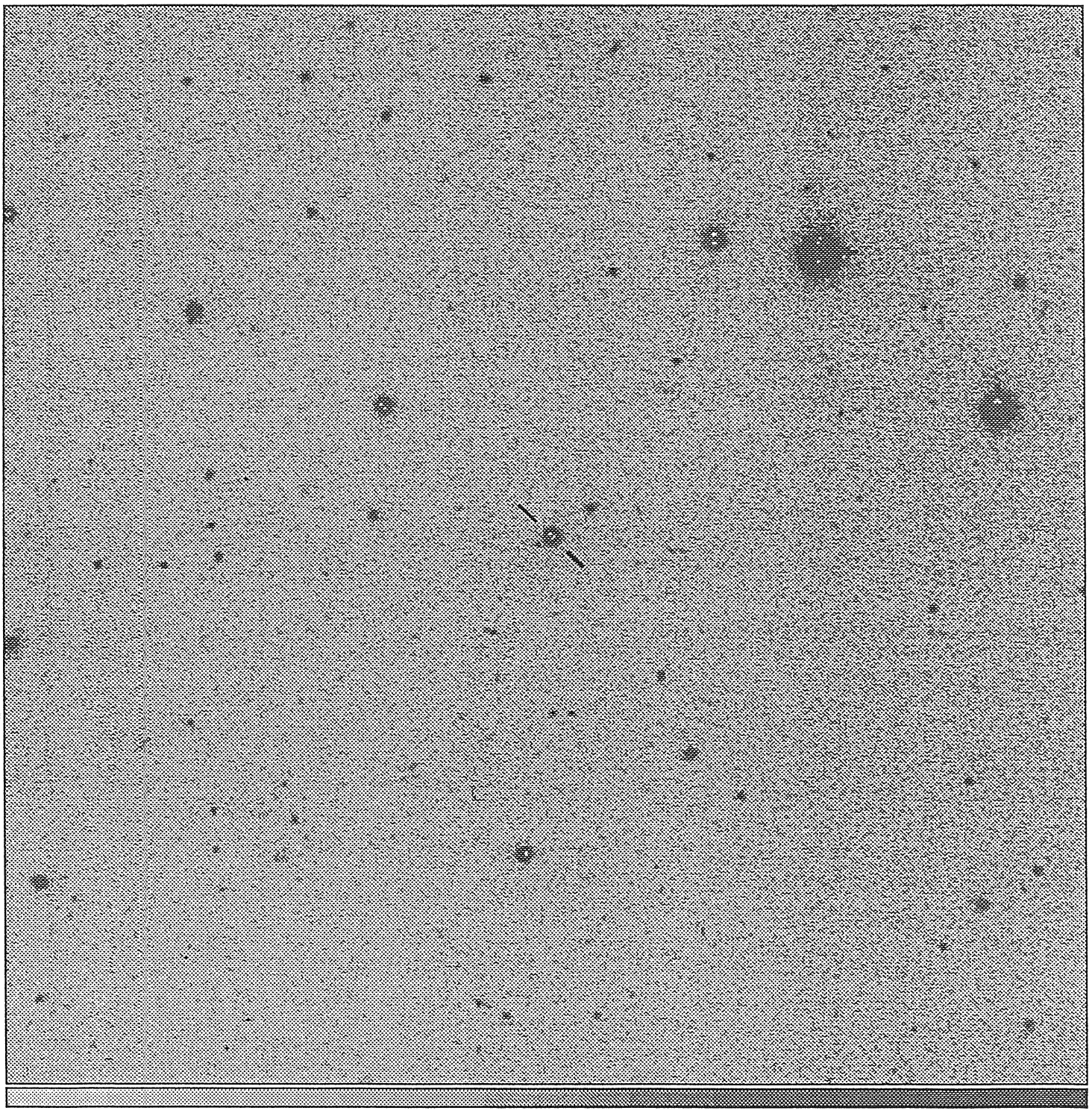

Figure A.2: PKS 0301–243 (ima048), redshift unknown, exp = 600s.

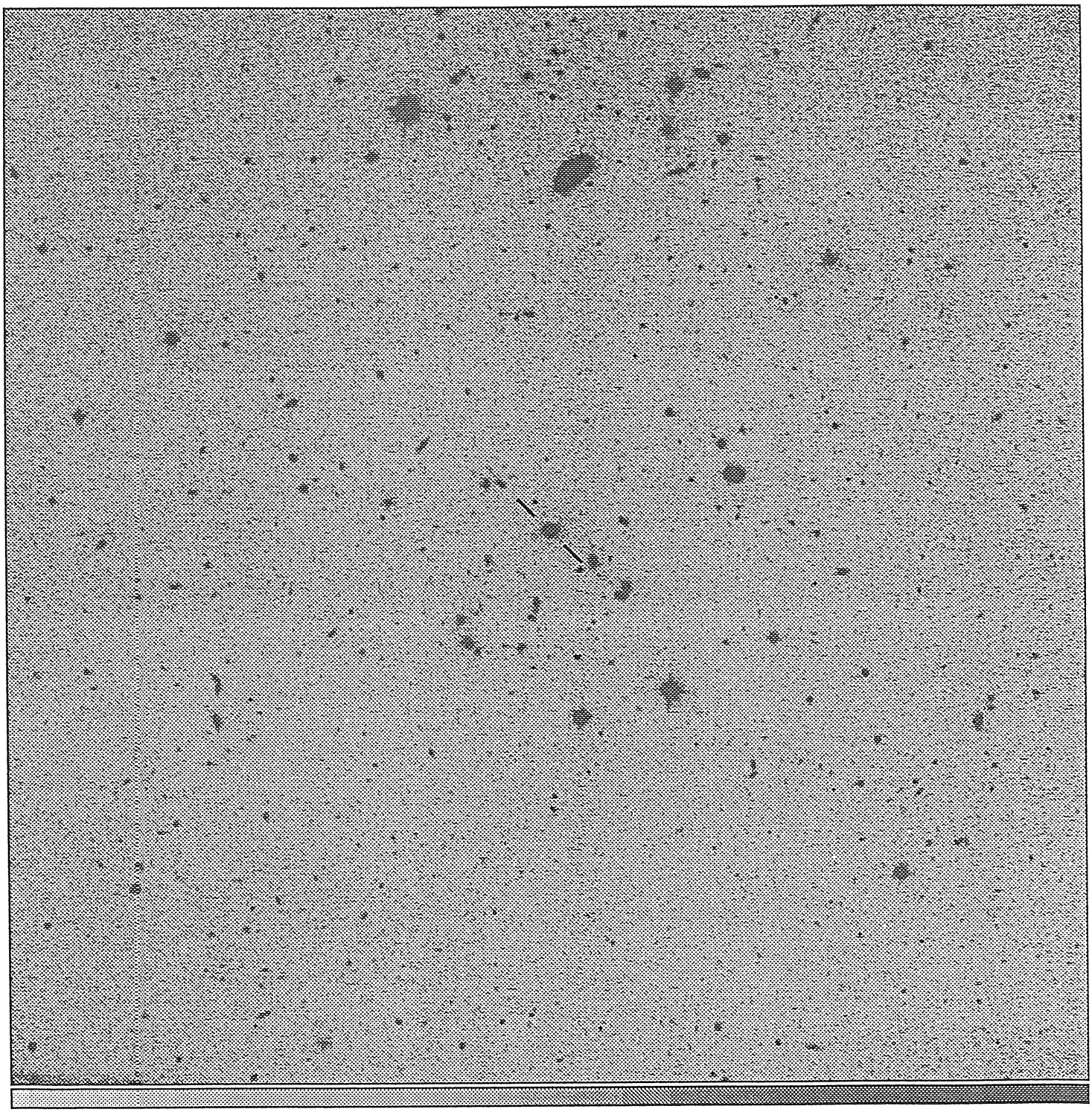

Figure A.3: H 0414+009 (average R frame), $z = 0.287$, exp = 90s.

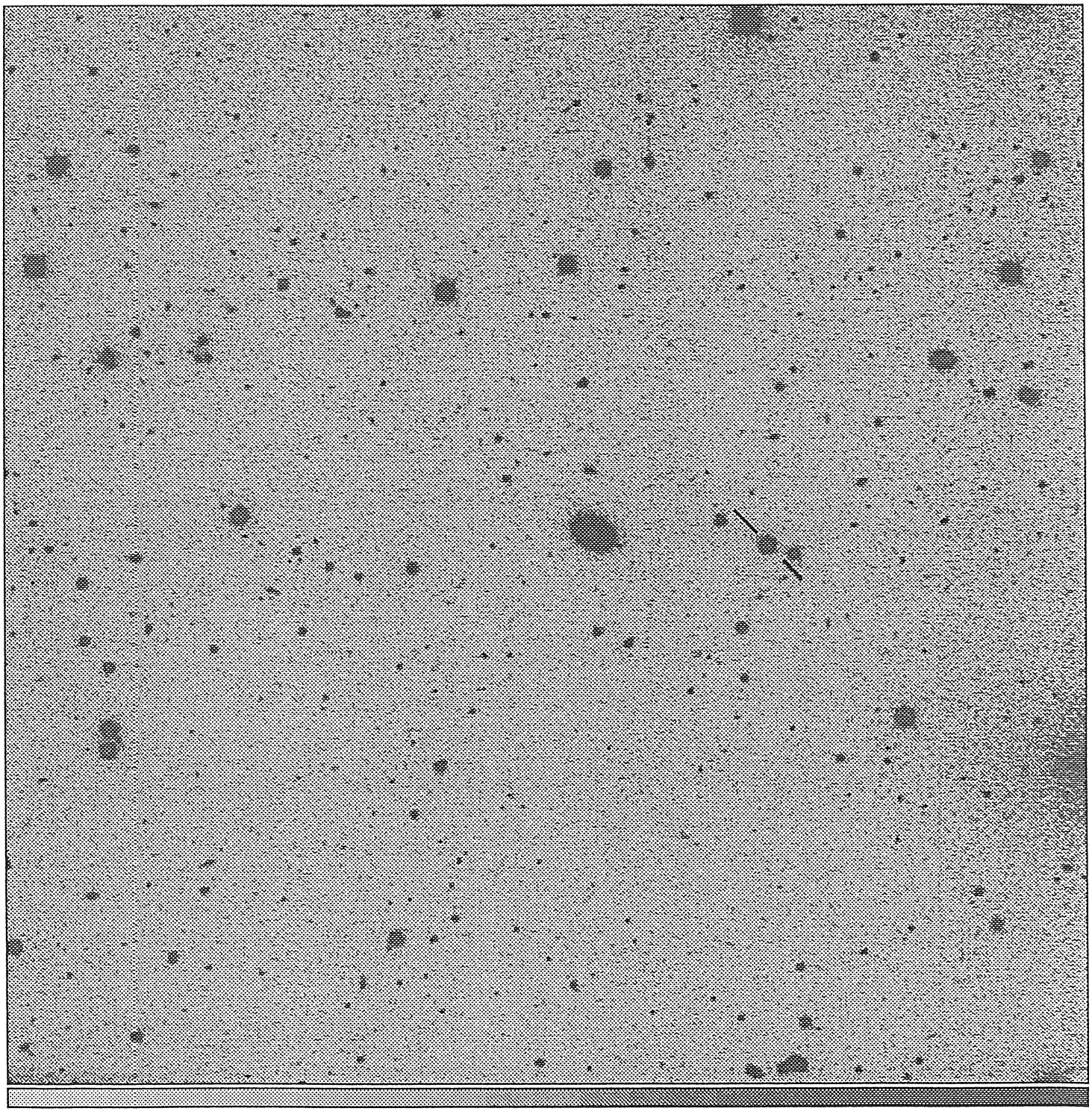

Figure A.4: PKS 0537–441 (average R frame), $z = 0.896$, exp = 180s.

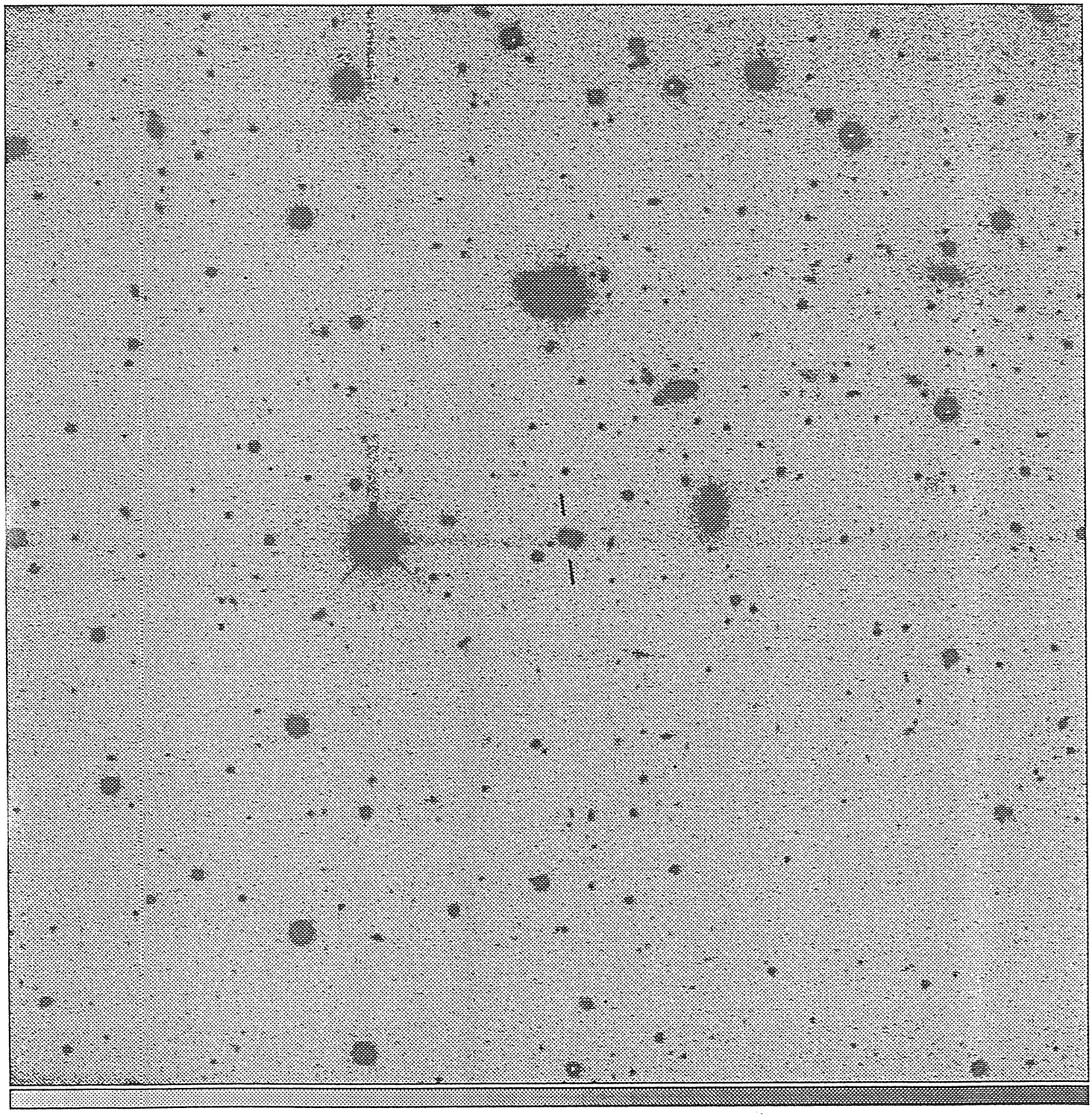

Figure A.5: PKS 0823+033 (ima004), $z = 0.506$, exp = 300s.

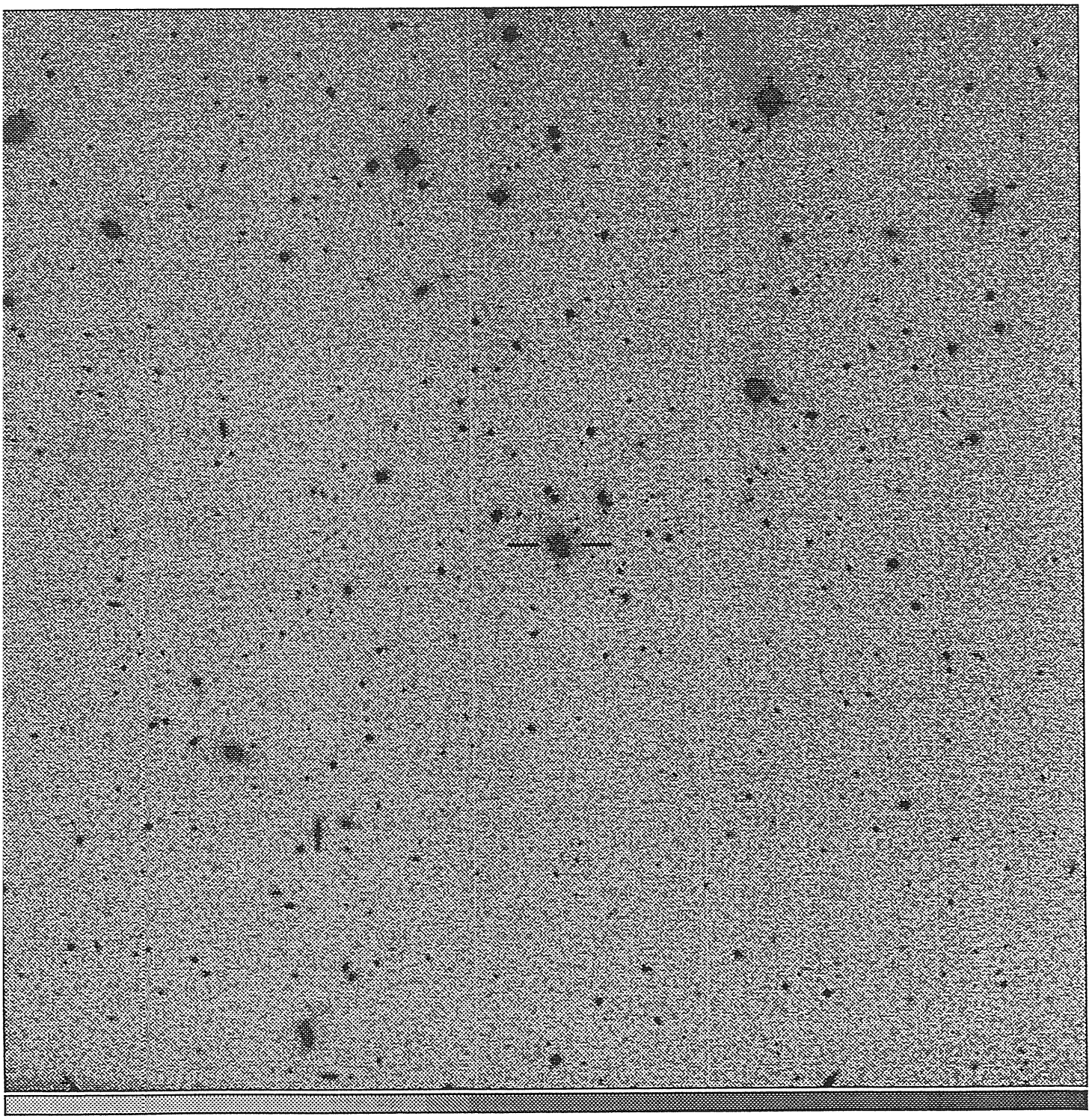

Figure A.6: PKS 0829+046 (average R frame), $z = 0.18$, exp = 60s.

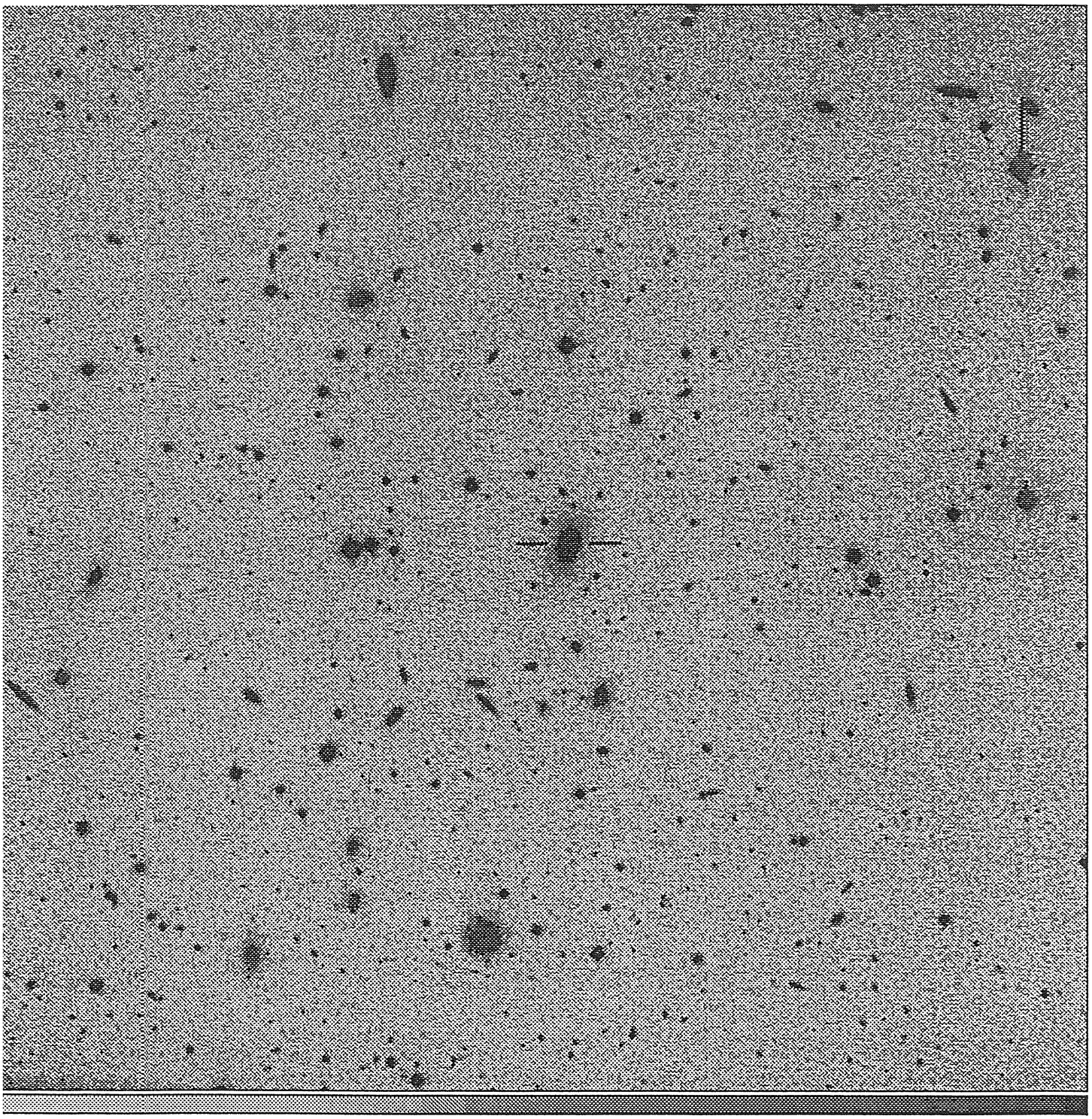

Figure A.7: H 1101–232 (average R frame), $z = 0.186$, exp = 330s.

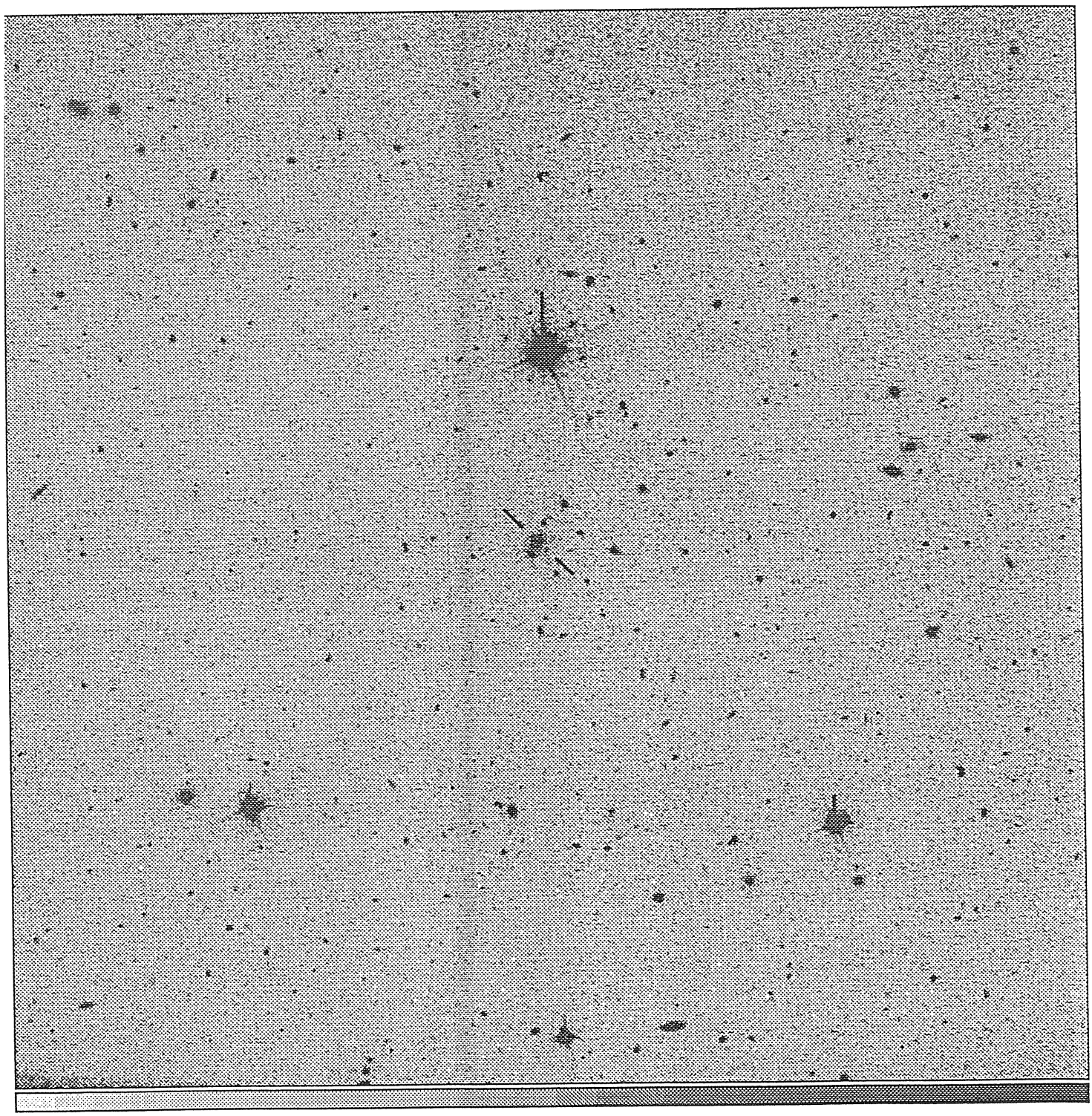

Figure A.8: PKS 1400+162 (average R frame), $z = 0.244$, exp = 330s.

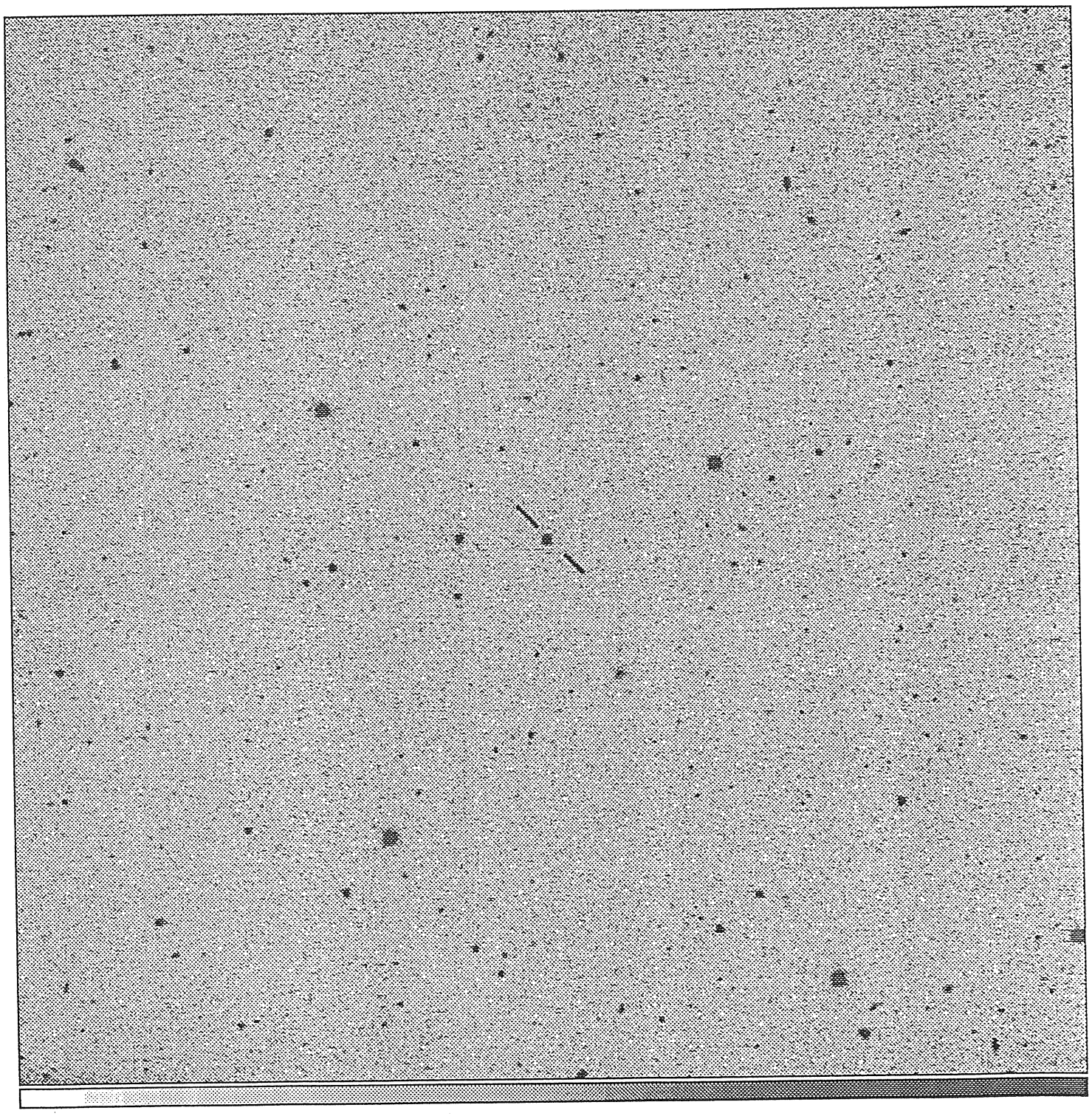

Figure A.9: MS 1402+042 (ima031), $z = 0.2$, exp = 120s.

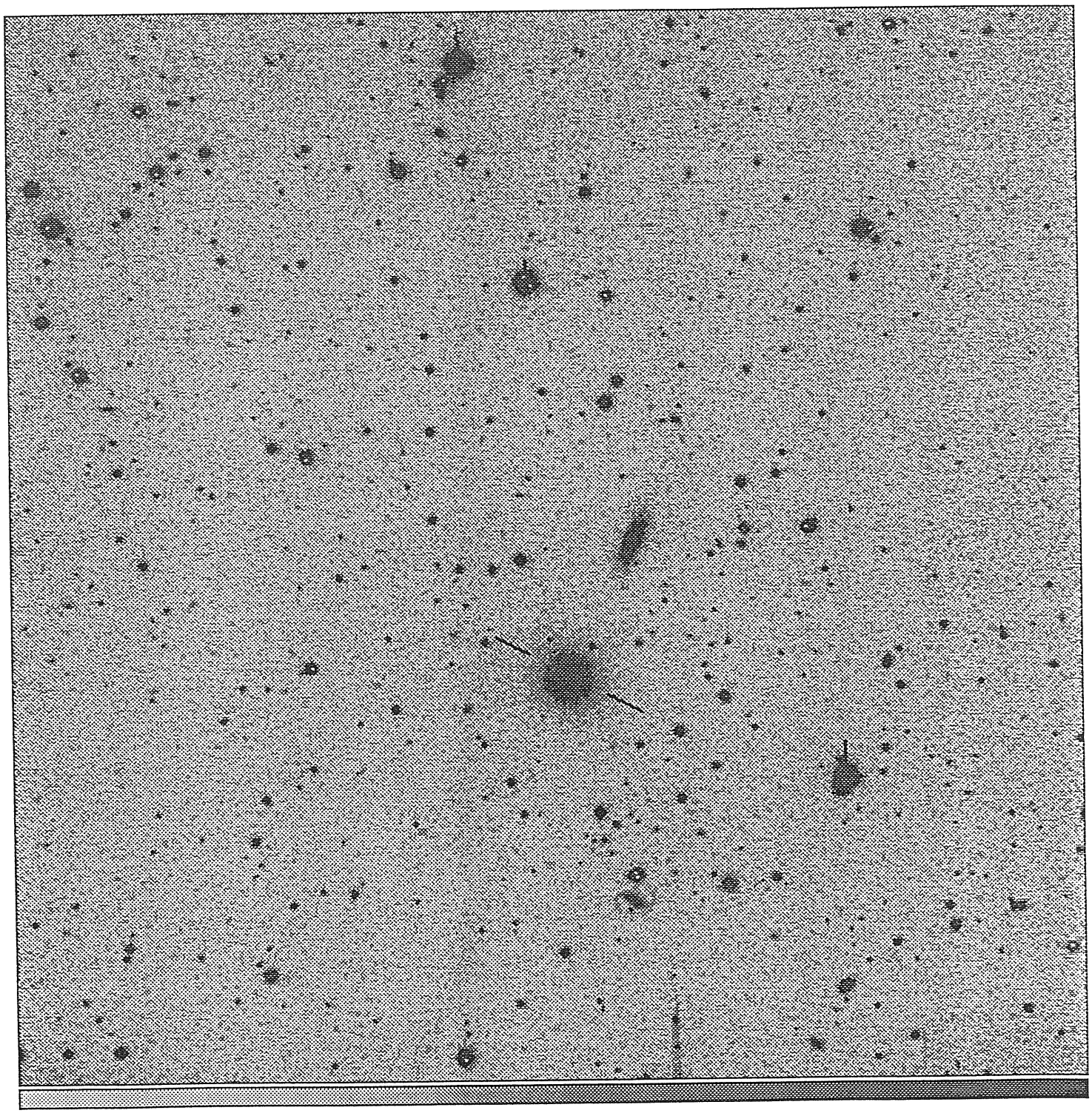

Figure A.10: PKS 1514–241 (ima051), $z = 0.0486$, exp = 600s.

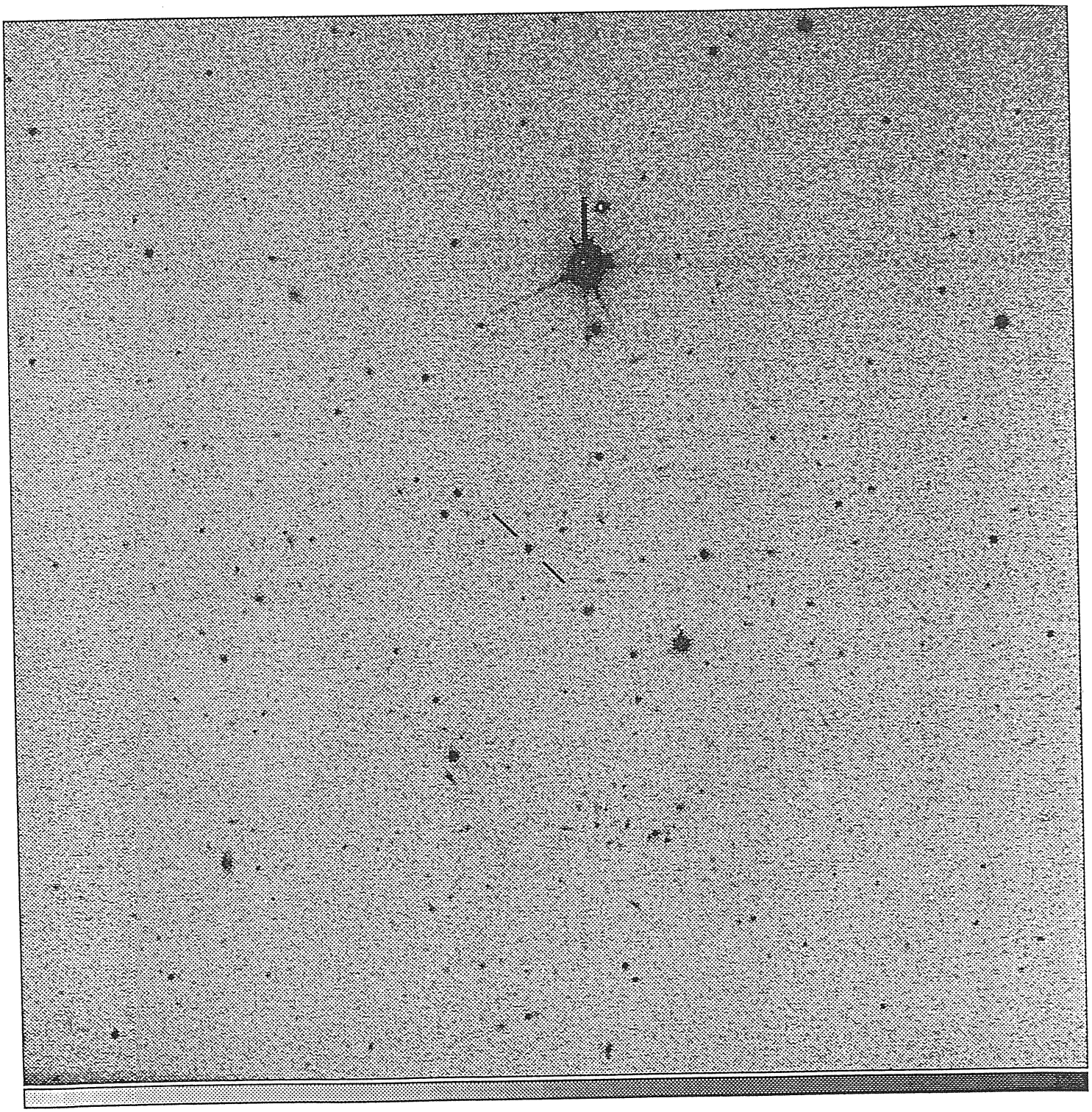

Figure A.11: PKS 1538+149 (ima034), $z = 0.605$, exp = 120.

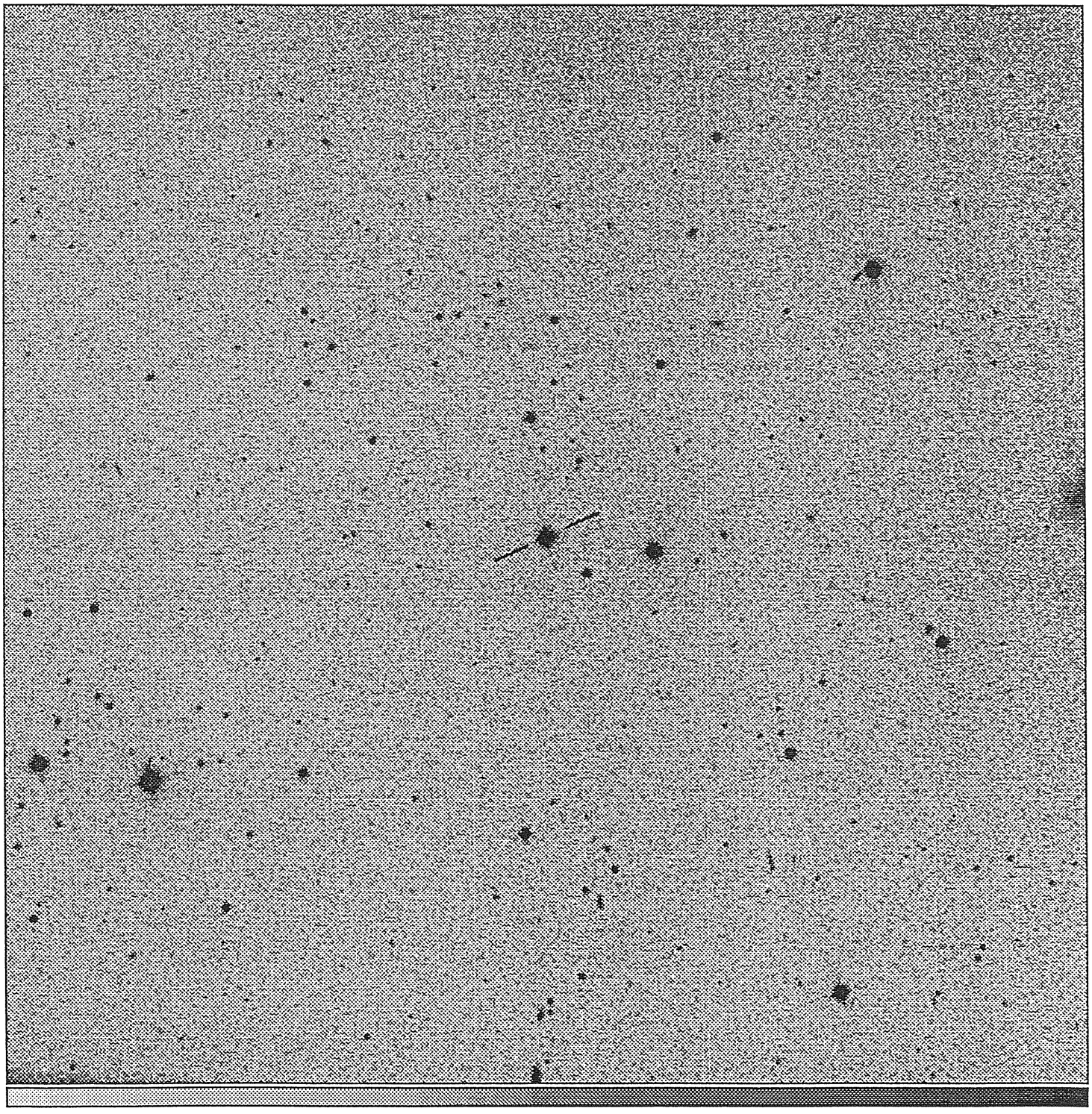

Figure A.12: PG 1553+113 (average R frame), redshift unknown, exp = 50s.

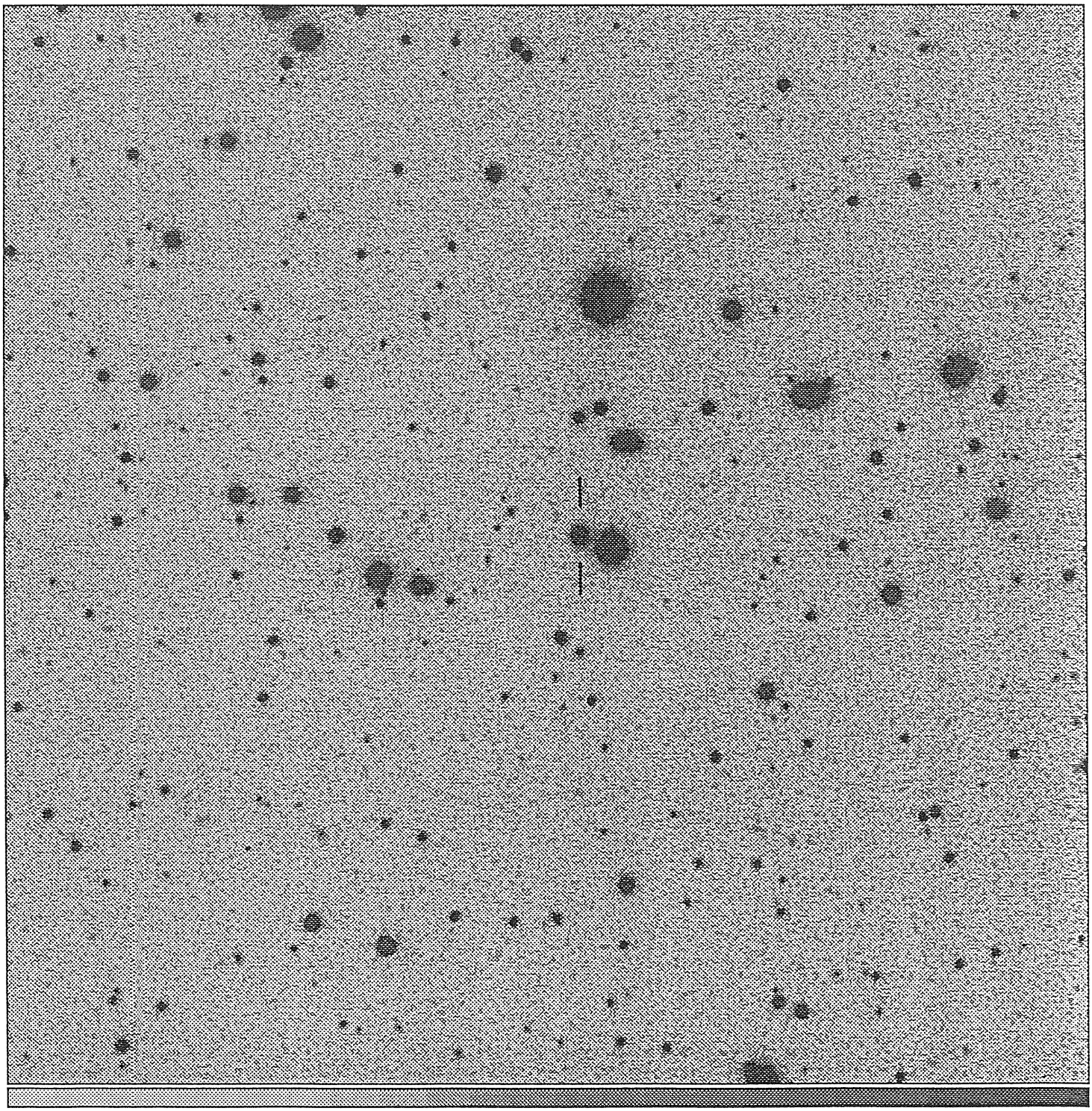

Figure A.13: H 1722+119 (ima003), redshift unknown, exp = 60s.

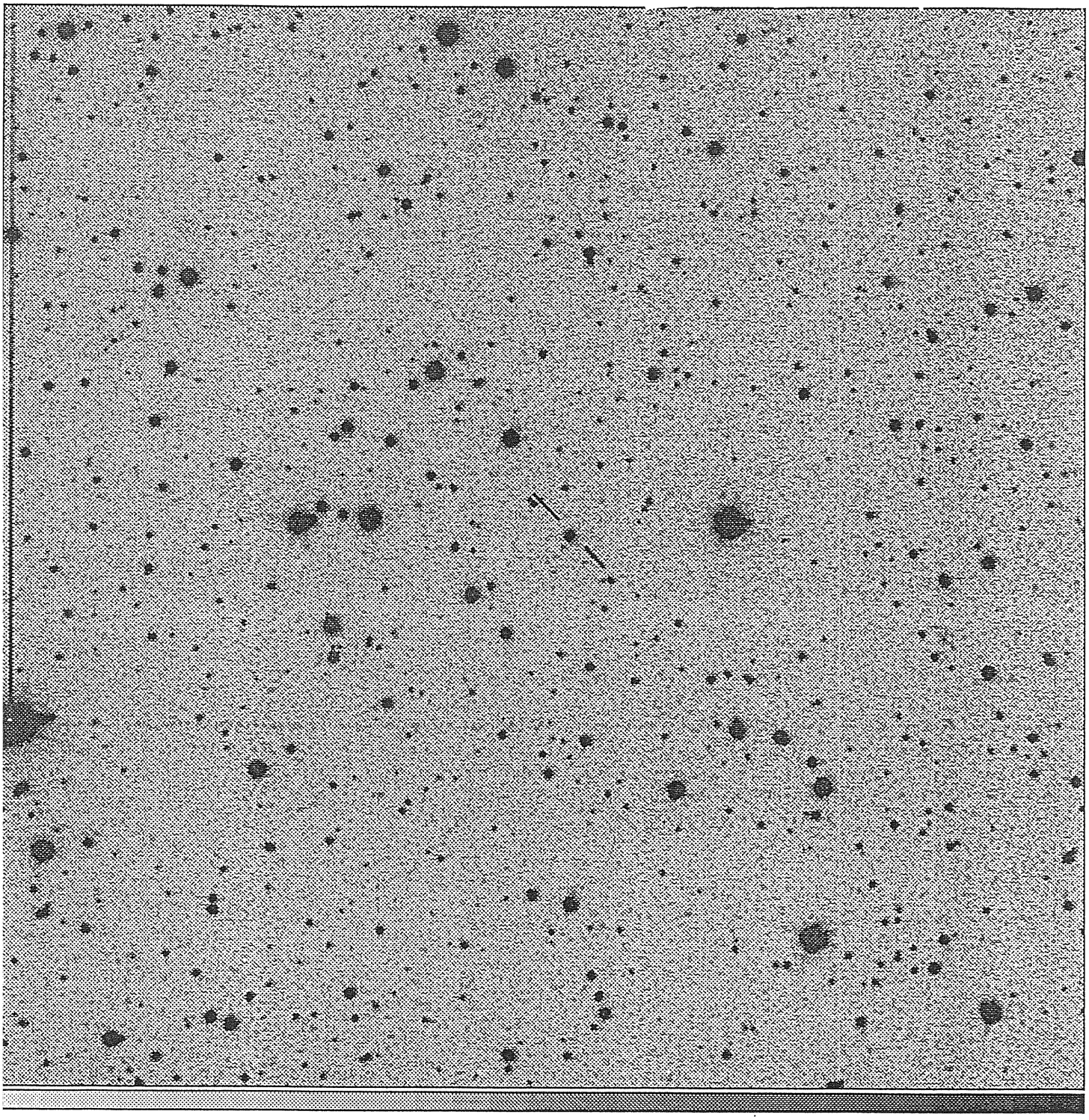

Figure A.14: 1749+096 (ima063), $z = 0.322$, exp = 300s.

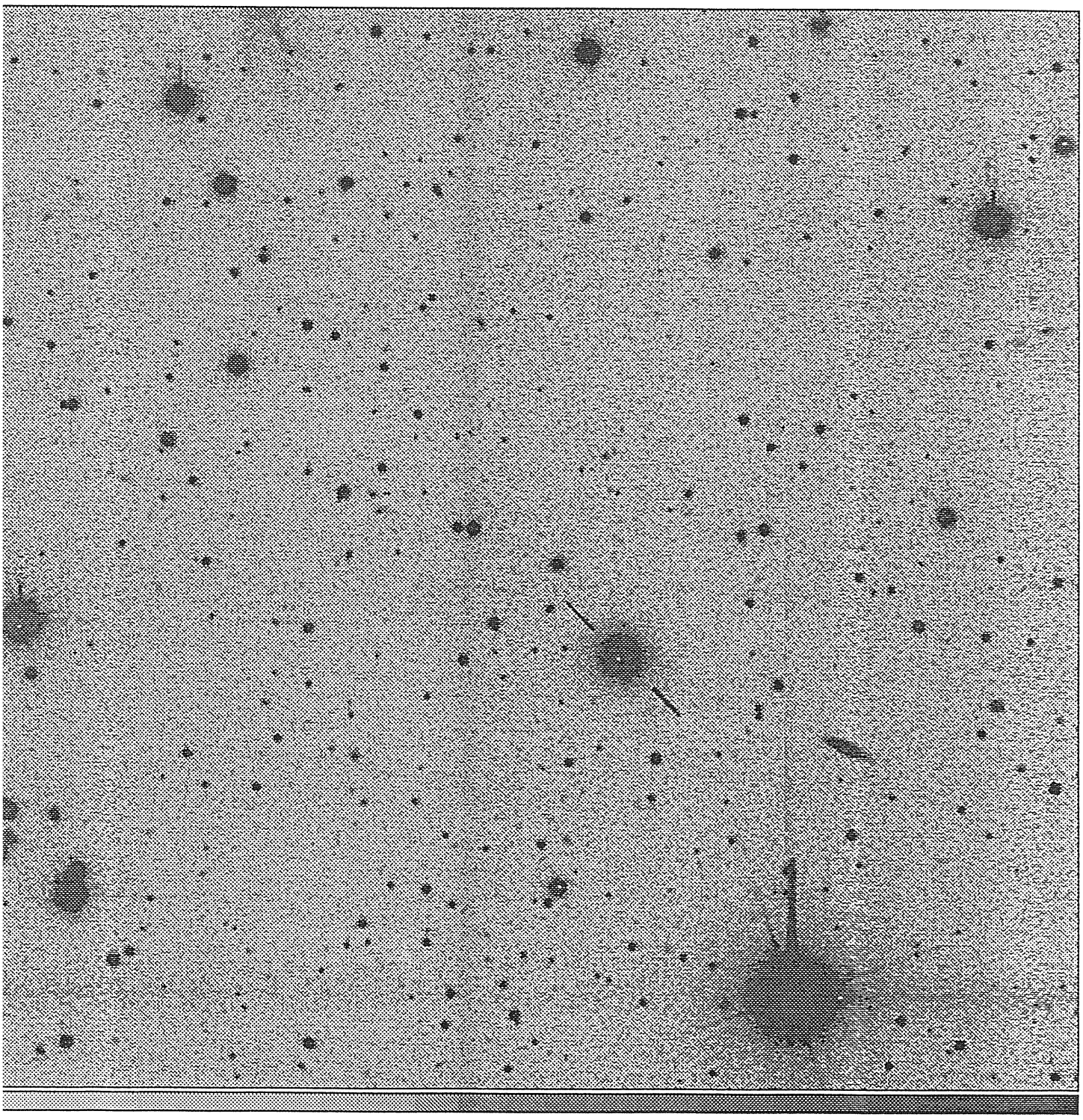

Figure A.15: PKS 2005–489 (ima010), $z = 0.071$, exp = 180s.

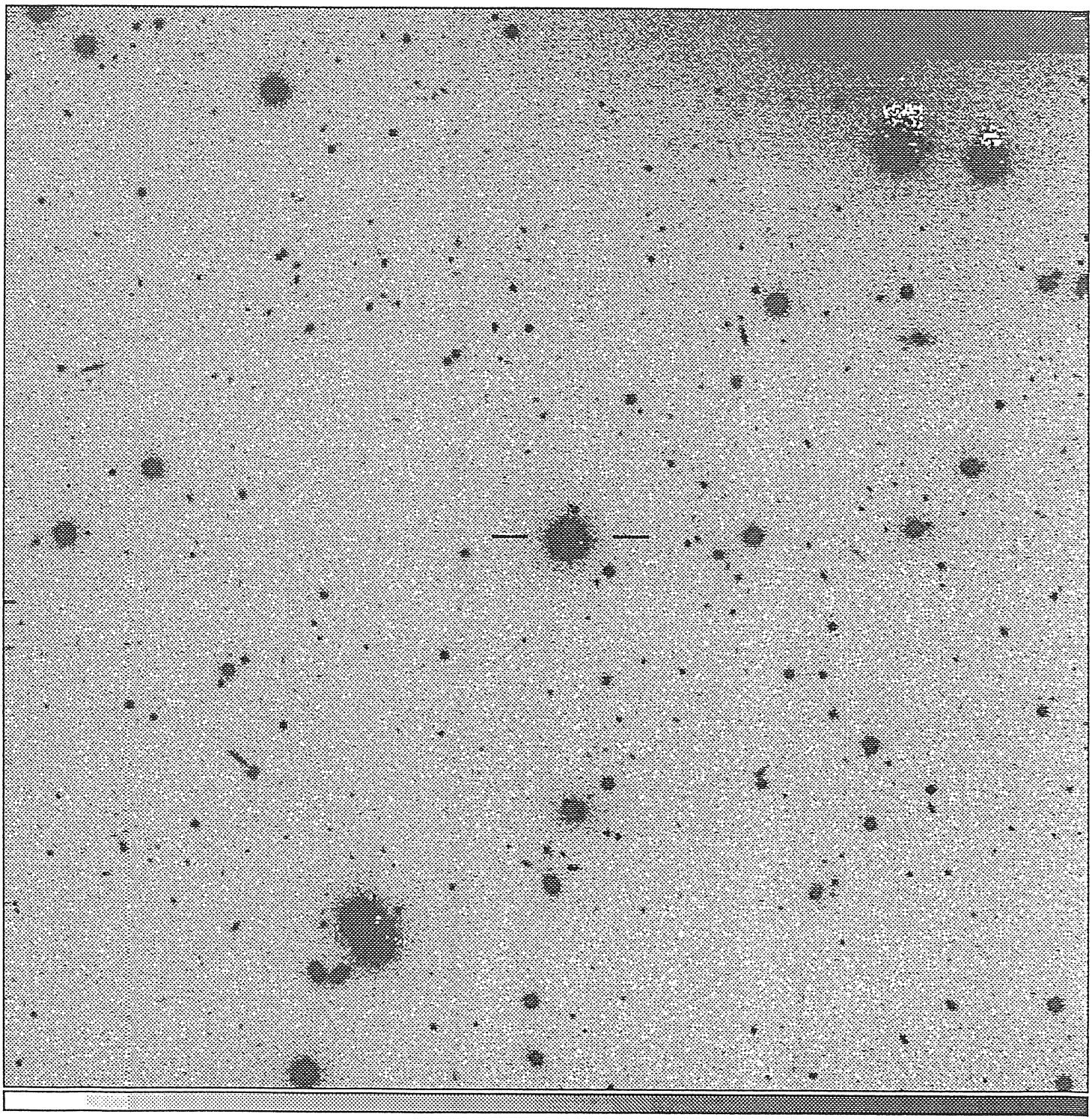

Figure A.16: PKS 2155–304 (average R frame), $z = 0.116$, exp = 150s.

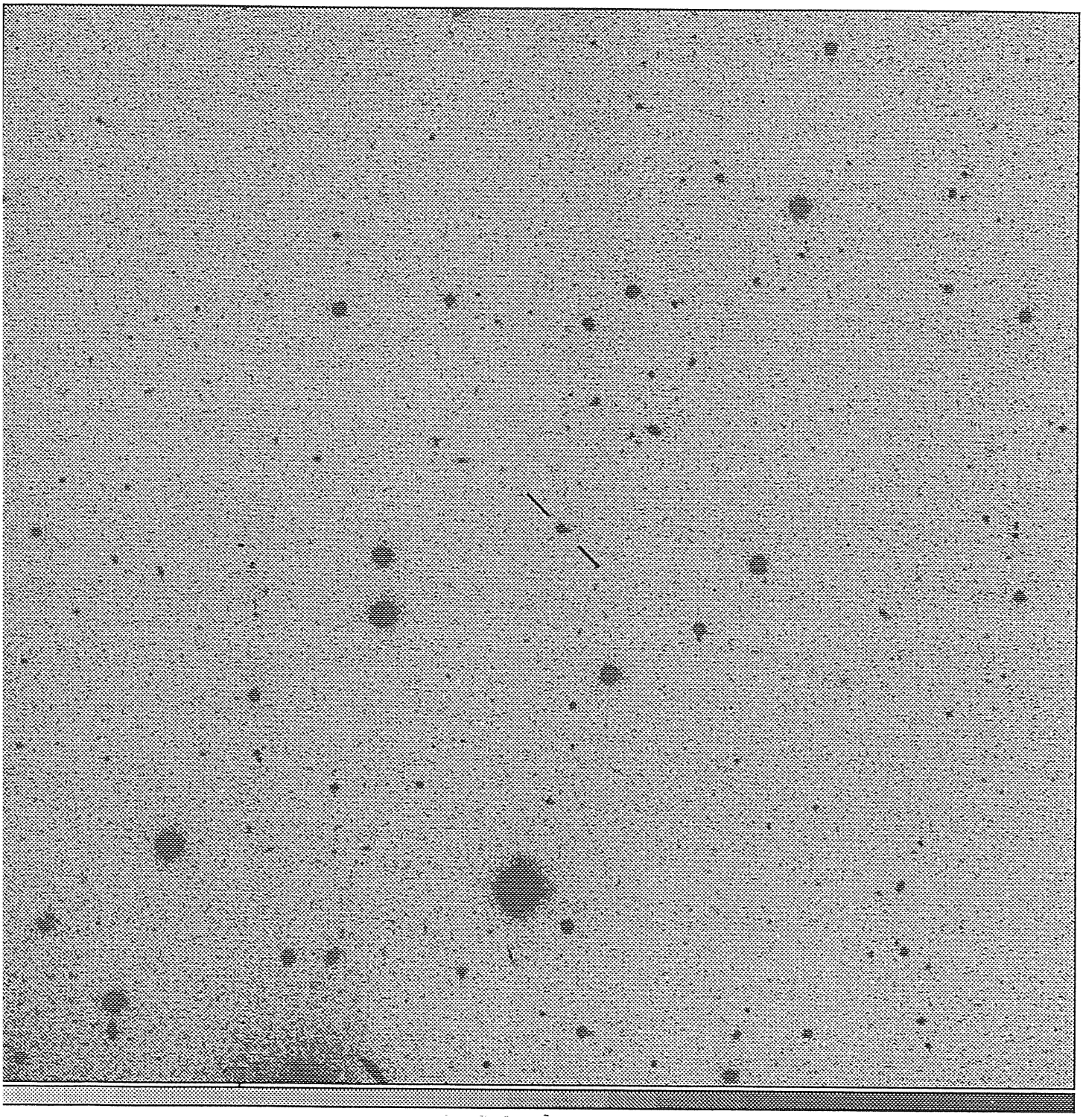

Figure A.17: PKS 2335+031 (average R frame), $z = 0.31$, exp = 120s.

APPENDIX B

V and I Radial Density Distributions of the Program Objects

This Appendix contains the V- and I-band radial galaxy density distributions for the program objects. For each figure, the arrow marks the 0.5 Mpc radius and the dashed line represents the local background value (determined from galaxies beyond 150 arcsec from the BL Lac). The magnitude limits used are given in the captions. The R-band distributions appear in Chapter V.

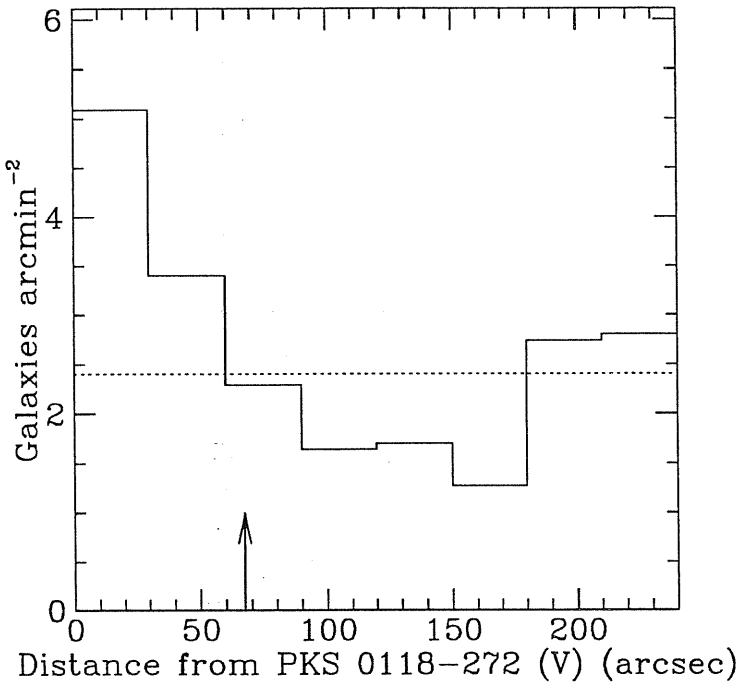

Figure B.1: PKS 0118–272, the V-band density distribution. The magnitude limit is 23.5.

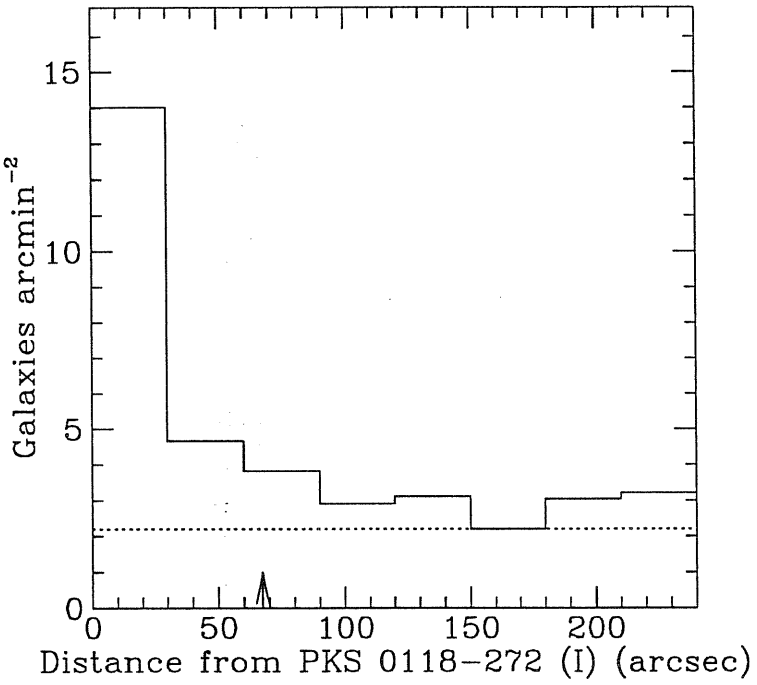

Figure B.2: PKS 0118–272, the I-band density distribution. The magnitude limit is 21.5.

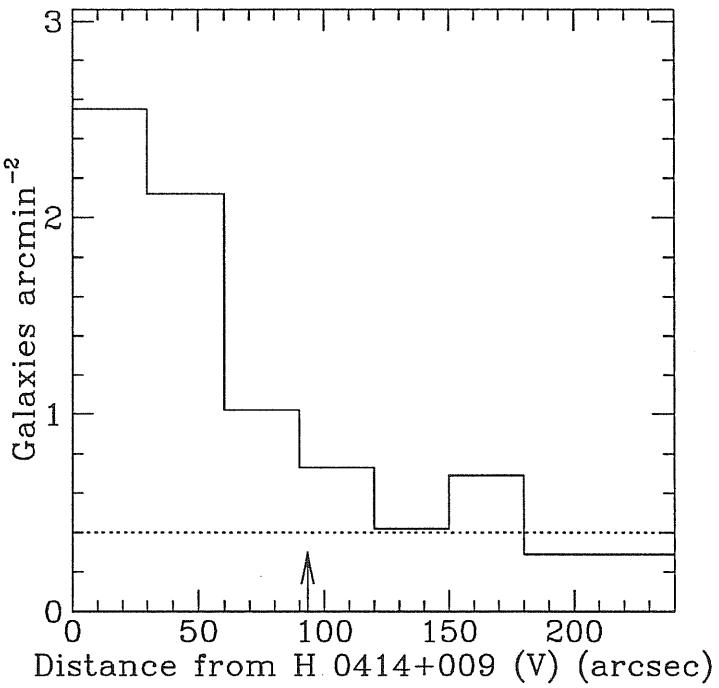

Figure B.3: H 0414+009, the V-band density distribution. The magnitude limit is 21.0.

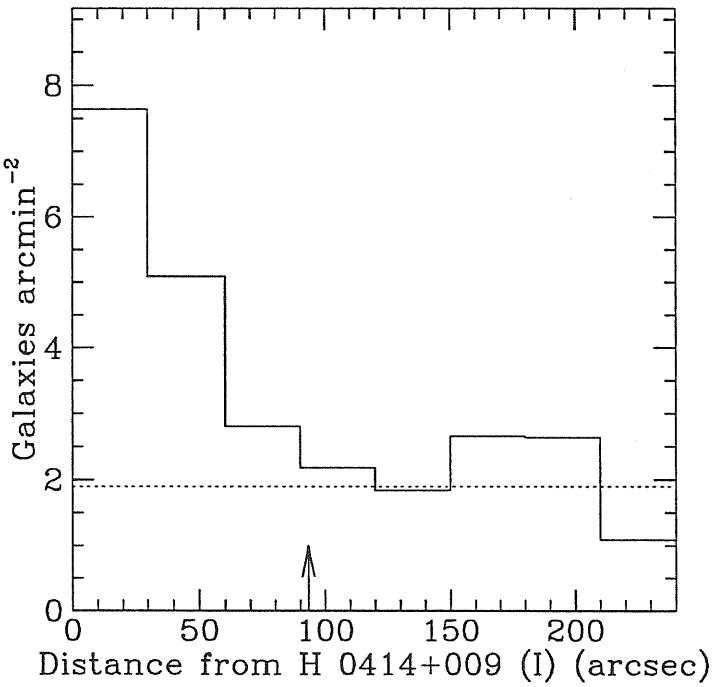

Figure B.4: H 0414+009, the I-band density distribution. The magnitude limit is 21.0.

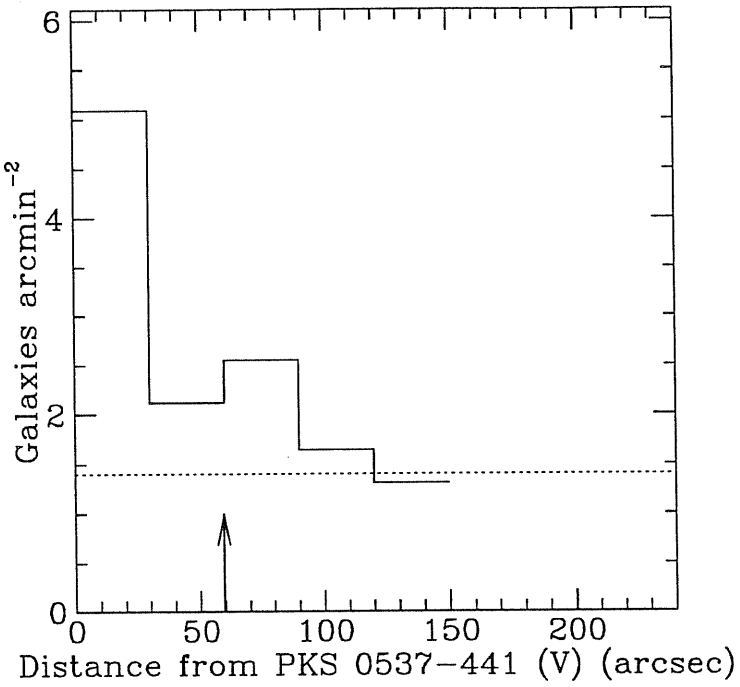

Figure B.5: PKS 0537–441, the V-band density distribution. The magnitude limit is 22.5.

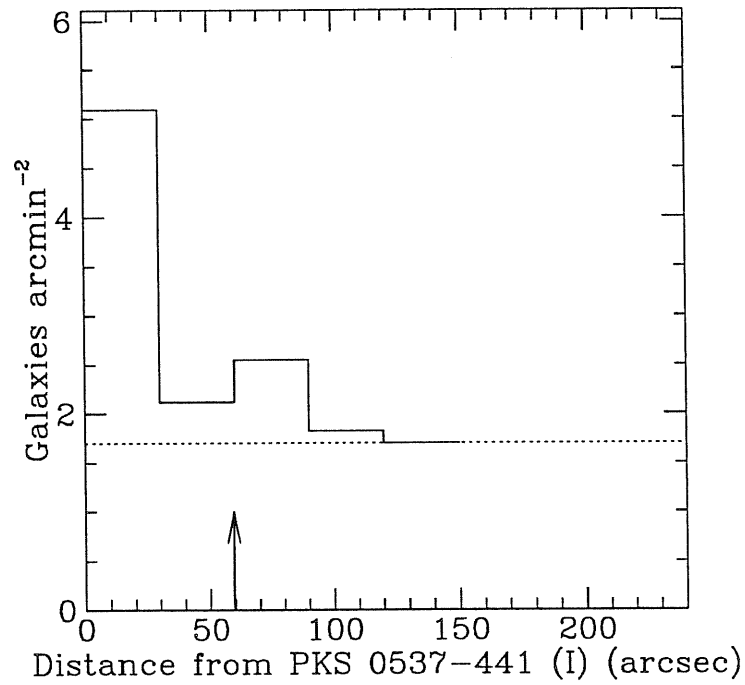

Figure B.6: PKS 0537–441, the I-band density distribution. The magnitude limit is 21.0.

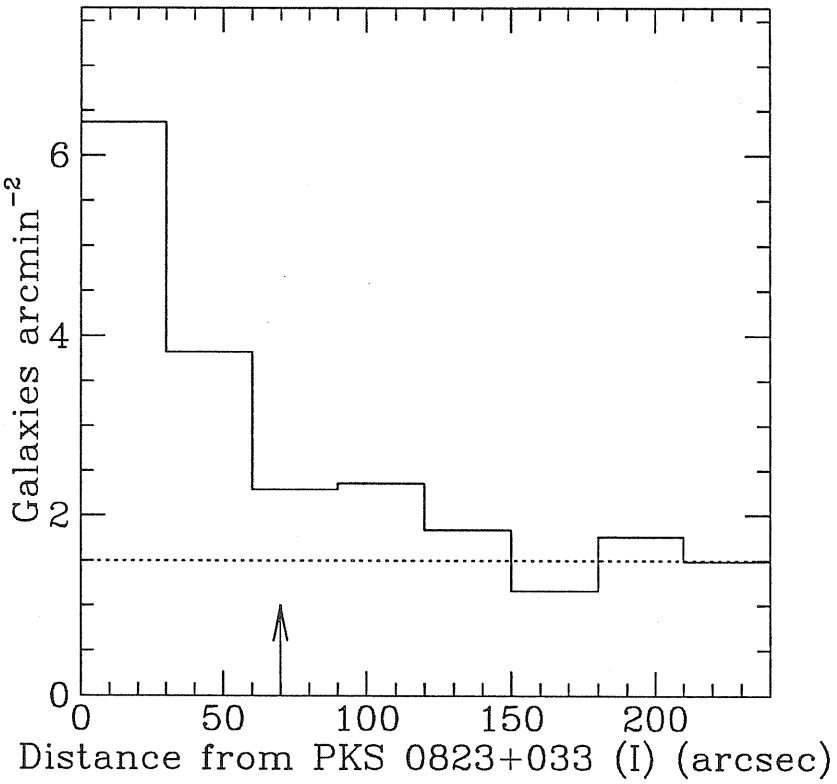

Figure B.7: PKS 0823+033, the I-band density distribution. The magnitude limit is 20.0.

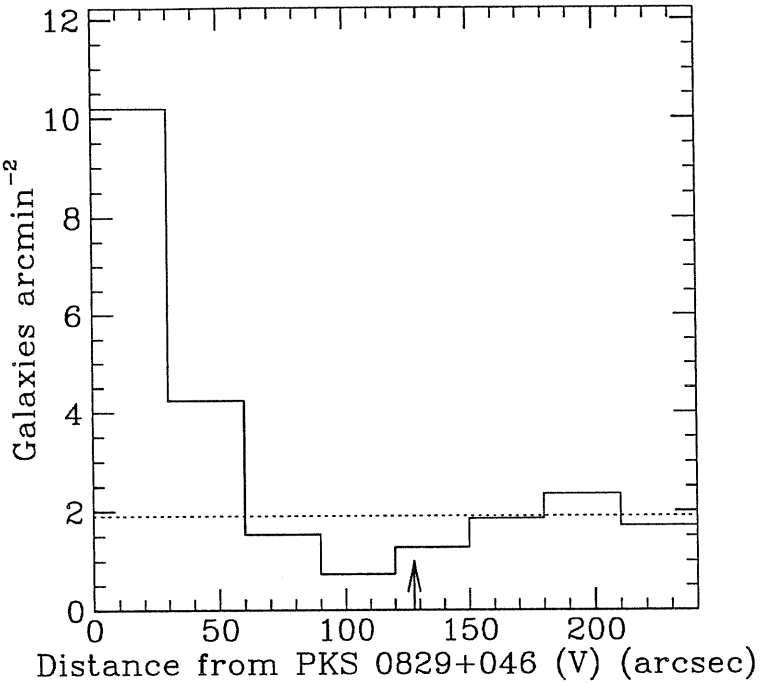

Figure B.8: PKS 0829+046, the V-band density distribution. The magnitude limit is 22.5.

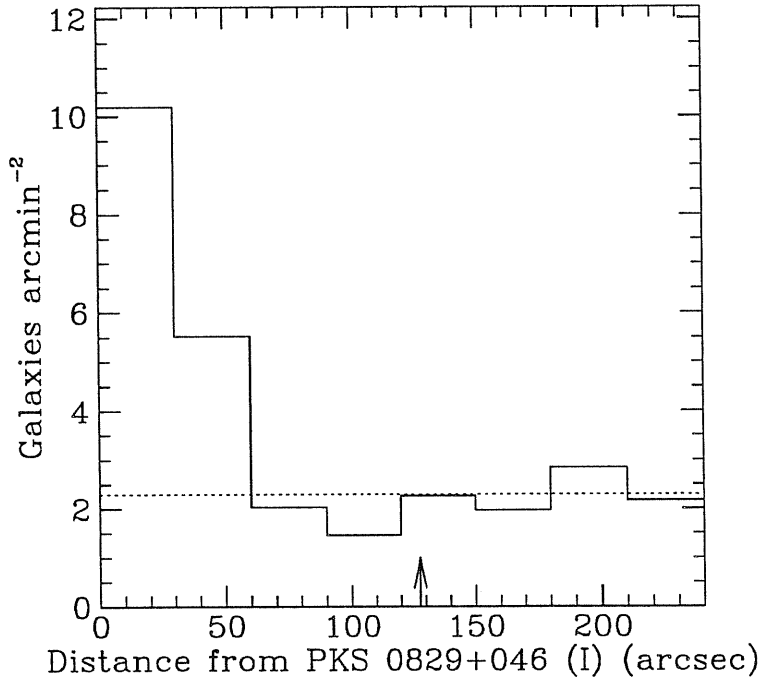

Figure B.9: PKS 0829+046, the I-band density distribution. The magnitude limit is 21.0.

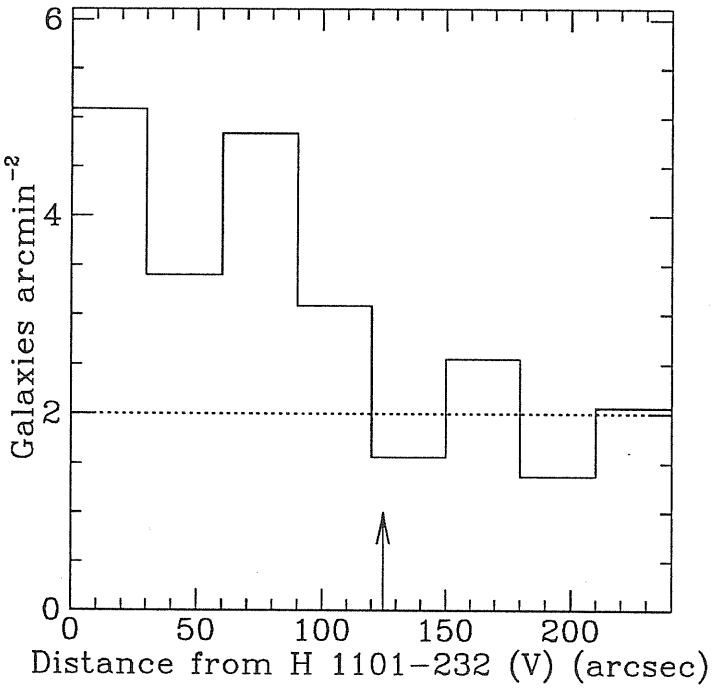

Figure B.10: H 1101–232, the V-band density distribution. The magnitude limit is 22.0.

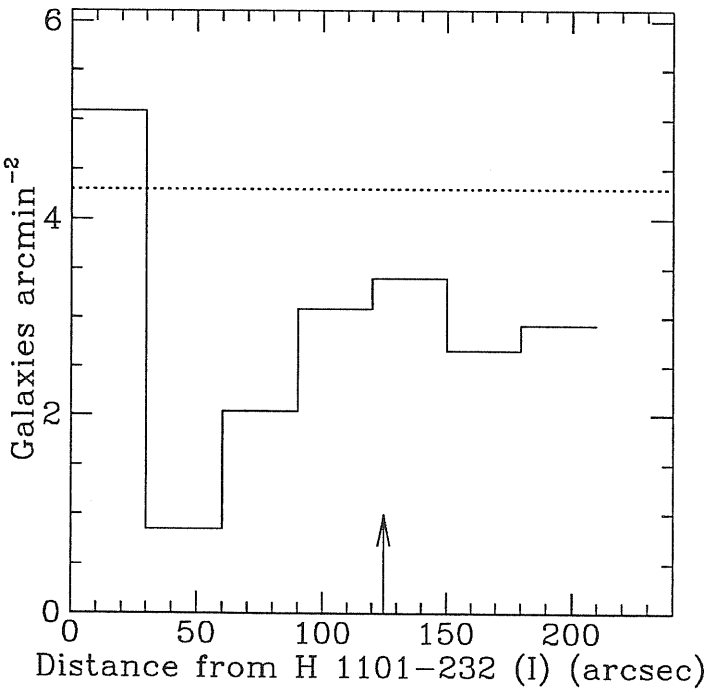

Figure B.11: H 1101–232, the I-band density distribution. The magnitude limit is 22.0.

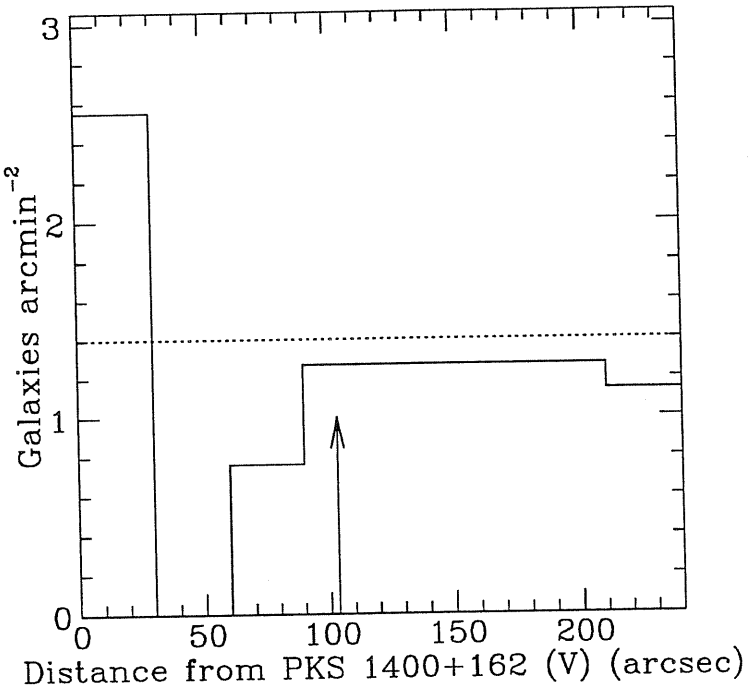

Figure B.12: PKS 1400+162, the V-band density distribution. The magnitude limit is 22.5.

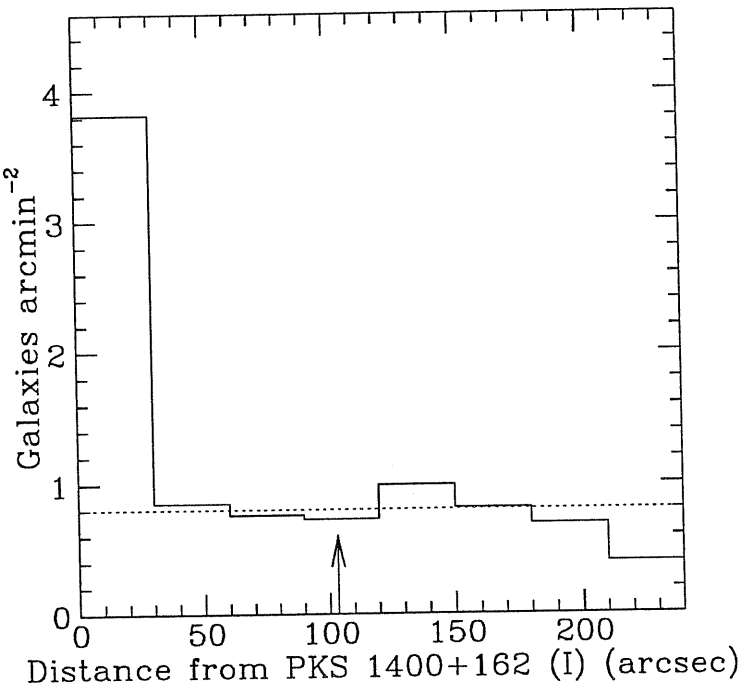

Figure B.13: PKS 1400+162, the I-band density distribution. The magnitude limit is 20.5.

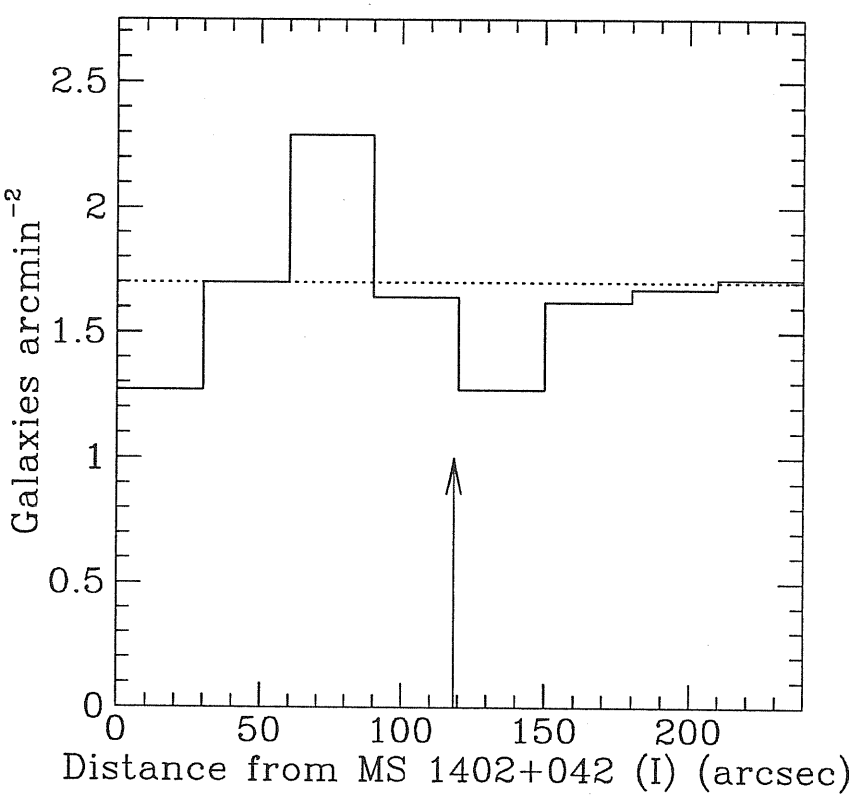

Figure B.14: MS 1402+042, the I-band density distribution. The magnitude limit is 21.0.

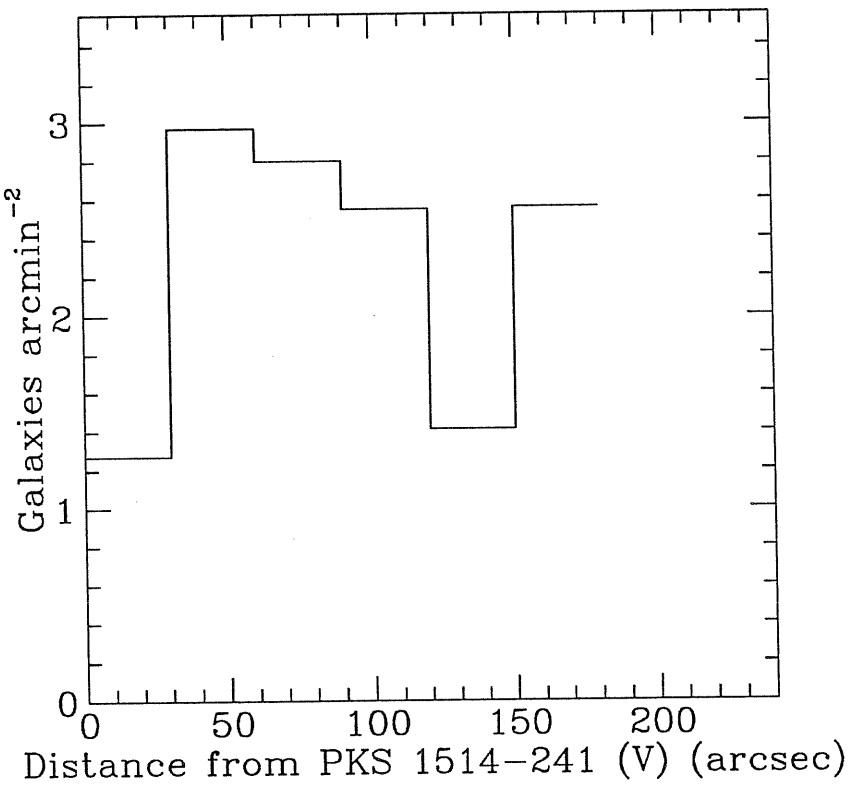

Figure B.15: PKS 1514–241, the V-band density distribution. The magnitude limit is 22.5. Because of the low redshift of this object, a local background has not been determined.

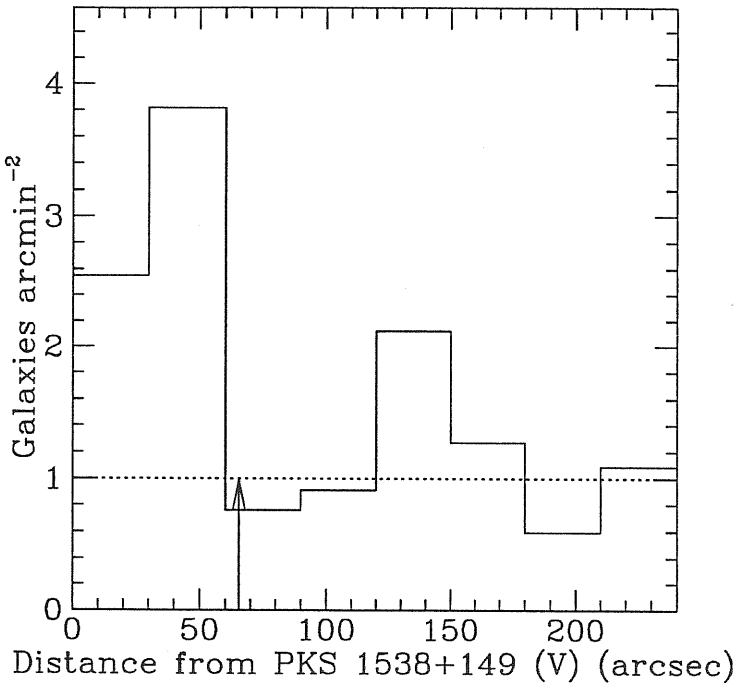

Figure B.16: PKS 1538+149, the V-band density distribution. The magnitude limit is 22.0.

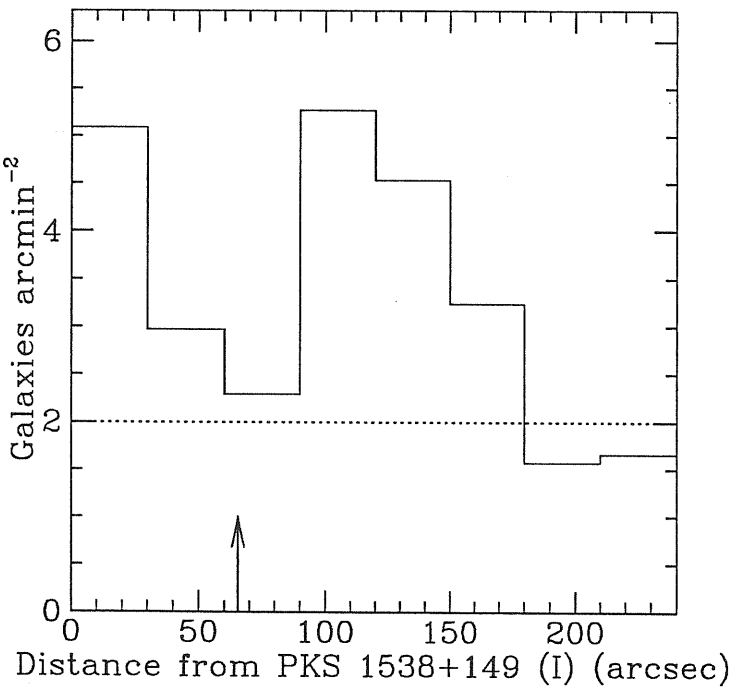

Figure B.17: PKS 1538+149, the I-band density distribution. The magnitude limit is 20.5.

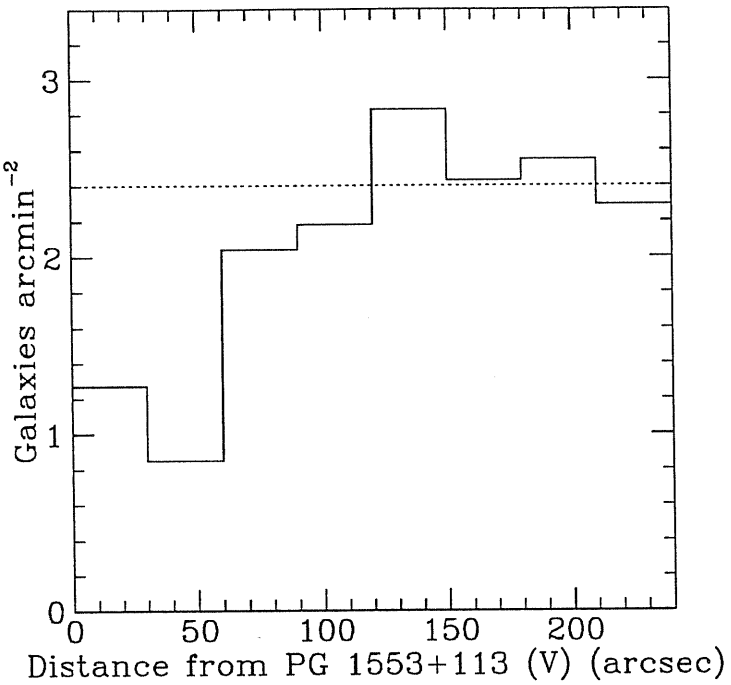

Figure B.18: PG 1553+113, the V-band density distribution. The magnitude limit is 23.0.

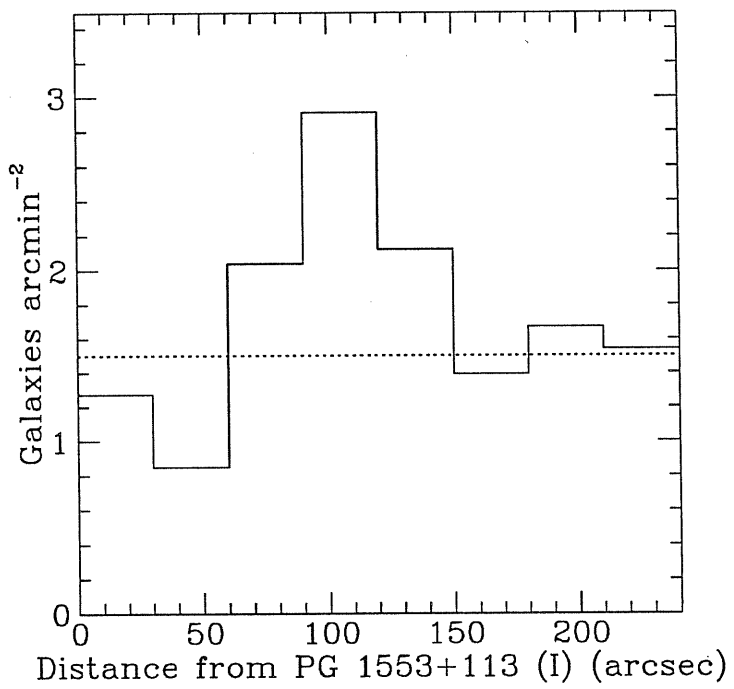

Figure B.19: PG 1553+113, the I-band density distribution. The magnitude limit is 21.0.

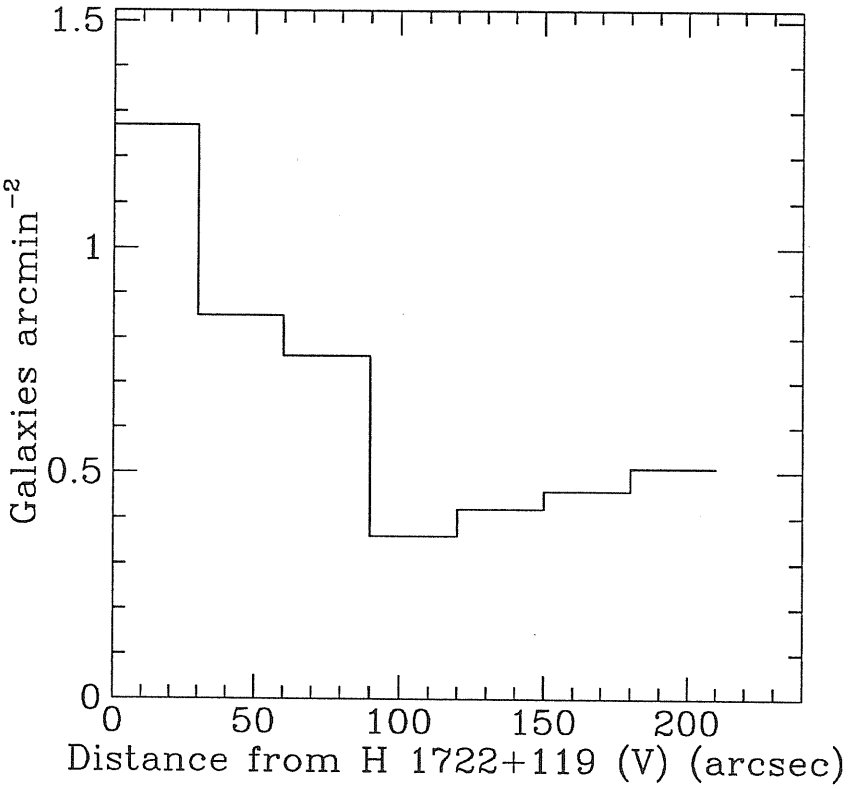

Figure B.20: H 1722+119, the V-band density distribution. The magnitude limit is 20.5. Because of the poor quality of this image, a local background has not been determined.

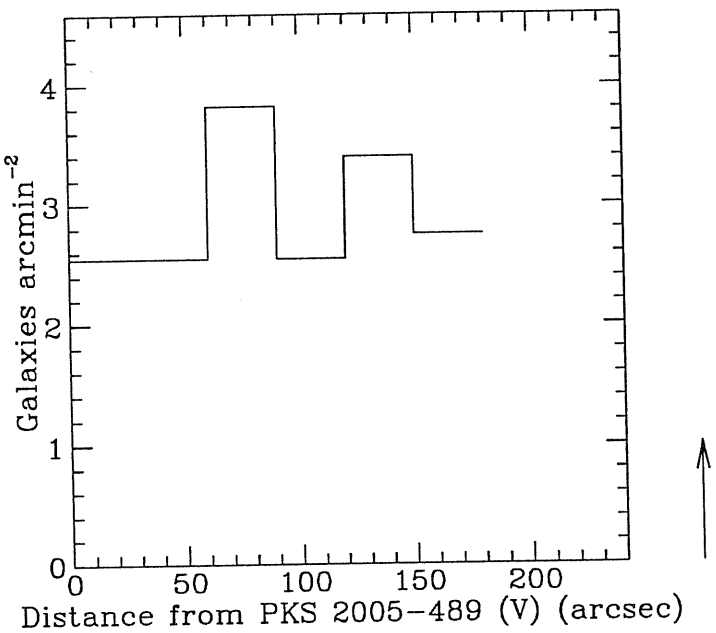

Figure B.21: PKS 2005–489, the V-band density distribution. The magnitude limit is 23.0. A local background has not been determined due to low redshift.

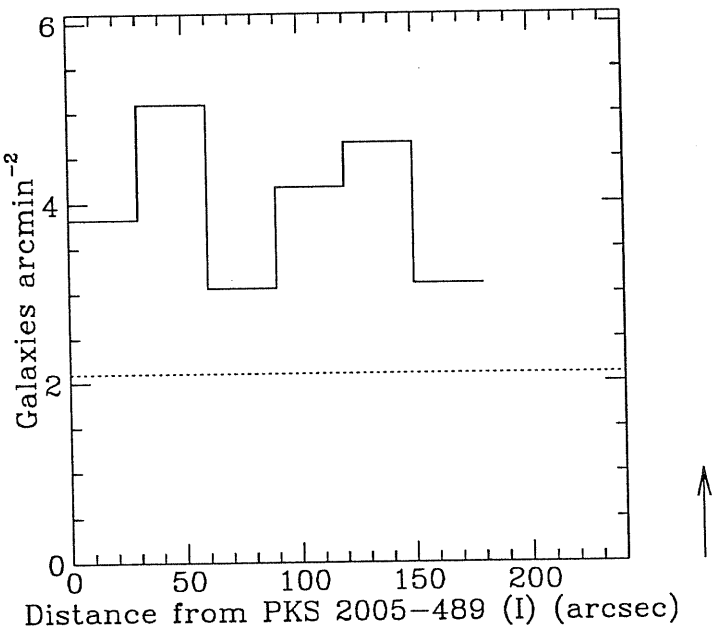

Figure B.22: PKS 2005–489, the I-band density distribution. The magnitude limit is 21.0. The average background has been used.

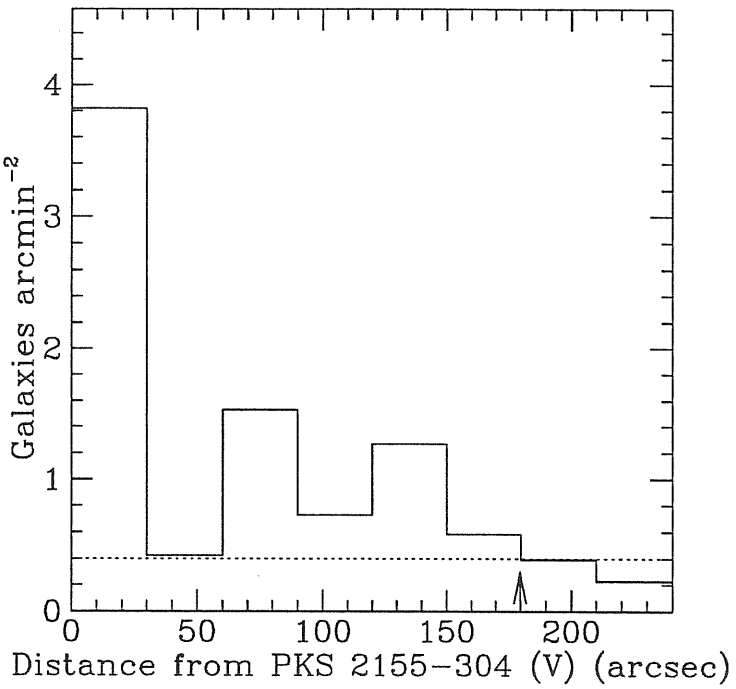

Figure B.23: PKS 2155–304, the V-band density distribution. The magnitude limit is 21.5.

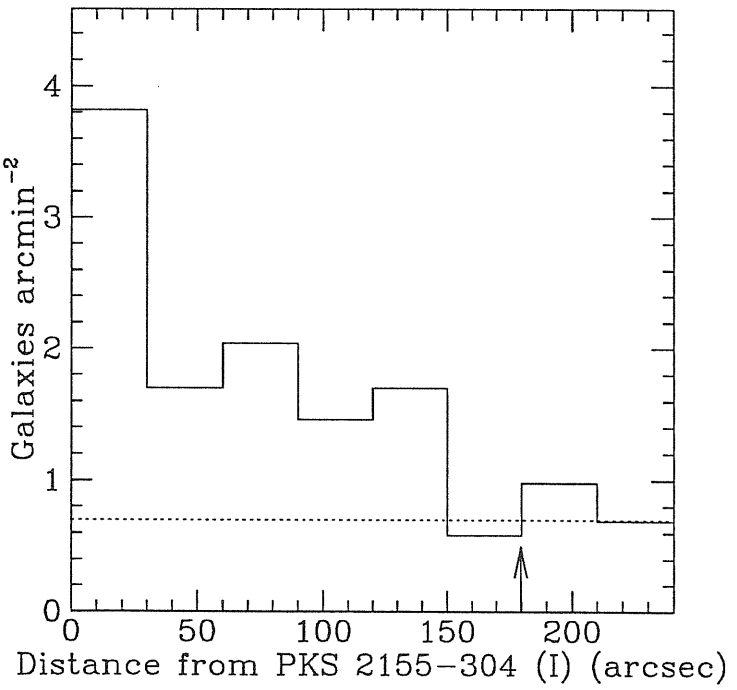

Figure B.24: PKS 2155–304, the I-band density distribution. The magnitude limit is 20.5.

APPENDIX C

Miscellaneous FOCAS Output

This Appendix contains examples of miscellaneous output (a complete collection of this data, plus program listings, can be obtained from the author). Examples of the diagrams used in the initial analysis phase are included. These are produced with FOCAS.SM using the catalog files as input. For each image there are two pages of output. The first gives a map of the galaxies, with the BL Lac at the center (top left), the galaxy radial density distribution (top right), a map of the stars (center left) and the stellar density distribution (center right), the differential galaxy counts for the entire frame (bottom left), and the integral galaxy counts (bottom right). Various data are given in the header at the top of the page.

The second page gives the scale-magnitude diagrams for the image (top left), isophotal magnitudes vs. total magnitudes (top right), aperture magnitudes vs. total magnitudes (center left), isophotal magnitudes vs. aperture magnitudes (center right), galaxy magnitudes vs. distance from object (bottom left), and stellar magnitudes vs. distance from object (bottom right).

For each object with observations in two or more filters, a page of diagrams corresponding to color information is provided. These diagrams give $R - I$ vs. R for galaxies within and beyond 0.5 Mpc (top left), $V - R$ for galaxies within and beyond 0.5 Mpc (top right), $R - I$ vs. distance from the object (center left), and $V - R$ vs. distance from the object (center right).

We also give a representative header file and FOCAS catalog for the V-band image of PKS 0118–272. The matched table for PKS 0118–272 is included. This gives the x and y coordinates in arcsec (with the BL Lac as the origin) and the distance (in arcsec) from the BL Lac. The following three columns give the R, I, and V, isophotal magnitudes. Finally, the values of $R - I$ and $V - R$ are listed.

FILE = V_0118.cat, FILTER = V, X_0 = 536, Y_0 = 521, MAGLIM = 100, BIN = 30, z = 0.559
$R_{0.5Mpc}$ =67.2953, N_{GALS} = 147 ($N_{\leq 0.5Mpc}$ = 15, $N_{>0.5Mpc}$ = 132), N_{STARS} = 50 Aug 16 12:38:11 1993
EXPOSURE = 600 sec, SEEING = 1.8 arcsec

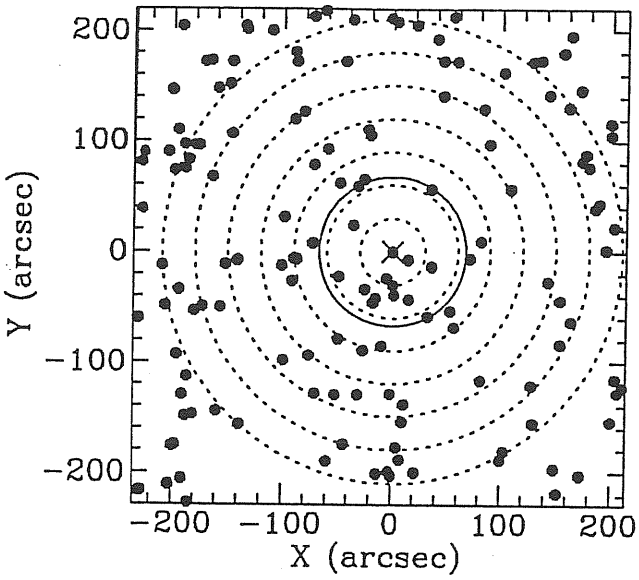

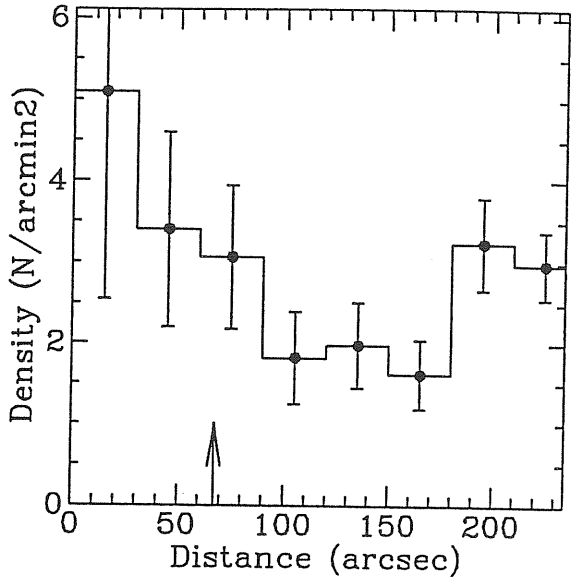

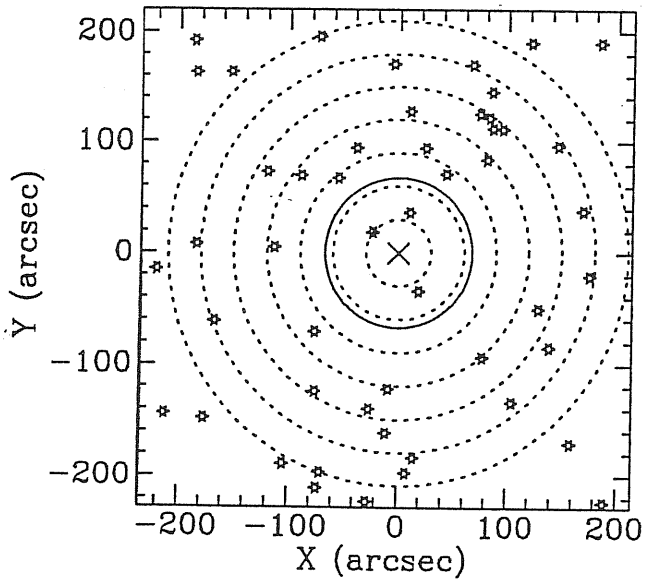

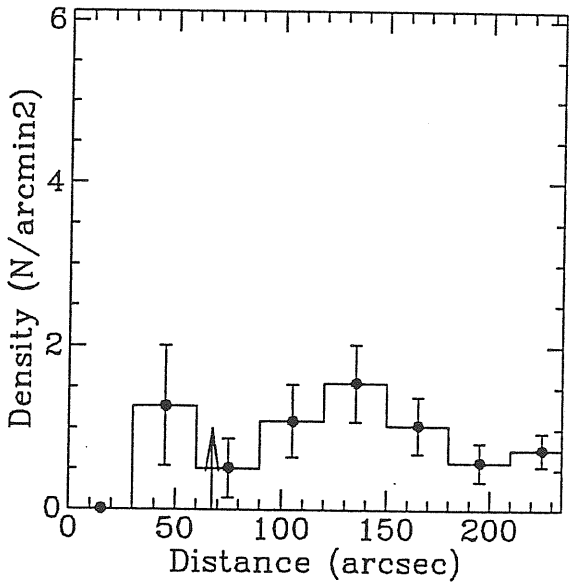

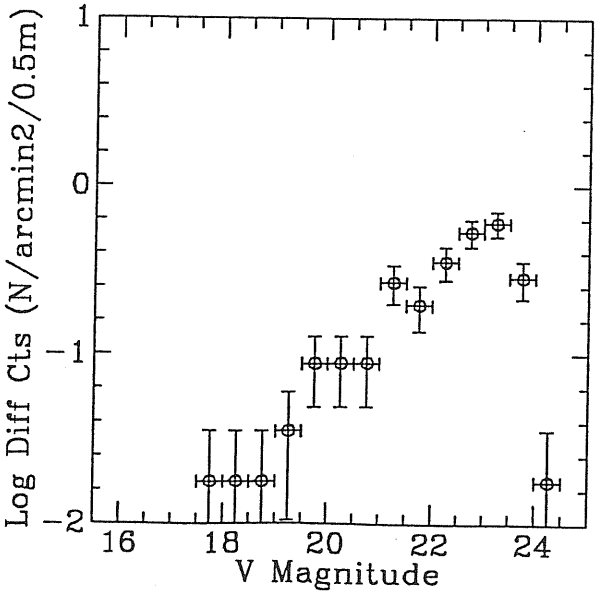

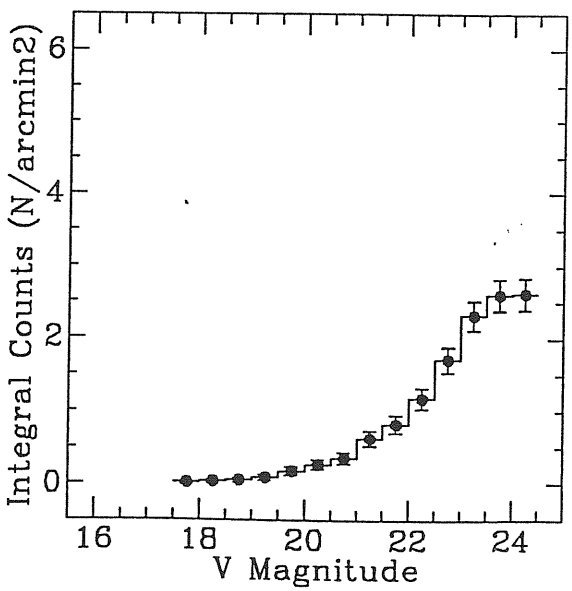

FILE = V_0118.cat, FILTER = V, MAGLIM = 100

Aug 16 12:44:59 199

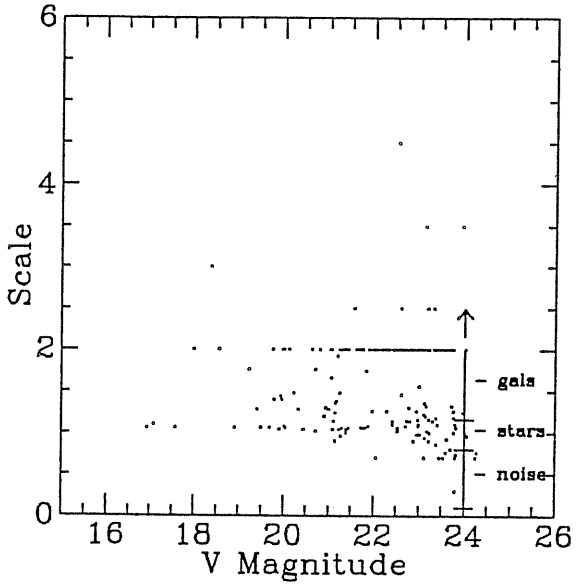

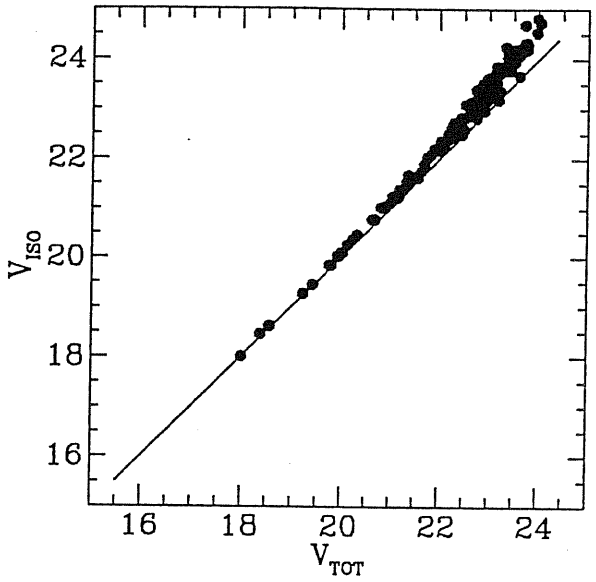

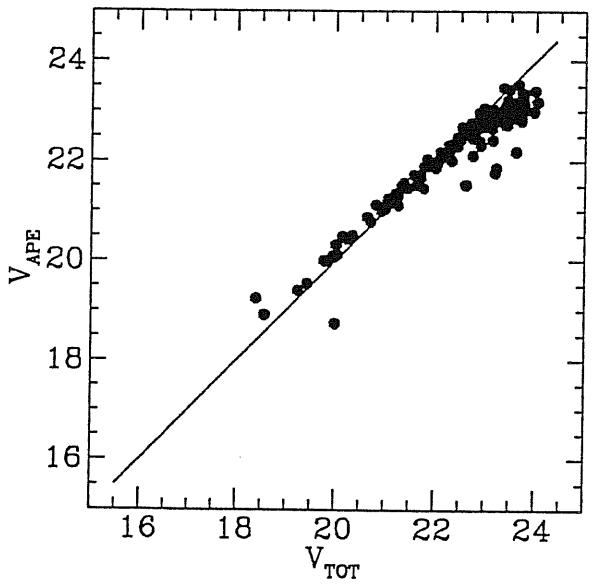

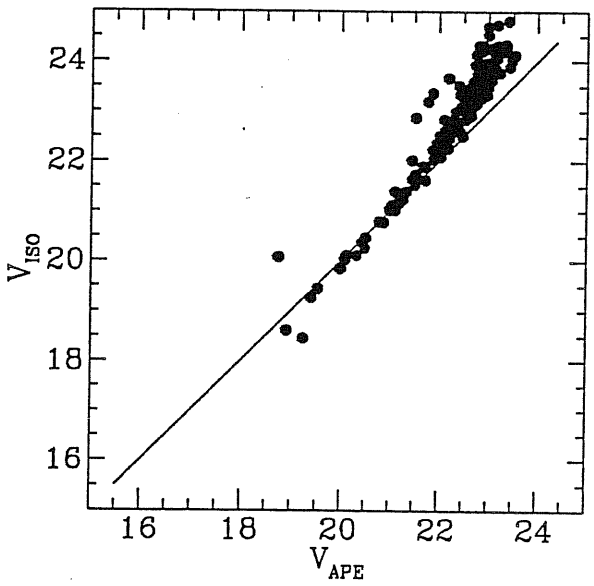

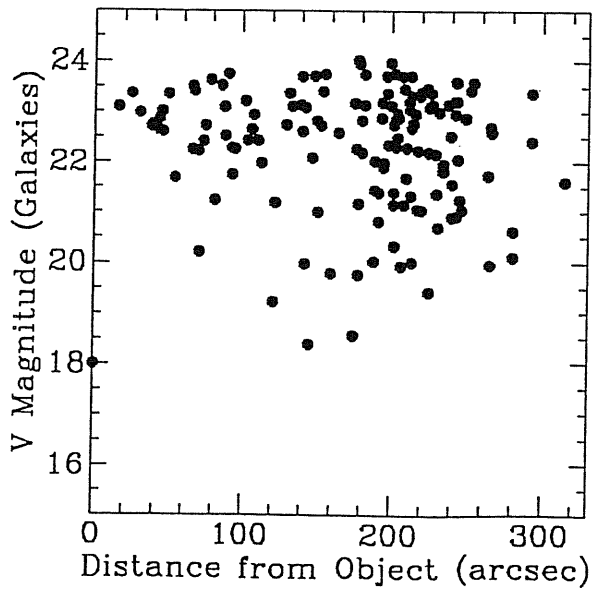

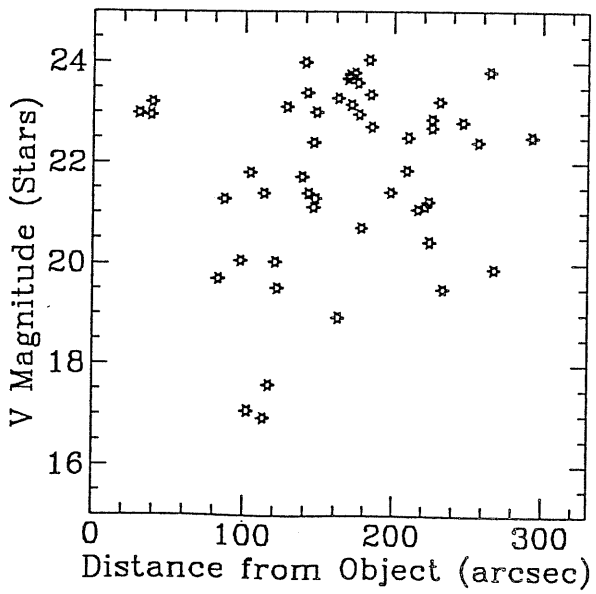

FILE = R_0118.cat, FILTER = R, X_0 = 536, Y_0 = 522, MAGLIM = 100, BIN = 30, z = 0.559

$R_{0.5Mpc}$ =67.2953, N_{GALS} = 142 ($N_{\leq 0.5Mpc}$ = 16, $N_{>0.5Mpc}$ = 126), N_{STARS} = 74 Aug 16 12:39:18 1993

EXPOSURE = 260 sec, SEEING = 1.7 arcsec

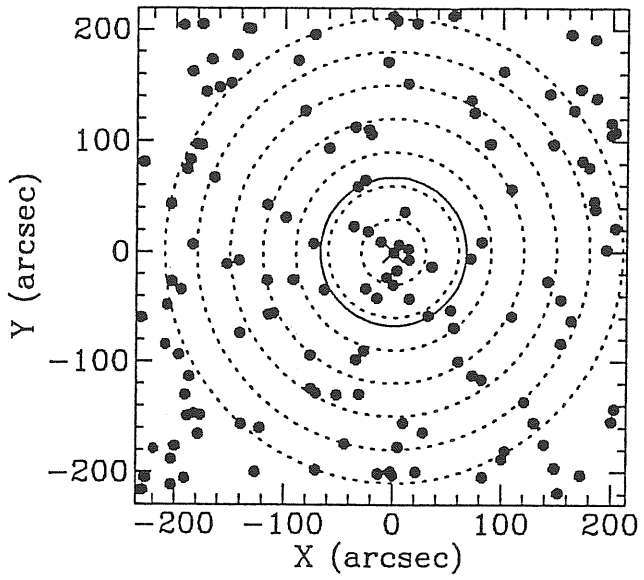

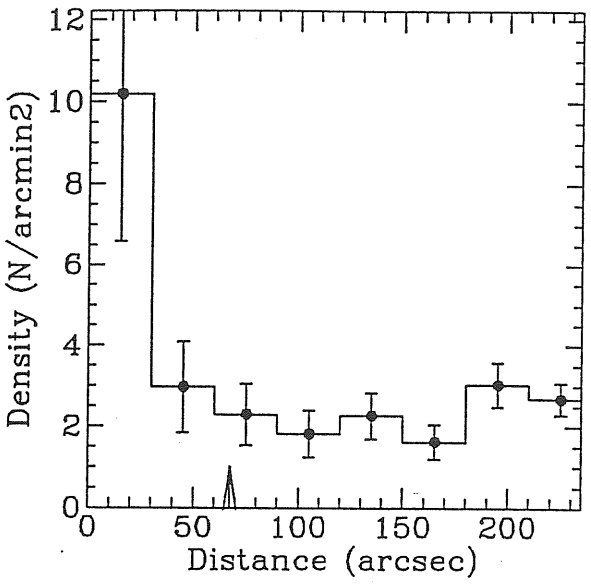

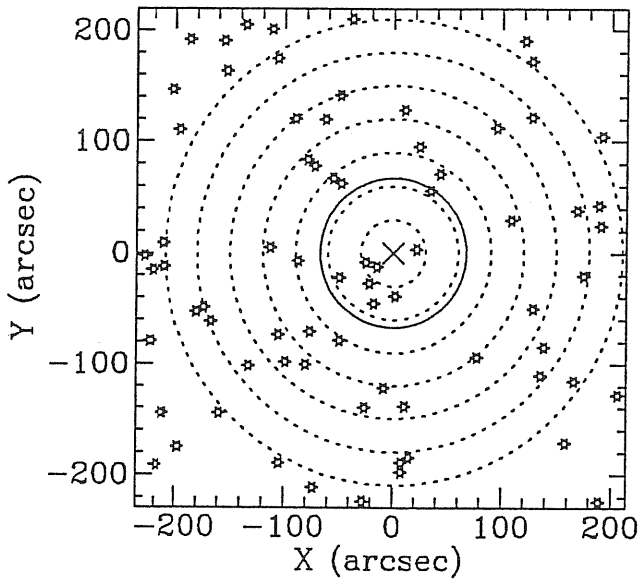

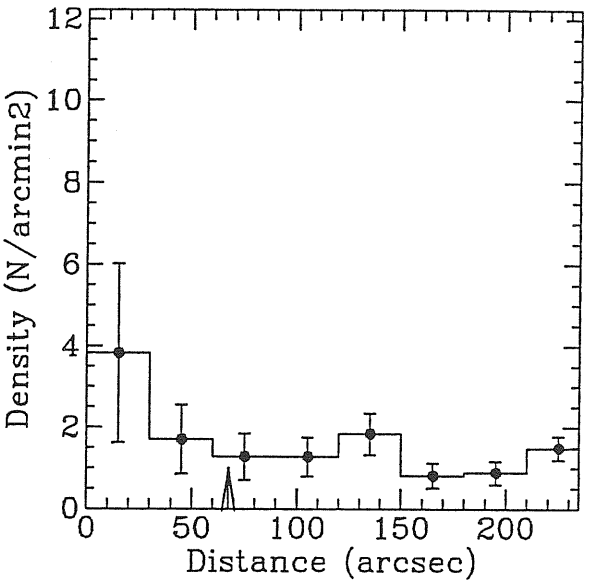

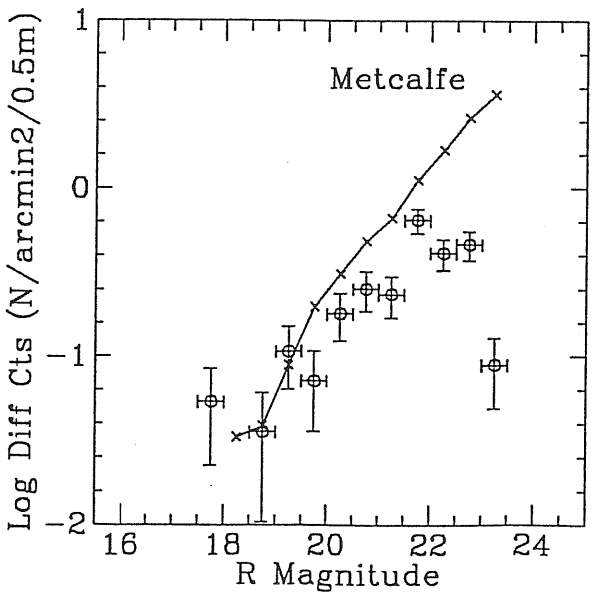

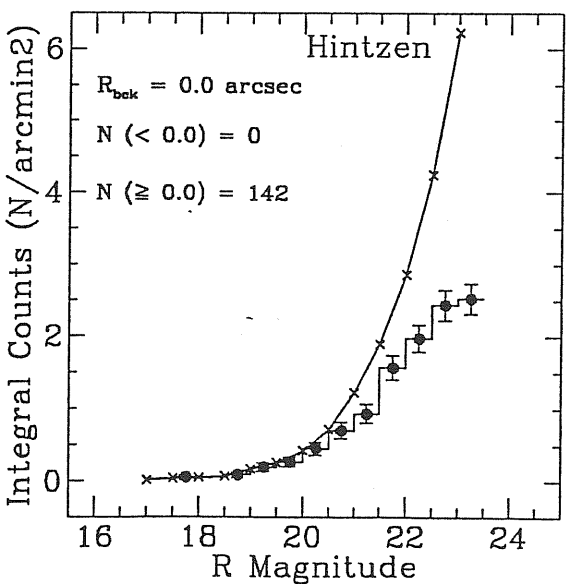

FILE = R_0118.cat, FILTER = R, MAGLIM = 100

Aug 16 12:44:03 199

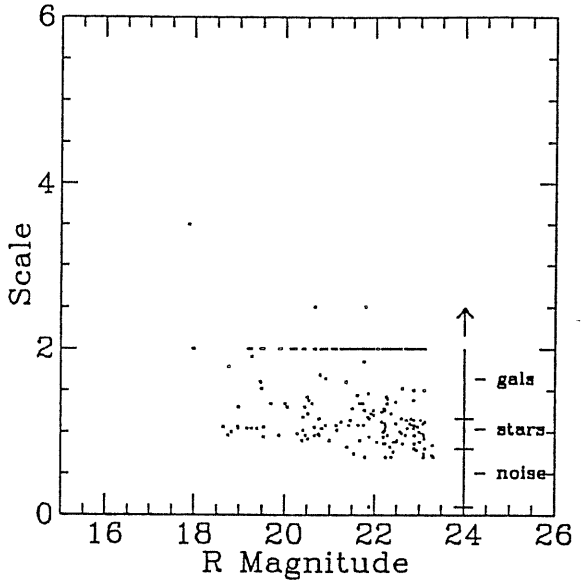

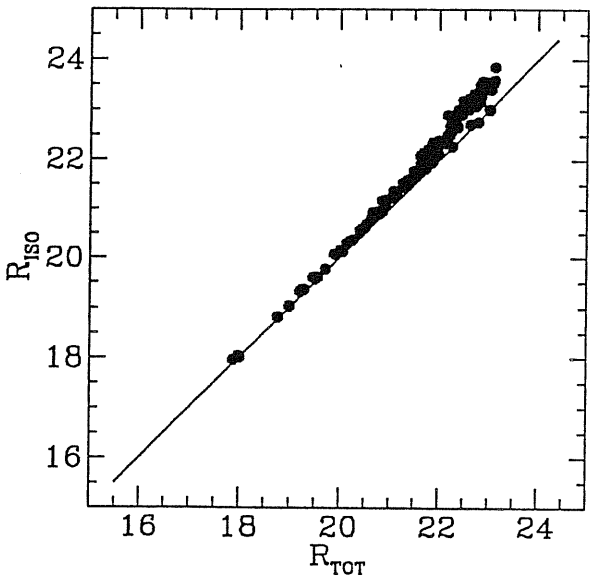

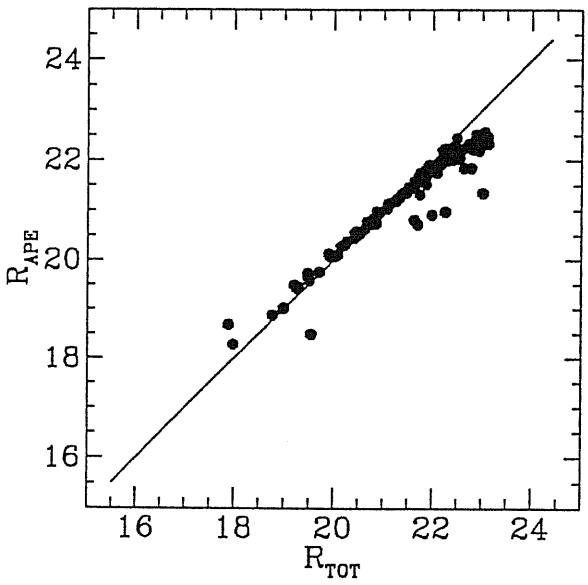

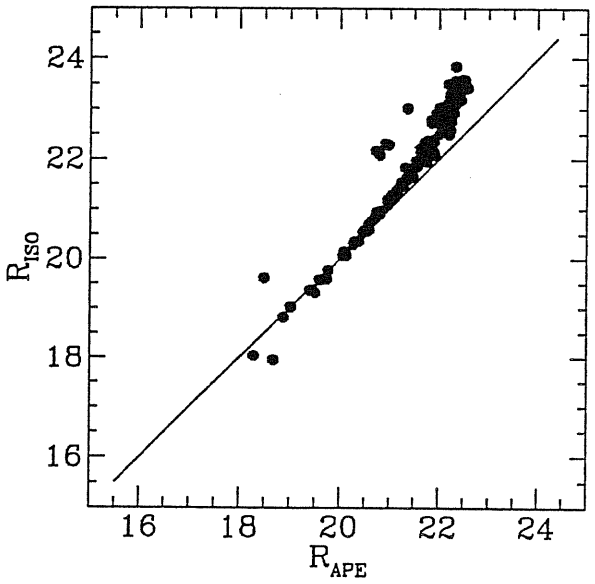

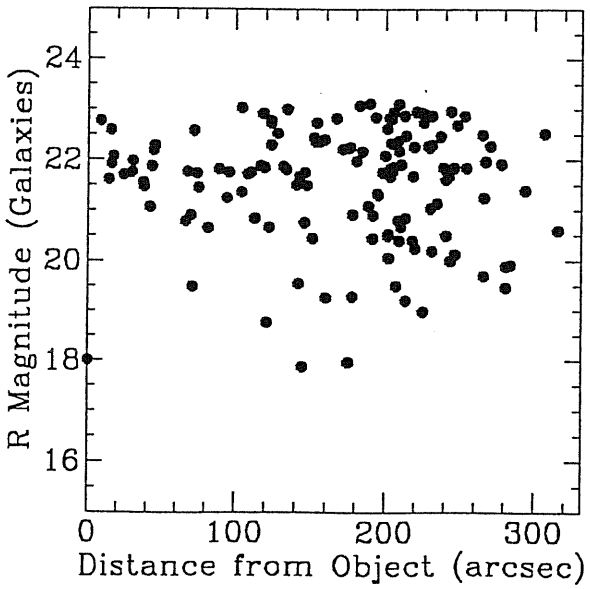

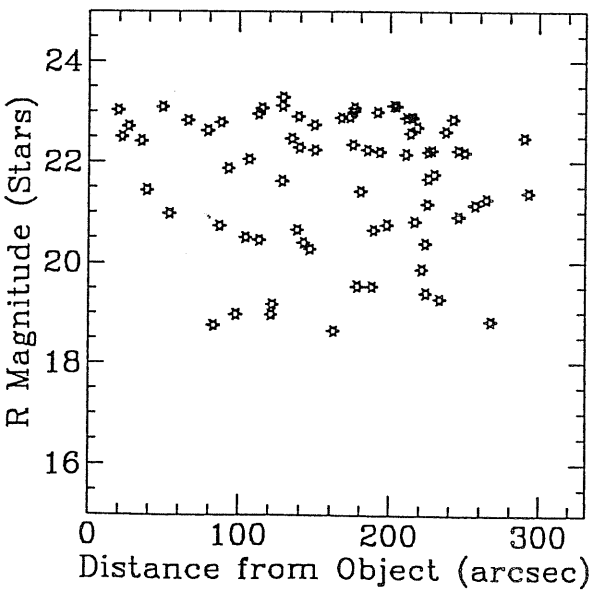

FILE = L0118.cat, FILTER = I, X_0 = 535, Y_0 = 521, MAGLIM = 100, BIN = 30, z = 0.559
$R_{0.5Mpc}$ =67.2953, N_{GALS} = 229 ($N_{\leq 0.5Mpc}$ = 29, $N_{>0.5Mpc}$ = 200), N_{STARS} = 57 Aug 16 12:42:02 1993
EXPOSURE = 600 sec, SEEING = 1.7 arcsec

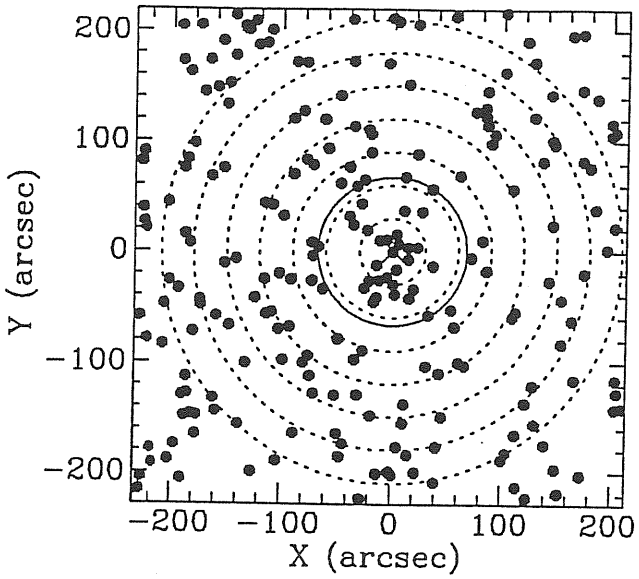

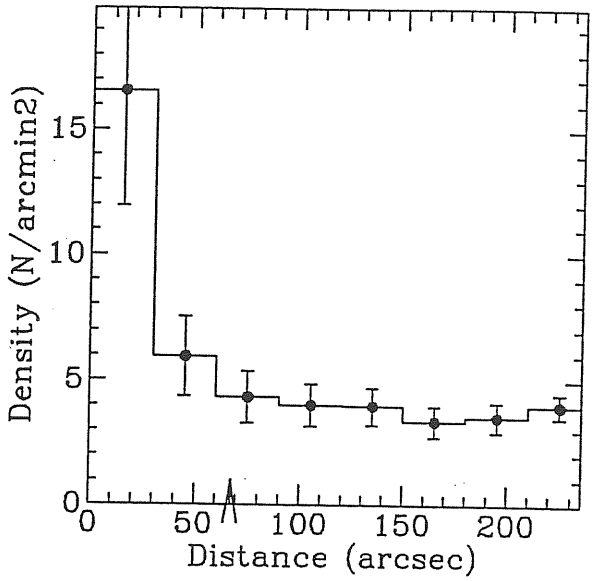

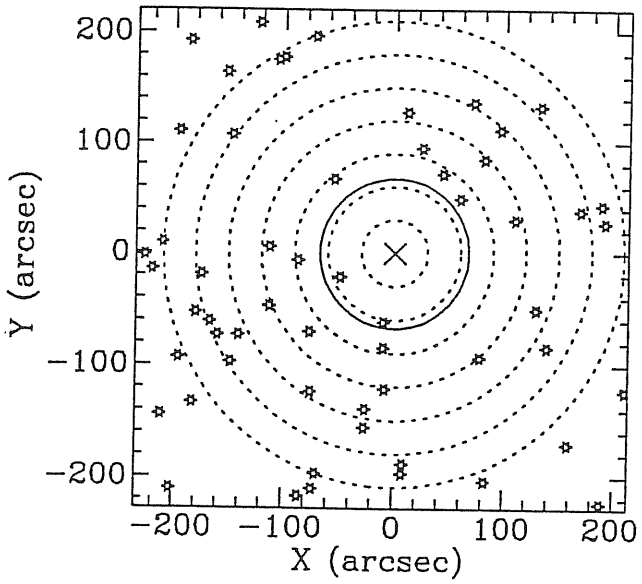

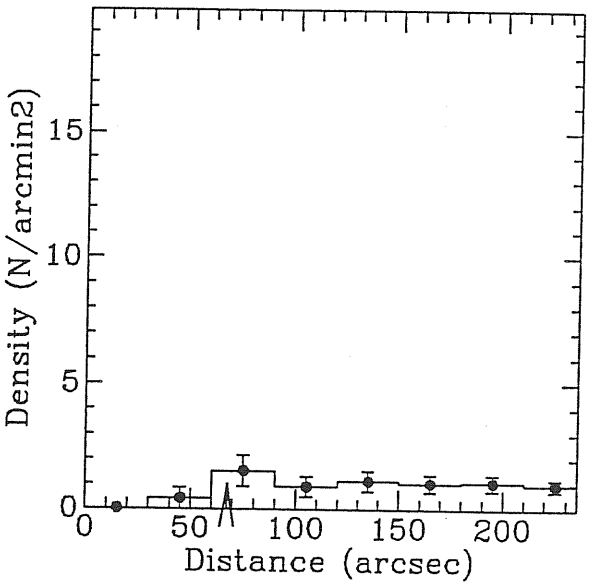

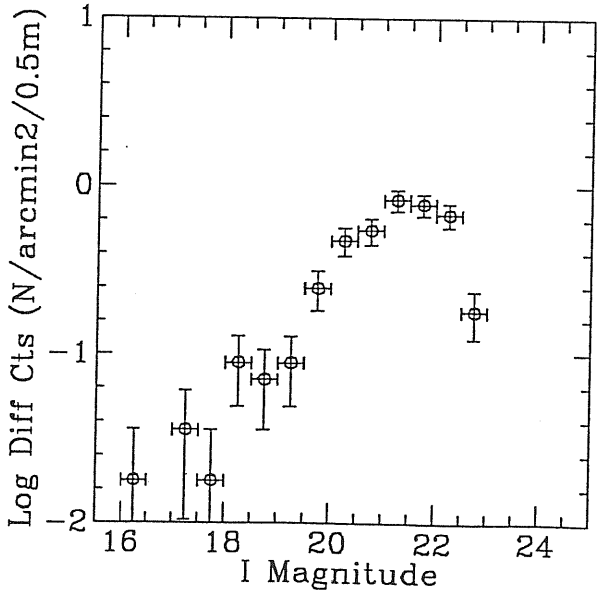

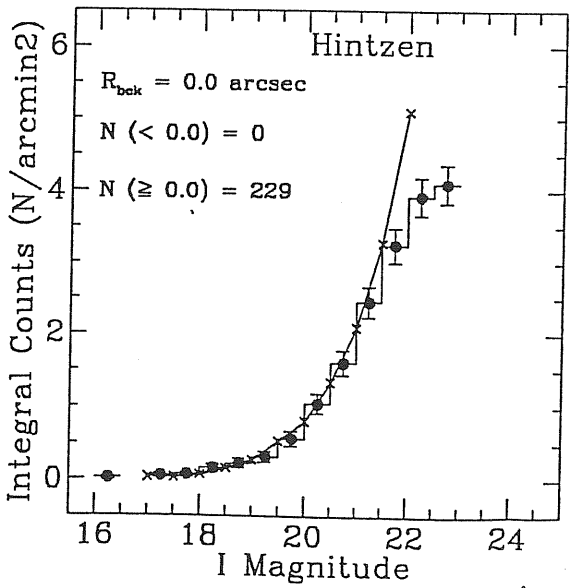

FILE = L_0118.cat, FILTER = I, MAGLIM = 100

Aug 16 12:43:12 1993

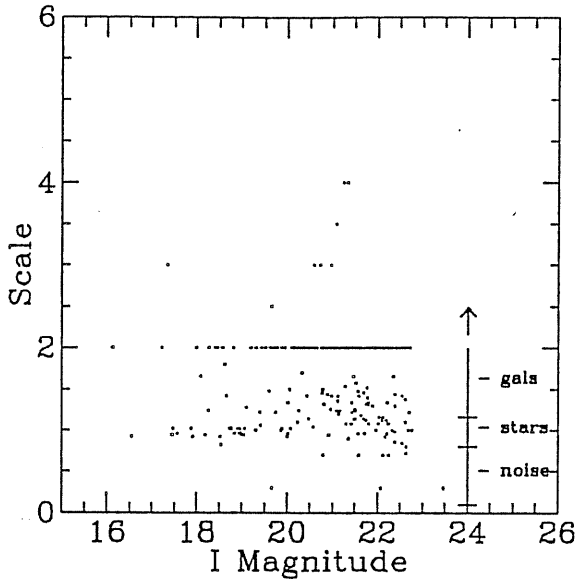

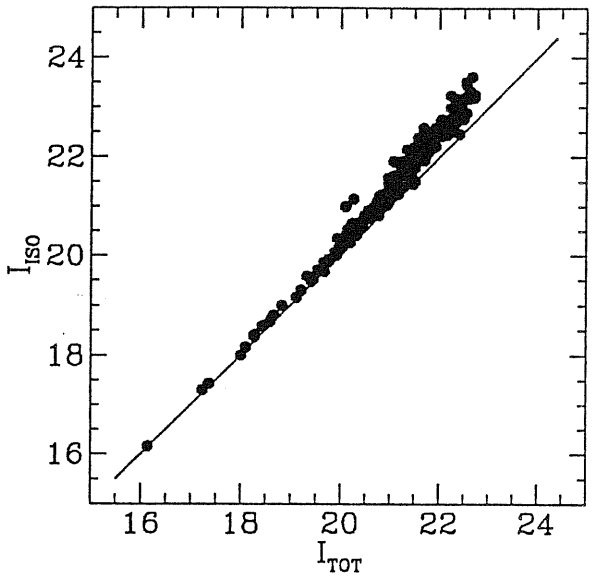

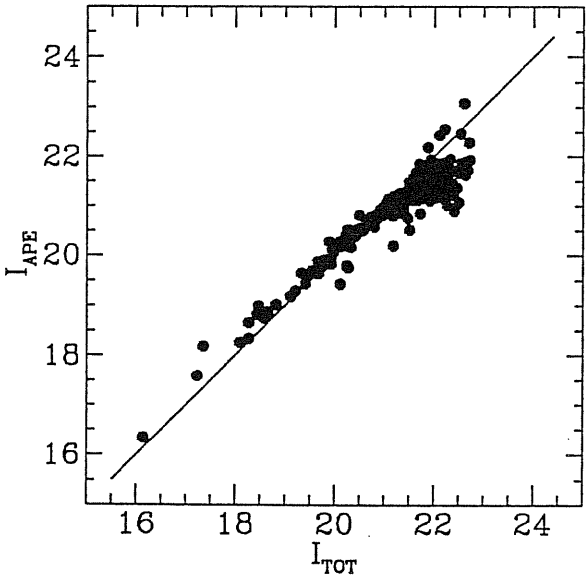

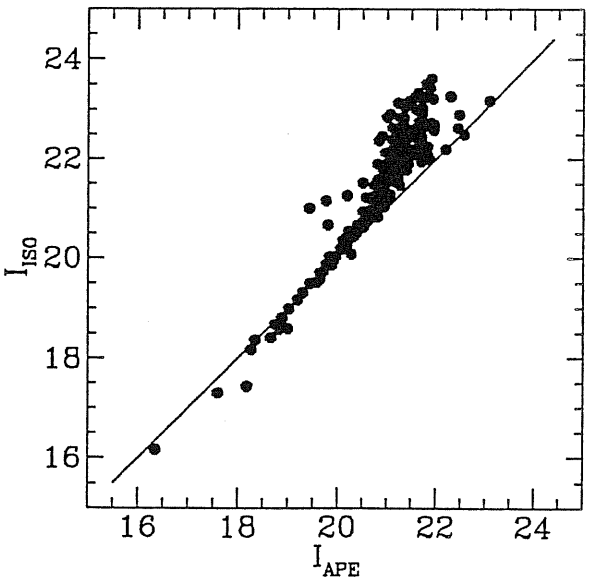

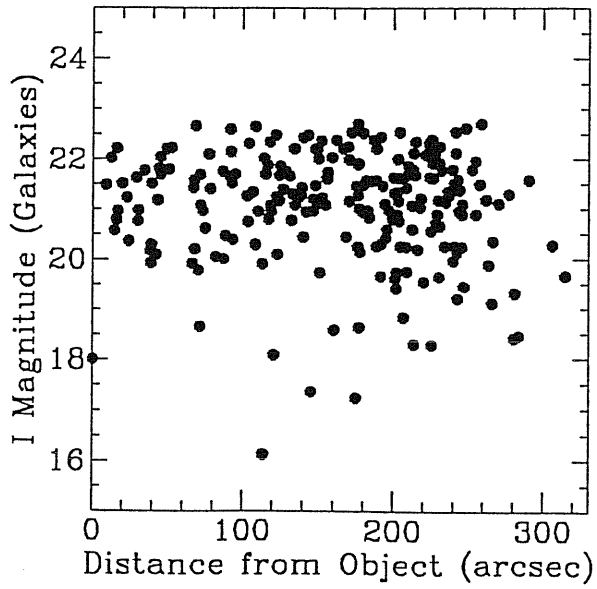

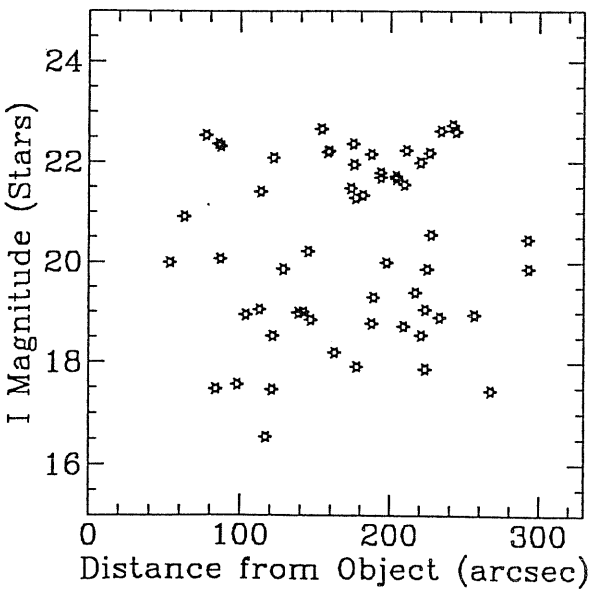

FILE = 0118_sm.mch, z = 0.559, $R_{0.5Mpc}$ = 67.2953 GALAXIES

Aug 16 12:49:41 1993

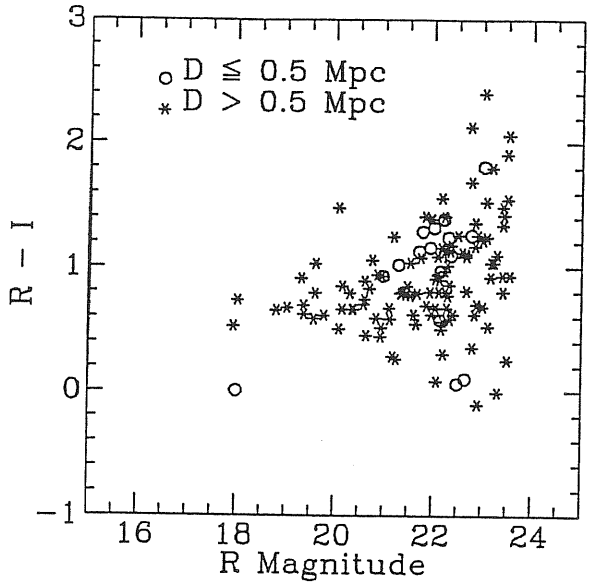

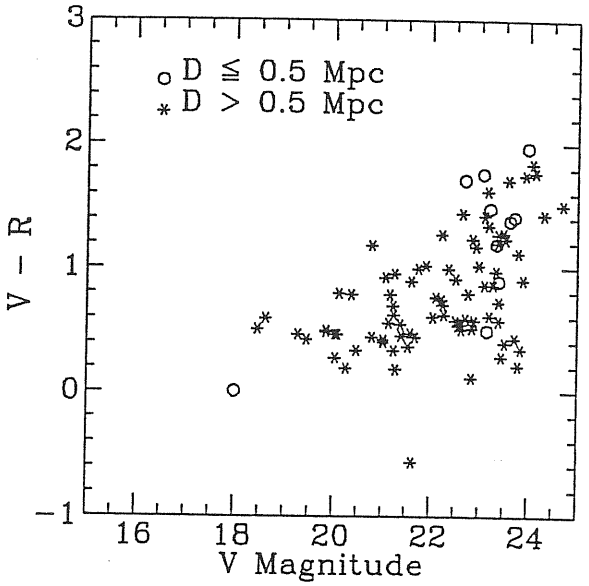

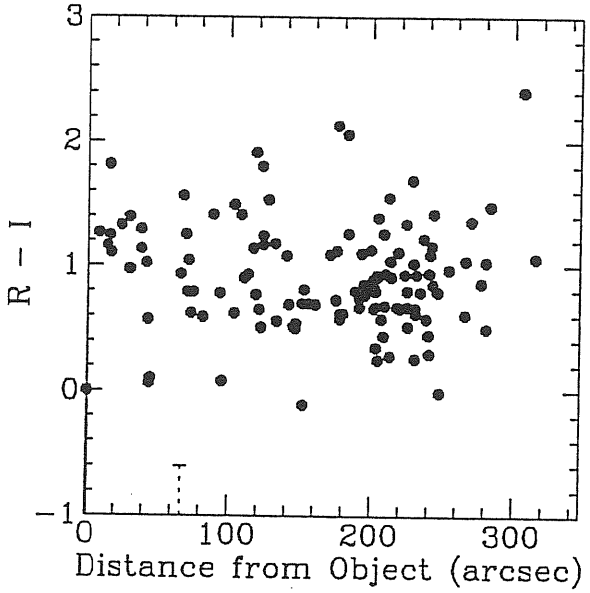

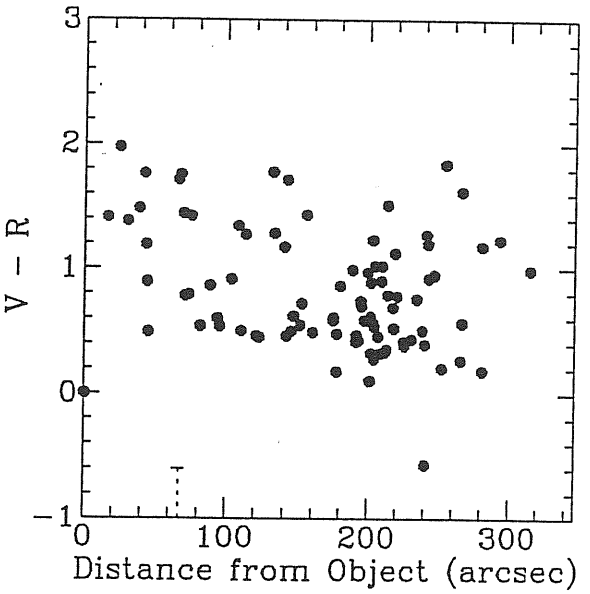

Catalog: v_0118.foc
Number of objects: Total = 266
Field image file: 0118_ima045
Field name: PKS0118-27/V/10M
Field epoch: 31/07/92
Field passband: V
Field coordinates: 0 0
Image exposure or integration: 600
Observer: Falomo
Origin: NTT
Field size: 1021 1021
Field scan origin: 1 1
Field corners in reference coordinates:
(1, 1) (1021, 1) (1, 1021) (1021, 1021)
Magnitude zero point: 31.415001
Catalog magnitude limit: 100.00
Radius of fixed circular aperature: 7.000000
Sigma of sky: 37.5462
Sigma above sky for detection: 3.500000
Sigma below sky for detection: 5.000000
Minimum area for detection: 10
Significance for evaluation and splitting: 0.2
Area file: 0118_im.ar

Comments:

Sat Jan 23 18:41:27 1993: setcat v_0118.foc
Sat Jan 23 18:43:00 1993: setcat v_0118.foc
Sat Jan 23 18:44:11 1993: detect v_0118.foc
sky: pts = 1016 avg = -0.257665 sigma = 37.5462
threshold above = 131.412 threshold below = 187.731

Sat Jan 23 18:44:26 1993: sky v_0118.foc
Sat Jan 23 18:44:41 1993: sky -3 -3.97481 v_0118.foc
Sat Jan 23 18:44:42 1993: evaluate v_0118.foc
Sat Jan 23 18:44:58 1993: splits v_0118.foc
Sat Jan 23 18:45:58 1993: setcat v_0118.foc
Sat Jan 23 18:46:00 1993: resolution v_0118.foc

Detection filter

Builtin filter

0	1	2	1	0
1	2	3	2	1
2	3	4	3	2
1	2	3	2	1
0	1	2	1	0

Transformation matrix

1	0	0
0	1	0
0	0	1

Instrumental intensity relation:

Linear

Point spread function template

3	-1	6	4	6	7	6	3	3	3	4
5	8	7	8	9	8	7	9	4	0	5
5	5	6	14	17	19	18	13	7	1	1
3	10	15	23	34	44	37	24	13	6	6
7	10	14	38	76	93	64	40	21	11	4
5	9	15	42	87	100	84	49	19	14	6

8	9	17	37	65	77	68	44	22	14	5
8	8	16	28	38	46	39	29	15	6	5
7	2	8	18	19	23	21	19	6	9	5
6	2	5	8	11	15	7	10	6	5	6
2	-3	2	-2	5	6	5	4	8	5	3

Classification rules:

0.00	100.00	0.10	0.79	0.00	1.00	n
0.00	100.00	0.80	1.15	0.00	1.00	s
0.00	100.00	1.16	6.00	0.00	1.00	g
0.00	100.00	6.01	100.00	0.00	1.00	d

```
#  24/1/93
#
# V_0118.CAT:  600s V image of 0118 (NTT) - ima045
#              seeing = 1.8s
#              The catalog header is located in V_0118.HEA and the
#              FOCAS readable catalog in V_0118.FOC
#
#              This catalog contains all objects classified as stars,
#              galaxies, noise or diffuse.  Border objects have been
#              removed as have all objects with 'm', 'u', 'long'
#              In addition, certain saturated stars have been misclassified,
#              these have been removed.
#
# The object has been added - magnitudes are NOT correct
###
0.0 536 521 2.0 0 4.26806 10.3028 654 0.0 18.0 18.0 g 0118
0.0  115 5 2 0.5 1.42678 1.58114 14 22.956 23.8902 23.381 g SE
1.0  964 11 1.02 1 2.09276 2.47207 36 22.478 22.8237 22.5233 s SE
2.0  472 12 1.08 1 1.98824 2.27894 31 22.5391 23.0361 22.7066 s SE
3.0  881 25 2 0.85 2.62321 2.96099 43 22.7487 23.147 22.7007 g SE
4.11  15 30 2 0.8 3.30018 3.74166 60 21.524 21.7432 21.6137 g SE
6.0  75 41 2 0.65 2.32937 2.54374 34 22.3179 22.8351 22.4273 g SE
7.0  369 40 1.04 1 2.77928 4.17998 108 20.4673 20.5057 20.4373 s SE
8.0  102 53 2 0.7 4.1992 5.32894 166 20.8707 20.7811 20.6323 g SE
9.0  927 61 1.4 1 3.68279 5.28376 171 20.078 20.0355 19.9604 g SE
10.0  505 63 1.28 1 3.75764 5.19372 158 20.511 20.4711 20.3268 g SE
11.1  535 60 2 0.7 2.77252 3.03158 42 22.0066 22.504 22.3124 g SE
11.2  529 68 2 0.8 2.26023 2.39565 23 22.4194 23.3235 23.1318 g SE
12.0  584 66 1.36 1 3.12168 4.00532 94 21.1957 21.2369 21.1498 g SE
13.0  375 72 1.06 1 2.03601 2.44949 37 22.4592 22.8255 22.5234 s SE
14.0  553 71 1.06 1 2.62041 3.41924 68 21.4486 21.5303 21.4336 s SE
15.0  875 74 1.66 1 3.92942 4.69874 128 21.2423 21.252 21.0544 g SE
16.0  401 89 1.24 1 1.79671 1.76068 10 23.3943 24.8158 23.9746 g SE
17.0  299 90 1.04 1 2.69031 3.81746 89 21.1016 21.1473 21.0852 s SE
19.0  553 92 2 0.25 2.64247 3.36579 70 21.4573 21.6357 21.4387 g SE
20.0  763 92 2 0.65 4.951 6.87249 264 20.3216 20.1066 20.0018 g SE
21.0  569 102 1.14 1 1.97681 2.26569 30 22.5 23.1883 22.7361 s SE
22.0  770 109 2 0.3 1.61697 1.80642 19 23.4189 23.8923 23.4626 g SE
23.0  546 117 2 0.9 4.63242 6.36854 240 19.9976 19.8527 19.7606 g SE
24.0  436 124 2 0.7 2.10347 2.31405 31 22.7828 23.2561 22.8299 g SE
25.1  87 122 2 0.4 2.38644 2.79384 36 21.4509 22.0205 21.7509 g SE
25.2  82 120 2.5 1 2.63299 2.78733 26 21.5235 22.8695 22.5998 g SE
27.0  896 132 1.06 1 3.16464 5.28874 171 19.5867 19.5607 19.5012 s SE
28.0  511 154 1.14 1 1.88564 2.07469 23 23.0449 23.6807 23.3009 s SE
29.0  881 156 0.7 1 1.36472 1.79505 18 22.9641 23.45 23.1084 n SE
30.0  220 164 2 0.65 3.04591 3.54745 77 21.7192 21.889 21.6857 g SE
31.0  558 169 1.26 1 1.63388 1.64751 14 23.1669 24.3078 23.7544 g SE
32.0  831 167 2 0.35 1.81915 1.97484 20 22.393 23.5074 22.8662 g SE
33.0  990 170 2 0.45 1.91701 1.94666 19 23.2143 23.7757 23.4318 g SE
34.0  135 183 1 1 1.74675 1.92931 18 22.8944 23.7617 23.2243 s SE
35.0  109 181 1.2 1 3.14094 4.3842 113 20.9936 21.025 20.9014 g SE
36.0  123 185 1.74 1 3.50084 4.14435 74 22.0315 22.0957 21.8272 g SE
37.0  173 192 2 0.55 1.69584 1.81659 20 23.0479 23.6187 22.9616 g SE
38.0  53 193 1.14 1 2.10024 2.5064 39 22.3727 22.6133 22.414 s SE
39.0  476 203 1.04 1 2.56952 3.52856 71 21.4088 21.4893 21.3898 s SE
40.0  561 206 2 0.65 1.99268 2.04124 18 22.776 23.8516 23.142 g SE
41.0  685 212 100 1 4.92983 4.89898 39 22.7236 23.1906 22.6004 d SE
42.0  774 217 1 1 2.35546 2.44949 12 23.5202 24.5317 23.7627 s SE
43.0  418 225 2 0.5 2.30783 2.60394 41 22.6346 22.9113 22.615 g SE
44.0  465 226 1.36 1 2.20153 2.35621 29 22.9818 23.4749 23.1161 g SE
45.0  532 227 2 0.55 3.95179 4.06003 31 22.5858 23.4004 22.746 g SE
46.0  102 225 1.76 1 3.80019 4.79276 136 20.7849 20.789 20.6941 g SE
47.0  114 229 0.7 1 1.34147 1.55839 14 23.1986 24.3066 23.7957 n SE
48.0  376 228 2 0.6 2.80721 3.23522 60 22.1776 22.2654 22.0894 g SE
49.0  1004 230 2 0.7 2.29487 2.51916 26 22.9829 23.4862 22.9604 g SE
50.0  1013 241 1.16 1 1.63764 1.73205 18 22.8626 23.7335 23.2135 g SE
```

51.0 364 238 1.14 1 2.89647 3.93232 95 21.1656 21.2212 21.1068 s SE
52.0 827 245 2 0.4 2.61655 3.06452 46 22.2051 22.4717 22.2673 g SE
53.0 516 244 1.06 1 3.31107 5.57355 186 19.5959 19.5508 19.4837 s SE
54.0 999 258 1.26 1 2.47193 2.99055 53 21.9664 22.1808 21.9666 g SE
55.0 111 263 2 0.6 2.31412 2.34521 20 22.9024 23.7833 23.3238 g SE
56.0 235 290 0.76 1 1.52379 1.69312 15 23.1071 23.9325 23.5888 n SE
59.0 310 297 2 0.8 1.61585 1.70782 12 22.8809 24.3145 23.7055 g SE
60.1 728 268 0 0 7.82542 9.77162 520 15.2444 14.5821 14.4883 s PSE
60.2 720 256 2 0.6 1.7041 1.83874 21 18.7463 20.0757 19.9819 g SE
61.0 90 309 2 0.5 3.32523 4.33474 100 21.2019 21.2229 21.0568 g SE
62.0 711 309 1.08 1 2.96374 4.69041 132 20.0634 20.0673 20.0076 s SE
63.0 363 307 1.76 1 4.41824 6.56229 267 19.3926 19.2709 19.2282 g SE
64.0 475 318 2 0.8 3.37819 3.83543 76 21.8768 22.0431 21.7637 g SE
65.0 513 327 2 0.4 1.52904 1.64082 13 22.8637 24.2049 23.5303 g SE
67.0 851 329 1.06 1 3.26978 6.02995 222 18.9886 18.9455 18.9139 s SE
68.11 910 318 0 0 6.47067 15.3202 1399 15.449 15.1515 15.147 s PSE
68.12 886 331 2 0.95 2.15387 2.19504 22 21.7692 23.1854 23.1808 g SE
69.0 424 342 1.26 1 2.46204 2.87995 51 22.2292 22.5512 22.2902 g SE
70.0 569 362 0.7 1 1.32929 1.65831 16 22.7667 23.4825 23.44 n SE
71.0 363 360 1.06 1 2.56311 3.35688 67 21.8469 21.973 21.7989 s SE
72.0 664 366 4.5 1 5.23315 5.29392 39 22.6695 23.0932 22.5282 g SE
74.0 156 381 1.02 1 2.65564 3.84386 89 20.763 20.815 20.7106 s SE
75.0 9 385 2 0.8 2.80738 2.97337 44 22.5322 22.8419 22.5221 g SE
76.0 907 378 2 0.65 5.546 8.77898 468 18.9121 18.6185 18.562 g SE
77.0 609 389 2 0.55 2.51356 2.80197 47 22.1694 22.6782 22.2604 g SE
78.0 656 400 2 0.3 2.06383 2.27894 31 22.4516 23.0922 22.7325 g SE
79.0 126 400 2 0.1 3.07007 4.88834 144 20.1166 20.1088 20.0248 g SE
80.0 180 408 2 0.85 2.8503 2.99537 36 22.5968 22.9811 22.5884 g SE
81.0 829 407 1.06 1 2.46848 3.24159 63 21.7158 21.8404 21.7192 s SE
82.0 142 410 2 0.2 2.23556 2.65922 42 22.0961 22.4131 22.1935 g SE
83.0 65 411 2 0.8 4.00984 4.59751 124 21.5055 21.5282 21.3201 g SE
84.0 495 417 2 0.15 2.08664 2.22539 21 23.4559 24.017 23.3614 g SE
85.0 500 426 2 0.5 2.21781 2.4037 27 22.9314 23.3836 23.0168 g SE
86.0 570 424 1.46 1 3.03336 3.14416 35 22.5314 23.1375 22.61 g SE
87.0 885 422 1.4 1 4.30909 6.39476 243 19.9801 19.8482 19.787 g SE
88.0 539 433 2 0.4 2.10196 2.36771 33 22.6379 23.2302 22.7594 g SE
90.0 578 443 0.9 1 1.61034 1.79947 21 22.8875 23.5972 23.2084 s SE
91.0 93 444 2 0.95 2.88862 3.05969 47 22.3399 22.7 22.3432 g SE
92.0 478 445 2 0.45 2.2027 2.5919 39 22.6359 23.0467 22.6602 g SE
93.0 536 453 2 0.3 1.62526 1.77482 20 22.6891 23.5953 22.9824 g SE
95.0 273 465 8.5 1 4.58124 4.75394 45 22.4798 23.0543 22.598 d SE
96.0 328 462 2 0.65 2.68621 3.10365 49 22.3188 22.6158 22.2706 g SE
97.0 523 467 2 0.75 1.9613 2.04634 16 22.7737 23.9736 23.3651 g SE
98.0 424 471 2 0.2 2.51254 3.16491 60 21.6593 21.8984 21.6877 g SE
99.0 860 460 3 1 8.1039 10.7587 695 19.2365 18.4553 18.383 g SE
100.0 934 475 1.08 1 1.73101 1.94489 23 22.7286 23.4922 22.9831 s SE
101.0 35 487 0.9 1 2.23774 3.32786 67 21.1471 21.1944 21.1384 s SE
102.0 617 491 2 0.7 2.25741 2.47933 34 22.4955 23.1887 22.7191 g SE
103.0 59 493 2 0.65 2.84825 3.15876 45 22.2657 22.7297 22.2888 g SE
104.0 306 493 2 0.25 1.5656 1.65831 16 22.8965 23.8502 23.2188 g SE
105.0 190 496 2 0.55 2.14539 2.39792 28 22.5548 23.3849 22.7342 g SE
107.0 214 504 2 0.45 2.43069 2.62927 23 22.9287 23.5698 23.0884 g SE
108.0 568 505 1.22 1 1.84163 1.94936 20 22.885 23.704 23.102 g SE
109.0 337 506 2 0.55 2.18705 2.41523 30 22.8759 23.4454 23.099 g SE
110.0 1002 506 0.7 1 1.50544 2.61795 41 21.9753 22.1516 22.0545 n SE
111.0 331 508 2 0.05 1.59469 1.82003 16 23.31 24.202 23.7539 g SE
112.0 697 507 1.48 1 3.97293 5.41882 176 20.4351 20.3739 20.2251 g SE
113.0 979 526 2 0.3 2.78594 3.34509 58 21.9684 22.2392 21.9877 g SE
115.0 279 532 1 1 2.42485 3.35517 70 21.3934 21.5114 21.3813 s SE
116.0 536 521 0 0 4.26806 10.3028 654 16.8425 16.7309 16.7151 s PSE
118.0 118 538 0.86 1 1.79723 1.94028 17 23.0301 23.7002 23.3711 s SE
119.0 370 539 2 0.75 2.60822 2.77746 42 22.3801 22.7522 22.4247 g SE
120.0 720 542 1.48 1 3.27008 4.03311 94 21.2959 21.3711 21.2453 g SE
121.0 482 564 1.1 1 1.91592 2.05363 23 22.929 23.623 22.9865 s SE
123.0 996 571 2 0.45 2.04236 2.2 25 22.8558 23.4372 22.9759 g SE
124.0 454 575 2 0.6 2.9158 2.97321 25 22.9612 23.3301 22.8717 g SE

125.0 311 592 2 0.5 2.51149 2.91548 50 22.4647 22.5034 22.4356 g SE
126.0 559 604 0.98 1 1.90145 2.12644 23 22.5664 23.4804 22.9576 s SE
127.0 920 608 1.1 1 1.34309 1.3784 10 23.2877 24.4842 23.7914 s SE
128.0 17 608 1.56 1 2.06095 2.16695 23 22.857 23.6362 23.0001 g SE
129.0 956 610 2 0.7 2.84376 3.32938 59 21.9395 22.3567 22.0239 g SE
130.0 272 619 0.74 1 1.42186 1.63299 15 23.6512 24.1878 23.8146 n SE
131.0 964 620 2 0.55 2.303 2.35407 24 22.7037 23.3938 22.8828 g SE
132.0 615 649 2 0.5 1.67372 1.8471 17 23.0862 23.9419 23.5122 g SE
133.0 463 655 2 0.8 1.81676 1.86295 17 22.7284 23.9258 23.4235 g SE
134.0 782 650 1.92 1 3.84589 4.41588 118 21.3401 21.3896 21.1962 g SE
135.0 426 661 2 0.45 1.83858 1.84391 15 23.5239 24.1222 23.6401 g SE
136.0 476 669 2 0.8 2.66319 2.89036 48 22.1215 22.6283 22.229 g SE
137.0 410 673 0.96 1 2.45983 3.38389 71 21.3024 21.4217 21.2645 s SE
138.0 162 674 1.38 1 3.39167 4.2893 108 21.2329 21.2808 21.1726 g SE
139.0 264 686 1 1 1.48803 1.55456 12 23.444 24.4312 24.0035 s SE
140.0 84 687 2 0.5 2.90821 3.03681 27 22.9848 23.485 23.0472 g SE
141.0 634 682 1.06 1 3.19805 5.28538 170 19.7645 19.7339 19.6914 s SE
142.0 333 678 1.06 1 3.87841 9.41387 546 17.0446 16.9534 16.9383 s SE
143.0 106 691 1.16 1 1.96953 2.23607 30 22.8519 23.3669 22.9706 g SE
145.0 942 695 2 0.95 3.30242 3.56571 63 21.9034 22.2064 21.8981 g SE
146.0 372 699 2 0.8 2.60758 2.72976 31 22.5336 23.0225 22.649 g SE
147.0 15 705 1.3 1 3.24743 4.21335 109 21.0147 21.0665 20.9278 g SE
148.0 929 707 2 0.9 3.35833 3.99078 95 21.4894 21.5729 21.3837 g SE
149.0 113 710 2 0.5 2.64514 3.01881 53 22.4208 22.5874 22.4829 g SE
150.0 936 722 2 0.35 1.43645 1.58114 14 22.9509 23.9277 23.3673 g SE
151.0 719 712 1.06 1 3.89157 8.88749 478 17.6938 17.6012 17.5807 s CSE
152.0 71 725 2 0.45 1.54333 1.73205 15 22.9447 23.9618 23.4755 g SE
153.0 20 724 2 0.2 2.42016 2.90517 50 22.024 22.2916 22.0627 g SE
154.0 400 732 2 0.35 2.58629 2.91956 42 22.2953 22.6206 22.4368 g SE
156.0 105 741 2.5 1 1.85941 2 18 22.9709 24.257 23.3272 g SE
157.0 592 736 1.06 1 2.91665 4.66267 131 20.0918 20.0986 20.0325 s SE
158.0 868 741 0.92 1 1.78158 1.83712 16 23.6391 23.9074 23.6075 s SE
159.0 737 742 1.18 1 1.49798 1.52752 12 22.7426 24.1302 23.3739 g SE
160.1 134 740 2 0.9 3.18073 3.3665 39 22.1069 22.8259 22.7388 g SE
160.2 126 740 2 0.9 2.70717 2.86972 34 22.3212 22.9747 22.8876 g SE
161.0 448 736 1.1 1 3.9618 9.24891 520 17.2011 17.1041 17.0837 s SE
162.0 703 736 0 0 3.76616 9.34735 539 17.0639 16.9809 16.9722 s PSE
163.0 202 764 2 0.05 1.51072 1.63299 12 23.3366 24.3326 23.7492 g SE
164.1 240 731 0 0 10.8113 20.1807 2471 15.0846 14.0746 14.0686 s PSE
164.2 239 759 9.5 1 2.55346 2.68328 10 19.4575 23.7032 23.6972 d SE
165.0 988 761 1.28 1 3.89233 6.37613 229 19.5328 19.45 19.4155 g SE
166.0 91 771 2 0.45 2.30761 2.72798 43 22.1022 22.4736 22.1998 g SE
168.1 483 772 2 0.95 2.90115 3.17774 51 21.8608 22.2212 21.9931 g SE
168.2 488 761 1.26 1 3.02122 3.22848 26 22.7548 23.1712 22.9431 g CSE
170.0 731 776 1.1 1 2.22605 2.24846 18 23.1532 24.1686 23.3996 s SE
171.0 752 775 1.06 1 2.43432 3.33234 67 21.3158 21.4307 21.2924 s SE
172.0 987 785 2 0.85 3.85962 4.38081 94 21.5539 21.6744 21.3676 g SE
173.0 332 794 2 0.6 2.2638 2.40139 30 22.6325 23.1623 22.8247 g SE
174.0 724 798 0.98 1 1.71587 1.97814 23 22.7827 23.4514 23.018 s SE
175.0 704 806 1.1 1 2.1428 2.55202 39 22.2524 22.7602 22.4112 s SE
176.0 559 811 0.94 1 1.83972 2.08474 26 22.8617 23.3627 23.1239 s SE
177.0 350 809 1.28 1 2.96535 3.82041 89 21.0534 21.1272 21.0006 g SE
178.0 724 816 2 0.45 1.87458 2.05866 21 23.1295 23.8559 23.4094 g SE
179.0 901 818 2 0.25 1.51433 1.5667 11 22.8011 24.307 23.704 g CSE
180.0 78 829 0.3 1 1.61067 1.7581 11 24.1621 24.7603 23.7866 n SE
181.0 639 842 1.32 1 1.5135 1.61245 15 23.3507 24.3018 23.7163 g SE
182.0 860 844 2 0.5 3.24063 4.04862 92 21.4942 21.5875 21.3859 g SE
183.0 729 852 0.8 1 1.8963 2.08637 17 23.8031 24.0484 23.6885 s CSE
184.0 925 854 2 0.65 1.97722 2.08893 22 22.646 23.4998 23.1136 g SE
185.0 78 854 2 0.9 2.59848 2.77537 37 22.8665 23.2709 22.8863 g SE
186.0 173 857 2 0.75 2.68981 2.94272 47 22.1662 22.5638 22.2291 g SE
188.0 197 866 2 0.65 1.52206 1.65145 11 22.9826 24.693 23.7159 g SE
189.0 105 858 0 0 5.27963 13.0113 1042 16.1993 16.0219 16.008 s PSE
192.0 116 891 1.14 1 1.86376 1.98956 24 22.7948 23.2403 22.8077 s SE
193.0 766 890 2 0.95 4.50192 5.43657 160 21.1113 21.0213 20.8068 g SE
194.0 189 892 1.04 1 2.49437 3.32327 68 21.2363 21.3636 21.2319 s SE

195.0 688 908 0.96 1 1.31355 1.4771 11 23.2323 24.6207 24.0531 s SE
197.0 258 910 0.76 1 1.59141 1.6641 13 23.1608 24.6806 24.2738 n SE
198.0 335 912 2.5 1 2.99662 3.25576 30 22.9723 23.7131 23.1866 g SE
199.0 523 909 1.02 1 2.77062 2.87772 32 23.0217 23.5573 23.1742 s CSE
200.0 588 914 0.7 1 2.4787 2.7303 11 23.6823 25.0215 24.2436 n SE
201.0 639 913 3.5 1 1.63785 1.81871 13 22.9806 24.5289 23.9542 g SE
202.0 826 912 1.3 1 2.14783 2.36234 31 22.567 23.0592 22.7733 g SE
203.0 292 915 9.5 1 3.07702 3.04594 18 23.0207 24.162 23.4495 d SE
204.0 436 912 2 0.35 1.59319 1.77951 12 23.1698 24.7293 24.024 g SE
205.0 668 912 1.2 1 1.83018 1.94235 22 23.0132 23.7723 23.1413 g SE
206.0 202 912 2 0.8 2.81248 2.74226 25 23.0494 23.91 23.3769 g SE
207.0 842 915 2 0.65 2.91189 3.00979 17 23.1035 24.0414 23.395 g SE
208.1 158 915 2.5 1 6.49002 7.01627 114 21.7184 21.6226 21.5643 g SE
208.2 146 912 2 0.85 2.18238 2.28035 20 22.1864 23.6615 23.6032 g SE
209.0 889 930 1.32 1 1.82285 2 17 22.7664 23.7422 23.1566 g SE
210.0 332 932 1.18 1 1.36726 1.3817 11 23.1214 24.2903 23.7656 g SE
211.0 811 954 0.9 1 1.81054 2.15473 28 23.0215 23.0696 22.879 s SE
212.0 954 954 1.06 1 1.46197 1.61721 13 23.2024 24.3895 23.8104 s SE
213.0 626 959 2 0.3 1.46464 1.5 12 23.0974 24.1916 23.7222 g SE
214.0 112 957 1.04 1 2.8818 4.53942 127 19.9584 19.9645 19.8959 s CSE
215.0 904 966 2 0.1 1.53812 1.74895 17 23.1637 24.072 23.5876 g SE
216.0 370 966 1.08 1 2.42484 3.13266 59 21.8676 22.0148 21.868 s SE
218.0 365 974 0.7 1 1.67102 1.74895 17 23.223 23.8074 23.5293 n SE
220.0 283 976 2 0.6 2.82922 3.16835 52 22.1207 22.4991 22.1708 g SE
221.0 47 977 100 1 3.24126 3.14181 31 25.2649 23.9004 0 d DE
223.1 228 986 2 0.1 2.42762 3.06715 54 21.1068 21.3878 21.2438 g SE
223.2 231 979 2 0.5 1.69764 1.78227 17 21.8604 23.3573 23.2133 g SE
224.0 98 985 2 0.9 5.03735 6.33283 229 20.4837 20.2649 20.1224 g SE
225.0 583 988 1.44 1 3.84197 5.5619 184 20.0941 20.0347 19.9301 g SE
227.0 450 998 2 0.6 2.58823 2.73861 34 22.6704 23.1261 22.6859 g SE
228.0 542 994 1.24 1 3.59299 4.62116 107 21.2724 21.2447 21.1445 g SE
229.0 530 1002 2 0.7 1.81801 1.88414 20 22.9206 23.8348 23.2006 g SE
230.0 370 1005 2 0.25 1.59181 1.77482 20 22.9746 23.5759 23.0905 g SE
231.0 660 1005 2 0.9 4.02349 4.99218 128 21.1943 21.1577 21.0359 g SE
232.0 393 1017 3.5 1 2.10436 2.20537 22 22.8863 23.5325 23.1373 g SE

0118: Match of R_0118 I_0118 and V_0118 (on two or more images)
25-2-92

--- arcsec ---							
x	y	d	R	I	V	R-I	V-R
0.0	0.0	0.0	18.00	18.00	18.00	0.00	0.00
5.1	6.6	8.3	22.77	21.51		1.26	
13.9	2.9	14.1	21.93	20.77		1.16	
-11.9	9.9	15.5	23.02	21.21		1.81	
14.1	-7.0	15.7	22.30	21.06	23.70	1.24	1.41
2.9	-16.5	16.7	22.36	21.26		1.10	
-6.2	-23.3	24.1	22.01	20.68	23.97	1.32	1.97
-0.2	-29.9	29.9	22.21	20.83	23.60	1.39	1.38
-23.5	19.1	30.3	22.15	21.18		0.97	
10.1	36.7	38.1	21.78	20.49		1.29	
35.8	-13.2	38.2	21.71	20.57	23.19	1.13	1.48
1.5	-38.7	38.7		20.35	23.23		
-25.5	-33.2	41.9	21.29	20.27	23.05	1.02	1.76
-36.1	23.7	43.2	22.14	21.57	23.33	0.57	1.19
-15.2	-41.6	44.2	22.49	22.43	23.38	0.06	0.89
14.9	-42.4	45.0	22.65	22.55	23.14	0.10	0.49
-17.6	-45.7	49.0		22.73	24.02		
32.3	-57.8	66.2	20.97	20.04	22.68	0.93	1.71
35.2	56.5	66.6		21.83	23.94		
-32.8	59.1	67.6	22.17	20.61	23.93	1.56	1.75
-26.2	64.9	69.9	21.19	19.94	22.63	1.25	1.44
71.0	-5.7	71.2	19.59	18.80	20.37	0.79	0.78
-63.1	-34.1	71.7	23.23	22.18		1.04	
-73.0	7.9	73.4	21.96	21.34	22.75	0.62	0.79
53.0	-53.0	74.9	21.67	20.88	23.09	0.79	1.42
-47.9	61.8	78.2		21.94	24.12		
81.1	9.5	81.7	20.83	20.24	21.37	0.59	0.54
56.1	-68.6	88.6	22.23	20.83	23.09	1.41	0.86
-49.0	-78.7	92.7		22.15	22.55		
-27.0	-89.7	93.7	21.44	20.66	22.04	0.78	0.60
-91.7	-25.5	95.2	22.07	22.00	22.62	0.08	0.54
-34.1	-97.6	103.4	23.41	21.92		1.49	
-98.7	31.4	103.6	21.60	20.97	22.50	0.62	0.91
-72.1	78.3	106.4		21.59	23.02		
-20.9	106.2	108.2	21.83	20.41	23.17	1.41	1.34
-59.1	93.2	110.4	22.12	21.22	22.62	0.90	0.50
-23.1	110.6	113.0	20.95	20.02	22.22	0.93	1.27
60.0	-100.3	116.8	22.24	21.10		1.14	
-35.6	113.0	118.5	23.49	21.58		1.91	
-115.9	-25.7	118.7	22.29	21.53		0.77	
-75.8	-94.1	120.9	18.81	18.16	19.27	0.65	0.46
108.6	56.7	122.5	20.94	20.42	21.39	0.51	0.45
-109.5	-55.4	122.7	23.19	21.39		1.80	
-115.9	43.1	123.6	22.85	21.68		1.17	
108.8	-59.1	123.9	23.08	21.84		1.24	
-113.9	-56.7	127.2	23.07	21.54		1.53	
88.6	97.8	132.0	22.36	21.18	24.13	1.18	1.77
-31.2	-129.5	133.2	22.19	21.63	23.47	0.56	1.28
11.0	-138.3	138.7		21.79	23.85		
-98.9	-98.3	139.4		21.95	24.31		
-51.7	-130.4	140.2	21.74	20.66	22.91	1.08	1.17
80.9	-116.5	141.9	19.61		20.08		0.46
-141.8	-7.3	142.0	21.86	21.17	23.57	0.69	1.71
142.5	-26.8	145.0	17.95	17.43	18.46	0.52	0.50
74.1	126.2	146.3	22.16	21.65		0.50	
-70.6	-128.6	146.7	21.65	21.11	22.27	0.54	0.62
-89.7	120.3	150.0		22.72	23.16		
-81.6	127.1	151.0	20.58	19.88	21.13	0.70	0.55
13.4	151.3	151.9	22.91	23.03		-0.11	
-152.1	-11.0	152.5	22.67	21.86	23.38	0.81	0.72
82.9	129.9	154.1		21.51	23.86		

9.7	-155.4	155.7	22.88	22.18	24.31	0.70	1.43
154.1	-43.5	160.1	19.36	18.67	19.85	0.69	0.49
-5.5	170.8	170.9	22.67	21.58		1.09	
163.3	-62.7	175.0	18.03	17.30	18.62	0.73	0.59
154.1	-83.3	175.2	22.58	21.46	23.19	1.12	0.61
146.6	97.2	175.9	22.75	20.62		2.13	
128.2	-121.1	176.4		21.75	22.47		
4.6	-177.4	177.5	19.37	18.75	19.85	0.62	0.48
-164.2	67.5	177.6	21.11	20.53	21.28	0.58	0.18
-44.2	-174.3	179.9	22.40	21.78	23.26	0.62	0.86
-173.2	-48.6	179.9		21.04	22.41		
120.9	-136.7	182.5	23.52	21.46		2.06	
-183.6	7.3	183.7	22.50	21.25		1.26	
184.5	38.7	188.5	21.37	20.57	22.36	0.80	0.99
100.9	162.5	191.3	20.60	19.86	21.02	0.74	0.42
173.0	82.0	191.5	21.10	20.44	21.57	0.67	0.47
-87.7	171.9	193.0	23.29	22.19	23.71	1.10	0.43
179.0	76.5	194.6	21.47	20.63	22.21	0.85	0.74
195.2	2.2	195.2	21.53	20.76	22.24	0.77	0.70
-194.3	-34.1	197.3	22.11	21.31	22.70	0.80	0.59
-2.4	-199.4	199.4	22.35	21.22	23.32	1.13	0.97
-176.5	96.3	201.1	22.72		22.83		0.11
21.3	-200.1	201.2	20.61	19.73	21.24	0.89	0.62
143.1	142.2	201.8	20.70	19.87	21.59	0.83	0.89
-13.4	-201.4	201.8	20.14	19.48	20.47	0.66	0.33
0.0	-202.5	202.5	21.93	21.13	22.50	0.80	0.57
129.9	-155.9	202.9	22.27	21.60	23.51	0.67	1.23
-188.9	75.0	203.2	22.80	22.45	23.37	0.35	0.57
202.7	21.8	203.9	23.16	22.24	23.44	0.92	0.28
-186.2	83.1	203.9	22.05	21.14	22.59	0.91	0.54
-202.7	-26.8	204.5	23.50	23.25		0.25	
-180.1	97.0	204.5	21.96	20.57	22.97	1.39	1.02
20.9	205.8	206.8	19.57	18.99	20.03	0.58	0.46
2.6	208.4	208.4	20.92	20.47	21.24	0.44	0.33
-203.8	43.8	208.4	22.90	21.64		1.26	
103.3	-181.8	209.1	23.00	22.32	23.89	0.68	0.90
-138.9	-156.8	209.5	20.86	19.93	21.89	0.94	1.02
-2.0	211.9	211.9	23.50	21.94	23.83	1.55	0.34
-207.3	-48.1	212.8	21.17	20.90	21.53	0.28	0.36
-149.1	152.4	213.1	23.18	22.14	24.69	1.04	1.51
-37.8	210.0	213.3		22.65	23.13		
100.0	-188.6	213.5	19.32	18.41	20.11	0.91	0.79
127.7	171.9	214.2		22.07	23.06		
-159.4	-144.4	215.1		22.83	23.62		
-196.3	-93.4	217.4	20.53		21.22		0.69
-159.6	148.4	217.9	22.04	21.37	22.56	0.67	0.53
-186.7	-113.7	218.5	22.66	21.55	23.78	1.11	1.12
54.5	213.0	219.9	20.37	19.71	21.16	0.66	0.78
139.2	-174.8	223.4	23.55	22.62		0.93	
-171.5	144.4	224.2	23.41	22.07		1.34	
-208.9	-84.2	225.2	23.42	22.61		0.80	
199.0	105.5	225.2	19.03	18.36	19.45	0.67	0.42
171.5	146.6	225.6	23.11	22.59	23.50	0.52	0.39
-143.8	177.4	228.4	22.77	21.08		1.69	
-111.0	200.3	229.0		21.25	22.50		
202.5	107.9	229.5	22.28	21.26		1.02	
199.0	116.3	230.5	21.24	20.98	21.67	0.26	0.44
-190.2	-130.4	230.6	20.35	19.69	20.79	0.66	0.44
-176.8	-148.4	230.8	22.84	22.22		0.62	
-227.8	38.5	231.0		22.83	23.64		
185.3	138.5	231.4	23.40	22.47		0.93	
203.8	-115.6	234.3		21.58	22.18		
-182.3	-147.3	234.3	21.33	20.54	22.10	0.79	0.76
-126.4	-199.8	236.5	23.01	21.79		1.22	
-230.8	-59.4	238.4	22.33	21.75	22.84	0.58	0.51
-188.0	-149.3	240.0	20.63	20.18	21.02	0.45	0.40

-131.7	201.2	240.4	22.09	21.15		0.94	
-166.6	173.5	240.5	22.20	21.90	21.62	0.30	-0.57
-132.8	201.4	241.2	22.09	21.00	23.36	1.09	1.27
205.6	-127.5	241.9		22.51	23.49		
-134.1	201.6	242.1	22.16	21.00	23.36	1.16	1.20
-229.1	81.1	243.0	20.15	19.30	21.07	0.85	0.92
-178.1	-165.8	243.3	23.43	22.02		1.42	
-226.7	89.5	243.7		21.07	22.29		
-135.2	204.7	245.3		20.66	21.39		
-184.5	162.5	245.8	22.24	21.44		0.80	
149.1	-196.5	246.7	20.30	19.52	21.25	0.79	0.95
202.9	-142.7	248.1	23.31	23.32		-0.01	
199.6	-154.6	252.5	23.57		23.78		0.21
162.5	195.9	254.5	22.23	21.26	24.07	0.97	1.84
-197.2	-175.2	263.8		20.07	22.02		
172.1	-202.5	265.8	19.77	19.16	20.04	0.61	0.27
151.9	-218.5	266.1	21.53	20.49	23.15	1.04	1.62
-199.8	-176.5	266.7	22.30		22.87		0.57
-175.7	205.1	270.1	22.85	21.48		1.36	
-203.1	-188.6	277.2	22.32	21.47		0.86	
-190.6	-205.8	280.5	19.60	18.58	20.78	1.03	1.18
-192.8	204.2	280.9	20.08	19.58	20.26	0.50	0.19
-219.6	-179.2	283.4	20.07	18.59		1.48	
-203.1	-211.3	293.1	21.60		22.84		1.23
-227.8	-204.7	306.2	23.03	20.64		2.40	
-229.5	-215.7	315.0	20.75	19.68	21.74	1.06	0.99